ALMA MATER STUDIORUM
UNIVERSITÀ DI BOLOGNA

DOTTORATO DI RICERCA IN

CHIMICA

Ciclo 38

Settore Concorsuale: 03/C1 - CHIMICA ORGANICA

Settore Scientifico Disciplinare: CHIM/06 - CHIMICA ORGANICA

EXCITED-STATE REACTIVITY OF 4-HYDROXYCOUMARINS: UNLOCKING NEW PHOTOCHEMICAL TRANSFORMATION

Presentata da: Hailong Wang

Coordinatore Dottorato

Cristina Puzzarini

Supervisore

Paolo Melchiorre

Co-supervisore

Luca Bernardi

Esame finale anno 2026

Acknowledgements

Looking back on the past several years in the Melchiorre group, I am deeply indebted to my supervisor, Professor Dr. Paolo Melchiorre, whose invaluable guidance, insightful advice, and continuous support have been the cornerstone of my doctoral studies. His passion for chemistry, intellectual rigor, and generosity in sharing knowledge have not only guided my research but also shaped my scientific mindset and personal growth.

I would also like to thank all my former and current colleagues in the Melchiorre group. In particular, I would like to thank Dr. Sumitava Mallik for the valuable discussions on the chemistry and for teaching me how to express my ideas more effectively. I sincerely thank Dr. Bixiao Li for the theoretical chemistry I learned from her and for her companionship during our time in the laboratory. I am thankful to Dr. Diyuan Li for his friendship and constructive discussions, both in the lab and beyond. My sincere thanks also go to Dr. Binlin Zhao for the chemistry I learned from him and for sharing your experience in scientific research. I am grateful to Dr. Gareth Surman for his kind assistance with my English writing. I would also like to thank Su Huang and Enrico Sfreddo for their collaboration and support. I would like to express my deepest appreciation to Isabella for her professional support with the administrative matters of my university.

I am grateful to Professor Dr. Daniele Leonori for his invaluable support and guidance during my visiting study in his research group. My heartfelt thanks extend to Dr. Giovanni Lonardi for his generous assistance, both in my chemical academic research and daily life during my stay in Aachen.

I am deeply grateful to my family—especially my mother, Shaofeng Hou, my father, Qingyu Wang, and my grandmother, Zongying Zhao for their unconditional love and unwavering support. I would like to thank my girlfriend, Jiayu Li, for her constant companionship and encouragement throughout this journey.

Finally, I would like to express my sincere gratitude to the China Scholarship Council (CSC) for supporting my research at the University of Bologna through a predoctoral fellowship (CSC202208350011).

Abstract

This PhD thesis examines how light excitation can be harnessed to reprogram the intrinsic reactivity of 4-hydroxycoumarins, compounds traditionally known for their ground-state nucleophilic behavior. By revealing how photochemical activation alters their fundamental reactivity patterns, this thesis establishes the unrecognized photoreactivity of 4-hydroxycoumarins in organic synthesis.

Firstly, we revealed that, upon deprotonation and excitation with purple light, 3-substituted 4-hydroxycoumarins reach an excited state and act as strong single-electron transfer (SET) reductants, generating radicals from stable substrates. This newfound reactivity enables the direct synthesis of 3,3-disubstituted 2,4-chromandiones via a radical dearomatization process. By enabling the incorporation of alkyl and perfluoroalkyl fragments, this protocol offers a straightforward and mild route to access synthetically valuable chromanone scaffolds featuring a quaternary stereocenter.

Based on our findings in the first project, we modified 4-hydroxycoumarins to design 3-thioaryl-4-hydroxycoumarins, a new family of cost-effective organic photocatalysts that leverage a stabilized charge-transfer (CT) excited state to achieve both strong reducing power and efficient energy transfer (EnT) behavior. The spatial separation of the HOMO and LUMO stabilizes the CT state, enhancing SET reactivity ($E^*_{red} = -3.08$ V vs. SCE) while maintaining a sufficiently high triplet energy (E_T = 67 kcal mol^{-1}) for EnT-driven transformations. This dual reactivity enables the activation of redox-inert substrates ($E_{red} < -2.8$ V vs. SCE) via SET reduction, generating radicals suitable for diverse C─S, C─P, C─B, and C─C bond-forming transformations, alongside EnT-based processes such as *E/Z* olefin isomerization and [2+2] photocycloadditions. Mechanistic studies, supported by photophysical and theoretical analyses, confirmed the catalyst's bifunctionality.

In conclusion, this work demonstrates that by exploiting light to control electronic excitation, 4-hydroxycoumarins can be transformed from simple ground-state nucleophiles into versatile photoactive scaffolds that enable previously inaccessible radical transformations.

Table of Contents

Chapter I

General Overview

This PhD thesis explores how light excitation can be used to reprogram the intrinsic reactivity of organic molecules, enabling radical-mediated transformations that are inefficient or inaccessible under thermal conditions. The central premise is straightforward: an electronically excited molecule is a different chemical species from its ground-state counterpart, with distinct redox properties and reactivity. Harnessing these differences allows us to reprogram reactions—to turn traditionally nucleophilic or inert motifs into photoreductants and triplet sensitizers—on demand. Within this framework, 4-hydroxycoumarins are repurposed from well-known ground-state nucleophiles into photoactive scaffolds that mediate either single-electron transfer (SET) or energy transfer (EnT) mechanisms upon light excitation.

This chapter introduces the conceptual ideas and the tools used in this PhD thesis (photochemistry, photoredox catalysis, SET, and EnT), thus providing the context and the background that have motivated this research.

1.1 Introduction

All photochemical processes begin with the interaction between light and matter through the absorption of a photon by a molecule.[1] This phenomenon underlies the principle of photochemical activation, also known as the Grotthuss–Draper law, which states that *"only absorbed light is effective in producing a photochemical change"*. Although this statement may sound self-evident, it is critical to understanding photochemistry: light that is not absorbed cannot induce a chemical event. Behind this law lies the quantum mechanical description of matter, in which molecules possess quantized energy levels ranging from the low-energy ground state to a number of higher excited states. Photon absorption occurs only when the photon energy matches the gap between an occupied and an unoccupied molecular orbital. Upon absorption of light of suitable energy, a molecule is electronically excited — an electron transitions from the highest occupied molecular orbital (HOMO) to the lowest unoccupied molecular orbital (LUMO, **Figure 1.1a**). In doing so, the molecule gains energy (hν, the energy of the photon, where *h* is Planck's constant), which is inversely proportional to the wavelength of light (λ), according to Planck's equation (**Eq. 1**).

$$E = h \cdot (c/\lambda) = E_f - E_i \qquad \textbf{(Eq. 1)}$$

[1] Balzani, V., Ceroni, P., Juris, A. "Photochemistry and Photophysics: Concept, Research and Applications" Weinheim, Wiley-VCH, **2014**.

These electronically excited states are described by the wave functions Ψ, with Ψ_i corresponding to the ground state and Ψ_f to the excited state (**Figure 1.1b**).

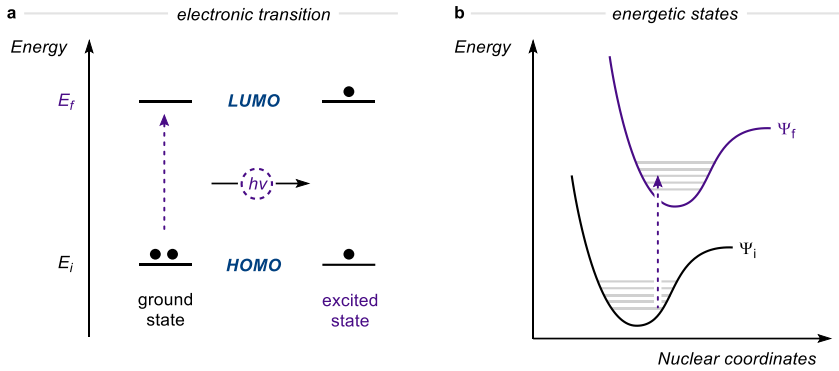

Figure 1.1. (**a**) Absorption of a photon promotes an electron from the HOMO to the LUMO. (**b**) Electronic transition from the ground state (Ψ_i) to the excited state (Ψ_f)

This electronic transition changes the physical and chemical properties of the molecule; therefore, an excited molecule can be considered a different compound from the ground state.[2] From the electronically excited state, a series of photophysical and photochemical events can take place. First, the excited molecule can return to the ground state S_0 through radiative and non-radiative deactivation pathways, including relaxation between vibrational levels, transitions between different excited states ($S_2 \rightarrow S_1$ or $S_1 \rightarrow T_1$) leading to luminescence from the lowest excited states, or thermal deactivation (**Figure 1.2**).[3] Another possibility for the excited molecule is to use this surplus of energy to initiate unimolecular or bimolecular photochemical processes, such as *single-electron transfer* (SET) or *energy transfer* (EnT), unlocking new reactivity inaccessible under thermal activation.

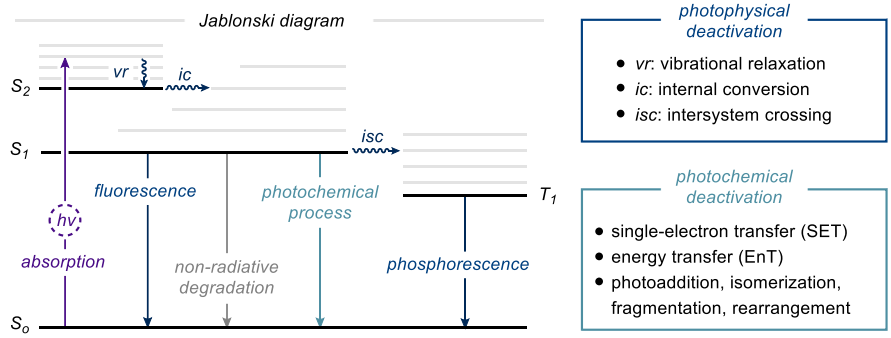

Figure 1.2. Photophysical and photochemical processes represented on a Jablonski diagram. Grey lines correspond to vibrational levels. *S*: singlet state; *T*: triplet state.

[2] Albini, A., Fagnoni, M. "Photochemically Generated Intermediates in Synthesis." John Wiley & Sons, **2013**.

[3] Lakowicz, J. R. "Principles of Fluorescence Spectroscopy." Springer, **2006**.

The earliest studies of photochemical phenomena date back to the 18th century,[4] but organic photochemistry only emerged as a distinct discipline in the early 20th century, following the pioneering sunlight-driven experiments of Giacomo Ciamician and Paul Silber.[5] From then until the late 2000s, only a limited number of synthetic chemists explored photochemical reactivity. Typically, the photochemical activation of colorless substrates required high-energy UV-light. Such energetic irradiation does not tolerate a wide range of functionality, often leading to inefficient and unselective reactivity. Furthermore, these processes required specialized equipment that limited a broad application of photochemistry.

These constraints were lifted with the introduction of visible-light photoredox catalysis, where colored photocatalysts mediate energy or electron transfer between visible light and otherwise non-absorbing substrates. This approach triggered a renaissance in the field around 2008–2009, following seminal reports by MacMillan,[6] Yoon,[7] and Stephenson,[8] who demonstrated the use of the tris(bipyridine)ruthenium(II) complex, $[Ru(bpy)_3]^{2+}$,[9] as a photocatalyst for SET and EnT processes under visible-light irradiation. Although this complex was already well known in artificial photosynthesis and water-splitting studies, its potential in organic synthesis had been largely unexplored.[10]

In their report (**Figure 1.3**),[6] MacMillan and co-workers combined organocatalysis and photoredox catalysis. Specifically, they used $[Ru(bpy)_3Cl_2]$ (**PC**) to generate radicals **II** by SET reduction of bromomalonates **2**. Meanwhile, condensation of MacMillan's imidazolidinone amine catalyst with aldehydes **1** generated the nucleophilic chiral enamine intermediate **I**, which could intercept the radicals **II** in a stereoselective fashion. The resulting α-amino radical **III** was then oxidized to iminium **IV** by the photoexcited Ru^{II} complex. Eventually, hydrolysis of **IV** delivered the enantioenriched α-alkylated aldehydes **3**, while turning over the organocatalyst. Later, Yoon and coworkers[11] clarified that a radical chain propagation mechanism accounted for product formation, with the excited Ru catalyst serving as an initiator. This reaction solved a long-standing challenge in polar chemistry: the

---

[4] (a) Roth, H. D. "The Beginnings of Organic Photochemistry." *Angew. Chem. Int. Ed.* **1989**, *28*, 1193–1207; (b) König, B. "Chemical Photocatalysis." Berlin/Boston, Walter de Gruyter GmbH, **2013**.

[5] (a) Ciamician, G., Silber, P. "Chemische Lichtwirkungen" *Ber. Dtsch. Chem. Ges.* **1910**, *43*, 45; (b) Ciamician, G. "The Photochemistry of the Future." *Science*, **1912**, *926*, 385–394.

[6] Nicewicz, D. A., MacMillan, D. W. C. "Merging Photoredox Catalysis with Organocatalysis: The Direct Asymmetric Alkylation of Aldehydes." *Science* **2008**, *322*, 77–80.

[7] Ischay, M. A.; Anzovino, M. E.; Du, J.; Yoon, T. P. "Efficient Visible Light Photocatalysis of [2+2] Enone Cycloadditions." *J. Am. Chem. Soc.* **2008**, *130*, 12886–12887.

[8] Narayanam, J. M. R.; Tucker, J. W.; Stephenson, C. R.J. "Electron-Transfer Photoredox Catalysis: Development of a Tin-Free Reductive Dehalogenation Reaction." *J. Am. Chem. Soc.* **2009**, *131*, 8756–8757.

[9] Paris, J. P., Brandt, W. W., "Charge Transfer Luminescence of a Ruthenium(II) Chelate" *J. Am. Chem. Soc.* **1959**, *81*, 5001–5002.

[10] (a) Grätzel, M. "Photochemical Conversion and Storage of Solar Energy." *Acc. Chem. Res.* **1981**, *14*, 376–384; (b) Meyer, T. "Chemical Approaches to Artificial Photosynthesis." J. *Acc. Chem. Res.* **1989**, *22*, 163–170.

[11] Cismesia, M. A. & Yoon, T. P. "Characterizing Chain Processes in Visible Light Photoredox Catalysis." *Chem. Sci.* **2015**, *6*, 5426–5434.

stereoselective intermolecular α-alkylation of aldehydes, achieved here through radical reactivity. Following this breakthrough, photoredox catalysis rapidly evolved into a central platform in modern synthesis. Numerous photocatalysts—ranging from transition-metal complexes to purely organic dyes—have since been developed, providing powerful tools to generate reactive intermediates through single-electron transfer or energy-transfer pathways.[12]

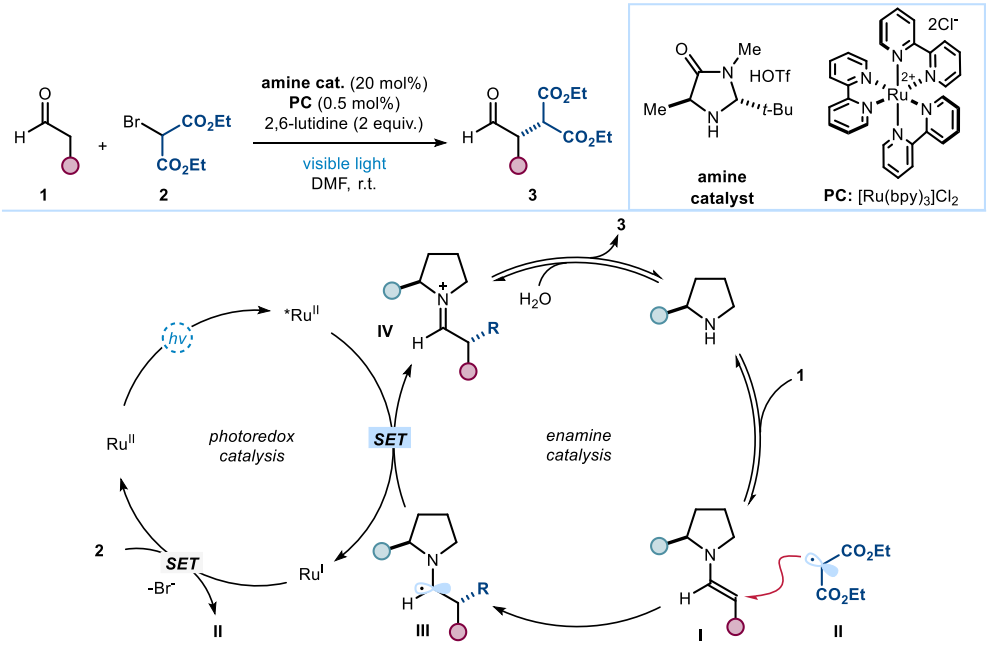

Figure 1.3. Merging photoredox and organocatalysis for the enantioselective α-alkylation of aldehydes. DMF: N, N-dimethylmethanamide.

While photoredox catalysis was transformative, it is not the only way to harness visible light. It is also possible to excite colored organic intermediates to trigger the formation of radicals. Specific non-covalent associations between electron-rich and electron-poor species may produce new visible-light-absorbing aggregates, known as electron donor–acceptor (EDA) complexes.[13] While the individual components are colorless, the EDA complex exhibits a red-shifted charge-transfer band, allowing visible-light excitation and radical generation. For example, our group discovered that mixing an enamine **I** with an electron-poor benzyl bromide **5** resulted in a color change of the solution from colorless to yellow (**Figure 1.4**).

[12] Shaw, M. H., Twilton, J., MacMillan, D. W. C. "Photoredox Catalysis in Organic Chemistry." *J. Org. Chem.* **2016**, *81*, 6898–6926.

[13] Crisenza, G. E. M.; Mazzarella, D.; Melchiorre, P. "Synthetic Methods Driven by the Photoactivity of Electron Donor–Acceptor Complexes." *J. Am. Chem. Soc.* **2020**, *142*, 5461–5476.

This observation was rationalized with the formation of an EDA complex between **I** and **5**.[14]

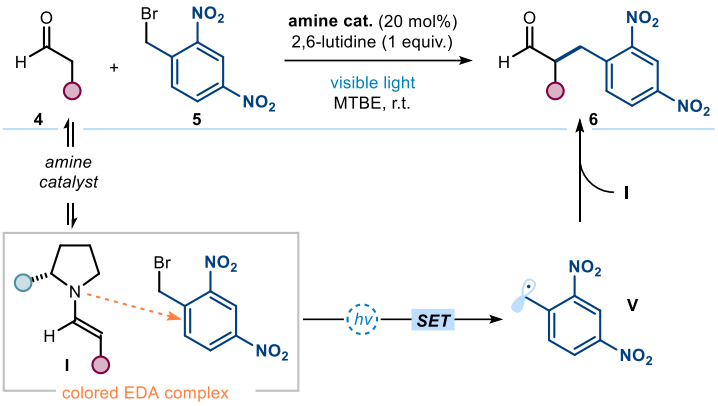

Figure 1.4. Photochemical stereoselective α-alkylation of aldehydes promoted by EDA complex formation. MTBE: 2-methoxy-2-methylpropane.

Upon irradiation with visible light, an intracomplex SET triggers the fragmentation of the bromide and formation of the benzyl radical **V**, which subsequently adds stereoselectively to the ground-state enamine **I** to ultimately afford α-benzyl aldehydes **6** with high enantioselectivity. This finding showed that organocatalysis can generate photoactive intermediates capable of accessing new reactivity under light activation.

Our laboratories later found that some organocatalytic intermediates directly absorb visible light without EDA complex formation, enabling excited-state reactivity upon direct excitation. For instance, enamine **I** can absorb near UV light (390 nm) to reach an electronically excited state (**Figure 1.5**). While enamines behave as nucleophiles in the ground state,[15] they act as strong SET reductants upon excitation.[16] This increased reducing power ($E^*(\mathbf{I}^{\bullet+}/\mathbf{I}^*)$ = -2.5 V vs Ag^+/Ag) was exploited to generate malonyl radicals **II** from bromomalonates **2**, substrates which would not engage in EDA complex formation with enamines. The ground-state nucleophilic chiral enamine **I** subsequently intercepted **II** in an enantioselective fashion to afford the α-amino intermediate **III**. This species then reduced another molecule of substrate **2** to sustain a radical chain mechanism. The resulting iminium ion **IV** was eventually hydrolyzed to product **3**, while releasing the aminocatalyst.

[14] Arceo, E.; Jurberg, I. D.; Álvarez-Fernández, A.; Melchiorre, P. "Photochemical Activity of a Key Donor-Acceptor Complex Can Drive Stereoselective Catalytic α-Alkylation of Aldehydes." *Nat. Chem.* **2013**, *5*, 750–756.

[15] Mukherjee, S., Yang, J. W., Hoffmann, S., List, B., "Asymmetric Enamine Catalysis." *Chem. Rev.* **2007**, *107*, 5471–5569.

[16] Silvi, M.; Arceo, E.; Jurberg, I. D.; Cassani, C.; Melchiorre, P. "Enantioselective Organocatalytic Alkylation of Aldehydes and Enals Driven by the Direct Photoexcitation of Enamines." *J. Am. Chem. Soc.* **2015**, *137*, 6120–6123.

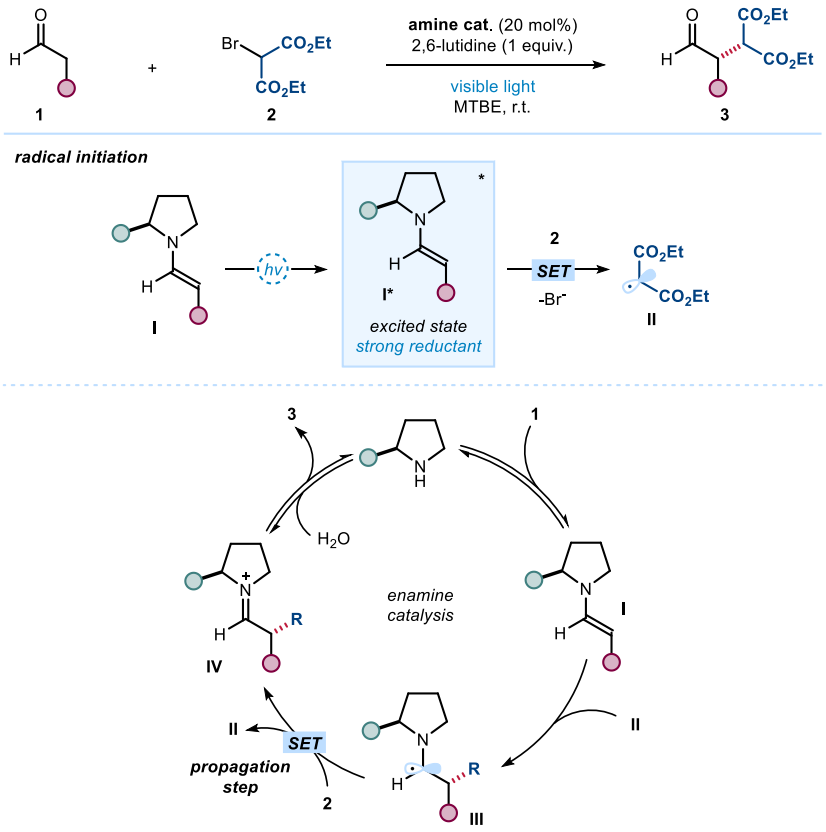

Figure 1.5. Direct photoexcitation of enamines **I** for the stereoselective α-alkylation of aldehydes.

This work highlighted how a well-established intermediate in ground-state polar chemistry could be repurposed using light to trigger new radical processes by employing its excited-state reactivity. [17]

Enamines (cornerstone intermediates of polar organocatalysis characterized by their nucleophilic reactivity) could be repurposed with photochemical activation to become strong SET reductants. By analogy, our group envisaged that electrophilic intermediates might act as SET oxidants in the excited state. The iminium ion[18] (the electrophilic counterpart of enamines in organocatalysis) also exhibits distinctive excited-state reactivity. We showed that electrophilic chiral iminium ions **VI** could absorb visible light to reach an electronically excited state (**Figure 1.6**).[19] These excited iminium ions **VI*** acted as strong oxidants (E^*(**VI***/**VIII**) = +2.40 V vs Ag^+/Ag) to generate radicals from organosilanes **8** through SET.

[17] Silvi, M., Melchiorre, P. "Enhancing the Potential of Enantioselective Organocatalysis with Light." *Nature* **2018**, *554*, 41–49.

[18] Erkkilä, A.; Majander, I.; Pihko, P. M.; "Iminium Catalysis." *Chem. Rev.* **2007**, *107*, 5416–5470.

[19] Silvi, M.; Verrier, C.; Rey, Y. P.; Buzzetti, L.; Melchiorre, P. "Visible-light excitation of iminium ions enables the enantioselective catalytic β-alkylation of enals." *Nat. Chem.* **2017**, *9*, 868–873.

The resulting benzylic and β-enaminyl radicals (**VII** and **VIII** respectively) coupled stereoselectively to eventually afford enantioenriched β-functionalized aldehydes **9**. This new reactivity enabled the enantioselective functionalization of enals **7** with non-nucleophilic partners **8**—reactivity inaccessible under conventional thermal conditions.

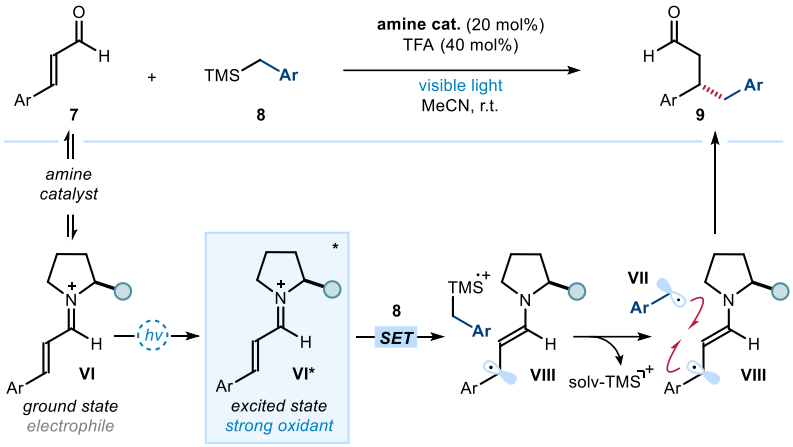

Figure 1.6. Photoexcitation of iminium ions for the enantioselective β-alkylation of enals. TMS: trimethylsilyl; TFA: 2,2,2-trifluoroacetic acid.

These examples illustrate the transformative power of photochemistry to convert simple molecules into reactive species with entirely new chemical behavior upon excitation, enabling the discovery of reactions inaccessible under thermal control. This concept forms the conceptual foundation of the research presented in this doctoral thesis, where excitation is deliberately used as a tool to redesign molecular reactivity.

The following section outlines the general objectives and specific goals that guided this work.

1.2 Chemical Properties of 4-Hydroxycoumarins

4-Hydroxycoumarins (4HCs) constitute one of the most important families of natural and synthetic organic compounds.[20] Beyond their biological relevance—as core motifs in anticoagulant drugs such as *warfarin*[21]—they are privileged scaffolds in synthetic chemistry owing to their well-defined acidity and nucleophilicity. Structurally, 4-hydroxycoumarin (also known as *4-hydroxy-2H-chromen-2-one*, *4-hydroxy-1-benzopyran-2-one*, or *2-hydroxychromen-4-one* in IUPAC nomenclature) possesses a lactone core with a conjugated carbonyl system and a hydroxyl group at the 4-position. The compound is acidic, readily deprotonated by mild bases to form a resonance-stabilized anion. This anionic species exhibits

[20] (a) Abdou, M. M.; El-Saeed, R. A.; Bondock, S. "Recent Advances in 4-Hydroxycoumarin Chemistry. Part 1: Synthesis and Reactions." *Arab. J. Chem.* **2019**, *12*, 88–121; (b) Lin, Y.; Shen, X.; Yuan, Q.; Yan, Y. "Microbial biosynthesis of the anticoagulant precursor 4-hydroxycoumarin." *Nat Commun.* **2013**, *4*, 2603.

[21] Melnikova, I. "The Anticoagulants Market." *Nat. Rev. Drug Discov.* **2009**, *8*, 353–353.

nucleophilic character primarily centered at the C3 carbon, enabling reactions such as Michael, Mannich, and Knoevenagel condensations.[22] The ionic pathway, however, typically leads to competing *O*-alkylation versus *C*-alkylation,[23] reflecting the ambident nature of the anion (**Figure 1.7**).

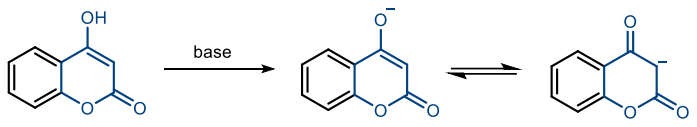

Figure 1.7. Deprotonation of 4-hydroxycoumarin and the resonance structures of the resulting nucleophilic anionic intermediate.

Despite their broad utility, such ground-state ionic transformations often lack regioselectivity and require strong bases or dehydrating agents. This limitation motivated us to explore how photoexcitation could be used to reprogram the intrinsic reactivity of 4-hydroxycoumarins — transforming a well-known nucleophile into a photoactive redox or energy-transfer agent capable of promoting new *radical-based* transformations under mild conditions.

1.3 General Objectives

Direct photoexcitation of organic molecules provides a powerful strategy to unlock new reactivity by temporarily altering their electronic structure. The research described in this doctoral thesis aimed to discover and develop new photochemical reactivity in natural product-derived scaffolds that are typically unreactive under conventional conditions. Specifically, the goal was to explore how 4-hydroxycoumarins—traditionally ground-state nucleophiles—could be transformed into photoactive scaffolds capable of engaging in both single-electron transfer and energy-transfer processes upon direct excitation. The combination of acid–base tunability, extended π-conjugation, and structural rigidity makes 4-hydroxycoumarins ideal candidates for photochemical activation. Their conjugated scaffold can support both charge-transfer and triplet-state manifolds, while the acidity of the 4-hydroxy group enables controlled generation of anionic species with distinct absorption and redox characteristics. These intrinsic features provided the rationale for this work: to determine whether 4-hydroxycoumarin derivatives could act not merely as reactive partners, but as functional chromophores—molecules whose excited states could be exploited to trigger new chemical reactivity.

---

[22] (a) Ramachary, D. B.; Kishor, M. "Direct Catalytic Asymmetric Synthesis of Highly Functionalized Tetronic Acids/Tetrahydro-Isobenzofuran-1,5-Diones via Combination of Cascade Three-Component Reductive Alkylations and Michael-Aldol Reactions." *Org. Biomol. Chem.* **2010**, *8*, 2859; (b) Yoda, J.; Djandé, A.; Cissé, L.; Abou, A.; Kaboré, L.; Saba, A. "Review on 4-Hydroxycoumarin Chemistry: Synthesis, Acylation and Photochemical Properties." *World Journal of Organic Chemistry*. **2019**, 7, 19-30.

[23] Cravotto, G.; Nano, G. M.; Palmisano, G. "4-Hydroxycoumarin and Related Systems: Sitoselectivity of the Mitsunobu Reaction with Prenyl Alcohols." *Heterocycles* **2003**, *60*, 1351–1358.

The overarching objective was thus to design and understand an organic platform capable of mastering both singlet and triplet excited-state reactivities, and to apply this understanding to the development of new radical and energy-transfer pathways for useful bond construction.

1.3.1 Radical Pathways for 2,4-Chromandione Synthesis via Photoexcitation of 4-Hydroxycoumarins

In Chapter II, we introduce a previously unrecognized radical mechanism for the synthesis of 2,4-chromandiones (**Figure 1.8**). Conventional methods for constructing these scaffolds rely on the ionic nucleophilic reactivity of the C3 position of 4-hydroxycoumarins, but often suffer from poor chemoselectivity, yielding mixtures of *O*- and *C*-alkylation products. Our strategy circumvents this limitation through a photochemical radical pathway, which enforces selective functionalization at the carbon center. Upon deprotonation and photoexcitation with violet light, 4-hydroxycoumarins are promoted to an anionic excited state capable of functioning as a strong photoreductant through an SET mechanism. This excited state can reduce alkyl or perfluoroalkyl halides to generate carbon radicals, which are then selectively captured at the C3 position of the coumarin core, yielding 3,3-disubstituted 2,4-chromandiones bearing a quaternary center.

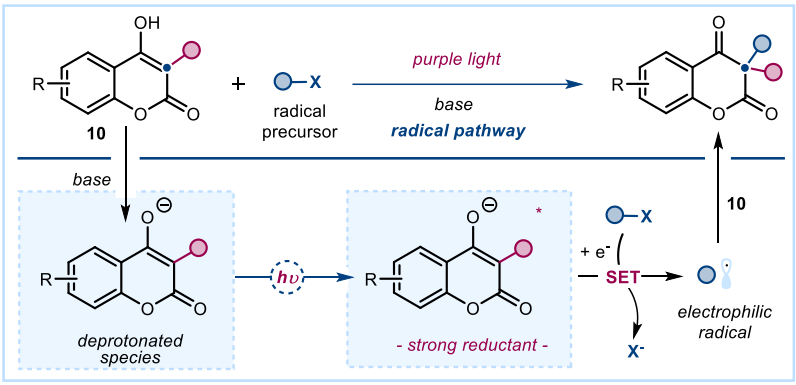

Figure 1.8. Radical pathway for the synthesis of 2,4-chromandiones via direct photoexcitation of deprotonated 4-hydroxycoumarins.

Comprehensive photophysical studies confirmed that the excited 4-hydroxycoumarin anion possesses a very negative excited-state reduction potential, validating its role as an efficient SET reductant for initiating radical transformations. This mechanistic switch—from ionic to radical—provides a milder, cleaner, and more selective route to valuable chromanone scaffolds.

1.3.2 A Bifunctional Organic Photocatalyst for Efficient Single-Electron and Energy-Transfer Activation

Building on the tunable photophysical properties of the excited 4-hydroxycoumarin core

established in Chapter II, these scaffolds offered an ideal platform for designing bifunctional photoactive systems. Their modular structure allows fine adjustment of absorption, redox potential, and triplet energy through minimal structural change. Guided by this idea, 3-thioaryl-4-hydroxycoumarins were developed as a new class of organic photocatalysts capable of mediating both single-electron transfer (SET) and energy-transfer (EnT) processes (**Figure 1.9**). Exploiting charge-transfer (CT) excited states with spatially separated HOMO and LUMO orbitals, these scaffolds overcome the usual trade-off between photoreduction strength and triplet energy, displaying $E^*_{red} = -3.08$ V vs. SCE and $E_T = 67$ kcal mol^{-1}. This balance grants access to complementary excited-state reactivities within a single, metal-free chromophore.

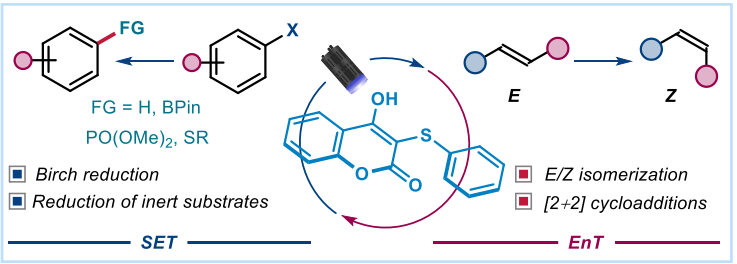

Figure 1.9. 3-Thioaryl-4-hydroxycoumarins as bifunctional organic photocatalysts combining SET and EnT reactivity through a stabilized charge-transfer excited state.

As a result, we have used these new bifunctional catalysts to:

- Activate relatively redox-inert substrates ($E^*_{red} < -2.8$ V vs. SCE) via SET reduction, forming radicals that participate in C–S, C–P, C–B, and C–C bond-forming reactions.
- Promote EnT-driven processes such as *E/Z* olefin isomerization and [2+2] photocycloadditions.

This discovery demonstrates that 3-thioaryl-4HCs unify two traditionally incompatible excited-state behaviors within one sustainable organic scaffold. Their cost-effectiveness and tunability make them a promising alternative to metal-based photocatalysts for dual photochemical activation.

In conclusion, this PhD work demonstrates that excited-state reactivity can be a practical synthetic tool. Through selective excitation of 4-hydroxycoumarins, we redefine how molecular structure governs their reactivity, enabling control over mechanism, selectivity, and outcome. The same scaffold can operate as a single-electron donor or triplet sensitizer, depending on its electronic state, providing a unified platform to access transformations beyond conventional ground-state chemistry. The following chapters detail how this principle was translated into general, operationally simple methods that harness light to trigger radical-based reactions.

Chapter II

Radical Pathways for 2,4-Chromandione Synthesis via Photoexcitation of 4-Hydroxycoumarins

Target

To develop a photochemical strategy for the synthesis of 3,3-disubstituted 2,4-chromandiones via a radical dearomatization of 4-hydroxycoumarins, enabling the incorporation of alkyl and perfluoroalkyl fragments to access valuable chromanone scaffolds featuring a quaternary stereocenter.

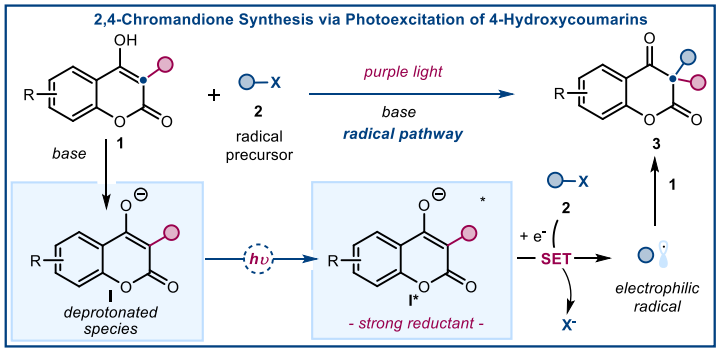

Tools

Upon deprotonation and excitation with 390 nm light, 3-substituted 4-hydroxycoumarins reach an excited state capable of single-electron transfer (SET) activation of alkyl or perfluoroalkyl halides, generating carbon-centered radicals that subsequently couple to the coumarin core.[1]

2.1 Introduction

4-Hydroxycoumarins (4HCs) have attracted considerable attention in medicinal chemistry due to their broad spectrum of biological activities and therapeutic potential.[2,3] Important

[1] The project discussed in this chapter has been conducted in collaboration with Dr. Sumitava Mallik and Enrico Sfreddo. I contributed to exploring the substrate scope of the reaction and conducted mechanistic investigations. This study has been published: Mallik, S.; Sfreddo, E.; Wang, H.; Melchiorre, P. "Radical pathways for 2,4-chromandione Synthesis via Photoexcitation of 4-hydroxycoumarins." *Chem. Sci.* **2025**, *16*, 124–129.

[2] Emami, S.; Dadashpour, S. "Current Developments of Coumarin-Based Anti-Cancer Agents in Medicinal Chemistry." *Eur. J. Med. Chem.* **2015**, *102*, 611–630.

[3] Li, X.; Huang, X.; Zhao, Y.; Zheng, Z.; Guo, M.; Chen, Z.; Chen, P.; Li, X.; Liao, J.; Jiang, M.; Cho, W.-J.; Cho, Y.-C.; Zeng, R.; Tang, Q.; Liang, G. "Design, Synthesis and Bioactivity Evaluation of 4-Hydroxycoumarin Derivatives as Potential Anti-Inflammatory Agents against Acute Lung Injury and Colitis." *Eur. J. Med. Chem.* **2024**, *272*, 116487.

applications of this scaffold are found in 3-alkylated 4-hydroxycoumarin derivatives, such as the approved drugs *warfarin*, *acenocoumarol*, and *phenprocoumon* (**Figure 2.1**), which are widely used as oral anticoagulants.[4]

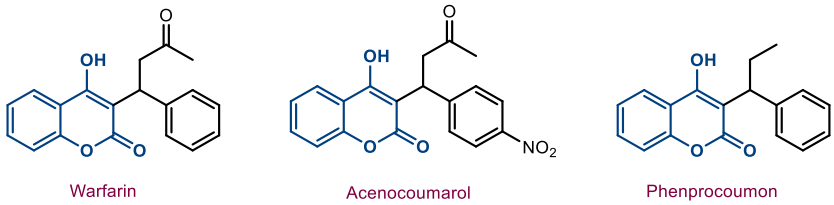

Figure 2.1. Approved anticoagulants containing the 4-hydroxycoumarin scaffold.

Beyond their biological relevance, 4-hydroxycoumarins are also reactive synthetic intermediates owing to their characteristic acidity at the 4-hydroxy position. Upon deprotonation, they form resonance-stabilized anionic species that exhibit pronounced nucleophilic behavior at the C3-position. This property has been widely exploited in classical coumarin chemistry. Consequently, numerous methods have been developed for the synthesis of 3-substituted 4-hydroxycoumarins, relying mainly on the ionic nucleophilic reactivity of the anion intermediate (**Figure 2.2**). These reactions typically involve electrophilic partners such as carbonyl compounds or activated halides, often under base or metal catalysis, to afford 3-alkylated or 3-arylated products.[5]

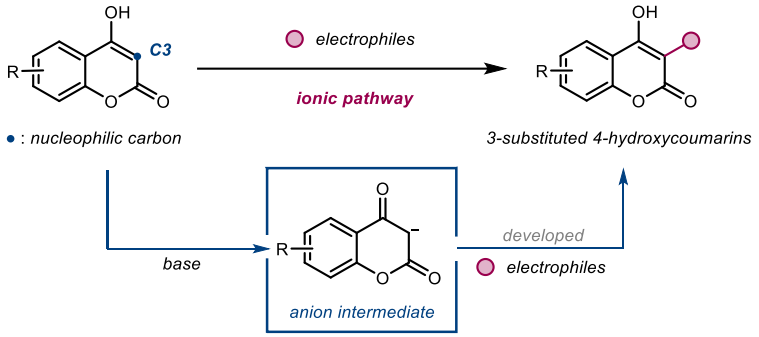

Figure 2.2. Typical reactivity of 4-hydroxycoumarins at C3 through nucleophilic reactivity.

In contrast, the direct synthesis of biologically relevant 3,3-disubstituted chromandiones through the functionalization of 3-substituted 4-hydroxycoumarins at their C3 has been much less investigated. In the following sections, I will first detail the intrinsic reactivity of 4-hydroxycoumarin derivatives and summarize the main strategies developed so far for their

---

[4] Melnikova, I. "The Anticoagulants Market." *Nat. Rev. Drug Discov.* **2009**, *8*, 353–353.

[5] Abdou, M. M.; El-Saeed, R. A.; Bondock, S. "Recent Advances in 4-Hydroxycoumarin Chemistry. Part 1: Synthesis and Reactions." *Arab. J. Chem.* **2019**, *12*, 88–121.

functionalization. Then, I will describe how we discovered a previously unknown *photoactivity of 4-hydroxycoumarins*, which allows access to a radical manifold. This photochemical pathway enables C–C bond formation via single-electron transfer processes, thus shifting their chemistry from traditional ionic reactivity to radical reactivity.

2.1.1 Chemical Properties of 4-Hydroxycoumarins

The 4-hydroxycoumarin scaffold represents the aromatic enol form of a six-membered β-keto lactone. As a result, it exists in equilibrium between three possible tautomeric forms (**Figure 2.3**): 4-hydroxy-2-chromenone (**1**), 2,4-chromandione (**1'**), and 2-hydroxy-4-chromenone (**1''**).

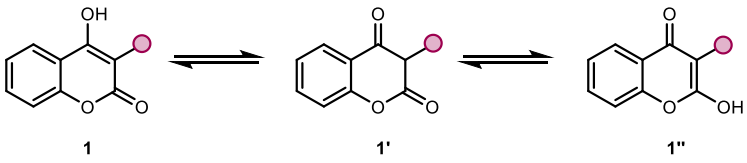

Figure 2.3. Tautomeric forms of 4-hydroxycoumarin.

The prototropic equilibria of these forms have been extensively investigated using spectroscopic, thermochemical, and computational methods. These studies indicate that the 4-hydroxy-2-chromenone form **1** is the most stable and predominant tautomer in both the solid state and solution.[6] The tautomeric structures of 4-hydroxycoumarin reveal a 1,3-dicarbonyl framework containing both electrophilic and nucleophilic centers (**Figure 2.4**). The C3 carbon is particularly nucleophilic and can undergo addition, condensation, halogenation, or cross-coupling reactions with electron-deficient substrates. In contrast, the hydroxyl oxygen atom is the preferred site for acylation and alkylation reactions. Generally, hard electrophiles react at the oxygen atom, whereas soft electrophiles favor substitution at the C3 carbon.[7]

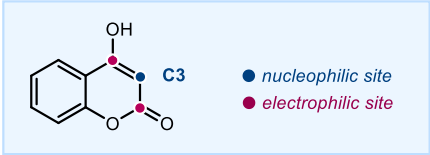

Figure 2.4. Nucleophilic and electrophilic sites of the 4-hydroxycoumarin scaffold.

Traditional methods for synthesizing 3-substituted 4-hydroxycoumarins mainly rely on

---

[6] Sousa, C. C. S.; Morais, V. M. F.; Matos, M. A. R. "Energetics of the Isomers: 3- and 4-Hydroxycoumarin." *J. Chem. Thermodyn.* **2010**, *42*, 1372–1378.

[7] Yoda, J.; Djandé, A.; Cissé, L.; Abou, A.; Kaboré, L.; Saba, A. "Review on 4-Hydroxycoumarin Chemistry: Synthesis, Acylation and Photochemical Properties." *World Journal of Organic Chemistry*, **2019**, *7*, 19-30.

classical ionic transformations such as Michael or Mannich additions, or Knoevenagel condensation followed by conjugate reduction (**Figure 2.5**). These strategies are well-established and remain among the most effective for introducing substituents at the C3-position of the coumarin core.[8]

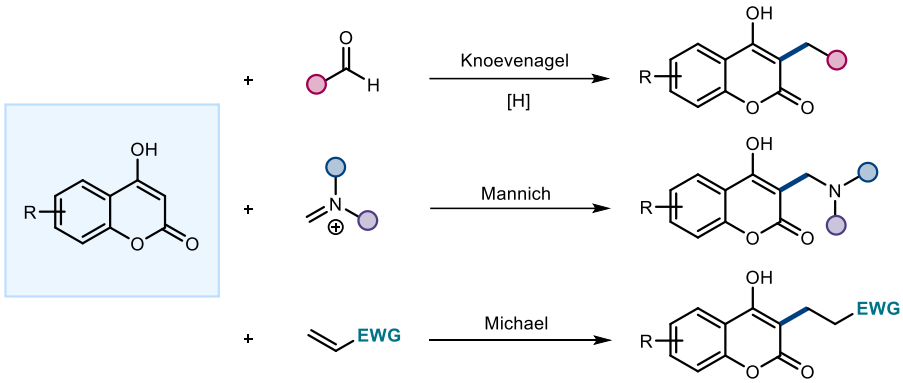

Figure 2.5. Representative strategies for C–C bond formation at the C3 position of 4HC. EWG: electron-withdrawing group.

An additional route to C3-functionalized derivatives involves Lewis acid-promoted alkylation. In this approach, allyl or benzyl alcohols act as alkylating agents in the presence of Lewis acids such as $FeCl_3$ or TMSOTf (**Figure 2.6**).[9,10] Coordination of the Lewis acid activates the alcohol, transforming the hydroxyl group into a better leaving group and enabling nucleophilic substitution by the 4HC anion. Under these conditions, the corresponding 3-alkylated products are obtained efficiently.

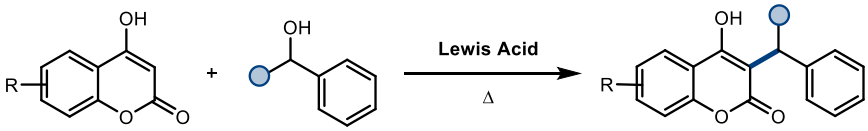

Figure 2.6. Lewis acid-promoted 3-alkylation of 4-hydroxycoumarins.

2.1.2 Synthesis of α-Disubstituted 2,4-Chromandiones

While the alkylation of 3-substituted 4-hydroxycoumarins could, in principle, provide a direct route to biologically relevant 3,3-disubstituted chromandiones, only a few methods have been

---

[8] Ramachary, D. B.; Kishor, M. "Direct Catalytic Asymmetric Synthesis of Highly Functionalized Tetronic Acids/Tetrahydro-Isobenzofuran-1,5-Diones via Combination of Cascade Three-Component Reductive Alkylations and Michael-Aldol Reactions." *Org. Biomol. Chem.* **2010**, *8*, 2859.

[9] Kischel, J.; Mertins, K.; Michalik, D.; Zapf, A.; Beller, M. "A General and Efficient Iron-Catalyzed Benzylation of 1,3-Dicarbonyl Compounds." *Adv. Synth. Catal.* **2007**, *349*, 865–870.

[10] Theerthagiri, P.; Lalitha, A. "Benzylation of β-Dicarbonyl Compounds and 4-Hydroxycoumarin Using TMSOTf Catalyst: A Simple, Mild, and Efficient Method." *Tetrahedron Lett.* **2010**, *51*, 5454–5458.

reported to achieve this transformation efficiently. Developing a versatile and straightforward approach to synthesize 3,3-disubstituted chromandiones would therefore be desirable, since this structural motif features a six-membered lactone ring with a quaternary carbon adjacent to the ester group — a synthetically and biologically significant framework.[11]

Two biologically active molecules that contain this framework are (−)-*herbertenolide*, a sesquiterpenoid known for its notable antifungal properties,[12] and *ammodoremin*, an epimeric mixture of prenylated chromandiones exhibiting in vivo haemorrhagic effects (**Figure 2.7**).[13]

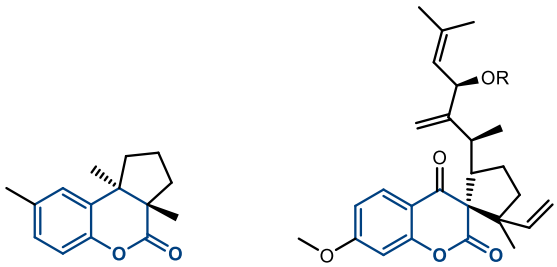

Figure 2.7. Biologically relevant 3,3-disubstituted chromandiones.

The few protocols available for the synthesis of substituted 2,4-chromandiones from 4-hydroxycoumarins generally involve direct C3-alkylation or Mitsunobu-type reactions, which typically provide the desired products only in low yields.[14,15] The main difficulty arises from poor regioselectivity, due to competing *O*-alkylation and *C*-alkylation pathways that lead to complex mixtures. For example, as shown in **Figure 2.8**, the Mitsunobu-type allylation of 4-hydroxycoumarin generates multiple products, including the *O*-alkylated compound **8**, the *C*,*O*-dialkylated derivative **9**, and two chromandione isomers (**10** and **11**), all in modest yields.

---

[11] Kelley, A. M.; Haywood, R. D.; White, J. C.; Petersen, K. S. "Enantioselective Desymmetrizations of Diesters to Synthesize Fully Substituted Chiral Centers of 3,4-Dihydrocoumarins." *ChemistrySelect.* **2020**, *5*, 3018–3022.

[12] Hu, J.; Ji, K.; Yan, L.; Yang, S.; Li, Y.; Wen, W.; Chen, L.; Wu, X.; Hu, Y.; Xie, W. A. "Concise Synthesis of Herbertenolide." *Org. Biomol. Chem.* **2022**, *20*, 2205–2208.

[13] Appendino, G.; Nano, G. M.; Viterbo, D.; De Munno, G.; Cisero, M.; Palmisano, G.; Aragno, M. "Ammodoremin, an Epimeric Mixture of Prenylated Chromandiones from Ammoniacum." *Helv. Chim. Acta* **1991**, *74*, 495–500.

[14] Garro Hugo, A.; Manzur Jimena, M.; Ciuffo Gladys, M.; Tonn Carlos, E.; Pungitore Carlos, R. "Inhibition of Reverse Transcriptase and Taq DNA Polymerase by Compounds Possessing the Coumarin Framework." *Bioorg. Med. Chem. Lett.* **2014**, *24*, 760–764.

[15] Cravotto, G.; Nano, G. M.; Palmisano, G. "4-Hydroxycoumarin and Related Systems: Sitoselectivity of the Mitsunobu Reaction with Prenyl Alcohols." *Heterocycles* **2003**, *60*, 1351 – 1358.

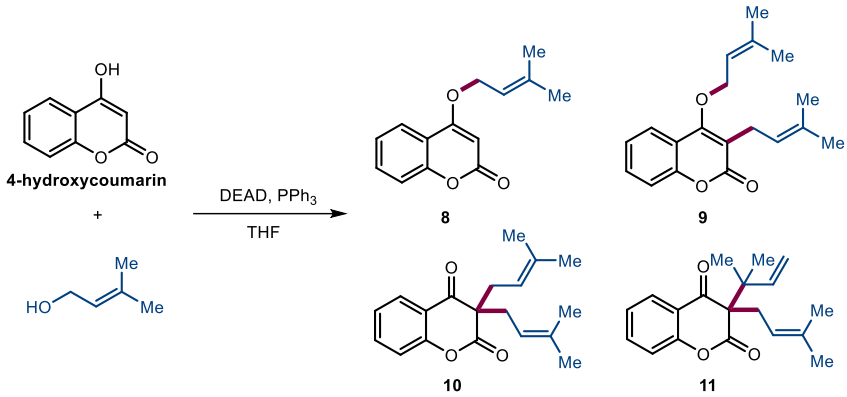

Figure 2.8. Selectivity issues in the Mitsunobu-type allylation of 4HC derivatives. DEAD: diethyl azodicarboxylate. THF: tetrahydrofuran.

Transition-metal-catalyzed routes have also been explored as alternative strategies to obtain 2,4-chromandiones bearing a quaternary α-carbon (**Figure 2.9**). In one example, the zinc enolate of 4-hydroxycoumarin **12** reacted with benzyl bromide in the presence of $Ni(PPh_3)_2Cl_2$ (2 mol%) to afford the dibenzylated keto lactone **13**, albeit in low yield (**Figure 2.9a**).[16] Manganese(III) acetate [$Mn(OAc)_3$] was also used to functionalize 3-substituted 4-hydroxycoumarins, yielding compound **15** (**Figure 2.9b**),[17] though only a single example was reported.

[16] Shin, U. S.; Joo, S.; Kim, S. "Zinc Enolate/Sulfinate Prepared from a Single-Run Reaction Using Zinc Dust with *O* -Tosylated 4-Hydroxy Coumarin and Pyrone." *Bull. Korean Chem. Soc.* **2016**, *37*, 1144–1147.

[17] Asahi, K.; Nishino, H. "Selective Synthesis of Trioxapropellanes Using Manganese(III) Acetate." *Heterocycl. Commun.* **2008**, *14*, 1–2.

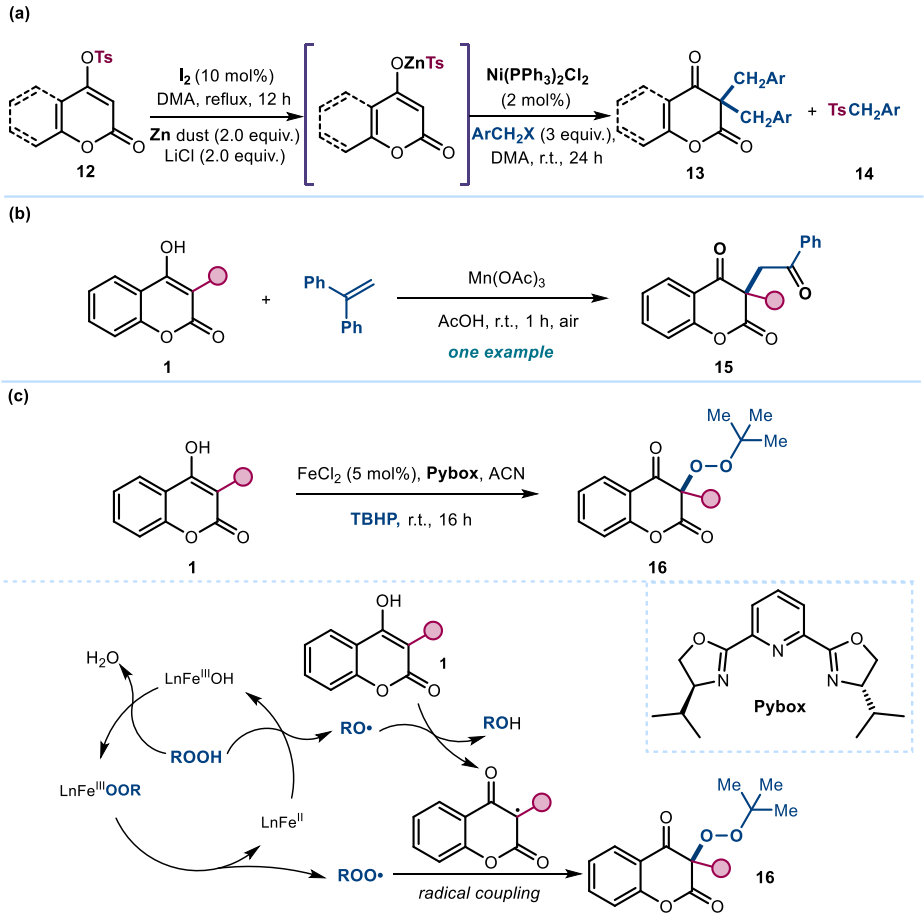

Figure 2.9. Selected metal-based methods for the synthesis of 2,4-chromandiones with an α-quaternary carbon. (**a**) Benzylation of 4HC zinc enolate. (**b**) Mn catalyzed the alkylation of 3-substituted 4HC. (**c**) Iron-catalyzed C-H peroxydation of 4-hydroxycoumarins. DMA: dimethylacetamide. ACN: acetonitrile.

More recently, a radical-based method was described to introduce a peroxide moiety at the C3 position (**Figure 2.9c**). This process involves the generation of an electrophilic peroxy radical that adds to electron-rich 4-hydroxycoumarins, furnishing the corresponding chromandione **16** containing a stereogenic center at C3 position.[18]

Despite these efforts, no general methodology currently exists for the preparation of 3,3-disubstituted chromandiones. Developing such a process would not only expand the synthetic scope of 4-hydroxycoumarins but also enable the conversion of an aromatic sp^2 carbon into a quaternary sp^3 center, thereby increasing molecular three-dimensionality — a valuable feature

[18] Chaudhari, M. B.; Moorthy, S.; Patil, S.; Bisht, G. S.; Mohamed, H.; Basu, S; Gnanaprakasam, B. "Iron-Catalyzed Batch/Continuous Flow C-H Functionalization Module for the Synthesis of Anticancer Peroxides." *J. Org. Chem.* **2018**, *83*, 1358-1368.

in drug design and synthesis.[19]

The intrinsic ionic reactivity of 4-hydroxycoumarins, while well established, inherently limits access to such transformations. We reasoned that when conventional two-electron (ionic) pathways reach their limits, *radical-based strategies* can offer a complementary solution. Radicals, with their unique reactivity and ability to access high-energy intermediates, enable reactions that are often beyond the reach of polar chemistry.[20] In recent years, visible-light-driven photocatalysis has emerged as a powerful and sustainable tool for generating radicals under mild conditions. In the next section, we will discuss the key developments in visible-light-induced radical reactions, which have inspired our own approach toward functionalizing 4-hydroxycoumarins.[21]

2.1.3 Photochemical Activation of Nucleophiles

In visible-light-mediated photocatalysis, several strategies have been developed to overcome the intrinsic limitations of ground-state reactivity. Some approaches rely on photoredox catalysts to mediate single-electron transfer (SET) events,[22] while others exploit the direct excitation of substrates. Our research laboratories have recently identified a photochemical method to functionalize electron-rich compounds without the use of external photoredox catalysts.[23] This process is based on the interaction between an electron-acceptor substrate (A) and a donor molecule (D) to form an electron donor-acceptor (EDA) complex.[24] Although the individual components cannot absorb visible light, the resulting complex does. Upon light irradiation, a SET occurs, generating radical intermediates under mild conditions. One early limitation of this approach was back electron transfer (BET), which regenerates the ground-state EDA complex. This issue can be overcome by introducing a suitable leaving group (LG) into the radical anion, enabling irreversible fragmentation and the formation of reactive radicals that can undergo productive bond-forming reactions (**Figure 2.10**).

---

[19] Lovering, F.; Bikker, J.; Humblet, C. "Escape from Flatland: Increasing Saturation as an Approach to Improving Clinical Success." *J. Med. Chem.* **2009**, *52*, 6752–6756.

[20] Smith, J. M.; Harwood, S. J.; Baran, P. S. "Radical Retrosynthesis." *Acc. Chem. Res.* **2018**, *51*, 1807–1817.

[21] (a) Melchiorre, P. "Introduction: Photochemical Catalytic Processes." *Chem. Rev.* **2022**, *122*, 1483–1484; (b) Albini, A.; Fagnoni, M. "Green Chemistry and Photochemistry Were Born at the Same Time." *Green Chem.* **2004**, *6*, 1; (c) Silvi, M.; Melchiorre, P. "Enhancing the Potential of Enantioselective Organocatalysis with Light." *Nature* **2018**, *554*, 41–49.

[22] Romero, N. A.; Nicewicz, D. A. "Organic Photoredox Catalysis." *Chem. Rev.* **2016**, *116*, 10075–10166.

[23] Crisenza, G. E. M.; Mazzarella, D.; Melchiorre, P. "Synthetic Methods Driven by the Photoactivity of Electron Donor–Acceptor Complexes." *J. Am. Chem. Soc.* **2020**, *142*, 5461–5476.

[24] (a) Mulliken, R. S. "Molecular Compounds and Their Spectra. III. The Interaction of Electron Donors and Acceptors." *J. Phys. Chem.* **1952**, *56*, 801–822; (b) RosokhaJay, S. V.; Kochi, K. "Fresh Look at Electron-Transfer Mechanisms via the Donor/Acceptor Bindings in the Critical Encounter Complex." *Acc. Chem. Res.* **2008**, *41*, 641–653.

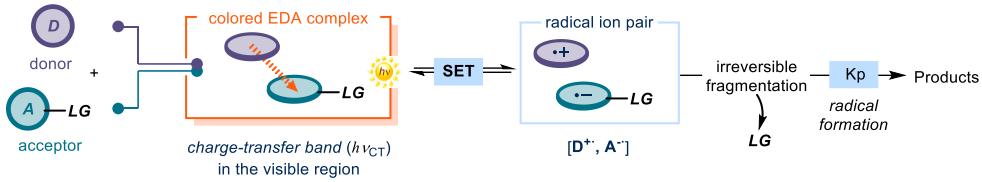

Figure 2.10. Productive strategy to make an EDA complex synthetically relevant. *Kp* is a kinetic constant.

Our group has employed EDA complex photochemistry to activate electron-rich intermediates that are nucleophilic in the ground state, enabling *radical* transformations that are otherwise inaccessible under dark conditions. For instance, chiral enamines can serve as effective electron donors for the formation of EDA complexes with an electron-deficient partner.[25] We also found that perfluoroalkyl iodides (R_F-I, where R_F is a perfluoroalkyl fragment) can serve as suitable electron-poor entities for EDA complex activation. These electron-deficient substrates efficiently interact with electron-rich compounds to form perfluoroalkyl radicals (R_F·) upon visible-light irradiation.[26]

Building on this platform, we developed strategies for the perfluoroalkylation of aromatic and carbonyl compounds through in situ generation of electron-rich species capable of forming EDA complexes with perfluoroalkyl iodides. This approach allowed the functionalization of nucleophiles such as enamines, α-cyanoesters, and β-keto esters.[27] For instance, a key study demonstrated the photochemical organocatalytic enantioselective perfluoroalkylation of β-ketoesters promoted by a chiral phase-transfer cinchona catalyst (**Figure 2.11**).[27c] In this process, chiral enolate **V**, generated by Cs_2CO_3 deprotonation of β-ketoester **17**, forms a photoactive EDA complex with perfluoroalkyl iodides (R_F-I) **2**. The formation of this complex was established through UV-Vis spectroscopic studies. Upon visible-light excitation, the EDA complex undergoes single-electron transfer, cleaving the C–I bond in **2** to generate a perfluoroalkyl radical **VI**. This radical is stereoselectively captured by the chiral enolate, forming a ketyl radical intermediate **VII** that propagates the chain through halogen-atom transfer (XAT).[28] The resulting intermediate **VIII** readily collapses to give the chiral product **18**. The halogen-atom abstraction by the ketyl radical corresponds to a propagation step within

---

[25] Arceo, E.; Jurberg, I. D.; Álvarez-Fernández, A.; Melchiorre, P. "Photochemical Activity of a Key Donor–Acceptor Complex Can Drive Stereoselective Catalytic α-Alkylation of Aldehydes." *Nat. Chem.* **2013**, *5*, 750–756.

[26] (a) Cantacuzene, D.; Wakeselman, C.; Dorme, R. "Condensation of Perfluoroalkyl Iodides with Unsaturated Nitrogen Compounds." *J. Chem. Soc. Perkin Trans. 1* **1977**, 1365-1371; (b) Postigo, A. "Electron Donor-Acceptor Complexes in Perfluoroalkylation Reactions." *Eur. J. Org. Chem.* **2018**, *2018*, 6391–6404.

[27] (a) Balletti, M.; Wachsmuth, T.; Di Sabato, A.; Hartley, W. C.; Melchiorre, P. "Enantioselective Catalytic Remote Perfluoroalkylation of α-Branched Enals Driven by Light." *Chem. Sci.* **2023**, *14*, 4923–4927; (b) Nappi, M.; Bergonzini, G.; Melchiorre, P. "Metal-Free Photochemical Aromatic Perfluoroalkylation of α-Cyano Arylacetates." *Angew. Chem. Int. Ed.* **2014**, *53*, 4921–4925; (c) Wozniak, L.; Murphy, J. J.; Melchiorre, P. "Photo-organocatalytic Enantioselective Perfluoroalkylation of β-Ketoesters." *J. Am. Chem. Soc.* **2015**, *137*, 5678–5681.

[28] Juliá, F.; Constantin, T.; Leonori, D. "Applications of Halogen-Atom Transfer (XAT) for the Generation of Carbon Radicals in Synthetic Photochemistry and Photocatalysis." *Chem. Rev.* **2022**, *122*, 2292–2352.

an atom transfer radical addition (ATRA) sequence, [29] initiated by EDA complex photoexcitation. The measured quantum yield ($\Phi = 1.2$) supports a chain-propagated radical mechanism being operative.[30]

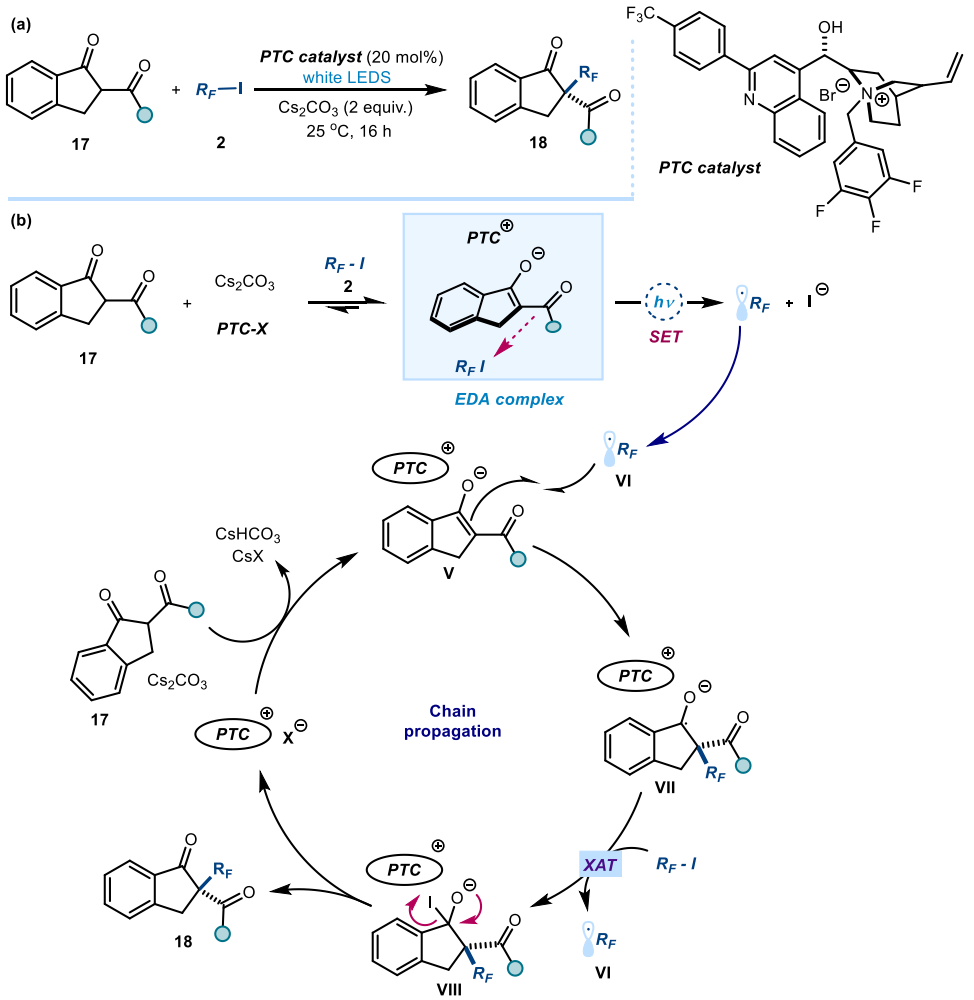

Figure 2.11. (**a**) Enantioselective perfluoroalkylation of β-ketoesters via EDA complex photoexcitation. (**b**) Proposed mechanism: initiation, triggered by the photoactivity of the EDA complex, and radical chain propagation; X = I, Br.

Our research team also found that, in some cases, even without EDA complex formation, reactions between electron-rich substrates and electron-poor reagents (including

---

[29] Stephenson, C.; Yoon, T.; MacMillan, D. W. C. "Visible Light Photocatalysis in Organic Chemistry," 1st ed.; Wiley, **2018**.

[30] (a) Cismesia, M. A.; Yoon, T. P. "Characterizing Chain Processes in Visible Light Photoredox Catalysis." *Chem. Sci.* **2015**, *6*, 5426–5434; (b) Buzzetti, L.; Crisenza, G. E. M.; Melchiorre, P. "Mechanistic Studies in Photocatalysis." *Angew. Chem. Int. Ed.* **2019**, *58*, 3730–3747.

perfluoroalkyl iodides) can still proceed. This occurs when the electron-rich substrate itself absorbs visible light, reaching an excited state with enhanced reducing power, capable of transferring an electron to the perfluoroalkyl halide to generate the corresponding radical. A representative example is the photochemical perfluoroalkylation of phenols developed by our group in 2015 (**Figure 2.12**).[31] This reaction proceeds without any external photoredox catalyst or ground-state EDA complex formation. Instead, the phenolate anion **IX**, formed upon deprotonation of phenol **19**, absorbs light directly and reaches an excited state that triggers single-electron transfer to R_FI. The resulting electron-deficient perfluoroalkyl radicals **VI** add to ground-state phenolate **IX**, forming a cyclohexadienyl radical **X**. Subsequent SET reduction of R_FI from **X** regenerates the perfluoroalkyl radical **VI** and forms intermediate **XI**, which, upon deprotonation, yields the final product **20** (upon acidic work-up).

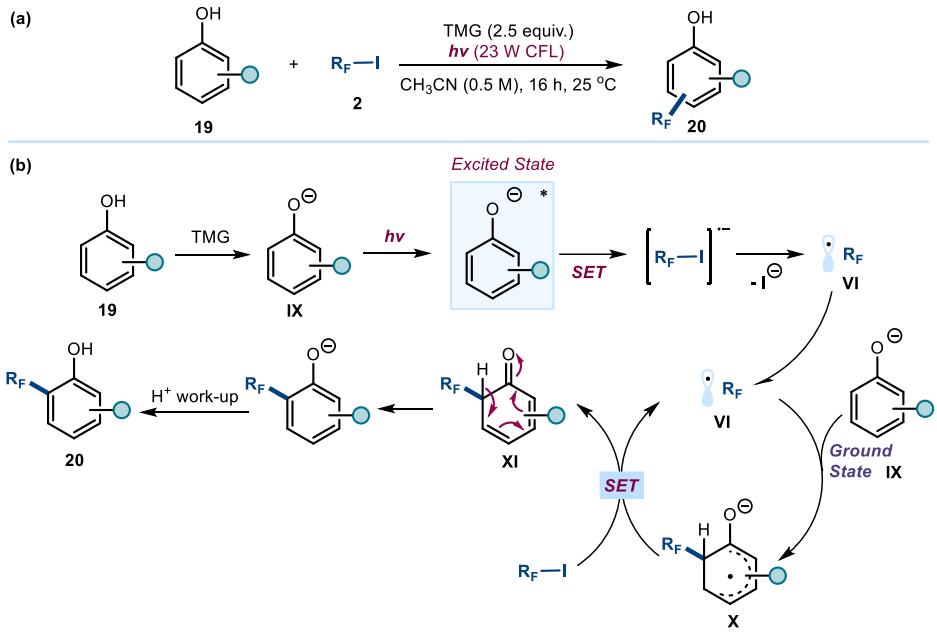

Figure 2.12. (**a**) Photochemical perfluoroalkylation of phenols. (**b**) Proposed mechanism. TMG = 1,1,3,3-tetramethylguanidine

These studies demonstrated how simple light excitation can turn simple nucleophilic substrates into strong SET reductants, suitable for initiating radical processes.

2.2 Design and Target of the Project

Our study aimed to develop a mild and metal-free protocol for 2,4-chromandione synthesis

[31] Filippini, G.; Nappi, M.; Melchiorre, P. "Photochemical Direct Perfluoroalkylation of Phenols." *Tetrahedron*, **2015**, *71*, 4535–4542.

using readily available 4-hydroxycoumarins and perfluoroalkyl iodides. The direct excitation of electron-rich substrates or their activation through EDA complexes under visible light are powerful strategies for initiating radical processes. Building on our previous experience, we sought to identify new electron-rich partners to expand this photochemical platform. As highlighted in **sections 2.1.1** and **2.2.2**, 4-hydroxycoumarin derivatives are highly nucleophilic at the C3 position. Given this inherent nucleophilicity, we surmised that they could fit within our photochemical reactivity platform. Moreover, 4-hydroxycoumarin derivatives are known for their absorption in the visible region and unique photophysical properties, including high non-radiative fluorescence,[32] making them potential candidates for visible-light activation. However, their excited-state reactivity in SET-based radical processes has remained completely unexplored.

We hypothesized that, under basic conditions, the deprotonated 3-substituted-4-hydroxycoumarin anion **I** could participate in visible-light-driven reactivity to directly form 3,3-disubstituted chromandiones **3** via a radical dearomatization mechanism (**Figure 2.13**).

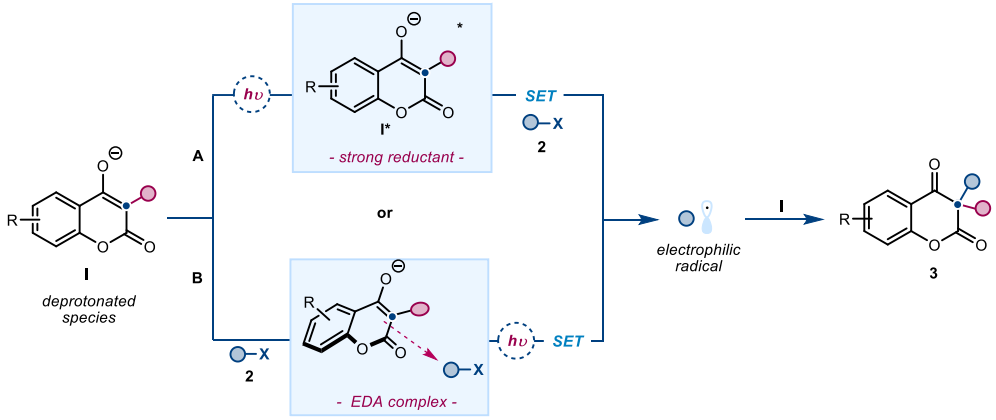

Figure 2.13. Our design plan for 2,4-chromadione synthesis: Path A: direct excitation of the deprotonated species as a strong reductant; Path B: formation of an EDA complex with perfluoroalkyl iodides.

In our design plan, deprotonation of the substrate generates an anion (**I**) that either (a) reaches an excited-state reductant (**I***) upon direct excitation (*Path A*), or (b) forms a photoactive EDA complex upon aggregation with the perfluoroalkyl iodide in the ground state (*Path B*). In both cases, reduction of the electron-deficient perfluoroalkyl iodide **2** produces a perfluoroalkyl radical, which can be captured by ground-state **I**, ultimately affording product **3** (**Figure 2.13**). Traditional ionic alkylation methods to decorate 4-hydroxycoumarins often suffer from poor

[32] (a) Bečić, E.; Šober, M.; Imamović, B.; Završnik, D.; Špirtović-Halilović, S. "UV/VIS Absorption and Fluorescence Spectroscopic Study of Some 3-substituted Derivatives of 4-hydroxycoumarin." *Pigment Resin Technol.* **2011**, *40*, 292–297; (b) Yoda, J.; Djandé, A.; Cissé, L.; Abou, A.; Kaboré, L.; Saba, A. "Review on 4-Hydroxycoumarin Chemistry: Synthesis, Acylation and Photochemical Properties." *World Journal of Organic Chemistry*. **2019**, *7*, 19-30.

regioselectivity, producing mixtures of *O*- and *C*-alkylated products. By employing a radical mechanism, we aim to achieve selective C3-functionalization, enabling access to 3,3-disubstituted chromandiones with enhanced efficiency.

Overall, this study seeks to uncover the photochemical reactivity of 4-hydroxycoumarins and establish them as versatile scaffolds for visible-light-mediated radical transformations.

2.3 Results and Discussion

2.3.1 Optimization of the Reaction Conditions

At the outset of our studies, we investigated the feasibility of our design plan by using 3-benzyl-4-hydroxycoumarin **1a** and perfluorohexyl iodide **2a** as the radical precursor (**Table 2.1**). The experiment was performed in acetonitrile (CH_3CN) as the solvent under irradiation by a purple Kessil lamp (λmax = 390 nm) at 20 °C in an inert atmosphere (nitrogen). The reactions, conducted using Cs_2CO_3 to facilitate the generation of the photoactive deprotonated intermediate, afforded the desired perfluoroalkylated 2,4-chromandione product **3a** in 82% yield (**Table 2.1**, entry 1). The control experiment established that light, base, and inert atmosphere were essential for product formation (entries 2-3). Extending the irradiation wavelength to 427–456 nm rendered the process inactive, highlighting the need for higher-energy light to drive the transformation.

Table 2.1. Optimization studies.[a]

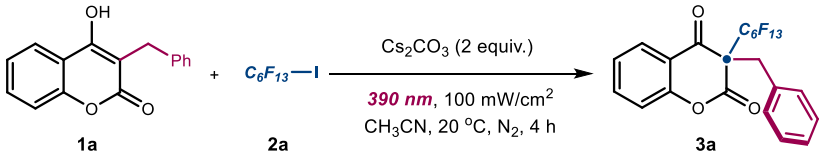

entry	deviation	[%] yield **3a**[b]
1	none	82
2	no light, no base	0
3	aerobic condition instead of N_2	0
4	427 nm, 440 nm, or 456 nm	0
5	DMSO, DMF instead of CH_3CN	<15
6	DCM instead of CH_3CN	5
7	DCE instead of CH_3CN	30
8	Na_2CO_3 instead of Cs_2CO_3	56
9	TMG instead of Cs_2CO_3	78
10	1.2 equiv. Cs_2CO_3 instead of 2 equiv.	37
11	1 equiv. 2a instead of 3 equiv.	15
12	2 equiv. 2a instead of 3 equiv.	40

[a] Reactions performed over 4 hours in 1 mL of CH_3CN using 0.15 mmol of **1a**, 0.45 mmol of **2a**, and base (2 equiv.) under irradiation by a Kessil lamp (λ_{max} = 390 nm, irradiance = 100 mW/cm^2). [b] Yield of **3a** determined by ^{1}H NMR analysis of the crude mixture using dibromomethane as the internal standard. DMSO: dimethyl sulfoxide; DMF: N, N-dimethylformamide. DCM: dichloromethane; DCE: 1,2-dichloroethane.

Using polar aprotic solvents, such as DMSO or DMF, resulted in a marked decrease in

reactivity, while less polar solvents, like DCM and DCE, also performed poorly (entries 5–7). When other bases, such as Na_2CO_3 or TMG, were tested, the reaction yield dropped to moderate levels (entries 8-9). Moreover, reducing the amount of base (1.2 equiv. of Cs_2CO_3 instead of 2) resulted in a significant decrease in yield to 37% (entry 10). Varying the equivalents of substrate **2a** also affected the outcome, affording the target product **3a** in 15% and 40% yield, respectively (entries 11 and 12).

2.3.2 Preliminary Mechanistic Studies

We then performed investigations to gain mechanistic insights. As shown in **Figure 2.14**, UV-visible spectroscopic analysis of 4-hydroxycoumarin **1a** indicated an absence of absorption in the visible region. The UV-Vis spectrum of **Ia** (the deprotonated form of **1a** formed in-situ in the presence of Cs_2CO_3) exhibited a significant bathochromic shift into the visible region compared to the neutral form **1a**, indicating that the deprotonated intermediate **Ia** acted as the chromophore in the photochemical process (red line). Upon addition of perfluorohexyl iodide **2a** to **Ia**, no significant spectral changes were observed, ruling out the formation of ground-state aggregates (i.e., no evidence of EDA complex formation was detected; see blue line).

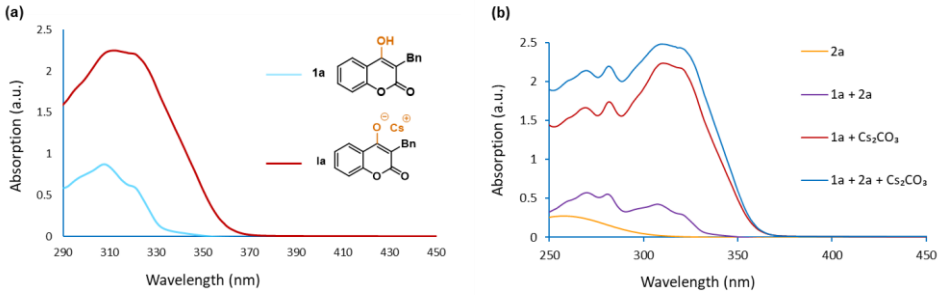

Figure 2.14. (**a**) Absorption spectra of neutral **1a** and deprotonated species **1a**. (**b**) Overlap of absorption spectra recorded for **1a**, and its deprotonated form (in situ generated from **1a** upon addition of Cs_2CO_3), and their mixture with perfluorohexyl iodide **2a** in CH_3CN ($1 \cdot 10^{-4}$ M).

Our attention then turned to the photophysical properties of the deprotonated hydroxycoumarin **Ia**, which was identified as the sole species absorbing at 390 nm, the wavelength used for irradiation in this study. Upon laser irradiation at 314 nm of a CH_3CN solution of **Ia** (in situ-generated by mixing **1a** with Cs_2CO_3), emission with a maximum at 407 nm was detected, confirming that **Ia** could reach an electronically excited state (Figure 2.15). The 0-0 transition energy ($E_{0,0}$) was determined to be 3.43 eV from the cross-section, located at 361 nm of the normalized UV-visible absorption and emission spectra (**Figure 2.15**).

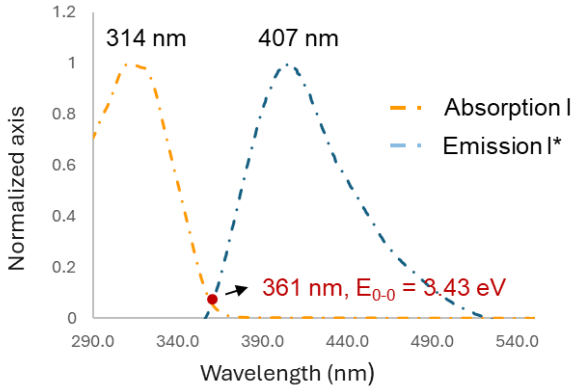

Figure 2.15. Emission of the excited deprotonated intermediate **Ia*** in CH_3CN (in situ generated mixing **Ia** with Cs_2CO_3) upon laser irradiation at 314 nm and its intercept at 361 nm with the absorption spectrum, with a 0–0 transition energy.

Next, cyclic voltammetry analysis of **Ia** revealed an irreversible oxidation peak at +0.66 V vs Ag/AgCl in CH_3CN. Applying the Rehm-Weller formalism,[33] the redox potential of excited **Ia** (E(**Ia**•/**Ia***)) was estimated to be -2.77 V vs SCE, confirming its strong reducing power upon excitation. Stern-Volmer quenching studies (**Figure 2.16**) showed that the fluorescence of excited **Ia**, induced by a laser at 310 nm, was effectively quenched by perfluorohexyl iodide **2a**. This supported the ability of excited **Ia** to activate **2a** via an SET mechanism.

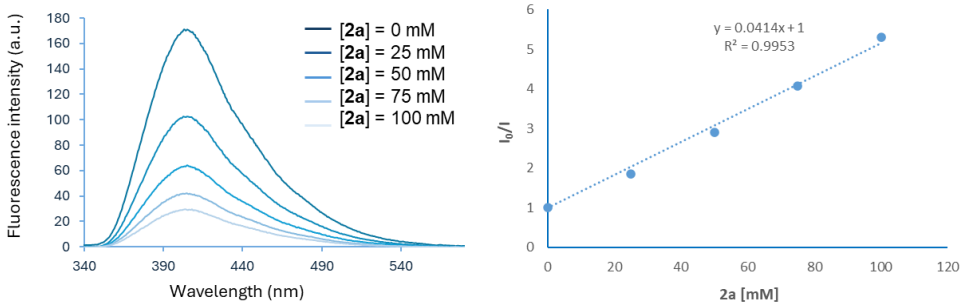

Figure 2.16. Stern−Volmer quenching studies of intermediate **Ia** ($1 \cdot 10^{-4}$ M in CH_3CN) with increasing amounts of perfluorohexyl iodide **2a** (excitation at 350 nm; emission was acquired from 360 nm to 440 nm).

Finally, the excited singlet-state lifetime of **Ia*** was measured as 5.1 ns by means of single photon counting technique, further confirming its potential for productive excited-state reactivity (**Figure 2.17**).

[33] Farid, S.; Dinnocenzo, J. P.; Merkel, P. B.; Young, R. H.; Shukla, D.; Guirado, G. "Reexamination of the Rehm–Weller Data Set Reveals Electron Transfer Quenching That Follows a Sandros–Boltzmann Dependence on Free Energy." *J. Am. Chem. Soc.* **2011**, *133*, 11580-11587.

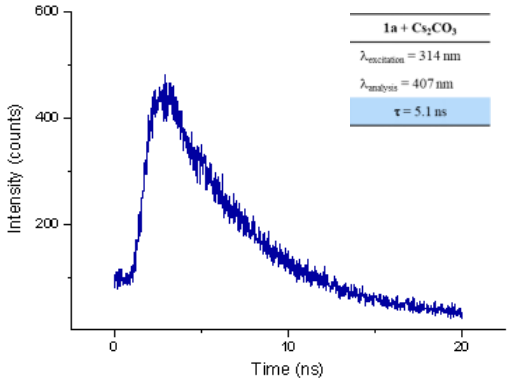

Figure 2.17. Time-resolved emission decay (excitation at 314 nm, analysis at 407 nm) of deprotonated **1a** (formed in situ in the presence of Cs_2CO_3 ($1 \cdot 10^{-4}$ M) in CH_3CN solution measured by TC-SPC (τ = 5.1 ns, from deconvolution and single-exponential fitting, X^2= 1.047).

2.3.3 Generality of the Photochemical Protocol

We then examined the scope of this photochemical strategy for the synthesis of 2,4-chromadione by using the optimal conditions reported in entry 1 of **Table 2.1**. Initially, we demonstrated that the process remained efficient on a preparative scale (5 mmol), affording 1.1 g of product **3a** in 50% yield. Then, the reactivity of substituted 3-benzyl-4-hydroxycoumarins **1** was explored. Our catalytic system can tolerate a series of substituents on the aromatic ring of the benzyl part (**Figure 2.18a**). Different electron-donating groups, such as methoxy and methyl, can work well affording products **3b-c** with a good yield of 75% and 58%, respectively. 4-Chloro substituent on the benzyl ring can afford the desired product **3d** in 65% yield, while a pyridyl group was also tolerated well, leading to product **3e** in high yield. Notably, aliphatic substituents at the 3-position of substrate **1** retained a productive photoreactivity, giving **3f** (68% yield) and **3g** (88% yield). However, introducing an aromatic substituent at the 3-position of **1** led to a complex reaction mixture, with only trace amounts of the desired 2,4-chromandione detected (see grey inset in the figure). A benzyl nitro substituent at the same position also proved poorly reactive, affording the product in only 15% yield. In contrast, modifying the electronic nature of the coumarin ring was well tolerated: both electron-withdrawing and electron-donating substituents on the aromatic ring of **1** furnished the corresponding perfluoroalkylated 2,4-chromandiones (**3h** and **3i**) in high yields.

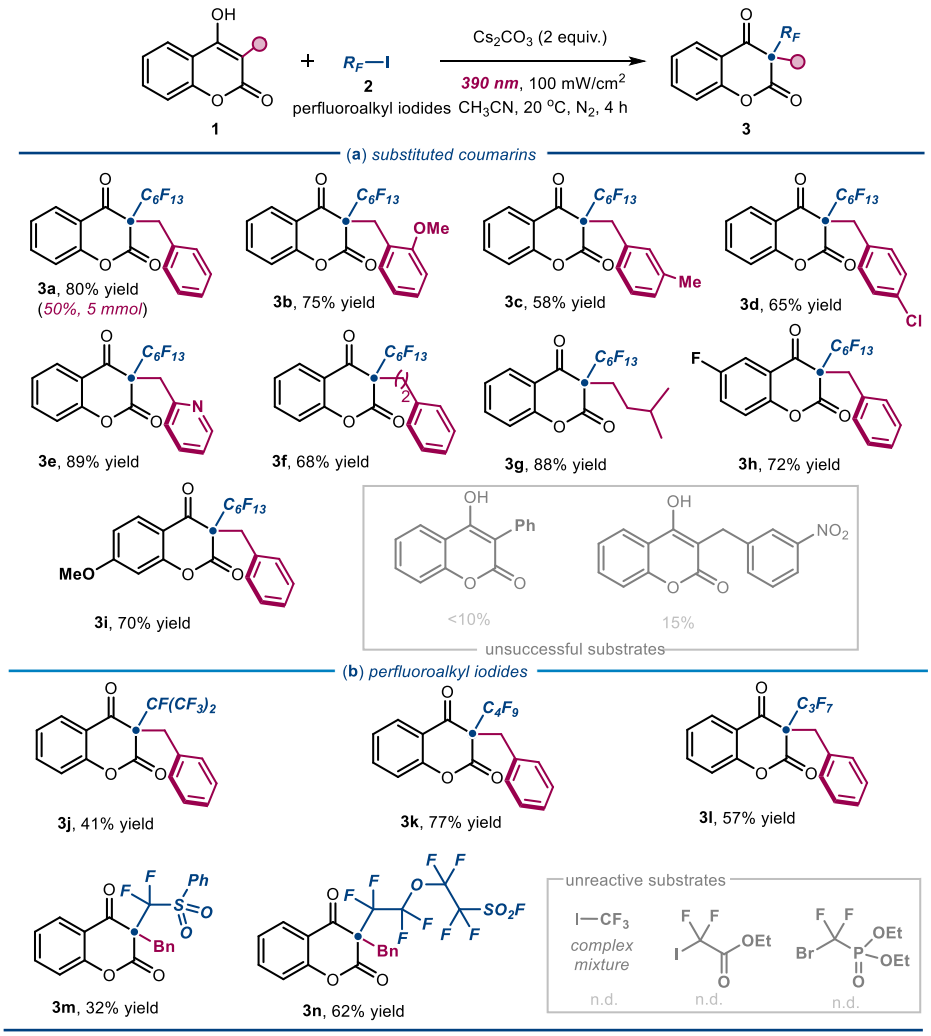

Figure 2.18. Photochemical radical synthesis of 2,4-chromandiones **3**: survey of the (**a**) 4-hydroxycoumarin derivatives **1** and (**b**) perfluoroalkyl iodides **2** that can participate in the process. Reactions performed using **1** (0.2 mmol), **2** (0.6 mmol), Cs_2CO_3 (2 equiv.) in 1 mL of CH_3CN under irradiation by a Kessil lamp (λmax = 390 nm, irradiance = 100 mW/cm^2). Yields of the isolated products **3** are reported below each entry; results are averaged from two runs. R_F: perfluoroalkyl chain. n.d.: not detected.

We next examined the range of perfluoroalkyl iodides compatible with this photochemical catalytic method (**Figure 2.18b**). A variety of perfluoroalkyl iodides with different chain lengths reacted smoothly with **1a**, affording the corresponding products **3j**–**3l** in good to high yields. We then found that iodo sulfonyl fluorides, despite their sensitivity, were suitable radical precursors, providing the corresponding products **3m** (32%) and **3n** (62%). However, attempts to use trifluoromethyl iodide as an electron-deficient radical precursor were unsuccessful, and likewise, α-difluorinated esters and phosphonates failed to deliver the desired products.

Next, we considered whether the strong reducing power acquired by the 4-hydroxycoumarin **1** upon excitation could be harnessed to activate radical precursors beyond perfluoroalkyl iodides, thus expanding the scope of the protocol (**Figure 2.19**). Firstly, (phenylsulfonyl)alkyl iodide **4a** was successfully activated to generate the corresponding electrophilic carbon-centered radical via SET reduction, which resulted in an 88% yield of product **5a**. We could also efficiently activate 2-bromo-*N,N*-dimethylacetamide **4b** and bromomalonate **4c** to afford the corresponding products **5b** and **5c** in moderate yield. A limitation of this method is that iodoacetonitrile proved unreactive, while Katritzky salts underwent reduction to the corresponding pyridinium species but formation of the desired chromandione product was not detected.

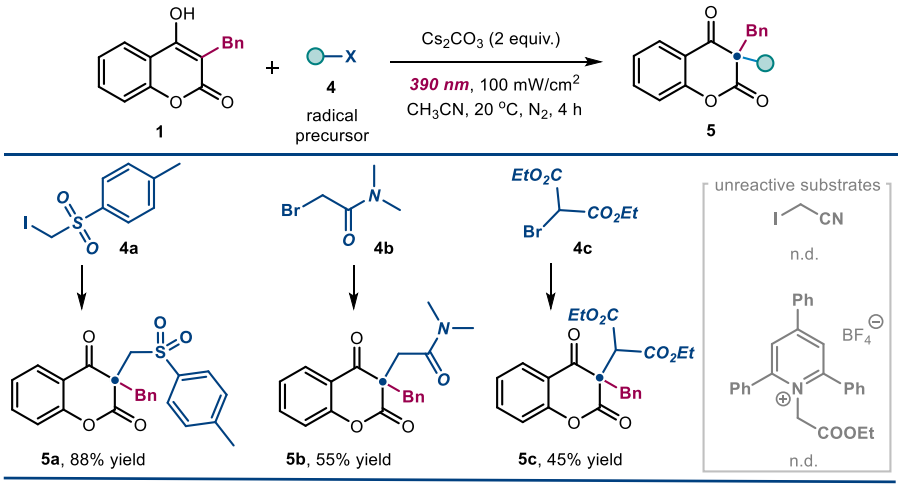

Figure 2.19. Expanding the pool of radical precursors. Reactions performed using **1** (0.2 mmol), **4** (0.6 mmol), Cs_2CO_3 (2 equiv.) in 1 mL of CH_3CN under irradiation by a Kessil lamp (λmax = 390 nm, irradiance = 100 mW/cm^2). Yields of the isolated products **5** are reported below each entry; results are averaged from two runs.

Importantly, in all experiments reported in this study, we observed complete regioselectivity for *C3* functionalization, with no *O*-alkylated products detected. This indicates that the radical pathway effectively circumvents the regioselectivity challenges commonly associated with polar mechanisms.

We then evaluated the potential to enhance the productivity of our photochemical protocol through the use of flow photochemistry (**Figure 2.20**).[34] The benefits of this method are improved light exposure and controlled residence time, resulting in more efficient and consistent reactions. We choose to use a 3D-printed flow reactor with a 0.5 mm inner diameter and a total volume of 2 mL, connected to a syringe pump for precise flow rate control. This

[34] Buglioni, L.; Raymenants, F.; Slattery, A.; Zondag, S. D. A.; Noël, T. "Technological Innovations in Photochemistry for Organic Synthesis: Flow Chemistry, High-Throughput Experimentation, Scale-up, and photoelectrochemistry." *Chem. Rev.* **2022**, *122*, 2752-2906.

system was irradiated with the same Kessil LED light source (λ_{max} = 390 nm) used in batch experiments. Interestingly, we achieved complete alkylation of 4-hydroxycoumarins in only ten minutes by using 1 equivalent of TMG as a soluble organic base, resulting in a significant reduction in reaction time relative to batch processes. High yields of alkylated products **3a**, **3k**, and **5a** were obtained with enhanced productivity under flow conditions. For comparison, a batch reaction produced **3a** in 80% yield after 240 minutes, whereas the flow system delivered the same product in just 10 minutes, using only half the amount of base. The flow process achieved a productivity of 0.924 mmol/h, representing a 23-fold increase over the batch process, which yielded 0.04 mmol/h. These findings highlight the significant advantages of flow photochemistry in terms of reaction speed, efficiency, and scalability.

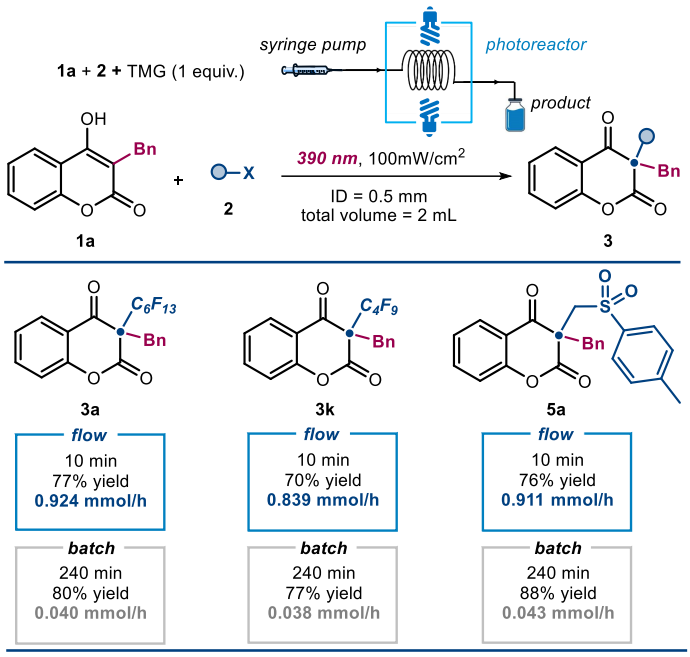

Figure 2.20. Flow photocatalysis for improved productivity. Reactions performed using **1** (0.2 mmol), **2** (0.6 mmol), TMG (1 equiv.) in 2 mL of CH_3CN under illumination by two single wavelength Kessil LED (λmax = 390 nm, irradiance = 100 mW/cm^2) inside a photoreactor. Yields of the isolated products **3** are reported below each entry. ID: inner diameter. Conditions for batch reactions are detailed in Figure 2.11 (4-hour reaction time, using 2 equiv. of Cs_2CO_3).

Finally, we hypothesized that our protocol could be extended to the alkylation of unsubstituted 4-hydroxycoumarins **6** by trapping electrophilic radicals generated upon photoexcitation. This strategy complements existing ionic approaches for the synthesis of 3-substituted 4-hydroxycoumarins **7** by introducing a radical-based pathway that broadens the synthetic scope. As illustrated in **Figure 2.21**, applying the optimized reaction conditions enabled the radical perfluoroalkylation of unsubstituted 4-hydroxycoumarins **6**. These substrates also exhibited productive photochemical reactivity upon irradiation with purple light, allowing the

generation of electrophilic radicals from a range of stable halide precursors, including trifluoromethyl iodide, which had previously shown no reactivity with 3-substituted analogues (adduct **7c**). The resulting perfluoroalkylated products (**7a**–**d**) were obtained in high yields, underscoring the efficiency and versatility of this methodology.

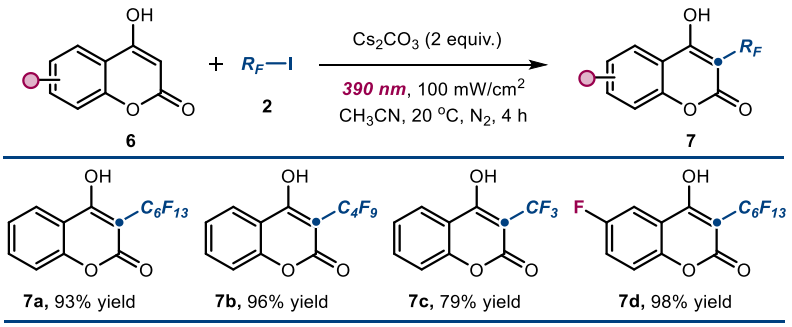

Figure 2.21. Extending the photochemistry to unsubstituted 4-hydroxycoumarins. Reactions performed using **6** (0.2 mmol), **2** (0.6 mmol), Cs_2CO_3 (2 equiv.) in 1 mL of CH_3CN under illumination by a single Kessil lamp (λmax = 390 nm, irradiance = 100 mW/cm^2). Yields of the isolated products **7** are reported below each entry. R_F: perfluoroalkyl chain.

2.3.4 Further Mechanistic Investigations

To gain a deeper understanding of the reaction mechanism, we conducted additional studies. Specifically, we determined the quantum yield (Φ) of the model reaction between **1a** and **2a**, which stood at 8.4, strongly supporting a radical chain mechanism.[30] Based on this result along with the photophysical studies and control experiments presented in **section 2.3.2**, we propose the mechanism detailed in **Figure 2.22**. Upon the irradiation of 390 nm purple light, intermediate **I**, generated from the deprotonation of 3-substituted 4-hydroxycoumarin **1** by Cs_2CO_3, can reach an excited state **I*** which serves as a strong SET reductant ($E(\mathbf{I}^{\cdot}/[\mathbf{I}^*]$ = -2.77 V). This excited state **I*** can reduce alkyl iodide **2** to form an electrophilic radical **II**, thus initiating the radical chain propagation process. Then, electrophilic radical **II** is intercepted by the ground-state nucleophilic 3-substituted 4-hydroxycoumarin **1**, generating a ketyl radical intermediate **III**. Radical **III** can undergo the XAT process with alkyl iodide **2**, generating intermediate **IV**[35] while affording radical intermediate **II**, thus propagation the chain. Intermediate **IV** collapses to afford product 2,4-chromandiones **3**. The overall

[35] Similar atom-transfer mechanisms have been invoked for the alkylation of enol ethers and enamides with electrophilic radicals; see: (a) Curran, D. P.; Ko, S.-B. "Additions of electrophilic radicals to electron-rich alkenes by the atom transfer method. Surmounting potentially reversible radical atom transfer reactions by irreversible ionic reactions." *Tetrahedron Lett.*, **1998**, *39*, 6629-6632; (b) Friestad, G. K.; Wu, Y. "Intermolecular Nonreductive Alkylation of Enamides via Radical−Polar Crossover." *Org. Lett.* **2009**, *11*, 819-822. See also: (c) Studer, A.; Curran, D. P. "Catalysis of Radical Reactions: A Radical Chemistry Perspective." *Angew. Chem. Int. Ed.,* **2016**, *55*, 58-102. However, a SET process that reduces substrate **2** from the ketyl radical intermediate **III** and regenerates the chain-propagating radical **II** cannot be excluded.

mechanism fits within the framework of an atom-transfer radical addition (ATRA) process.[36]

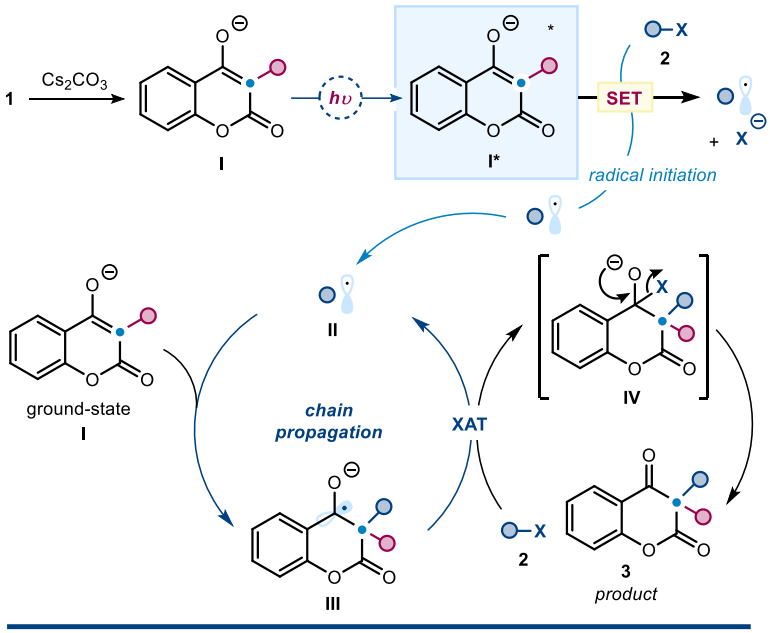

Figure 2.22. Proposed catalytic cycle

2.4 Conclusions

In summary, we have reported a photochemical, radical-based method for the dearomatization of 4-hydroxycoumarin derivatives, enabling the efficient introduction of fluoroalkyl and alkyl substituents at the *C3* position. This strategy exploits the unique excited-state reactivity of hydroxycoumarins, which serve as potent SET reductants under purple light irradiation to drive radical generation. This newly uncovered photochemical reactivity broadens the scope of functionalization for biologically relevant hydroxycoumarins and offers direct access to 2,4-chromandiones bearing quaternary stereogenic centers.

2.5 Experimental Section

General Information. The ^{1}H NMR, ^{19}F{1H} NMR, ^{13}C{1H} NMR spectra are available in the literature[1] and are not reported in the present dissertation.

The NMR spectra were recorded at 400 MHz and 600 MHz for ^{1}H, 101 or 150 MHz for ^{13}C and 376 MHz for ^{19}F{1H}. The chemical shift (δ) for ^{1}H and ^{13}C are given in ppm relative to residual signals of the solvents ($CHCl_3$ @ 7.26 ppm ^{1}H NMR and 77.16 ppm ^{13}C NMR).

---

[36] Pintauer, T.; Matyjaszewski, K. in *Encyclopedia of Radicals*, volume 4, pp.1851–1894, Wiley (**2012**).

Coupling constants are given in Hertz. The following abbreviations are used to indicate the multiplicity: s, singlet; d, doublet; q, quartet; m, multiplet; br, broad signal.

High resolution mass spectra (HRMS) were obtained from the Mass Facility unit on a Waters Xevo Q Tof spectrometer with electrospray ionization (ESI). UV-vis measurements were carried out on a Cary 3500 Multicell UV-vis spectrophotometer. Cyclic voltammetry studies were carried out on a CHI660C potentiostat, offering compliance voltage up to ± 100 V (available at the counter electrode), ± 10 V scan range, and ±2 A current range. Fluorescence measurements were carried out on an Edinburgh FLSP920 spectrometer equipped with a 450 W xenon arc lamp, double excitation and single emission monochromators, and a Peltier-cooled Hamamatsu R928P photomultiplier tube (185−850 nm).

Yields refer to isolated materials of >95% purity as determined by ^{1}H NMR analysis.

General Procedures. All reactions were set up under an argon atmosphere in oven-dried glassware. Synthesis grade and anhydrous solvents were used as purchased from commercial sources. Chromatographic purification of products was accomplished using forced-flow chromatography (FC) on silica gel (230-400 mesh). For thin-layer chromatography (TLC) analysis throughout this work, Merck pre-coated TLC plates (silica gel 60 GF254, 0.25 mm) were employed, using UV light as the visualizing agent and an acidic mixture of vanillin or basic aqueous potassium permanganate ($KMnO_4$) stain solutions, and heat as developing agents. Organic solutions were concentrated under reduced pressure on a Büchi rotatory evaporator.

Materials. Commercial-grade reagents and solvents were purchased at the highest quality from commercial suppliers and used as received, unless otherwise stated.

2.5.1 Synthesis of the Substrates

Compound **1a** and other coumarin substrates **1** were synthesized according to previously reported procedures (Figure 2.23),[37] with slight modifications as outlined below.

General Procedure A:

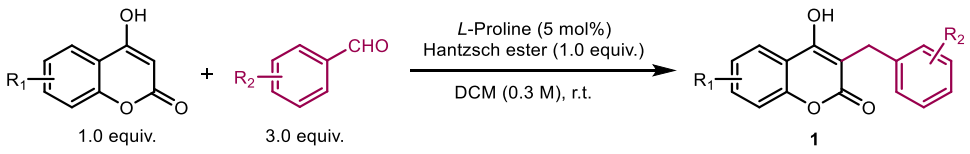

[37] (a) Ramachary, D. B.; Kishor, M. "Direct catalytic asymmetric synthesis of highly functionalized tetronic acids/tetrahydro-isobenzofuran-1,5-diones via combination of cascade three-component reductive alkylations and Michael-aldol reactions." *Org. Biomol. Chem*. **2010**, *8*, 2859-2867; (b) Montagut-Romans, A.; Boulven, M.; Lemaire, M.; Popowycz, F. "3-Methylene-2,4-chromandione in situ trapping: introducing molecular diversity on 4-hydroxycoumarin." *RSC Adv*. **2016**, *6*, 4540-4544.

An oven-dried flask was charged with 4-hydroxycoumarin (1.0 equiv.), aldehyde (3.0 equiv.), Hantzsch ester (1.0 equiv.), and proline (0.05 equiv.), which were dissolved in 0.3 M dichloromethane. The reaction mixture was stirred at room temperature overnight. The reaction was monitored by TLC analysis, and the excess solvent was evaporated using a rotary evaporator. The crude reaction mixture was purified by flash column chromatography on silica gel, using 50% ethyl acetate in hexanes as the eluent, to afford the final benzylated 4-hydroxycoumarin substrate **1** as a white solid.

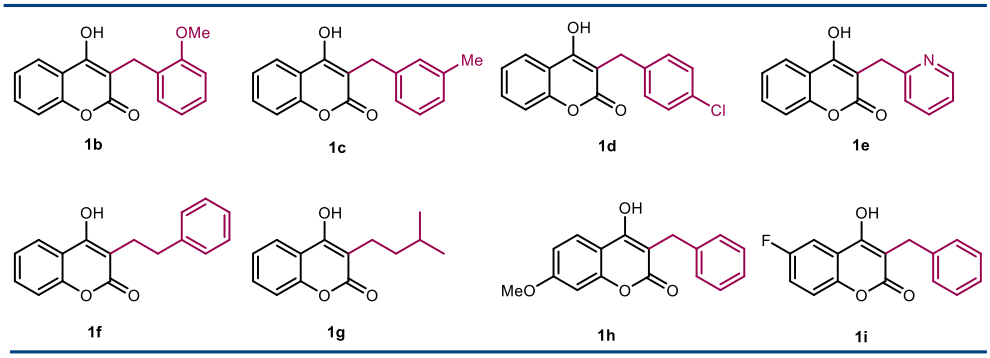

Figure 2.23. Starting materials synthesized according to **General procedure A**.

Characterization of substrates 1:

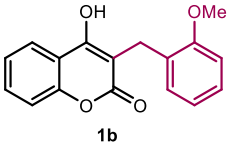

4-hydroxy-3-(2-methoxybenzyl)-2H-chromen-2-one (1b): Synthesized according to the general procedure **A** using 4-hydroxycoumarin (250 mg, 1.54 mmol, 1.0 equiv.), 2-methoxybenzaldehyde (630 mg, 4.63 mmol, 3.0 equiv.) and Hantzsch ester (391 mg, 1.54 mmol, 1.0 equiv.), and L-proline (8.9 mg, 0.077 mmol, 0.05 equiv.). The crude mixture was purified by flash column chromatography on silica gel (Hexane:EtOAc = 1:1 as eluent) to afford **1b** (292 mg, 67% yield) as a light yellow solid.

^{1}H NMR (400 MHz, DMSO) δ= 7.99 – 7.92 (m, 1H), 7.62 (ddd, *J* = 8.6, 7.2, 1.6 Hz, 1H), 7.42 – 7.33 (m, 2H), 7.17 (ddd, *J* = 8.1, 7.2, 1.9 Hz, 1H), 6.97 (dd, *J* = 8.2, 1.1 Hz, 1H), 6.89 – 6.75 (m, 2H), 3.83 (s, 3H), 3.81 (s, 2H) ppm.

^{13}C{^{1}H} NMR (151 MHz, DMSO): δ= 162.8, 161.1, 157.1, 152.1, 131.8, 127.3, 127.7, 126.9, 123.9, 123.3, 120.1, 116.3, 116.2, 110.3, 102.3, 55.3, 23.8 ppm.

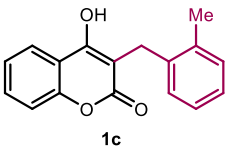

4-hydroxy-3-(3-methylbenzyl)-2H-chromen-2-one (1c): Synthesized according to the general procedure **A** using 4-hydroxycoumarin (250 mg, 1.54 mmol, 1.0 equiv.), 3-methylbenzaldehyde (556 mg, 4.63 mmol, 3.0 equiv.) and Hantzsch ester (391 mg, 1.54 mmol, 1.0 equiv.), and L-proline (8.9mg,

0.077mmol, 0.05 equiv.). The crude mixture was purified by flash column chromatography on silica gel (Hexane:EtOAc = 1:1 as eluent) to afford **1c** (337 mg, 82% yield) as a white solid.

^{1}H NMR (400 MHz, DMSO) δ= 7.96 (dd, *J* = 8.2, 1.6 Hz, 1H), 7.63 – 7.54 (m, 1H), 7.38 – 7.29 (m, 2H), 7.12 (t, *J* = 7.5 Hz, 1H), 7.06 – 6.89 (m, 3H), 3.82 (s, 2H), 2.23 (s, 3H) ppm.

^{13}C{^{1}H} NMR (151 MHz, DMSO): δ= 163.0, 161.4, 152.1, 140.1, 137.1, 131.6, 128.7, 128.0, 126.4, 125.2, 123.7, 123.5, 116.8, 116.1, 103.8, 29.1, 21.0 ppm.

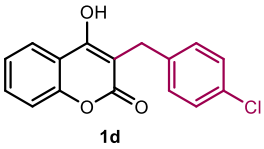

1d

3-(4-chlorobenzyl)-4-hydroxy-2H-chromen-2-one (1d): Synthesized according to the general procedure **A** using 4-hydroxycoumarin (1.0 g, 6.17 mmol, 1.0 equiv.), 4-chlorobenzaldehyde 2.6 g, 18.5 mmol, 3.0 equiv.) and Hantzsch ester (1.56 g, 6.17 mmol, 1.0 equiv.), and L-proline (35.5 mg, 0.31 mmol, 0.05 equiv.). The crude mixture was purified by flash column chromatography on silica gel (Hexane:EtOAc = 1:1 as eluent) to afford **1d** (1.15 g, 65% yield) as a white solid.

^{1}H NMR (600 MHz, DMSO): δ= 8.00 – 7.95 (m, 1H), 7.61 (ddd, *J* = 8.7, 7.4, 1.6 Hz, 1H), 7.39 – 7.35 (m, 2H), 7.30 (d, *J* = 8.5 Hz, 2H), 7.26 (d, *J* = 8.5 Hz, 2H), 3.86 (s, 2H) ppm.

^{13}C{^{1}H} NMR (151 MHz, DMSO): δ= 162.8, 160.8, 152.1, 138.9, 132.0, 130.5, 130.0, 128.1, 124.0, 123.4, 116.3, 116.2, 103.8, 28.6 ppm.

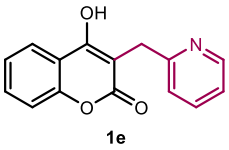

1e

4-hydroxy-3-(pyridin-2-ylmethyl)-2H-chromen-2-one (1e): Synthesized according to the general procedure **A** using 4-hydroxycoumarin (250 mg, 1.54 mmol, 1.0 equiv.), 2-pyridinecarboxaldehyde (495 mg, 4.63 mmol, 3.0 equiv.) and Hantzsch ester (391 mg, 1.54 mmol, 1.0 equiv.), and L-proline (8.9 mg, 0.077 mmol, 0.05 equiv.). The crude mixture was purified by flash column chromatography on silica gel (Hexane:EtOAc = 1:1 as eluent) to afford **1e** (206 mg, 53% yield) as a light yellow solid.

^{1}H NMR (400 MHz, DMSO): δ 8.56 (ddd, *J* = 5.1, 1.8, 0.9 Hz, 1H), 7.93 (dd, *J* = 8.1, 1.6 Hz, 1H), 7.88 (td, *J* = 7.7, 1.8 Hz, 1H), 7.60 (ddd, *J* = 8.4, 7.3, 1.7 Hz, 1H), 7.45 (d, *J* = 7.9 Hz, 1H), 7.42 – 7.30 (m, 3H), 4.10 (s, 2H) ppm.

^{13}C{^{1}H} NMR (151 MHz, DMSO): δ 163.8, 162.9, 159.2, 152.2, 147.1, 139.0, 131.8, 123.8, 123.4, 123.3, 122.4, 117.3, 116.0, 100.7, 31.8 ppm.

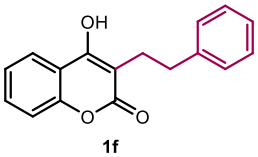

1f

4-hydroxy-3-phenethyl-2H-chromen-2-one (1f): Synthesized according to the general procedure **A** using 4-hydroxycoumarin (250 mg, 1.54 mmol, 1.0 equiv.), 2-phenylacetaldehyde (556 mg, 4.63 mmol, 3.0 equiv.) and Hantzsch ester (391 mg, 1.54 mmol, 1.0 equiv.), and L-proline (8.9 mg, 0.077 mmol, 0.05 equiv.). The crude

mixture was purified by flash column chromatography on silica gel (Hexane:EtOAc = 1:1 as eluent) to afford **1f** (211 mg, 51% yield) as a white solid.

^{1}H NMR (600 MHz, DMSO): δ= 7.92 (dd, *J* = 7.8, 1.6 Hz, 1H), 7.58 (ddd, *J* = 8.5, 7.3, 1.6 Hz, 1H), 7.36 – 7.30 (m, 2H), 7.30 – 7.24 (m, 4H), 7.23 – 7.11 (m, 1H), 2.82 – 2.76 (m, 2H), 2.76 – 2.70 (m, 2H) ppm.

^{13}C{^{1}H} NMR (151 MHz, DMSO): δ= 162.8, 160.2, 151.9, 141.6, 131.6, 128.3, 128.2, 125.8, 123.8, 123.3, 116.5, 116.1, 104.2, 33.6, 25.7 ppm.

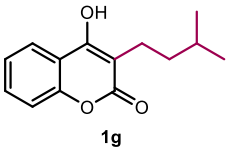

1g

4-hydroxy-3-isopentyl-2H-chromen-2-one (1g): Synthesized according to the general procedure **A** using 4-hydroxycoumarin (250 mg, 1.54 mmol, 1.0 equiv.), isovaleraldehyde (398 mg, 4.63 mmol, 3.0 equiv.) and Hantzsch ester (391 mg, 1.54 mmol, 1.0 equiv.), and L-proline (8.9 mg, 0.077 mmol, 0.05 equiv.). The crude mixture was purified by flash column chromatography on silica gel (Hexane:EtOAc = 1:1 as eluent) to afford **1g** (283 mg, 79% yield) as a white solid.

^{1}H NMR (400 MHz, DMSO): δ= 7.92 (dd, *J* = 8.2, 1.6 Hz, 1H), 7.61 – 7.52 (m, 1H), 7.37 – 7.28 (m, 2H), 1.56 (dp, *J* = 13.3, 6.7 Hz, 1H), 1.37 – 1.27 (m, 2H), 0.91 (d, *J* = 6.7 Hz, 6H) ppm.

^{13}C{^{1}H} NMR (151 MHz, DMSO): δ= 162.8, 159.8, 151.8, 131.4, 123.7, 123.1, 116.5, 116.0, 105.5, 36.9, 27.6, 22.5, 21.7 ppm.

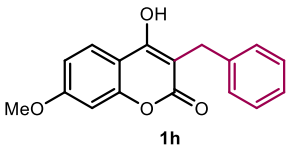

1h

3-benzyl-4-hydroxy-7-methoxy-2H-chromen-2-one (1h): Synthesized according to the general procedure **A** using 4-hydroxy-7-methoxycoumarin (150 mg, 0.78 mmol, 1.0 equiv.), benzaldehyde (249 mg, 2.34 mmol, 3.0 equiv.) and Hantzsch ester (198 mg, 0.78 mmol, 1.0 equiv.), and L-proline (4.5 mg, 0.04 mmol, 0.05 equiv.). The crude mixture was purified by flash column chromatography on silica gel (Hexane:EtOAc = 1:1 as eluent) to afford **1h** (159 mg, 72% yield) as a light brown solid.

^{1}H NMR (400 MHz, DMSO): δ= 7.88 (d, *J* = 9.5 Hz, 1H), 7.27 – 7.20 (m, 5H), 7.24 – 7.09 (m, 1H), 6.96 – 6.88 (m, 2H), 3.83 (s, 3H), 3.81 (s, 2H) ppm.

^{13}C{^{1}H} NMR (151 MHz, DMSO): δ= 163.4, 162.1, 153.89, 140.6, 128.1, 128.1, 125.6, 124.7, 111.5, 110.1, 101.0, 100.3, 55.8, 29.1 ppm.

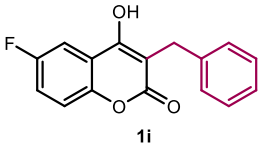

1i

3-benzyl-6-fluoro-4-hydroxy-2H-chromen-2-one (1i): Synthesized according to the general procedure **A** using 6-fluoro-4-hydroxycoumarin (200 mg, 1.11 mmol, 1.0 equiv.), benzaldehyde (353 mg, 3.33 mmol, 3.0 equiv.) and Hantzsch ester

(281 mg, 1.11 mmol, 1.0 equiv.), and L-proline (6.40 mg, 0.056 mmol, 0.05 equiv.). The crude mixture was purified by flash column chromatography on silica gel (Hexane:EtOAc = 1:1 as eluent) to afford **1i** (247 mg, 82% yield) as a white solid.

^{1}H NMR (600 MHz, DMSO): δ= 7.69 (dd, *J* = 9.2, 3.0 Hz, 1H), 7.43 (td, *J* = 8.6, 3.0 Hz, 1H), 7.38 (dd, *J* = 9.0, 4.5 Hz, 1H), 7.25 – 7.20 (m, 4H), 7.13 (tt, *J* = 5.6, 2.5 Hz, 1H), 3.83 (s, 2H) ppm.

^{13}C{^{1}H} NMR (151 MHz, DMSO): δ= 162.9, 161.2, 158.7, 157.1, 148.5, 140.2, 128.1 (2×C), 125.7, 118.8, 118.7, 118.2, 118.1, 109.1, 109.0, 104.0, 29.3 ppm.

^{19}F{^{1}H} NMR (565 MHz, DMSO): δ= -118.43 ppm.

2.5.2 Experimental Procedures

Experimental Setup

- ***Photochemical Set-up 1*** *390 nm Kessil lamp setup* with PhotoRedOx Box TC™ (**Figure 2.24**)

The reactions were performed using a PhotoRedOx Box TC™ reactor under the illumination of a Kessil lamp (max 52 W, λmax = 390 nm, positioned 2-3 cm away from the vial), with a fan to maintain a cool temperature. Under these conditions, the reaction temperature within the vessel was measured to be between 20-22 ºC.

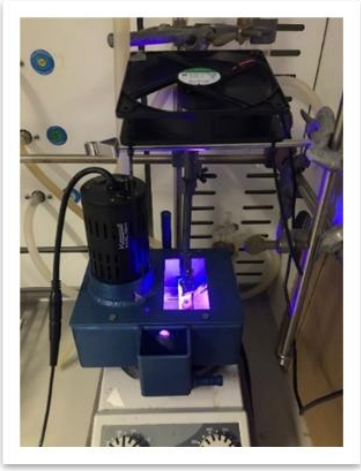

Figure 2.24. Reaction setup using PhotoRedOx Box TC™ reactor with 390 nm Kessil lamp.

- ***Set-up 2*** Gram scale experiment (**Figure 2.25**)

The gram scale reaction was performed using a PhotoRedOx Box TC™ reactor with a 390 nm Kessil lamp (max 52W, λmax= 390 nm, 2-3 cm away from the vial), and a fan to cool down the temperature.

Figure 2.25. Setup for the gram-scale experiment using PhotoRedOx Box TC™ reactor with 390 nm Kessil lamp

2.5.3 Preparation of the 3,3-disubstituted 2,4-chromandiones from 4-hydroxycoumarins and alkyl halides

General Procedure A for the 3,3-disubstituted 2,4-chromandiones

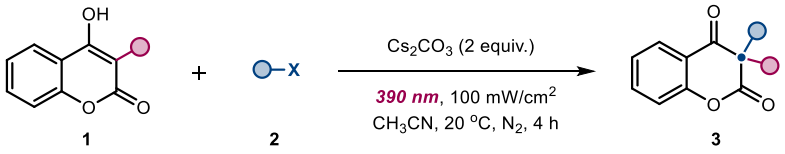

To a 4 mL glass vial, 4-hydroxycoumarins **1** (0.2 mmol, 1.0 equiv.) and Cs_2CO_3 (0.4 mmol, 2 equiv.) were sequentially added. The vial was sealed with a screw-top cap with septum and then vacuumed and backfilled with nitrogen for 3 times. Afterwards, fluoroalkyl halides **2** (0.6 mmol, 3 equiv.), followed by argon-sparged CH_3CN (0.2 M, 1.0 mL) were added *via* syringe. The vial was sealed with Parafilm and then stirred under the irradiation of 390 nm *Kessil* lamp with PhotoRedOx Box TC™ reactor for 4 hours using ***Set-up 1*** detailed in **Figure 2.24**. After the reaction was completed, the reaction mixture was transferred to an extraction funnel, 10 mL of H_2O and 2 mL of brine were added, and the organic layer was extracted with EtOAc. The organic layer was washed with brine twice. The combined organic layers were dried over anhydrous Na_2SO_4, filtered, and concentrated to dryness. The crude residue was purified by column chromatography to afford the corresponding product **3**.

Characterization of Products

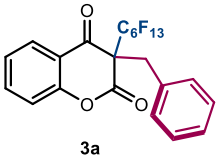

3a

3-Benzyl-3-(perfluorohexyl)-chromane-2,4-dione (3a): Synthesized according to the General Procedure using **1a** (50 mg, 0.2 mmol, 1.0 equiv.), **2a** (268 mg, 0.6 mmol, 3.0 equiv.), and cesium carbonate (130 mg, 0.4 mmol, 2.0 equiv.). The crude mixture was purified by flash column chromatography on silica gel (Hexane: EtOAc = 99: 1 as eluent) to afford **3a** (91 mg, 80% yield) as a colorless oil.

^{1}H NMR (400 MHz, $CDCl_3$) δ= (ddd, *J* = 8.7, 7.2, 1.7 Hz, 1H), 7.22 (td, *J* = 7.6, 1.1 Hz, 1H), 7.10 (q, *J* = 3.4 Hz, 5H), 6.99 (dd, *J* = 8.2, 1.0 Hz, 1H), 4.36 – 3.37 (m, 2H) ppm.

^{13}C{^{1}H} NMR (151MHz, $CDCl_3$): δ= 185.7, 162.6, 153.7, 138.2, 131.4, 130.8, 128.9, 128.2, 127.4, 125.7, 118.8, 117.6, 63.1, 39.1 ppm.

^{19}F{^{1}H} NMR (376 MHz, $CDCl_3$): δ= -80.81 (t, *J* = 10.0 Hz), -108.55 – -112.32 (m), -116.1– -117.9 (m), -121.71 (bs), -122.6 – -122.8 (m), -124.18 – -129.13 (m) ppm.

HRMS (ESI): calculated for $C_{22}H_{12}F_{13}O_3$ ($M+Na^+$): 593.0398, found 593.0399.

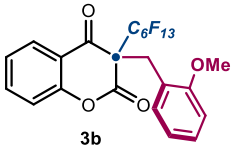

3b

3-(2-Methoxybenzyl)-3-(perfluorohexyl)-chromane-2,4-dione (3b): Synthesized according to the General Procedure using **1a** (56 mg, 0.2 mmol, 1.0 equiv.), **2b** (268 mg, 0.6 mmol, 3.0 equiv.), and cesium carbonate (130 mg, 0.4 mmol, 2.0 equiv.). The crude mixture was purified by flash column chromatography on silica gel (Hexane: EtOAc = 99: 1 as eluent) to afford **3b** (90 mg, 75% yield) as a colourless oil.

^{1}H NMR (600 MHz, $CDCl_3$) δ 7.87 – 7.83 (m, 1H), 7.58 (ddd, *J* = 8.3, 7.3, 1.7 Hz, 1H), 7.28 – 7.19 (m, 1H), 7.15 – 7.08 (m, 2H), 7.07 – 7.02 (m, 1H), 6.82 (td, *J* = 7.4, 1.1 Hz, 1H), 6.54 (dt, *J* = 8.1, 0.8 Hz, 1H), 3.90 – 3.77 (m, 1H), 3.40 (s, 3H) ppm.

^{13}C{^{1}H} NMR (151MHz, $CDCl_3$): δ 184.9, 162.4, 157.0, 153.9, 137.3, 132.7, 129.5, 127.3, 125.2, 121.3, 121.0, 119.0, 117.3, 109.9, 54.2, 29.9 ppm.

^{19}F{^{1}H} NMR (376 MHz, $CDCl_3$): δ -80.8 (t, *J* = 9.9 Hz), -107.0 – -113.8 (m), -114.5 – -118.2 (m), -119.2 – -123.8 (m), -126.1 (dt, *J* = 47.3, 14.1 Hz) ppm.

HRMS (ESI): calculated for $C_{23}H_{13}F_{13}O_4$ ($M+Na^+$): 623.0498, found 623.0504.

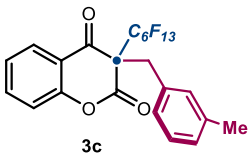

3c

3-(3-Methylbenzyl)-3-(perfluorohexyl)-chromane-2,4-dione (3c): Synthesized according to the General Procedure using **1a** (53 mg, 0.2 mmol, 1.0 equiv.), **2c** (268 mg, 0.6 mmol, 3.0 equiv.), and cesium carbonate (130 mg, 0.4 mmol, 2.0 equiv.). The crude mixture was purified by flash column chromatography on silica gel (Hexane: EtOAc = 99: 1 as eluent) to afford **3c** (69 mg, 58% yield) as a colourless oil.

^{1}H NMR (600 MHz, $CDCl_3$) δ 7.90 (dd, *J* = 7.9, 1.7 Hz, 1H), 7.57 (ddd, *J* = 8.3, 7.3, 1.7 Hz,

1H), 7.22 (ddd, *J* = 8.1, 7.3, 1.1 Hz, 1H), 7.02 – 6.95 (m, 2H), 6.93 – 6.83 (m, 3H), 4.42 – 3.31 (m, 2H), 2.16 (s, 3H) ppm.

$^{13}C\{^1H\}$ NMR (151MHz, $CDCl_3$): δ 185.8, 162.6, 153.8, 138.6, 138.1, 135.0, 131.5, 131.3, 128.9, 128.7, 127.7, 127.3, 125.6, 117.6, 63.1, 39.1, 21.3.

$^{19}F\{^1H\}$ NMR (565 MHz, $CDCl_3$): δ -80.8 (t, *J* = 9.8 Hz), -108.1 – -111.2 (m), -114.5 – -118.7 (m), -121.7 (ddd, *J* = 56.1, 27.9, 13.3 Hz), -122.3 – -123.7 (m), -125.1 – -127.8 (m).

HRMS (ESI): calculated for $C_{23}H_{13}F_{13}O_3$ ($M+Na^+$): 607.0549, found 607.0555.

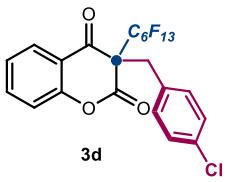

3d

3-(4-Chlorobenzyl)-3-(perfluorohexyl)-chromane-2,4-dione (3d): Synthesized according to the General Procedure using **1a** (57 mg, 0.2 mmol, 1.0 equiv.), **2d** (268 mg, 0.6 mmol, 3.0 equiv.), and cesium carbonate (130 mg, 0.4 mmol, 2.0 equiv.). The crude mixture was purified by flash column chromatography on silica gel (Hexane: EtOAc = 99: 1 as eluent) to afford **3d** (79 mg, 65% yield) as a colourless oil.

^1H NMR (400 MHz, $CDCl_3$) δ 7.90 (dd, *J* = 7.9, 1.7 Hz, 1H), 7.62 (ddd, *J* = 8.3, 7.3, 1.7 Hz, 1H), 7.33 – 7.23 (m, 1H), 7.14 – 7.08 (m, 2H), 7.04 (dd, *J* = 8.4, 1.4 Hz, 3H), 4.13 – 3.51 (m, 2H).

^{13}C NMR (151 MHz, $CDCl_3$) δ 185.5, 162.4, 153.7, 138.5, 134.4, 132.3, 130.1, 129.1, 127.4, 126.0, 118.7, 117.8, 63.1, 37.9.

^{19}F NMR (565 MHz, $CDCl_3$) δ -80.8 (t, *J* = 10.0 Hz), -100.2 – -114.3 (m), -114.51 – -119.1 (m), -120.3 – -122.1 (m), -122.1 – -123.7 (m), -126.1 (dtd, *J* = 121.5, 15.6, 7.7 Hz).

HRMS: calculated for $C_{22}H_{12}F_{13}O_3$ ($M+Na^+$): 627.0009, found 627.0009.

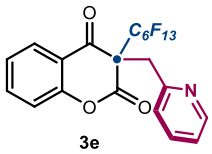

3e

3-(Pyridin-2-ylmethyl)-3-(perfluorohexyl)-chromane-2,4-dione (3e): Synthesized according to the General Procedure using **1a** (51 mg, 0.2 mmol, 1.0 equiv.), **2e** (268 mg, 0.6 mmol, 3.0 equiv.), and cesium carbonate (130 mg, 0.32 mmol, 2.0 equiv.). The crude mixture was purified by flash column chromatography on silica gel (Hexane: EtOAc = 98: 2 as eluent) to afford **3e** (102 mg, 89% yield) as a colorless oil.

^1H NMR (600 MHz, $CDCl_3$) δ 7.92 (dd, *J* = 7.8, 1.7 Hz, 1H), 7.86 (ddd, *J* = 5.0, 1.7, 1.0 Hz, 1H), 7.70 (ddd, *J* = 8.1, 7.3, 1.7 Hz, 1H), 7.58 (td, *J* = 7.7, 1.7 Hz, 1H), 7.33 – 7.25 (m, 3H), 6.98 (ddd, *J* = 7.4, 5.0, 1.1 Hz, 1H), 4.84 – 3.65 (m, 2H).

^{13}C NMR (151 MHz, $CDCl_3$) δ 185.2, 163.4, 154.2, 154.0, 147.3, 137.0, 136.7, 127.1, 125.0, 123.0, 121.9, 120.3, 117.6, 60.9, 39.8.

^{19}F NMR (565 MHz, $CDCl_3$) δ -80.8 (t, *J* = 9.7 Hz), -109.4 (ddtt, *J* = 40.4, 20.9, 11.2, 5.1 Hz), -115.7 – -120.1 (m), -121.4 (t, *J* = 18.3 Hz), -122.7 (dddq, *J* = 19.9, 15.1, 10.2, 5.5 Hz), -126.1 (dt, *J* = 41.9, 14.0 Hz).

HRMS: calculated for $C_{21}H_{10}F_{13}N_1O_3$ ($M+Na^+$): 594.0345, found 594.0351.

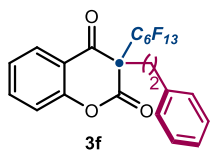

3f

3-Phenethyl-3-(perfluorohexyl)-chromane-2,4-dione (3f): Synthesized according to the General Procedure using **1a** (53 mg, 0.2 mmol, 1.0 equiv.), **2f** (268 mg, 0.6 mmol, 3.0 equiv.), and cesium carbonate (130 mg, 0.4 mmol, 2.0 equiv.). The crude mixture was purified by flash column chromatography on silica gel (Hexane: EtOAc = 98: 2 as eluent) to afford **3f** (80 mg, 68% yield) as a colourless oil.

^{1}H NMR (600 MHz, $CDCl_3$) δ 7.98 (dd, *J* = 7.9, 1.7 Hz, 1H), 7.74 (ddd, *J* = 8.4, 7.3, 1.7 Hz, 1H), 7.43 – 7.30 (m, 2H), 7.25 – 7.20 (m, 2H), 7.19 – 7.14 (m, 1H), 7.13 – 7.07 (m, 2H), 2.95 (td, *J* = 12.2, 5.4 Hz, 1H), 2.78 (ddd, *J* = 12.8, 11.7, 4.7 Hz, 1H), 2.60 – 2.53 (m, 1H), 2.50 – 2.39 (m, 1H).

^{13}C NMR (151 MHz, $CDCl_3$) δ 185.4, 162.8, 154.3, 138.9, 138.4, 128.8, 128.7, 127.7, 127.0, 125.9, 119.0, 117.9, 62.2, 35.0, 30.6.

^{19}F NMR (565 MHz, $CDCl_3$) δ -80.8 (t, *J* = 10.1 Hz), -108.8 – -111.9 (m), -116.2 – -119.0 (m), -120.6 – -121.9 (m), -122.1 – -123.6 (m), -126.1 (dt, *J* = 98.1, 16.0 Hz).

HRMS: calculated for $C_{23}H_{13}F_{13}O_3$ ($M+Na^+$): 607.0549, found 607.0555.

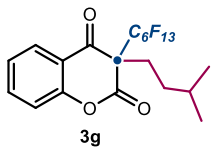

3g

3-Isopentyl-3-(perfluorohexyl)-chromane-2,4-dione (3g): Synthesized according to the General Procedure using **1a** (46 mg, 0.2 mmol, 1.0 equiv.), **2g** (268 mg, 0.6 mmol, 3.0 equiv.), and cesium carbonate (130 mg, 0.4 mmol, 2.0 equiv.). The crude mixture was purified by flash column chromatography on silica gel (Hexane: EtOAc = 99: 1 as eluent) to afford **3g** (97 mg, 88% yield) as a colourless oil.

^{1}H NMR (400 MHz, $CDCl_3$) δ 8.00 (dd, *J* = 7.9, 1.7 Hz, 1H), 7.74 (ddd, *J* = 8.8, 7.4, 1.7 Hz, 1H), 7.35 (td, *J* = 7.7, 1.1 Hz, 1H), 7.29 – 7.22 (m, 1H), 2.85 – 2.53 (m, 1H), 2.46 (td, *J* = 12.5, 4.3 Hz, 1H), 1.15 – 1.01 (m, 1H), 0.87 – 0.84 (m, 6H).

^{13}C NMR (151 MHz, $CDCl_3$) δ 185.9, 163.1, 154.3, 138.3, 127.6, 125.9, 119.0, 118.0, 62.2, 32.8, 29.9, 28.4, 22.2, 22.2.

^{19}F NMR (565 MHz, $CDCl_3$) δ -80.8 (t, *J* = 10.0 Hz), -109.3 – -111.7 (m), -116.5 – -118.7 (m), -121.7 (ddd, *J* = 37.0, 25.2, 12.8 Hz), -122.0 – -123.6 (m), -125.1 – -127.1 (m).

HRMS: calculated for $C_{20}H_{15}F_{13}O_3$ ($M+Na^+$): 573.0706, found 573.0711.

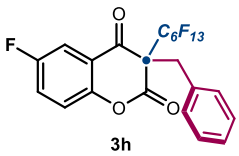

3h

3-Benzyl-6-fluoro-3-(perfluorohexyl)-chromane-2,4-dione (3h): Synthesized according to the General Procedure using **1a** (54 mg, 0.2 mmol, 1.0 equiv.), **2h** (268 mg, 0.6 mmol, 3.0 equiv.), and cesium carbonate (130 mg, 0.4 mmol, 2.0 equiv.). The crude mixture was purified by flash column chromatography on silica gel (Hexane:

EtOAc = 99: 1 as eluent) to afford **3h** (85 mg, 72% yield) as a pale-yellow liquid.

^{1}H NMR (400 MHz, $CDCl_3$) δ 7.53 (dd, *J* = 7.6, 3.1 Hz, 1H), 7.33 – 7.25 (m, 1H), 7.17 – 7.11 (m, 3H), 7.10 – 7.06 (m, 2H), 7.00 (dd, *J* = 9.0, 4.0 Hz, 1H), 4.08 – 3.50 (m, 2H).

^{13}C NMR (151 MHz, $CDCl_3$) δ 185.2, 160.2, 158.6, 149.8, 131.1, 130.8, 129.0, 128.4, 125.7, 125.5, 119.7, 112.8, 77.4, 76.9, 68.1, 39.3.

^{19}F NMR (565 MHz, $CDCl_3$) δ -80.8 (t, *J* = 9.7 Hz), -106.5 – -112.0 (m), -113.1 – -115.5 (m), -115.7 – -118.1 (m), -121.2 – -122.2 (m), -122.3 – -123.3 (m), -124.8 – -127.7 (m).

HRMS: calculated for $C_{22}H_{10}F_{14}O_3$ ($M+Na^+$): 611.0304, found 611.0304.

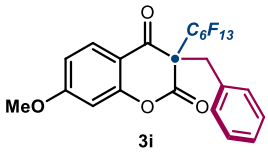

3i

3-Benzyl-7-methoxy-3-(perfluorohexyl)-chromane-2,4-dione (3i): Synthesized according to the General Procedure using **1a** (56 mg, 0.2 mmol, 1.0 equiv.), **2i** (268 mg, 0.6 mmol, 3.0 equiv.), and cesium carbonate (130 mg, 0.4 mmol, 2.0 equiv.). The crude mixture was purified by flash column chromatography on silica gel (Hexane: EtOAc = 99: 1 as eluent) to afford **3i** (84 mg, 70% yield) as a colourless oil.

^{1}H NMR (400 MHz, $CDCl_3$) δ 7.83 (d, *J* = 8.9 Hz, 1H), 7.18 – 7.06 (m, 5H), 6.73 (dd, *J* = 8.9, 2.4 Hz, 1H), 6.40 (d, *J* = 2.3 Hz, 1H), 3.92 (d, *J* = 12.3 Hz, 1H), 3.82 (s, 3H), 3.71 (d, *J* = 12.5 Hz, 1H).

^{13}C NMR (151 MHz, $CDCl_3$) δ 207.1, 167.5, 162.9, 155.8, 131.7, 130.8, 129.3, 128.8, 128.1, 113.6, 112.5, 101.1, 62.6, 56.2, 31.1.

^{19}F NMR (376 MHz, $CDCl_3$) δ -80.7 – -81.0 (m), -109.9 – -110.4 (m), -117.4 (dtd, *J* = 53.5, 16.6, 8.8 Hz), -121.6 - -121.8 (m, *J* = 44.9 Hz), -122.1 – -123.4 (m), -125.3 – -126.9 (m).

HRMS: calculated for $C_{23}H_{13}F_{13}O_4$ ($M+Na^+$): 623.0498, found 623.0504.

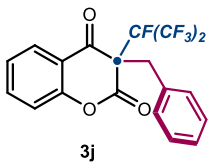

3j

3-Benzyl-3-(perfluoroisopropyl)-chromane-2,4-dione (3j): Synthesized according to the General Procedure using **1a** (50 mg, 0.2 mmol, 1.0 equiv.), **2j** (178 mg, 0.6 mmol, 3.0 equiv.), and cesium carbonate (130 mg, 0.4 mmol, 2.0 equiv.). The crude mixture was purified by flash column chromatography on silica gel (Hexane: EtOAc = 99: 1 as eluent) to afford **3j** (35 mg, 41% yield) as a colourless oil

^{1}H NMR (400 MHz, $CDCl_3$) δ 7.87 (ddd, *J* = 7.9, 1.8, 0.4 Hz, 1H), 7.56 (ddd, *J* = 8.3, 7.3, 1.7 Hz, 1H), 7.23 – 7.18 (m, 1H), 7.15 – 7.03 (m, 5H), 7.01 – 6.94 (m, 1H), 4.07 – 3.75 (m, 2H).

^{13}C NMR (151 MHz, $CDCl_3$) δ 207.6, 186.6, 162.9, 153.5, 138.1, 131.7, 131.3, 128.8, 128.1, 127.4, 1257, 118.7, 117.4, 77.4, 62.5, 39.9, 30.3.

^{19}F NMR (565 MHz, $CDCl_3$) δ -68.6 (td, *J* = 11.1, 6.0 Hz), -69.1 (qd, *J* = 11.1, 5.8 Hz), -177.8 (p, *J* = 6.0 Hz).

HRMS: calculated for $C_{19}H_{11}F_7O_3$ ($M+Na^+$): 443.0409, found 443.0494.

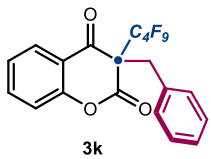

3k

3-Benzyl-3-(perfluorobutyl)-chromane-2,4-dione (3k): Synthesized according to the General Procedure using **1a** (50 mg, 0.2 mmol, 1.0 equiv.), **2k** (208 mg, 0.6 mmol, 3.0 equiv.), and cesium carbonate (130 mg, 0.4 mmol, 2.0 equiv.). The crude mixture was purified by flash column chromatography on silica gel (Hexane: EtOAc = 99: 1 as eluent) to afford **3k** (72 mg, 77% yield) as a colorless oil.

^{1}H NMR (400 MHz, $CDCl_3$) δ 7.89 (dd, *J* = 7.9, 1.7 Hz, 1H), 7.57 (ddd, *J* = 8.3, 7.3, 1.7 Hz, 1H), 7.22 (ddd, *J* = 8.1, 7.3, 1.1 Hz, 1H), 7.17 – 7.05 (m, 5H), 6.99 (dd, *J* = 8.3, 1.0 Hz, 1H), 3.94 – 3.37 (m, 2H).

^{13}C NMR (151 MHz, $CDCl_3$) δ 207.5, 185.7, 162.5, 153.7, 138.2, 131.4, 130.8, 128.9, 128.2, 127.4, 125.7, 118.8, 118.7, 117.7, 63.0, 39.0.

^{19}F NMR (565 MHz, $CDCl_3$) δ -80.8 (t, *J* = 9.7 Hz), -109.1 – -111.7 (m), -116.6 – -119.4 (m), -124.8 – -126.9 (m). **HRMS:** calculated for $C_{20}H_{11}F_9O_3$ ($M+Na^+$): 493.0457, found 493.0462.

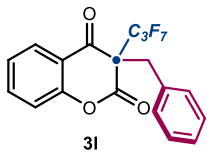

3l

3-Benzyl-3-(perfluoropropyl)-chromane-2,4-dione (3l): Synthesized according to the General Procedure using **1a** (50 mg, 0.2 mmol, 1.0 equiv.), **2l** (178 mg, 0.6 mmol, 3.0 equiv.), and cesium carbonate (130 mg, 0.4 mmol, 2.0 equiv.). The crude mixture was purified by flash column chromatography on silica gel (Hexane: EtOAc = 99: 1 as eluent) to afford **3l** (48 mg, 57% yield) as a colourless oil.

^{1}H NMR (600 MHz, $CDCl_3$) δ 7.89 (dd, *J* = 7.9, 1.7 Hz, 1H), 7.57 (ddd, *J* = 8.3, 7.3, 1.7 Hz, 1H), 7.22 (ddd, *J* = 8.1, 7.4, 1.0 Hz, 1H), 7.16 – 7.07 (m, 5H), 6.99 (dd, *J* = 8.3, 1.0 Hz, 1H), 4.79 – 3.01 (m, 2H).

^{13}C NMR (151 MHz, $CDCl_3$) δ 185.7, 162.5, 153.8, 138.2, 131.5, 130.8, 128.9, 128.2, 127.4, 125.7, 118.8, 117.6, 63.0, 38.8.

^{19}F NMR (565 MHz, $CDCl_3$) δ -75.6 – -88.1 (m), -107.3 – -112.1 (m), -119.5 – -123.7 (m).

HRMS: calculated for $C_{19}H_{11}F_7O_3$ ($M+Na^+$): 443.0489, found 443.0494.

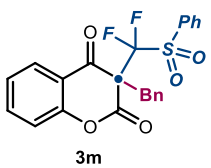

3m

3-Benzyl-3-(difluoro(phenylsulfonyl)methyl) -chromane-2,4-dione (3m): Synthesized according to the General Procedure using **1a** (50 mg, 0.2 mmol, 1.0 equiv.), **2m** (191 mg, 0.6 mmol, 3.0 equiv.), and cesium carbonate (130 mg, 0.4 mmol, 2.0 equiv.). The crude mixture was purified by flash column chromatography on silica gel (Hexane: EtOAc = 98: 2 as eluent) to afford **3m** (28 mg, 32% yield) as a white semi-solid.

^{1}H NMR (400 MHz, $CDCl_3$) δ 7.94 (ddd, *J* = 8.1, 6.0, 1.6 Hz, 3H), 7.82 – 7.74 (m, 1H), 7.66

– 7.59 (m, 2H), 7.55 (ddd, *J* = 8.6, 7.3, 1.7 Hz, 1H), 7.22 (ddd, *J* = 8.3, 7.3, 1.0 Hz, 1H), 7.15 – 7.07 (m, 5H), 7.00 (dd, *J* = 8.3, 1.0 Hz, 1H), 4.42 – 3.17 (m, 2H).

^{13}C NMR (151 MHz, CDCl$_3$) δ 186.0, 163.0, 154.0, 137.7, 136.1, 132.1, 131.6, 131.3, 131.0, 130.7, 129.7, 129.6, 128.8, 128.2, 127.4, 125.4, 117.6, 62.6, 39.9.

^{19}F NMR (565 MHz, CDCl$_3$) δ -95.88 (d, *J* = 226.9 Hz), -99.02 (d, *J* = 226.9 Hz).

HRMS: calculated for $C_{23}H_{16}F_2O_5S$ ($M+Na^+$): 465.0579, found 465.0584.

3-Benzyl-3-(1,1,2,2-tetrafluoro-2-(1,1,2,2-tetrafluoroethoxy) ethane-1-sulfonylfluoride)-chromane-2,4-dione (3n): Synthesized according to the General Procedure using **1a** (50 mg, 0.2 mmol, 1.0 equiv.), **2n** (256 mg, 0.6 mmol, 3.0 equiv.), and cesium carbonate (130 mg, 0.4 mmol, 2.0 equiv.). The crude mixture was purified by flash column chromatography on silica gel (Hexane: EtOAc = 99: 1 as eluent) to afford **3n** (68 mg, 62% yield) as a colourless oil.

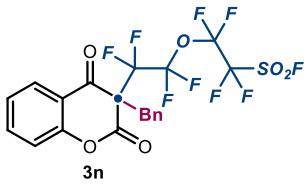

3n

^{1}H NMR (400 MHz, CDCl$_3$) δ 7.89 (dd, *J* = 7.9, 1.8 Hz, 1H), 7.59 (dddd, *J* = 8.2, 7.3, 1.8, 0.8 Hz, 1H), 7.23 (ddd, *J* = 8.1, 7.3, 1.0 Hz, 1H), 7.18 – 7.02 (m, 5H), 7.00 (dd, *J* = 8.3, 1.0 Hz, 1H), 4.60 – 3.08 (m, 2H).

^{13}C NMR (151 MHz, CDCl$_3$) δ 185.5, 162.2, 153.8, 138.4, 131.7, 130.8, 129.0, 128.9, 128.2, 127.5, 125.8, 118.6, 118.6, 117.7, 63.0, 38.7.

^{19}F NMR (565 MHz, CDCl$_3$) δ 51.4 – 38.0 (m), -63.0 – -91.3 (m), -111.9, -112.2 – -117.2 (m).

HRMS: calculated for $C_{20}H_{11}F_9O_6S$ ($M+Na^+$): 573.0025, found 573.0031.

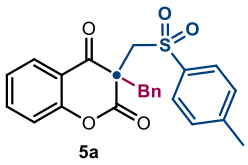

5a

3-Benzyl-3-(tosylmethyl)-chromane-2,4-dione (5a): Synthesized according to the General Procedure using **1a** (50 mg, 0.2 mmol, 1.0 equiv.), 1-((iodomethyl)sulfonyl)-4-methylbenzene **4a** (178 mg, 0.6 mmol, 3.0 equiv.), and cesium carbonate (130 mg, 0.4 mmol, 2.0 equiv.). The crude mixture was purified by flash column chromatography on silica gel (Hexane: EtOAc = 98: 2 as eluent) to afford **5a** (74 mg, 88% yield) as a white solid.

^{1}H NMR (600 MHz, CDCl$_3$) δ 7.88 (dd, *J* = 7.7, 1.7 Hz, 1H), 7.84 – 7.79 (m, 1H), 7.73 – 7.63 (m, 1H), 7.53 – 7.47 (m, 1H), 7.39 – 7.30 (m, 3H), 7.19 (t, *J* = 7.5 Hz, 1H), 7.08 – 7.02 (m, 2H), 6.98 – 6.90 (m, 3H), 4.53 – 3.98 (m, 2H), 3.14 (q, *J* = 12.9 Hz, 2H), 2.44 (s, 3H).

^{13}C NMR (151 MHz, CDCl$_3$) δ 191.6, 168.9, 145.1, 138.1, 137.2, 131.7, 130.1, 129.9, 129.8, 128.5, 128.2, 127.9, 127.5, 127.0, 125.0, 117.5, 62.9, 60.1, 46.4, 21.8.

HRMS: calculated for $C_{24}H_{20}O_5S$ ($M+Na^+$): 443.0924, found 443.0929.

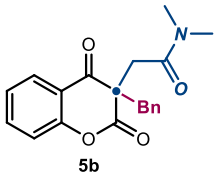

5b

2-(3-benzyl-2,4-dioxo-3-chroman-3-yl)-N,N-dimethylacetamide (5b): Synthesized according to the General Procedure using **1a** (50 mg, 0.2 mmol, 1.0 equiv.), 2-bromo-N,N-dimethylacetamide **4b** (100 mg, 0.6 mmol, 3.0 equiv.), and cesium carbonate (130 mg, 0.4 mmol, 2.0 equiv.). The crude mixture was purified by flash column chromatography on silica gel (Hexane: EtOAc = 70: 30 as eluent) to afford **5b** (37 mg, 55% yield) as a colourless oil liquid.

^{1}H NMR (400 MHz, $CDCl_3$) δ 7.79 (dd, *J* = 7.8, 1.7 Hz, 1H), 7.40 (ddd, *J* = 8.3, 7.2, 1.7 Hz, 1H), 7.14 – 7.06 (m, 1H), 7.05 – 7.00 (m, 3H), 6.99 – 6.92 (m, 2H), 6.87 (dd, *J* = 8.4, 1.1 Hz, 1H), 3.68 – 3.34 (m, 2H), 3.16 (s, 2H), 3.05 (s, 3H), 2.83 (s, 3H).

^{13}C NMR (151 MHz, $CDCl_3$) δ 194.4, 171.3, 169.7, 154.4, 136.3, 133.3, 129.7, 128.3, 127.7, 126.5, 124.4, 119.7, 117.3, 59.4, 44.9, 43.4, 37.4, 35.6.

HRMS: calculated for $C_{20}H_{19}NO_4$ ($M+Na^+$): 360.1206, found 360.1212.

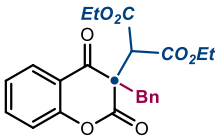

5c

Diethyl-2-(3-benzyl-2,4-dioxo-3-chroman-3-yl)malonate (5c): Synthesized according to the General Procedure using **1a** (50 mg, 0.2 mmol, 1.0 equiv.), diethyl bromomalonate **4c** (143 mg, 0.6 mmol, 3.0 equiv.), and cesium carbonate (130 mg, 0.4 mmol, 2.0 equiv.). The crude mixture was purified by flash column chromatography on silica gel (Hexane: EtOAc = 98: 2 as eluent) to afford **5c** (37 mg, 45% yield) as a pale-yellow liquid.

^{1}H NMR (400 MHz, $CDCl_3$) δ 7.79 (dd, *J* = 7.8, 1.7 Hz, 1H), 7.46 (ddd, *J* = 8.3, 7.3, 1.7 Hz, 1H), 7.14 (td, *J* = 7.6, 1.0 Hz, 1H), 7.09 – 6.99 (m, 5H), 6.91 (dd, *J* = 8.3, 1.1 Hz, 1H), 4.34 (s, 1H), 4.31 – 4.22 (m, 4H), 3.69 – 3.42 (m, 2H), 1.28 (td, *J* = 7.2, 4.7 Hz, 6H).

^{13}C NMR (151 MHz, $CDCl_3$) δ 192.76, 169.25, 168.31, 168.19, 154.20, 136.94, 132.85, 130.14, 128.36, 127.87, 126.86, 124.86, 119.20, 117.29, 62.69, 62.44, 62.40, 56.60, 43.74, 13.99.

HRMS: calculated for $C_{23}H_{22}O_7$ ($M+Na^+$): 433.1258, found 433.1263.

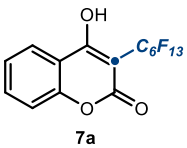

7a

3-(perfluorohexyl)-4-hydroxycoumarin (7a): Synthesized according to the General Procedure using **6a** (32 mg, 0.2 mmol, 1.0 equiv.), perfluorohexyl iodide **2a** (268 mg, 0.6 mmol, 3.0 equiv.), and cesium carbonate (130 mg, 0.4 mmol, 2.0 equiv.). After the reaction was completed, the reaction mixture was transferred to an extraction funnel, 10 mL of H_2O and 2 mL of brine were added, and the organic layer was extracted with EtOAc. The organic layer was washed with brine twice. The combined organic layers were dried over anhydrous Na_2SO_4, filtered, and concentrated to dryness to get product **7a** (89 mg, 93% yield) as a sticky yellow solid.

^{1}H NMR (400 MHz, MeOD) δ 7.97 (dd, *J* = 7.9, 1.6 Hz, 1H), 7.50 (ddd, *J* = 8.3, 7.2, 1.7 Hz, 1H), 7.26 – 7.13 (m, 2H).

^{13}C NMR (101 MHz, MeOD) δ 177.8, 165.4, 155.1, 133.2, 126.4, 124.1, 123.5, 117.0, 89.7.

^{19}F NMR (376 MHz, MeOD) δ -82.5 (t, *J* = 10.1 Hz), -105.9 – -106.2 (m), -122.5, -123.7 (tdd, *J* = 14.1, 6.7, 3.4 Hz), -127.0 – -127.6 (m).

HRMS: calculated for $C_{15}H_5F_{13}O_3$ ($M+Na^+$): 502.9923, found 502.9929.

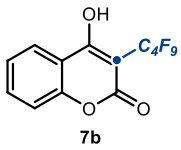

7b

3-(perfluorobutyl)-4-hydroxycoumarin (7b): Synthesized according to the General Procedure using **6b** (32 mg, 0.2 mmol, 1.0 equiv.), perfluorobutyl iodide **2k** (208 mg, 0.6 mmol, 3.0 equiv.), and cesium carbonate (130 mg, 0.4 mmol, 2.0 equiv.). After the reaction was completed, the reaction mixture was transferred to an extraction funnel, 10 mL of H_2O and 2 mL of brine were added, and the organic layer was extracted with EtOAc. The organic layer was washed with brine twice. The combined organic layers were dried over anhydrous Na_2SO_4, filtered, and concentrated to dryness to get product **7b** (73 mg, 96% yield) as a sticky yellow solid.

^{1}H NMR (400 MHz, MeOD) δ 7.97 (dd, *J* = 8.0, 1.8 Hz, 1H), 7.50 (ddd, *J* = 8.2, 7.2, 1.7 Hz, 1H), 7.26 – 7.13 (m, 2H).

^{13}C NMR (151 MHz, DMSO) δ 173.4, 160.7, 153.6, 131.3, 125.1, 122.6, 122.1,115.5, 85.2.

^{19}F NMR (376 MHz, MeOD) δ -82.5 (ddd, *J* = 13.2, 6.5, 2.9 Hz), -105.7 (ddt, *J* = 16.5, 14.0, 2.9 Hz), -123.7 (ddt, *J* = 12.5, 10.0, 4.8 Hz), -127.2 – -127.4 (m).

HRMS: calculated for $C_{13}H_5F_9O_3$ ($M+Na^+$): 402.9987, found 402.9993.

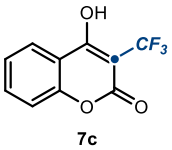

7c

3-(trifluoromethyl)-4-hydroxycoumarin (7c): Synthesized according to the General Procedure with some modification, using **6c** (32 mg, 0.2 mmol, 1.0 equiv.) and cesium carbonate (130 mg, 0.4 mmol, 2.0 equiv.) were taken in a Schlenk tube and degassed 3 times with argon. Then 1ml dry CH_3CN was added and the Schlenk tube was cooled using a liquid nitrogen bath. After that trifluoromethyl iodide **2c** (117 mg, 0.6 mmol, 3.0 equiv.) was added via syringe. Once addition of trifluoromethyl iodide was over, the Schlenk tube was placed under the irradiation of 390 nm *Kessil* lamp with PhotoRedOx Box TC™ reactor for 4 hours. After the reaction was completed, the reaction mixture was transferred to an extraction funnel, 10 mL of H_2O and 2 mL of brine were added, and the organic layer was extracted with EtOAc. The organic layer was washed with brine twice. The combined organic layers were dried over anhydrous Na_2SO_4, filtered, and concentrated to dryness to get product **7c** (72 mg, 79% yield) as a sticky yellow solid.

^{1}H NMR (400 MHz, DMSO) δ 7.83 (dd, *J* = 7.7, 1.7 Hz, 1H), 7.43 (ddd, *J* = 8.4, 7.4, 1.8 Hz,

1H), 7.17 – 7.05 (m, 2H).

^{13}C NMR (101 MHz, DMSO) δ 172.9, 160.7, 153.6, 131.4, 125.1, 122.6, 122.2, 115.6, 87.9.

^{19}F NMR (376 MHz, DMSO) δ -52.9.

HRMS: calculated for $C_{10}H_5F_3O_3$ (M^+): 230.0191, found 230.0113.

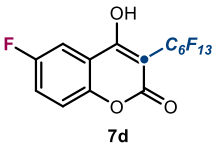

7d

3-(perfluorohexyl)-6-fluoro-4-hydroxycoumarin (7d): Synthesized according to the General Procedure using **6d** (36 mg, 0.2 mmol, 1.0 equiv.), perfluorohexyl iodide **2a** (268 mg, 0.6 mmol, 3.0 equiv.), and cesium carbonate (130 mg, 0.4 mmol, 2.0 equiv.). After the reaction was completed, the reaction mixture was transferred to an extraction funnel, 10 mL of H_2O and 2 mL of brine were added, and the organic layer was extracted with EtOAc. The organic layer was washed with brine twice. The combined organic layers were dried over anhydrous Na_2SO_4, filtered, and concentrated to dryness to get product **7d** (98 mg, 98% yield) as a sticky red solid.

^{1}H NMR (400 MHz, DMSO) δ 7.47 (dd, J = 9.0, 3.2 Hz, 1H), 7.28 (ddd, J = 8.9, 8.2, 3.2 Hz, 1H), 7.14 (dd, J = 8.9, 4.4 Hz, 1H).

^{13}C NMR (101 MHz, DMSO) δ 172.3, 160.6, 158.8, 156.4, 149.8, 123.9, 118.4, 117.5, 110.2, 85.5.

^{19}F NMR (376 MHz, DMSO) δ -80.58 (tt, J = 9.6, 2.7 Hz), -102.97 (tt, J = 13.8, 3.7 Hz), -121.08 (td, J = 8.6, 4.6 Hz), -121.48 (ddd, J = 21.5, 11.4, 4.9 Hz), -121.98 (t, J = 15.1 Hz), -122.53 – -122.75 (m), -126.02 (td, J = 13.8, 5.6 Hz).

HRMS: calculated for $C_{15}H_4F_{14}O_3$ ($M+Na^+$): 520.9829, found 520.9835.

2.5.4 Photophysical studies

Sample Preparation:

Three 25 mL glass vials, each containing either **1a**, **2a**, or a mixture of **1a** and Cs_2CO_3, were sealed with septa, degassed, and then dry CH_3CN (20 mL) was added to each vial to prepare 0.1 M solutions. From these stock solutions, **1a** (10^{-4} M), **2a** (10^{-4} M), and **1a** with Cs_2CO_3 (10^{-4} M) were prepared accordingly. Then, 2.5 mL of each solution was transferred into an argon-filled quartz cuvette (10 x 10 mm light path) equipped with a septum.

UV-visible Absorption Spectra

UV-Vis measurements were carried out on a Cary 3500 Multicell UV-Vis spectrophotometer equipped with two silicon diode detectors, double beam optics, and Xenon pulse light (**Figure 2.26**).

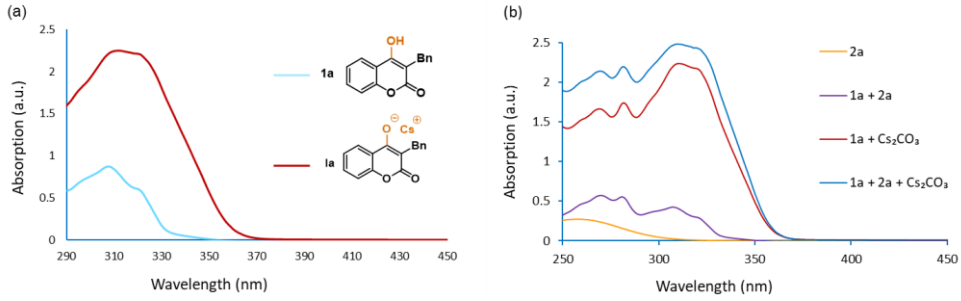

Figure 2.26. (**a**) Absorption spectra recorded for **1a** (10^{-4} M; blue line) and **Ia** (in situ generated mixing **1a** with Cs_2CO_3; red line) measured in CH_3CN. (**b**) All samples in CH_3CN. *Yellow line*: [**2a**] = 10^{-4} M; *purple line*: [**1a**] = 10^{-4} M and [**2a**] =3. 10^{-4} M; *red line*: [**1a**] = 10^{-4} M and [Cs_2CO_3] = $2x10^{-4}$ M; and *blue line*: [**1a**] = $1x10^{-4}$ M, [**2a**] = $3x10^{-4}$ M, and [Cs_2CO_3] = $2x10^{-4}$ M.

Emission Spectra

Fluorescence measurements were carried out on an Edinburgh FLSP920 spectrometer equipped with a 450 W xenon arc lamp, double excitation and single emission monochromators, and a Peltier-cooled Hamamatsu R928P photomultiplier tube (185−850 nm). The emission spectrum of the deprotonated substrate **Ia** (formed in situ form **1a** upon the addition of Cs_2CO_3 in degassed CH_3CN according to the same procedure mentioned before) was recorded from 320 nm to 600 nm after excitation with a 314 nm laser (**Figure 2.27**).

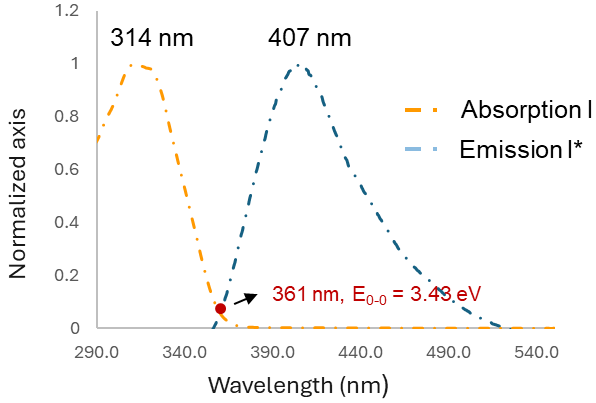

Figure 2.27. Stern-Volmer quenching studies of the photoactive species **Ia** (formed upon deprotonation of **1a**) in CH_3CN using **2a** as quencher.

Stern-Volmer Quenching Studies

Fluorescence measurements were carried out on an Edinburgh FLSP920 spectrometer equipped with a 450 W xenon arc lamp, double excitation and single emission monochromators. A 0.025 M solution of the quencher substrate (**2a**) in degassed CH_3CN (HPLC grade) was prepared and 20 µL of this stock solution was added to the solution of the deprotonated photoactive species **Ia**, prepared according to the procedure detailed in the

beginning of section E. The addition of the substrate solution **2a** was repeated four times. After each addition, the solution was mixed and the emission spectra of the excited catalyst were acquired from 320 nm to 600 nm (the excitation wavelength was fixed at 314 nm). A solvent blank was subtracted from all the measurements. The excitation wavelength was chosen to avoid saturation of the emission detector.

The results shown in **Figure 2.28** indicate that all substrates quenched the excited state emission of the deprotonated substrate **Ia**. The Stern-Volmer plot shows a linear correlation between the amounts of substrates and the ratio I_0/I, following the relationship: $I_0/I = 1 + KSV[Q]$ (Q = Quencher) (**Figure 2.28**).

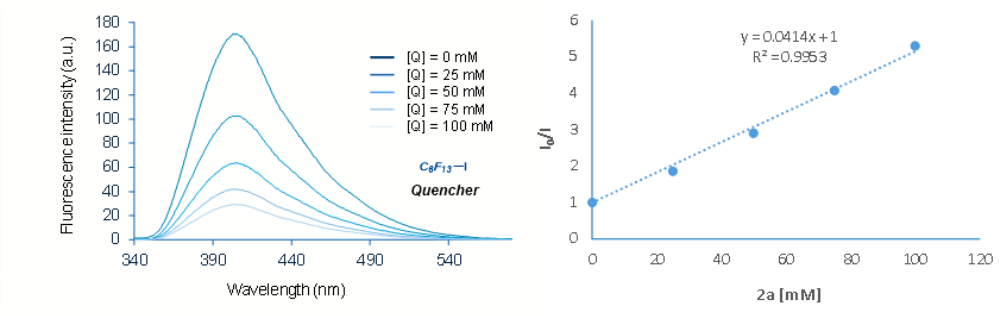

Figure 2.28. Stern-Volmer quenching studies using perfluorohexyl iodide (**2a**) as the quencher Q

Electrochemical Studies

Cyclic voltammetry (CV) measurements were carried out on a CHI660C instrument with a glassy carbon disk electrode (diameter: 3 mm) as working electrode. A silver wire coated with AgCl immersed in a 3.0 M aqueous solution of KCl and separated from the analyte by a fritted glass disk was employed as the reference electrode and a Pt wire counter-electrode completed the electrochemical setup. The scan rate was 100 mV/s unless otherwise stated. The substrates were measured at a concentration of 0.02 M in CH_3CN with $TBAPF_6$ (0.1 M) as electrolyte. The deprotonated substrate **Ia** was at a concentration of 0.02 M. Potentials are quoted with the following notation: E_p^C (E_{Red}) refers to the cathodic peak potential, E_p^A (E_{Ox}) refers to the anodic peak potential (**Figures 2.29** and **2.30**).

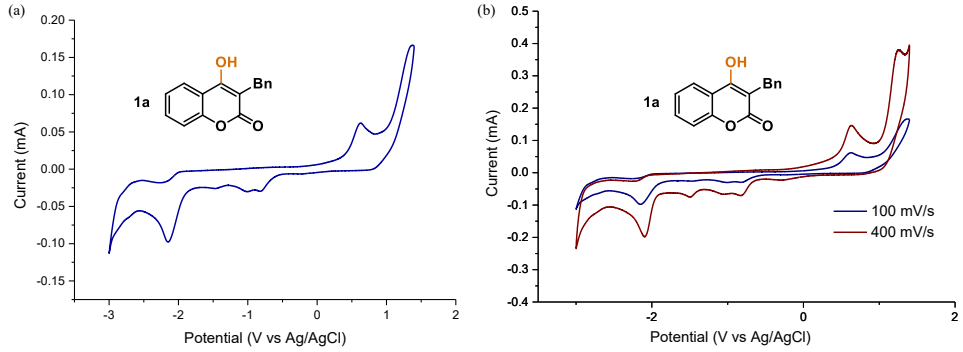

Figure 2.29. (left) CV of the 4-hydroxycoumarin substrate **1a** in CH_3CN starting with the oxidation, reversible oxidation, and reduction, Ep^A = 0.61 V and Ep^C = -2.13 V; (right) CV of **1a** in CH_3CN starting with the oxidation with a sweep rates of 100 and 400 mV/s.

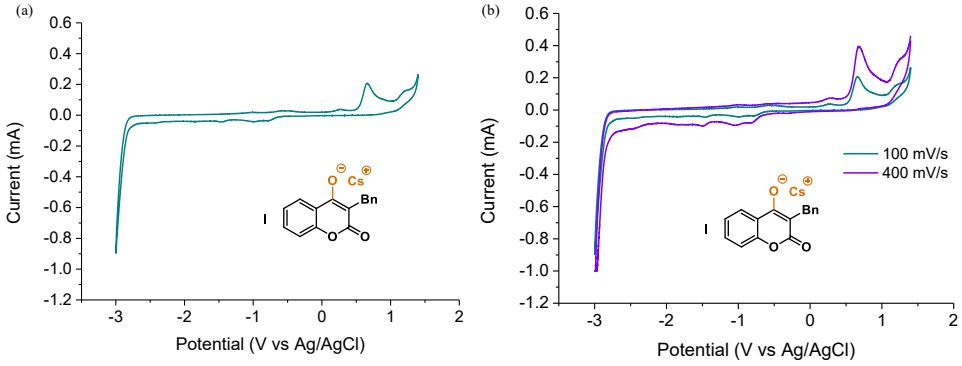

Figure 2.30. (left) CV of the in situ deprotonated species **Ia** in CH_3CN starting with the oxidation, reversible oxidation, and reduction, Ep^A = 0.66 V and Ep^C = -2.44 V; (right) CV of **Ia** in CH_3CN starting with the oxidation with a sweep rates of 100 and 400 mV/s.

Conversion of the Potential from Ag/AgCl to SCE

The conversion of the redox potential from Ag/AgCl to SCE was done according to the literature by measuring the redox potential of ferrocene as a reference in CH_3CN (**Figure 2.31**).[38]

[38] Pavlishchuk, V.V.; Addison, A.W. "Conversion Constants for Redox Potentials Measured versus Different Reference Electrodes in Acetonitrile Solutions at 25°C." *Inorganica Chim. Acta.* **2000**, *298*, 97–102.

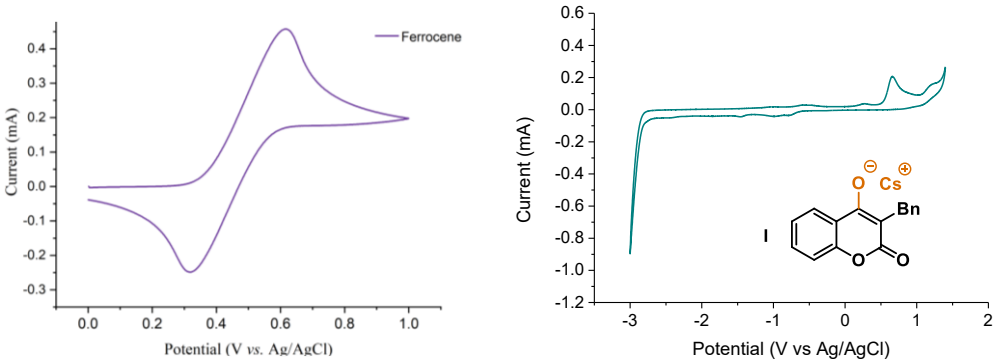

Figure 2.31. (left) CV of ferrocene in CH_3CN, reversible reduction and oxidation $E_{1/2}$ = 0.46 V. (right) CV of deprotonated substrate **Ia** in CH_3CN, reversible oxidation E_p^A = 0.66 V.

With the reference CV, the redox potential *vs.* SCE in CH_3CN was calculated using the following equations:

$$E_p^A \text{ (Ag/AgCl to Fc/Fc}^+\text{)} = 0.66 - 0.46 = 0.20 \text{ V } \textit{vs.}\text{ Fc/Fc}^+$$

$$E_p^A \text{ (Fc/Fc}^+\text{ to SCE)} = 0.20 + 0.38 = 0.58 \text{ V } \textit{vs.}\text{ SCE}$$

Evaluation of the excited-state potential of the excited deprotonated substrate 1a

Using the data collected from the CV studies (**Figure 2.29-2.31**) and from the absorption and emission spectra (**Figure 2.27**) of deprotonated substrate **Ia**, we could estimate the redox potential of the excited state with the following Equation:

$$E(\mathbf{Ia}^{\bullet+}/\ \mathbf{Ia}^{*}) = E(\mathbf{Ia}^{\bullet+}/\ \mathbf{Ia}) - E_{0\text{-}0}(\mathbf{Ia}^{*})/(\ \mathbf{Ia})$$

Since the electrochemical oxidation of deprotonated substrate **Ia** is reversible (**Figure 2.29**), the reversible peak potential E_p anode was used for $E(Pc^{\bullet+}/Pc)$. The oxidation potential was calculated to be 0.58 V *vs.* SCE (in ACN). $E_{0\text{-}0}(\mathbf{Ia}^{*})/(\mathbf{Ia})$ was approximately determined spectroscopically from the tail of absorption spectrum (roughly at 314 nm for deprotonated substrate **Ia**) to have values of 3.43 eV.

The oxidation potential of the excited **Ia***:

$$E(\mathbf{Ia}^{\bullet+}/\ \mathbf{Ia}^{*}) = 0.66 - 3.43 = \textit{-2.77 V vs. Ag/AgCl}$$

$$E(\mathbf{Ia}^{\bullet+}/\ \mathbf{Ia}^{*}) = 0.58 - 3.43 = \textit{-2.85 V vs. SCE}$$

Time-resolved Emission Decay

Emission lifetimes (τ) were determined with the single photon counting technique (TCSPC) with the same Edinburgh FLSP920 spectrometer using pulsed picosecond LED (EPLED 365, FWHM < 800ps) as the excitation source, with repetition rates between 1 kHz and 1 MHz,

and the above-mentioned R928P PMT as detector. The goodness of fit was assessed by minimizing the reduced $\chi 2$ function and by visual inspection of the weighted residuals (**Figure 2.32**).

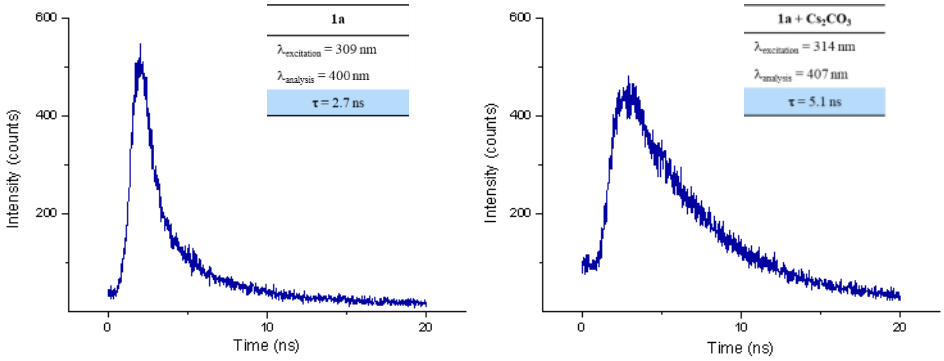

Figure 2.32. (left) Time-resolved emission decay (excitation at 309 nm, analysis at 400 nm) of **1a** ($1 \cdot 10^{-4}$ M) in CH_3CN solution measured by TC-SPC (τ = 2.7 ns, from deconvolution and single-exponential fitting, X^2= 1.319) (right) Time-resolved emission decay (excitation at 314 nm, analysis at 407 nm) of **1a** with Cs_2CO_3 ($1 \cdot 10^{-4}$ M) in CH_3CN solution measured by TC-SPC (τ = 5.1 ns, from deconvolution and single-exponential fitting, X^2= 1.047)

Quantum Yield Determination

-Experimental Setup

The experiments for the quantum yield determination were conducted under illumination by a 390 Kessil lamp (setup depicted in **Figure 2.33**), using a 3D printed photoreactor. The intensity was fixed to the maximum value.

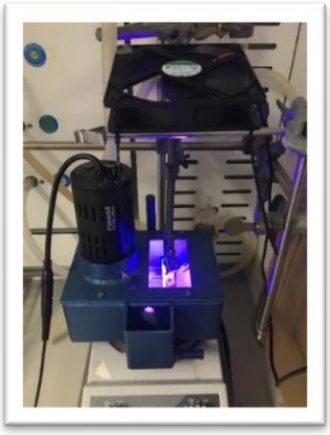

Figure 2.33. Kessil lamp set-up for the quantum yield determination

General Procedure for photon Flux (F) determination:[39]

$$\Phi = M / (F \cdot t \cdot f) \quad (1)$$

$$f = 1\text{-}10^{-A} \quad (2)$$

M is the moles of product formed (mol), **F** is the number of photons emitted per second (einstein s^{-1}), **t** is the time (s) and **f** is fraction of light absorbed which can be calculated using eq. 2, where **A** is the measured absorbance at 390 nm.

The number of photons emitted per second was determined using azobenzene as actinometer. Using the reaction setup depicted in **Figure 2.30**, a glass vial was filled with a solution of Z-azobenzene (0.1 mmol) in CD_3OD (0.1M) and irradiated at 390 nm. The trans-cis isomerization was monitored by ^{1}H-NMR using dibromomethane as an internal standard (**Figure 2.34**).

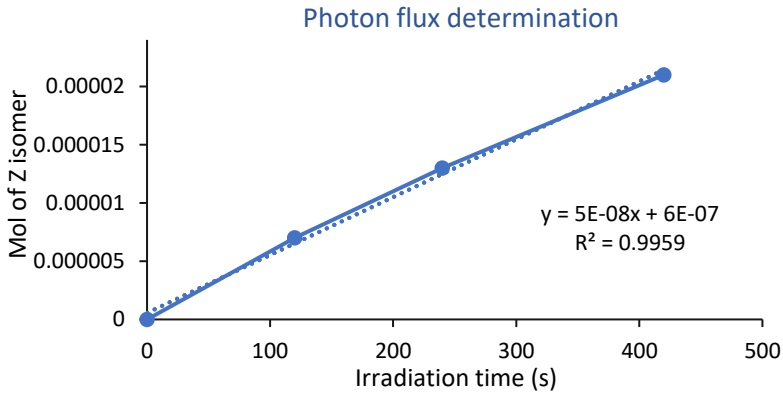

Figure 2.34. Plot of moles of *cis*-azobenzene formed vs irradiation time (s)

The actinometer solution was irradiated for 0 min, 2 min, 4 min, and 7 min. According to the eq. (**1**), (**2**) and estimated quantum yield of trans-cis isomerization process at 390 nm (Φ = 0.262), the number of photons emitted per time unit (**F**) was determined (2.08 x 10^{-8} mol s^{-1}).

Quantum Yield Determination:

Following the general procedure, three model perfluoroalkylation reactions between **1a**, and **2a** using Cs_2CO_3 were performed separately. Each reaction mixture was irradiated for 0 min, 3 min, 6 min, 9 min, and 12 min. After irradiation reactions were worked up and the amount of product **3a** formed was determined by ^{1}H NMR analysis of the crude using

[39] Ladányi, V.; Dvořák, P.; Al Anshori, J.; Vetráková, L.; Wirz, J.; Heger, D. "Azobenzene Photoisomerization Quantum Yields in Methanol Redetermined." *Photochem. Photobiol. Sci.*, **2017**, *16*, 1757–1761.

dibromomethane as the internal standard. The fraction of light absorbed *f* was recognized as 1. The moles of the formed product **3a** are plotted against the number of incident photons (**Figure 2.35**). The quantum yield was calculated to be $\Phi = 8.4$ based on the slope and eq. (**1**), (**2**).

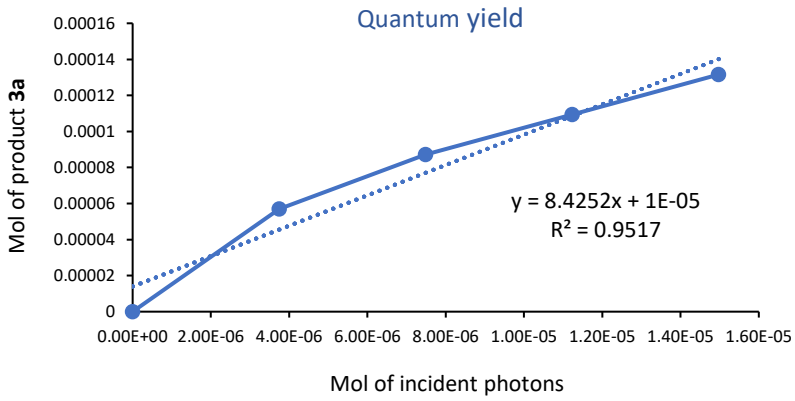

Figure 2.35. Plot of moles of incident photons vs moles of product **3a** formed.

2.5.5 Flow photocatalysis

-Experimental Setup

Figure 2.36 details a schematic representation of the photoflow catalysis setup. In this setup, a 4 mL glass vial containing **1a** (0.2 mmol, 1 equiv.) and tetramethyl guanidine (0.2 mmol, 1 equiv.) was sealed with a screw-top cap with a septum, then evacuated and backfilled with argon three times. Next, electrophilic radical precursors **2** (0.6 mmol, 3 equiv.) were added, followed by 2 mL of argon-sparged CH_3CN via a syringe. The resulting solution was drawn into a 5 mL syringe, which was then connected to a flow reactor equipped with two 390 nm Kessil lamps. The temperature of the photoreactor was maintained at 20 °C using a temperature controller connected to an external chiller. The syringe pump delivered the solution at a flow rate of 0.5 mL/min for 10 minutes, and the crude product mixture was collected in a separate vial (**Figure 2.37**).

After the reaction, the mixture was transferred to an extraction funnel, and 10 mL of H_2O and 2 mL of brine were added. The organic layer was then extracted with EtOAc and washed with brine twice. The combined organic layers were dried over anhydrous Na_2SO_4, filtered, and concentrated to dryness. The crude residue was purified by column chromatography to yield the corresponding products **3a**, **3k**, and **5a**.

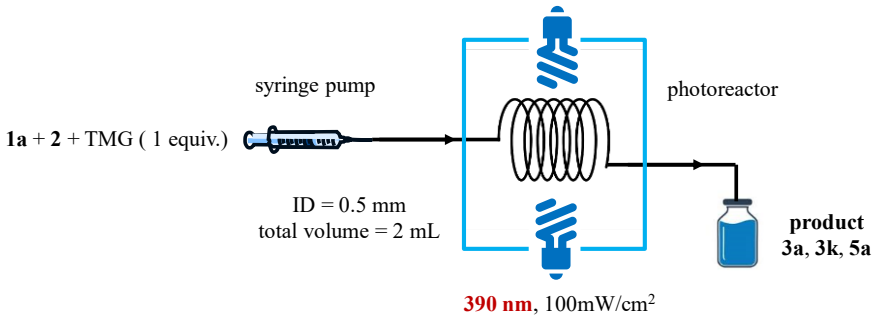

Figure 2.36. Schematic representation of the flow setup. ID = internal diameter.

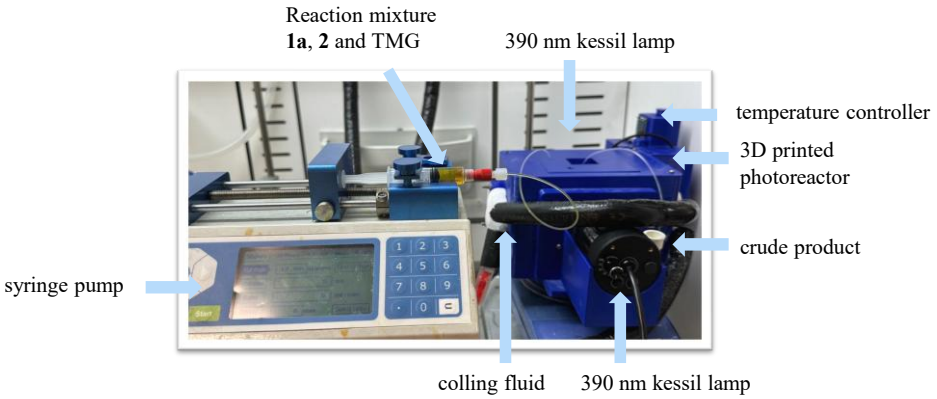

Figure 2.37. The photoreactor shown in Figure 2.33 was formed by a 3D-printed holding a cylindrical flow coil with 2 Kessil 390 nm LEDs pointing toward the flow coil inside the reactor. The distance between the LEDs is 2 cm and the tubing is 2 mm.

Chapter III

A Bifunctional Organic Photocatalyst for Efficient Single-Electron and Energy Transfer Activation

Target

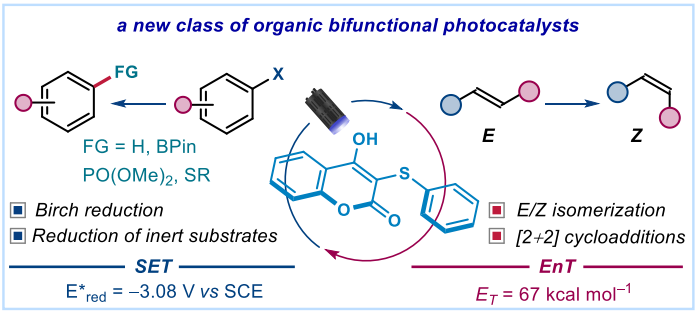

To develop a new family of bifunctional organic photocatalysts that unify single-electron transfer and energy transfer reactivity within a single molecular scaffold. The design exploits charge-transfer excited states in 3-thioaryl-4-hydroxycoumarins to combine strong reducing power ($E^*_{red} \approx -3.0$ V vs. SCE) with high triplet energy ($E_T \approx 67$ kcal mol^{-1}), enabling diverse radical and triplet-sensitized photochemical transformations under visible light.

Tools

Upon deprotonation, 3-thioaryl-4-hydroxycoumarins generate anionic species that absorb at 390 nm and, upon excitation, act as strong single-electron transfer (SET) reductants for otherwise redox-inert substrates. In their neutral form, the same scaffolds absorb at 370 nm and exhibit long-lived triplet states that mediate EnT processes, including *E/Z* isomerization and [2 + 2] photocycloaddition.[1]

3.1 Introduction

Photocatalysis has become a central tool in modern organic synthesis, enabling highly selective transformations under mild and sustainable conditions.[2] Depending on the nature of the excited state involved, reactions typically proceed through either single-electron transfer

[1] The project discussed in this chapter was conducted in collaboration with Dr. Sumitava Mallik, Nunzio Matera, Dr. Bixiao Li, and Professor Stefano Stagni. I contributed to the catalyst modification, the optimization of reaction conditions and substrate scope, the discovery and development of energy transfer reactivity, and performed mechanistic studies. This study has been published: Mallik, S.; Wang, H.; Matera, N.; Li, B.; Stagni, S.; Melchiorre, P. "A Bifunctional Organic Photocatalyst for Efficient Single-Electron and Energy Transfer Activation." *Angew. Chem. Int. Ed.* **2025**, *64*, e202509770.

[2] For a special issue on photochemical catalytic processes., see: *Chem. Rev.* **2022**, *122*, 1483–2980.

(SET)[3] or energy transfer (EnT)[4] mechanisms. In SET photocatalysis, the excited catalyst acts as a strong oxidant or reductant to initiate radical processes via electron exchange. In EnT catalysis, the photocatalyst transfers its excitation energy to a substrate, usually generating a reactive triplet state that can participate in pericyclic or isomerization reactions.

In the context of SET catalysis, the activation of inert substrates such as aryl chlorides and fluorides, alkyl halides, and unactivated arenes remains a major challenge because of their large bond dissociation energies (BDEs) and highly negative reduction potentials ($E_{red} < -2.5$ V vs. SCE; **Figure 3.1a**).[5] Conventional photocatalysts—typically based on Ru, Ir, or organic dyes—are generally limited to redox potentials above –2.2 V vs. SCE and are therefore unable to engage such demanding substrates (**Figure 3.1b**, left).[6] Yet, these halides are widely available[7] and represent valuable aryl radical precursors for synthetic applications, including pharmaceutical intermediates (**Figure 3.1b**, right).[8]

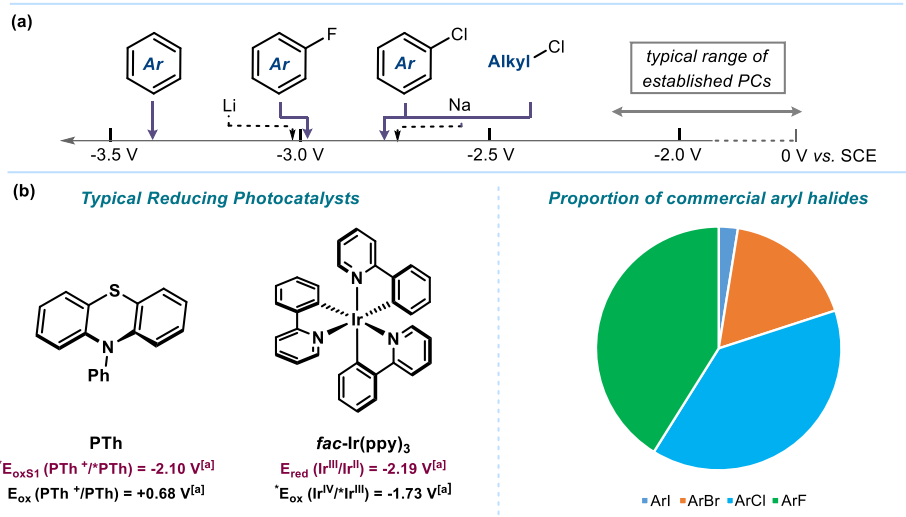

Figure 3.1. (**a**) Reduction potentials of redox-inert substrates and typical established photocatalysts; (**b**) Selected examples of photoredox catalysts and aryl halides. [a] Redox potentials reported as V vs. SCE.

---

[3] Shaw, M. H.; Twilton, J.; MacMillan, D. W. C. "Photoredox Catalysis in Organic Chemistry." *Org. Chem.* **2016**, *81*, 6898.

[4] Großkopf, J.; Kratz, T.; Rigotti, T.; Bach, T. "Enantioselective Photochemical Reactions Enabled by Triplet Energy Transfer." *Chem. Rev.* **2022**, *122*, 1626–1653.

[5] (a) Amii, H.; Uneyama, K. "C–F Bond Activation in Organic Synthesis." *Chem. Rev.* **2009**, *109*, 2119–2183; (b) Cheng, L. J.; Mankad, N. P. "C–C and C–X Coupling Reactions of Unactivated Alkyl Electrophiles Using Copper Catalysis". *Chem. Soc. Rev.* **2020**, *49*, 8036–8064; (c) Rabideau, P. W.; Marcinow, Z. "The Birch Reactions of Aromatic Compounds." *Organic Reactions*, **1992**, 1–334; (d) Yan, M.; Kawamata, Y.; Baran, P. S. "Synthetic Organic Electrochemical Methods Since 2000: On the Verge of a Renaissance." *Chem. Rev.* **2017**, *117*, 13230–13319.

[6] Tay, N. E. S.; Lehnherr, D.; Rovis, T. "Photons or Electrons? A Critical Comparison of Electrochemistry and Photoredox Catalysis for Organic Synthesis." *Chem. Rev.* **2022**, *122*, 2487–2649.

[7] Liu, X.; Dong, S.; Zhu, J.; Inoue, S. "Dialumene as a Dimeric or Monomeric Al Synthon for C–F Activation in Monofluorobenzene." *J. Am. Chem. Soc.* **2024**, *146*, 23591–23597.

[8] Grudzień, K.; Zlobin, A.; Zadworny, J.; Rybicka-Jasińska, K.; Sadowski, B. "Modern Photo- and Electrochemical Approaches to Aryl Radical Generation." *Org. Chem. Front.* **2024**, *11*, 5232–5277.

Their activation usually requires strong reducing agents such as alkali metals, low-valent transition-metal complexes, or electrochemical methods,[6] which often involve harsh conditions and generate undesired by-products. Developing photocatalysts capable of promoting these transformations under mild and sustainable conditions thus remains a significant goal in modern photochemistry.

Energy transfer (EnT) catalysis represents an alternative approach for activating organic molecules through triplet–triplet energy exchange.[9] Efficient triplet-sensitized processes require photocatalysts with suitably high triplet energies and sufficiently long triplet-state lifetimes to ensure productive energy transfer. Since the 1950s, spectroscopic studies have established the triplet energies of many common substrates, which generally exceed 50 kcal mol^{-1} (**Figure 3.2a)**.[10]

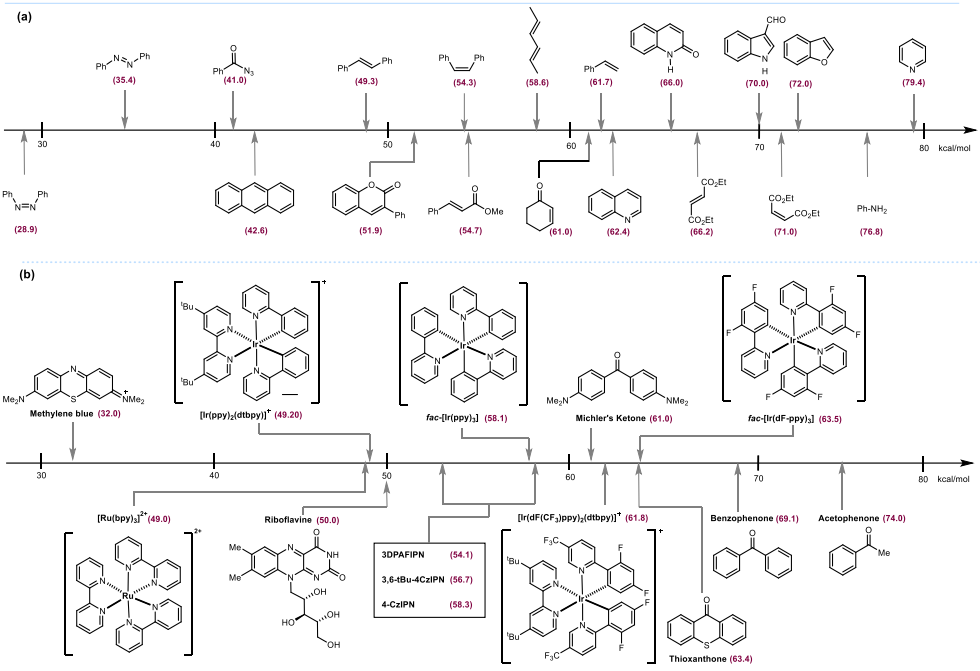

Figure 3.2. Triplet state energies (given in kcal/mol) of (**a**) selected organic substrates and (**b**) commonly used photosensitizers.

Although several organic molecules, such as benzophenone and acetophenone, exhibit high

---

[9] Zhou, Q. Q.; Zou, Y. Q.; Lu, L. Q.; Xiao, W. J. "Visible-Light-Induced Organic Photochemical Reactions through Energy-Transfer Pathways." *Angew. Chem. Int. Ed.* **2019**, *58*, 1586–1604.

[10] (a) Murov, S. L.; Charmichael, I.; Hug, G. L. Handbook of Photochemistry, Marcel Dekker Inc., New York, **1993**; (b) Strieth-Kalthoff, F.; James, M. J.; Teders, M.; Pitzer, L.; Glorius, F. "Energy Transfer Catalysis Mediated by Visible Light: Principles, Applications, Directions." *Chem. Soc. Rev.* **2018**, *47*, 7190–7202; (c) Dutta, S.; Erchinger, J. E.; Strieth-Kalthoff, F.; Kleinmans, R.; Glorius, F. "Energy Transfer Photocatalysis: Exciting Modes of Reactivity." *Chem. Soc. Rev.* **2024**, *53*, 1068–1089.

triplet energies, their short excited-state lifetimes often limit catalytic performance. Iridium-based complexes, including fac-[Ir(dF-ppy)$_3$] and [Ir(dF(CF$_3$)ppy)$_2$(dtbpy)], possess both high triplet energies and long lifetimes, but their use is restricted by cost and sustainability concerns. Among purely organic photosensitizers, thioxanthone remains the most prominent example with suitable triplet energy and lifetime (**Figure 3.2b**).

Although both mechanisms have been extensively exploited, photocatalysts capable of efficiently mediating *both* SET and EnT processes remain scarce.[11,12] Strong photoreductants suitable for SET typically possess low triplet energies, whereas effective triplet sensitizers often have poor redox activity.[13,14] Reconciling these contrasting properties within a single molecular framework represents a major challenge in photocatalyst design.

For this reason, the development of a *bifunctional photocatalyst* that combines strong reducing ability with high triplet energy under visible light excitation is highly desirable. The next section discusses representative examples of previously reported bifunctional photocatalysts and outlines the strategies employed to reconcile SET and EnT reactivity in a single molecular framework.

3.1.1 Bifunctional Metal-Based Photocatalysts

Transition-metal complexes have long served as versatile photocatalysts owing to their favorable photophysical characteristics,[15] including efficient intersystem crossing,[16] long-lived triplet excited states,[17] and tunable redox potentials.[18,19] These properties allow such complexes to mediate both SET and triplet–triplet energy transfer processes, positioning them as early examples of bifunctional photocatalysts.

---

[11] Glaser, F.; Wenger, O. S. "Recent Progress in the Development of Transition-metal Based Photoredox Catalysts." *Coord. Chem. Rev.* **2020**, *405*, 213129.

[12] Nikitas, N. F.; Gkizis, P. L.; Kokotos, C. G. "Thioxanthone: a powerful photocatalyst for organic reactions." *Org. Biomol. Chem.* **2021**, *19*, 5237–5253

[13] DiLuzio, S.; Mdluli, V.; Connell, T. U.; Lewis, J.; Van-Benschoten, V.; Bernhard, S. "High-Throughput Screening and Automated Data-Driven Analysis of the Triplet Photophysical Properties of Structurally Diverse, Heteroleptic Iridium(III) Complexes." *J. Am. Chem. Soc.* **2021**, *143*, 1179–1194.

[14] Dedeian, K.; Djurovich, P. I.; Garces, F. O.; Carlson, G.; Watts, R. "A New Synthetic Route to the Preparation of a Series of Strong Photoreducing Agents: fac Tris-Ortho-Metala ted Complexes of Iridium(III) with Substituted 2-Phenylpyridines." *Inorg. Chem.* **1991**, *30*, 1685–1687.

[15] Morselli, G.; Reber, C.; Wenger, O. S. "Molecular Design Principles for Photoactive Transition Metal Complexes: A Guide for "Photo-Motivated" Chemists." *J. Am. Chem. Soc.* **2025**, *147*, 11608–11624.

[16] Teegardin, K.; Day, J. I.; Chan, J.; Weaver, J. "Advances in Photocatalysis: A Microreview of Visible Light Mediated Ruthenium and Iridium Catalyzed Organic Transformations." *Org. Process Res. Dev.* **2016**, *20*, 1156−1163.

[17] Mills, I. N.; Porras, J. A.; Bernhard, S. "Judicious Design of Cationic, Cyclometalated Ir(III) Complexes for Photochemical Energy Conversion and Optoelectronics." *Acc. Chem. Res.* **2018**, *51*, 352−364.

[18] Förster, C.; Heinze, K. "Photophysics and photochemistry with Earth-abundant metals – fundamentals and concepts." *Chem. Soc. Rev.* **2020**, *49*, 1057–1070.

[19] Bevernaegie, R.; Wehlin, S. A. M.; Piechota, E. J.; Abraham, M.; Philouze, C.; Meyer, G. J.; Elias, B.; Troian-Gautier, L. "Improved Visible Light Absorption of Potent Iridium(III) Photo-oxidants for Excited-State Electron Transfer Chemistry." *J. Am. Chem. Soc.* **2020**, *142*, 2732−2737.

Among them, the benchmark complex $[Ru(bpy)_3]^{2+}$ remains a prototypical system exhibiting dual reactivity.[20,21] Its excited state can participate in *SET*-driven photoredox processes, as demonstrated by Hu and co-workers in the decarboxylative C(sp^3)–N coupling of redox-active esters with anilines (**Figure 3.3**).[22] Here, photoexcited $[Ru(bpy)_3]^{2+}$ reduces the redox-active ester **13** to generate an alkyl radical **IV** that subsequently undergoes copper-mediated amination. However, the moderate excited-state reduction potential (E^*_{red} = –0.81 V vs. SCE) limits its scope to relatively easy-to-reduce substrates.

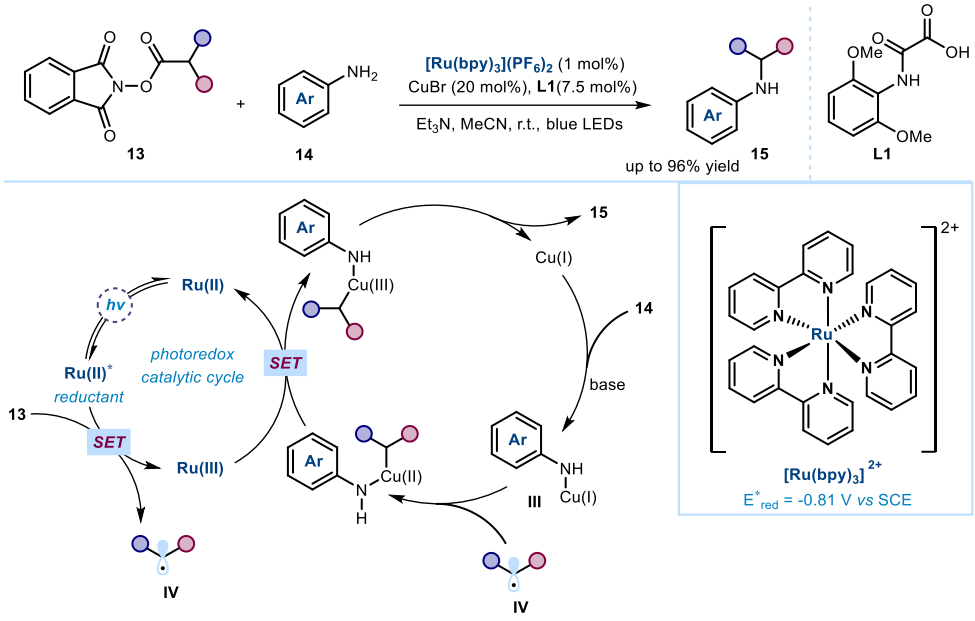

Figure 3.3. Photoredox reactivity of $[Ru(bpy)_3]^{2-}$ catalyst.

The same $[Ru(bpy)_3]^{2+}$ catalyst can also function as an *energy-transfer* photosensitizer. Kutal and co-workers first demonstrated its ability to mediate a [2+2] photocycloaddition of norbornadiene via EnT (**Figure 3.4a**).[23] Because the redox potentials of norbornadiene **16** lie outside the accessible range of $[Ru(bpy)_3]^{2+}$, this reaction proceeds exclusively through triplet energy transfer. Later, Yoon and co-workers exploited this EnT ability to achieve an

---

[20] Pitre, S. P.; McTiernan, C. D.; Vine, W.; Pucchio, R. D.; Grenier, M.; Scaiano, J. C. "Visible-Light Actinometry and Intermittent Illumination as Convenient Tools to Study Ru(bpy)$_3$Cl$_2$ Mediated Photoredox Transformations." *Sci. Rep.* **2015**, *5*, 16397.

[21] Schmitz, M.; Bertrams, M. S.; Sell, A. C.; Glaser, F.; Kerzig, C. "Efficient Energy and Electron Transfer Photocatalysis with a Coulombic Dyad." *J. Am. Chem. Soc.* **2024**, *146*, 25799–25812.

[22] Mao, R.; Frey, A.; Balon, J.; Hu, X. "Decarboxylative C(sp^3)–N Cross-coupling via Synergetic Photoredox and Copper Catalysis." *Nat. Catal.* **2018**, *1*, 120–126.

[23] Ikezawa, H.; Kutal, C.; Yasufuku, K.; Yamazaki, H. "Direct and Sensitized Valence Photoisomerization of a Substituted Norbornadiene. Examination of the Disparity between Singlet- and Triplet-state Reactivities." *J. Am. Chem. Soc.* **1986**, *108*, 1589–1594.

enantioselective intermolecular [2+2] photocycloaddition of 2′-hydroxychalcones **18** and styrenes **19** using a Lewis-acid-assisted strategy (**Figure 3.4b**).[24] Coordination of $Sc(OTf)_3$ to the chalcone substrate **18** lowered its triplet energy, enabling efficient excitation by $[Ru(bpy)_3]^{2+}$ and high enantioselectivity. These examples illustrate how a single Ru-based photocatalyst can switch between SET and EnT mechanisms depending on the energetic match with the substrate.

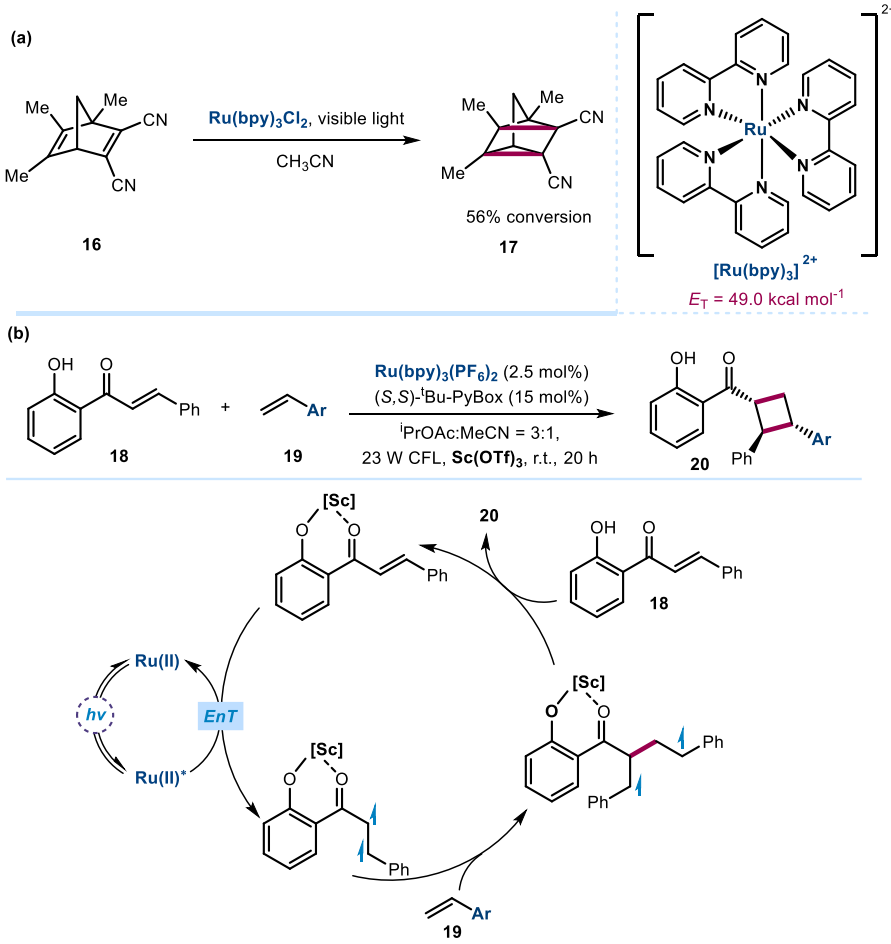

Figure 3.4. (**a**) Intramolecular [2+2] photocycloaddition of norbornadiene via an EnT catalysis. (**b**) Intermolecular [2+2] photocycloaddition reactions of 2'-hydroxychalcones.

Cyclometalated iridium complexes, such as $Ir(ppy)_3$, display an even broader range of

[24] (a) Miller, Z. D.; Lee, B. J.; Yoon, T. P. "Enantioselective Crossed Photocycloadditions of Styrenic Olefins by Lewis Acid Catalyzed Triplet Sensitization." *Angew. Chem. Int. Ed.* **2017**, *56*, 11891–11895; (b) Blum, T. R.; Miller, Z. D.; Bates, D. M.; Guzei, I. A.; Yoon, T. P. "Enantioselective Photochemistry Through Lewis Acid–Catalyzed Triplet Energy Transfer." *Science*. **2016**, *354*, 1391–1395.

bifunctional behavior due to their strong excited-state redox potentials and high triplet energies. In photoredox chemistry, Ir(ppy)$_3$ acts as a potent photoreductant (E^*_{red} = –1.73 V vs. SCE),[25] as shown in MacMillan's enantioselective α-benzylation of aldehydes **21** via an enamine radical pathway (**Figure 3.5**).

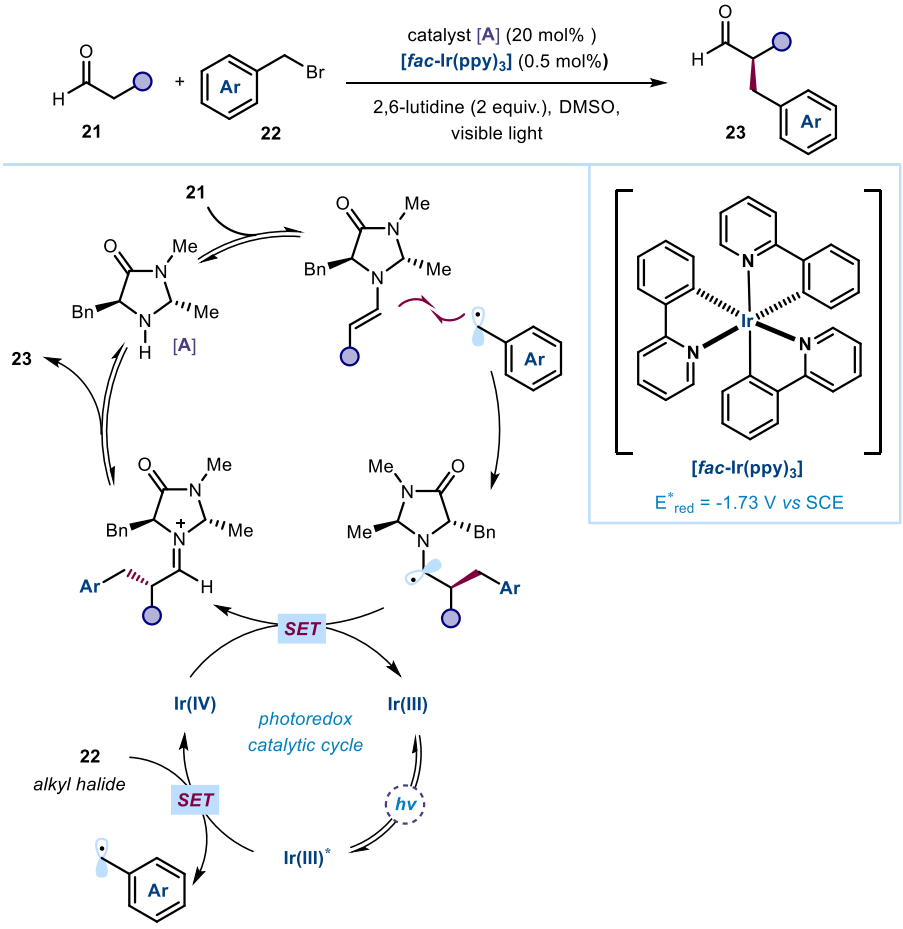

Figure 3.5. Ir(ppy)$_3$ in a SET-driven process.

The same catalyst can also operate via EnT. Weaver and co-workers reported an $E \rightarrow Z$ isomerization of cinnamyl amines **24** mediated by triplet energy transfer from Ir(ppy)$_3$ (**Figure 3.6a**),[26] while Brown's group used the same complex to promote visible-light-induced [2+2]

[25] Shih, H.W.; Vander Wal, M. N.; Grange, R. L.; MacMillan, D.W. C. "Enantioselective α-Benzylation of Aldehydes via Photoredox Organocatalysis." *J. Am. Chem. Soc.* **2010**, *132*, 13600–13603.

[26] Singh, K.; Staig, S. J.; Weaver, J. D. "Facile Synthesis of Z-Alkenes via Uphill Catalysis." *J. Am. Chem. Soc.* **2014**, *136*, 5275−5278.

cycloadditions of alkenylboronates **26** with alkenes **27** (**Figure 3.6b**).[27] These studies established Ir(ppy)$_3$ as a bifunctional photocatalyst capable of switching between SET and EnT manifolds. However, its moderate triplet energy ($E_T \approx 55$ kcal·mol^{-1}) confines its EnT activity to substrates with relatively low triplet energies, thereby limiting its general applicability.

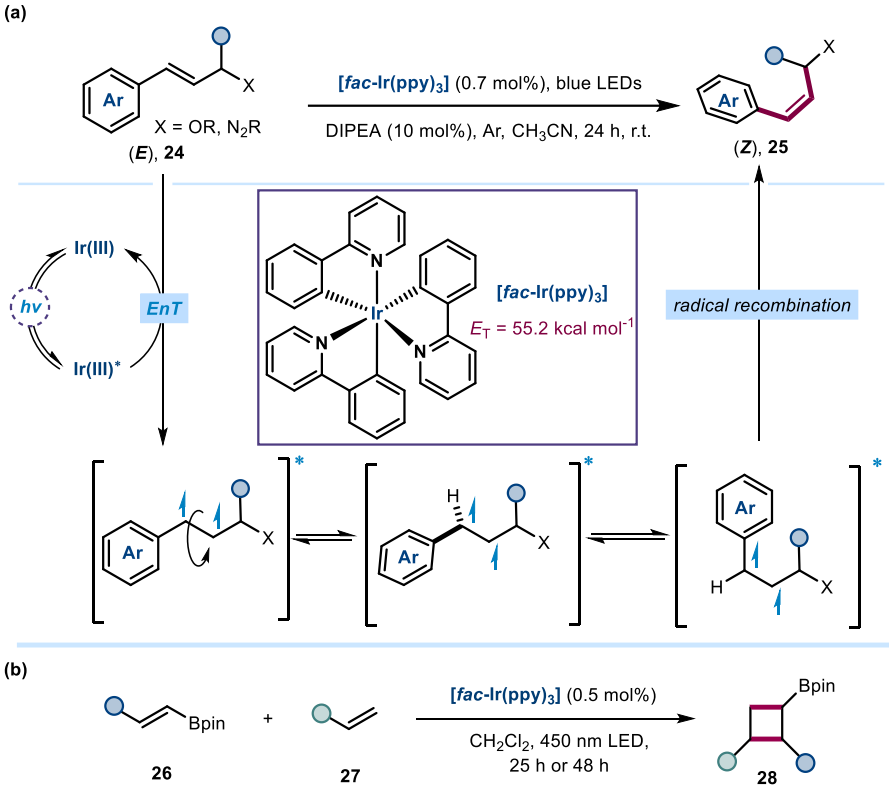

Figure 3.6. EnT reactivity of Ir(ppy)$_3$. (**a**) E → Z isomerization and (**b**) [2+2] photocycloaddition.

Structural modification of the iridium chromophore allows tuning the EnT power. For instance, Ir(dFppy)$_3$ ($E^*_{red} = -1.44$ V vs. SCE, $E_T = 63.5$ kcal·mol^{-1}) can catalyze both SET reductive and energy-transfer processes. Jiang and co-workers employed it in the annulation–alkynylation of alkenes through a visible-light-driven SET pathway (**Figure 3.7a**),[28] whereas Schindler's group demonstrated its EnT capacity in an intermolecular *aza-Paternò–Büchi*

[27] Liu, Y.; Ni, D.; Stevenson, B. G.; Tripathy, V.; Braley, S. E.; Raghavachari, K.; Swierk, J. R.; Brown, M. K. "Photosensitized [2+2]-Cycloadditions of Alkenylboronates and Alkenes." *Angew. Chem. Int. Ed.* **2022**, *61*, e202200725.

[28] Zhao, Q.; Hao, W.; Shi, H.; Xu, T.; Tu, S.; Jiang, B. "Photocatalytic Annulation–Alkynyl Migration Strategy for Multiple Functionalization of Dual Unactivated Alkenes." *Org. Lett.* **2019**, *21*, 9784–9789.

reaction between oximes **32** and alkenes **33** to give azetidines **34** (**Figure 3.7b**).[29]

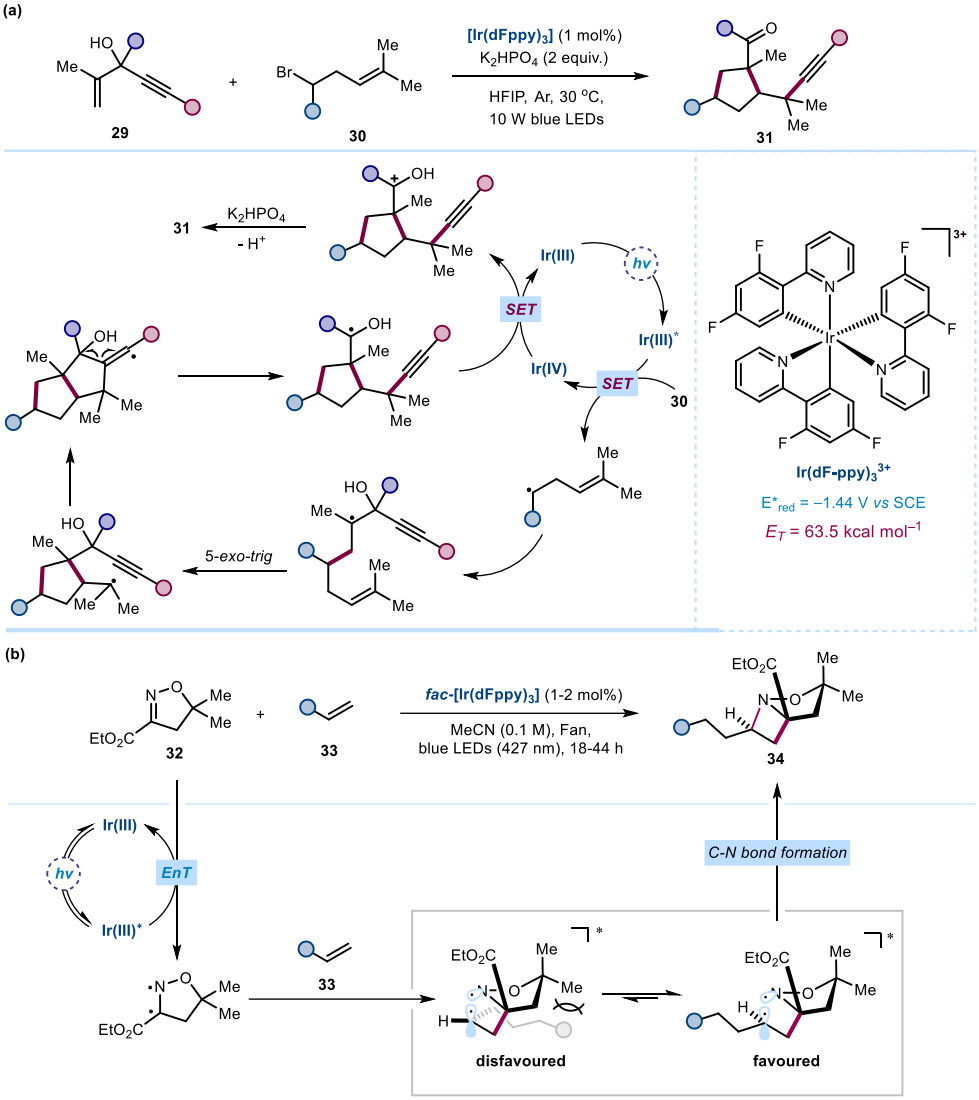

Figure 3.7. Ir(dFppy)$_3$. (**a**) SET reactivity of Ir(dFppy)$_3$ and (**b**) EnT reactivity of Ir(dFppy)$_3$.

Further examples of bifunctional photocatalysts include [Ir(dF(CF$_3$)ppy)$_2$(dtbbpy)]$^+$, which exhibits strong photoreducing ability (E[*Ir^{III}/Ir^{II}] = +1.21 V vs SCE) while maintaining high triplet energy. Hashmi and co-workers exploited the SET activity to reduce *gem*-difluoroalkenes **36** under visible light, forming fluoroalkenyl radicals that participate in cross-coupling reactions (**Figure 3.8a**).[30] Glorius later demonstrated its performance as a triplet

[29] Becker, M. R.; Wearing, E. R.; Schindler, C. S. "Synthesis of Azetidines via Visible-light-mediated Intermolecular [2+2] Photocycloadditions." *Nat. Chem.* **2020**, *12*, 898–905.

[30] Xie, J; Yu, J.; Rudolph, M.; Rominger, F.; Hashmi, A. S. K. "Monofluoroalkenylation of Dimethylamino Compounds through Radical–Radical Cross-Coupling." *Angew.Chem. Int. Ed.* **2016**, *55*, 9416–9421.

sensitizer in a dearomative cycloaddition of bicyclic azaarenes **38** and olefins **39**,[31] where coordination to a Lewis acid lowered substrate triplet energy, enabling efficient EnT activation (**Figure 3.8b**).

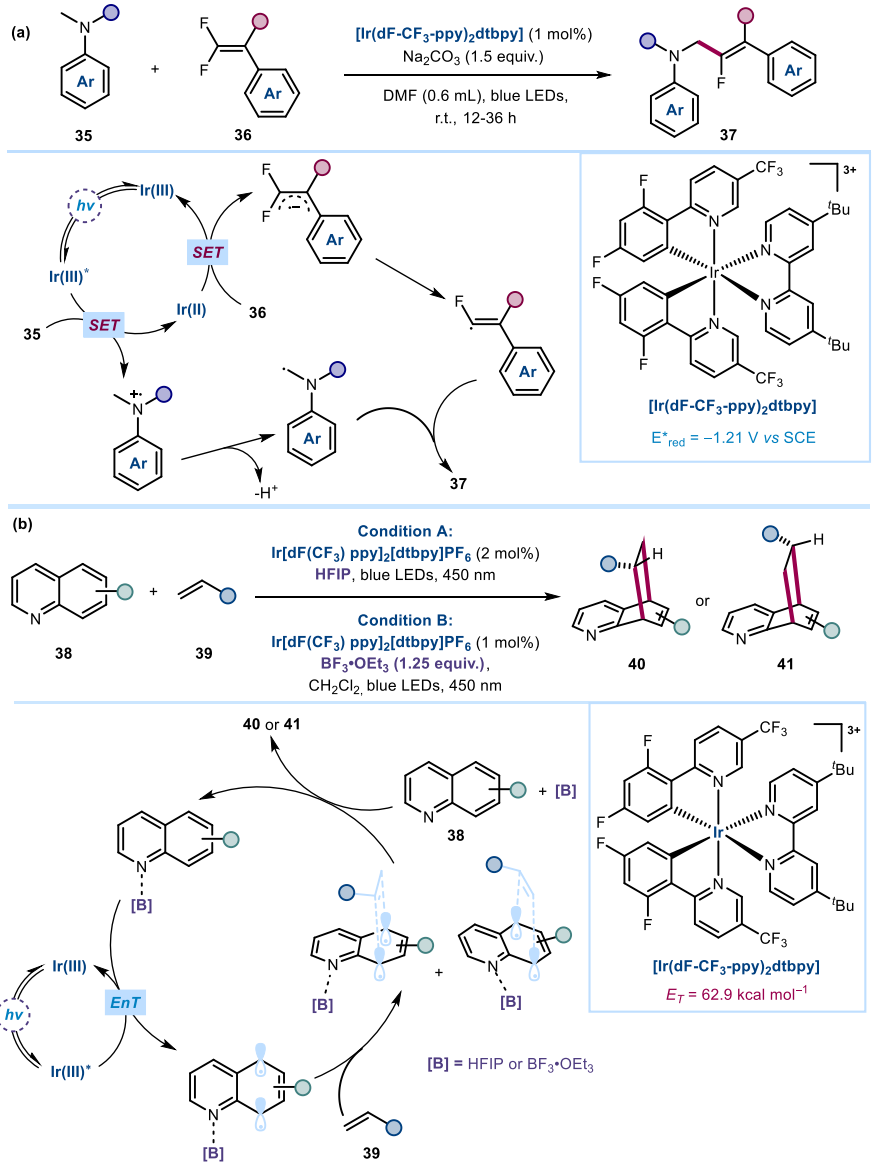

Figure 3.8. The reactivity of photocatalyst $[Ir(dF\text{-}CF_3\text{-}ppy)_2(dtbbpy)]^{3+}$. (**a**) SET reactivity and (**b**) EnT reactivity. HFIP: Hexafluoro-2-propanol.

[31] Ma, J.; Chen, S.; Bellotti, P.; Guo, R.; Schäfer, F.; Heusler, A.; Zhang, X.; Daniliuc, C.; Brown, M. K.; Houk, K. N.; Glorius, F. "Photochemical intermolecular dearomative cycloaddition of bicyclic azaarenes with alkenes." *Science.* **2021**, *371*, 1338–1345.

Beyond noble-metal systems, Wenger and co-workers introduced zinc(II) complexes with intraligand charge-transfer triplet states, capable of both EnT and photoinduced SET (**Figure 3.9**).[32] Although their reactivity remains moderate, these results highlight the potential of earth-abundant metals as sustainable bifunctional photocatalysts.

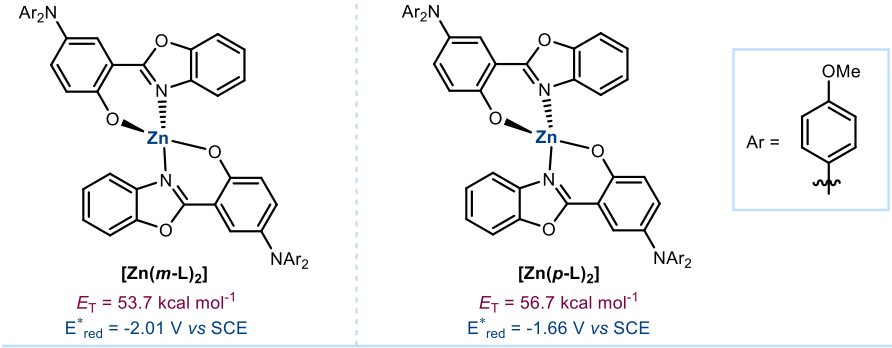

Figure 3.9. Zinc(II) Complexes with Triplet Charge-Transfer Excited States Enabling Energy-Transfer Catalysis, Photoinduced Electron Transfer

The bifunctional concept reached an important milestone with the development of iridium(III) isocyanoborato complexes, which uniquely combine strong photoreductive ability ($E^*_{red} = -2.42$ V vs. SCE) with high triplet energy (E_T = 68.9 kcal mol^{-1}).[33] These chromophores exhibit both potent SET and EnT reactivity under visible light, representing the most balanced bifunctional performance among known metal-based photocatalysts. Wenger and co-workers demonstrated their versatility across diverse transformations, including intramolecular [2+2] photocycloadditions of alkenes and carbonyls, [1,3]-sigmatropic alkyl shifts, and reductive dehalogenations of aryl halides (**Figure 3.10**). In these examples, substrates with reduction potentials around –2.0 V vs SCE[34] were efficiently activated, while high triplet energies enabled productive energy-transfer chemistry within the same catalytic system. These results illustrate how rational molecular design—through incorporation of strong-field isocyanoborato ligands—can simultaneously enhance redox and triplet properties, effectively reconciling SET and EnT reactivity within a single metal complex.

---

[32] Kübler, J. A.; Pfund, B.; Wenger, O. S. "Zinc(II) Complexes with Triplet Charge-Transfer Excited States Enabling Energy-Transfer Catalysis, Photoinduced Electron Transfer, and Upconversion." *JACS Au* **2022**, *2*, 2367–2380.

[33] Schmid, L.; Glaser, F.; Schaer, R.; Wenger, O. S. "High Triplet Energy Iridium(III) Isocyanoborato Complex for Photochemical Upconversion, Photoredox and Energy Transfer Catalysis." *J. Am. Chem. Soc.* **2022**, *144*, 963–976.

[34] Glaser, F.; Kerzig, C.; Wenger, O. S. "Sensitization-Initiated Electron Transfer via Upconversion: Mechanism and Photocatalytic Applications." *Chem. Sci.* **2021**, *12*, 9922−9933.

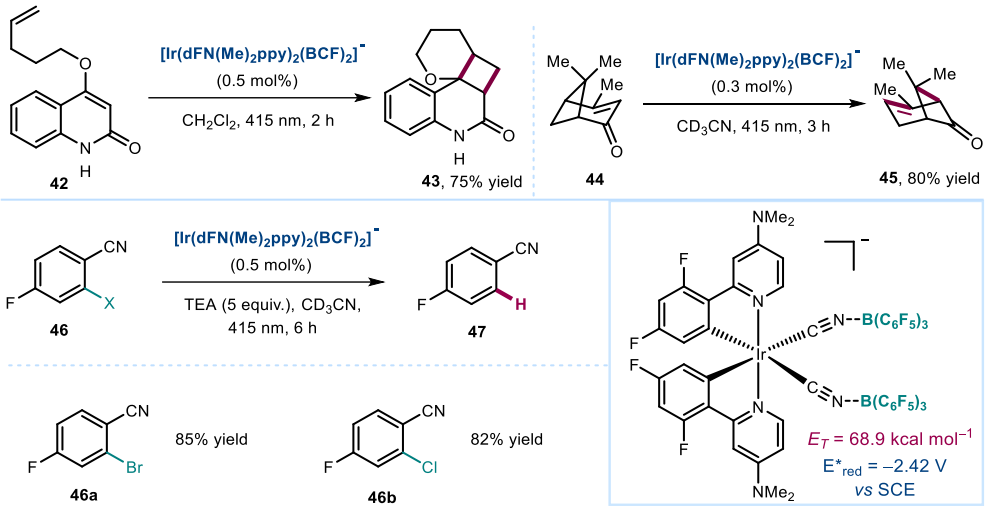

Figure 3.10. Iridium(III) isocyanoborato complex combining strong reducing power and high triplet energy for dual SET and EnT catalysis. TEA: Triethylamine.

Overall, transition-metal complexes—especially Ru(II), Ir(III), and Zn(II) derivatives—represent foundational examples of *bifunctional photocatalysts*. Their capacity to undergo both SET and EnT processes arises from long-lived triplet states and tunable excited-state energetics. However, their reliance on scarce metals and limited sustainability motivated the search for organic photocatalysts capable of delivering comparable dual reactivity under environmentally benign conditions.

3.1.2 Limitations of Organic Bifunctional Photocatalysts

Although transition-metal complexes have demonstrated genuine bifunctionality, the development of purely organic photocatalysts capable of efficiently mediating both SET and EnT processes remains far less advanced. Organic systems are attractive due to their low cost, structural tunability, and sustainability;[35,36] however, achieving the combination of strong redox activity and high triplet energy within a single organic scaffold has proven difficult.

Aromatic ketones, particularly *thioxanthone* (TXT) and its derivatives,[37,38] represent the most explored class of organic chromophores for dual photochemical reactivity.[39] In 2017, Ooi and

---

[35] Romero, N. A.; Nicewicz, D. A. "Organic Photoredox Catalysis." *Chem. Rev.* **2016**, *116*, 10075–10166.

[36] Vega-Peñaloza, A.; Mateos, J.; Companyó, X.; Escudero-Casao, M.; Dell'Amico, L. "A Rational Approach to Organo-Photocatalysis: Novel Designs and Structure-Property Relationships." *Angew. Chem. Int. Ed.* **2021**, *60*, 1082–1097.

[37] Elliott, D. L.; Kayal, S.; George, M. W.; Booker-Milburn, K. "Rational Design of Triplet Sensitizers for the Transfer of Excited State Photochemistry from UV to Visible." *J. Am. Chem. Soc.* **2020**, *142*, 14947–14956.

[38] Kang, W.; Li, B.; Zhao, Z.; Sun, S.; Feng, C.; Hu, K.; Houk, K. N.; Guo, H. "Generation of Thioxanthone Hydrogen Anion by Double Photoreduction and Uses for Catalytic Photoreductions." *ACS Catal.* **2023**, *13*, 13588–13596.

[39] (a) Recent studies suggest that other organic scaffolds may also enable dual SET and EnT reactivity. For example, 2,4,6-triarylpyrylium salts have shown such potential: Bao, L.; Cheng, J.; Wang, Z.; Chen, X. Y. "Pyrylium Salts Acting as Both Energy Transfer and Electron Transfer Photocatalysts for E → Z Isomerization of Activated Alkenes and

co-workers employed TXT as a photoredox catalyst for the reduction of 3,5-bis(trifluoromethyl)phenylacyloxyphthalimide **49**, enabling the imidation and acyloxylation of arenes **48** (**Figure 3.11**). The reaction proceeds through photoexcitation of TXT followed by intersystem crossing to its triplet state, which then engages in a reductive SET step. The electron-donating 4,4′-dimethoxy derivative displayed improved reducing power (E^*_{red} = –1.32 V vs. SCE) compared to TXT (E^*_{red} = –1.12 V vs. SCE), highlighting the tunability of this scaffold. However, the relatively low redox potential still limits the activation of more challenging substrates.

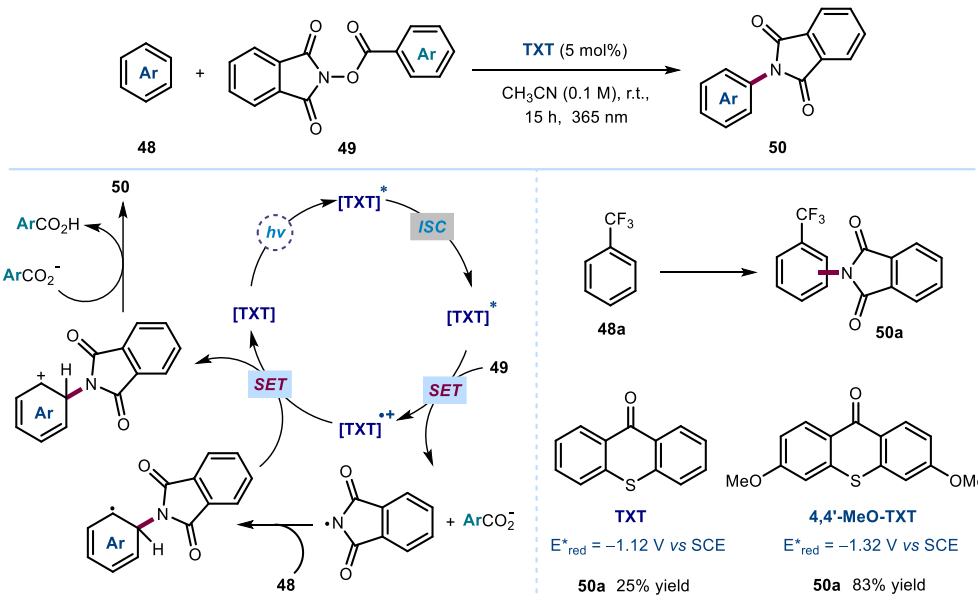

Figure 3.11. Thioxanthone with limited redox power.

Thioxanthone also serves as an efficient *triplet sensitizer*. In 2022, Glorius and co-workers demonstrated that TXT can activate coumarins **51** for [2π+2σ] photocycloadditions with bicyclo[1.1.0]butanes **52** via triplet–triplet energy transfer (**Figure 3.12**).[40] This strain-release-driven process, mediated by TXT (E_T = 63.4 kcal mol^{-1}), showcased its capacity for effective EnT catalysis.

Cyclization of Cinnamic or Biaryl Carboxylic Acids." *Org. Chem. Front.* **2022**, *9*, 648–659; (b) Additionally, (−)-riboflavin has been demonstrated to combine SET and EnT activation modes in a single catalytic sequence. Metternich, J. B.; Gilmour, R. "One Photocatalyst, n Activation Modes Strategy for Cascade Catalysis: Emulating Coumarin Biosynthesis with (−)-Riboflavin." *J. Am. Chem. Soc.* **2016**, *138*, 1040−1045.

[40] Kleinmans, R.; Pinkert, T.; Dutta, S.; Paulisch, T. O.; Keum, H.; Daniliuc, C. G.; Glorius, F. "Intermolecular [2π+2σ]-Photocycloaddition Enabled by Triplet Energy Transfer." *Nature*. **2022**, *605*, 477–482.

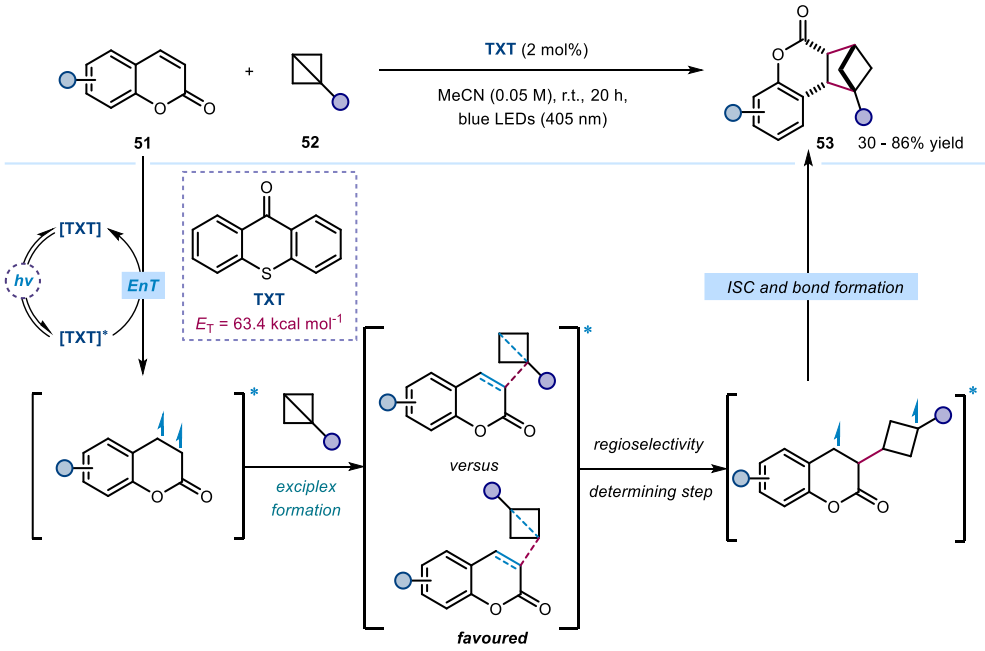

Figure 3.12. Thioxanthone as an efficient EnT catalyst

Overall, thioxanthone exemplifies the dual potential of organic photocatalysts, yet its moderate photoreductive power underscores the challenge of designing *truly bifunctional* organic systems.

3.2 Target of the Project: Design of Bifunctional 4-Hydroxycoumarin Photocatalysts

This project was motivated by the lack of examples of bifunctional organic photocatalysts capable of mediating both SET and EnT with high efficiency. In the course of our research on the functionalization of 4-hydroxycoumarins, we investigated the direct photoexcitation of 4-hydroxycoumarins under visible light. We discovered that *in situ* deprotonation of 3-substituted 4-hydroxycoumarins produces an anionic form that, when irradiated at 390 nm, reaches a highly reducing excited state capable of activating alkyl halides through SET (**Figure 3.13**). The details of this SET reactivity are described in Chapter II.

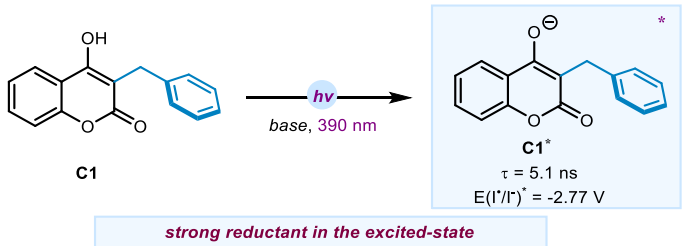

Figure 3.13. Singlet excited-state SET reactivity of **C1**.

In addition, a few early studies already indicated that 4-hydroxycoumarins could reach an excited triplet state and participate in light-driven transformations.[41, 42] In particular, Roantree[43] and Sharma[44] demonstrated that 4-hydroxycoumarin could be photoexcited to its triplet state under UV light, reacting with cyclohexene or oxygen to give characteristic photocyclization or oxidation products (**Figure 3.14a** and **3.14b**). Later, photophysical investigations by Esteves da Silva and co-workers confirmed that 4-hydroxycoumarin undergoes efficient intersystem crossing ($S_1 \rightarrow T$) and generates a long-lived triplet state with measurable phosphorescence (**Figure 3.14c**),[45] while recent data from Ye and colleagues indicated a high triplet energy of about 65.5 kcal mol^{-1}.[46] These observations highlight the intrinsic ability of 4-hydroxycoumarins to act as triplet high-energy donors.

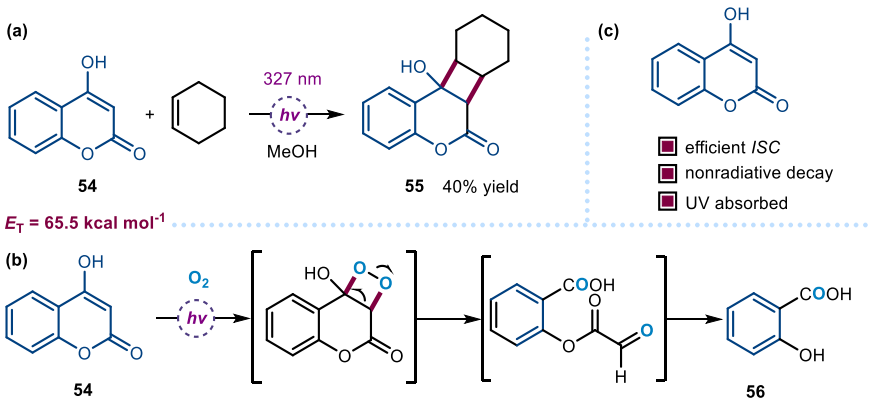

Figure 3.14. Seminal study for triplet state reactivity of 4-hydroxycoumarin.

Based on these findings, we envisioned that structural modification of the coumarin core could enable access to both strong reducing power and efficient triplet sensitization within the same organic framework. In particular, 3-thioaryl-4-hydroxycoumarins were designed to enhance light absorption and stabilize the photoexcited states. Upon deprotonation, the resulting anion can reach a highly reducing excited state under 390 nm irradiation, capable of promoting SET-driven reactions, while the neutral form retains a sufficiently high triplet energy ($E_T \approx 67$ kcal

---

[41] Kim, M.; Hong, S.; Jeong, J.; Hong, S. "Visible-Light-Active Coumarin- and Quinolinone-Based Photocatalysts and Their Applications in Chemical Transformations." *Chem. Rec.* **2023**, *23*, e202200267.

[42] Haywood, D. J.; Hunt, R. G.; Potter, C. J.; Reid, S. T. "Photochemical Transformations. Part 10. Photocycloaddition Reactions of 4-Hydroxycoumarin with Cycloalkenes." *J. Chem. Soc. Perkin Trans. 1* **1977**, 2458–2461.

[43] Hunt, R. G.; Potter, C. J.; Reid, S. T.; Roantree, M. L. "The Photoaddition of 4-Hydroxycoumarin and N-Methyl-4-hydroxyquinol-2-one to Cyclohexene." *Tetrahedron Lett.* **1975**, *16*, 2327–2330.

[44] Kuznetsova, N. A.; Kaliya, O. L. "The Photochemistry of Coumarins." *Russ. Chem. Rev.* **1992**, *61*, 683–696.

[45] Pinto da Silva, L.; Simkovitch, R.; Huppert, D.; Esteves da Silva, J. C. G. "Combined Experimental and Theoretical Study of the Photochemistry of 4- and 3-hydroxycoumarin." *J. Photochem. Photobiol. A Chem.* **2017**, *338*, 23–36.

[46] Chang, R.; Pang, Y.; Ye, J. "Divergent Photosensitizer Controlled Reactions of 4-Hydroxycoumarins and Unactivated Olefins: Hydroarylation and Subsequent [2 + 2] Cycloaddition." *Angew. Chem. Int. Ed.* **2023**, *62*, e202309897.

mol⁻¹) for efficient EnT activation.

This dual photoreactivity under visible light inspired the design of a new family of bifunctional organic photocatalysts capable of promoting both reductive and energy-transfer transformations, including the activation of redox-inert substrates through C–F and C–Cl bond cleavage, or EnT-mediated reactions like *E/Z* isomerization and [2+2] photocycloadditions (**Figure 3.15**).

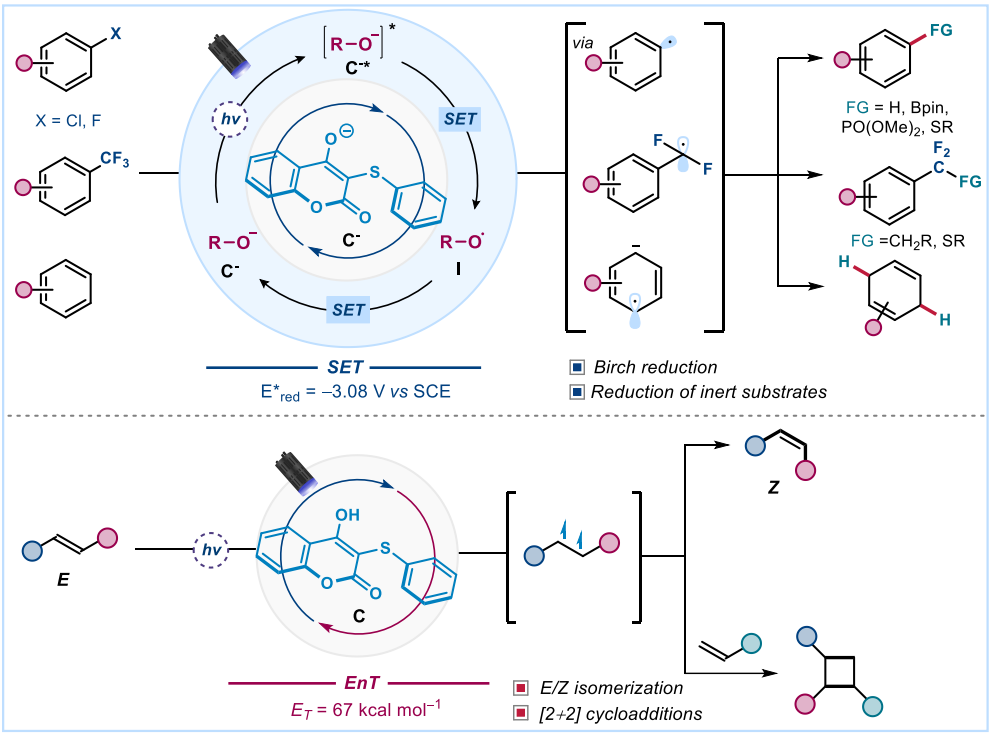

Figure 3.15. The dual reactivity of our new bifunctional photocatalyst.

Overall, the goal of this project is to establish 4-hydroxycoumarin derivatives as a new class of cost-effective, metal-free photocatalysts capable of combining SET and EnT reactivity within a single molecular architecture.

3.3 Results and Discussion

3.3.1 Developing Efficient Single-Electron Transfer Catalysts

We first examined the ability of the hydroxycoumarin **C1** and the newly designed 3-thioaryl-4-hydroxycoumarin-based catalysts **C2**–**C5** as strong SET reductants upon excitation. To evaluate the reducing power of our organic catalysts, we tested the hydrodechlorination of 4-chloroanisole (**1a**, E_{red} = −2.9 V vs. SCE) and the more challenging defluorination of 4-fluoroanisole (**1b**, E_{red} < −3.0 V vs. SCE), both requiring highly negative redox potentials. Reactions were conducted with 10 mol% of catalyst **C**, Cs_2CO_3 as the base (3 equiv.), γ-terpinene as the hydrogen donor, and under irradiation by 390 nm light in *N*-methyl-2-

pyrrolidone (NMP, **Table 3.1**). The 3-benzyl-4-hydroxycoumarin catalyst **C1**, which we used in our previous project discussed in Chapter II as a substrate, has an excited-state reduction potential (E^*_{red}) upon deprotonation of −2.85 V vs. SCE.[47] **C1** yielded 20% of product **2a** from **1a** but was ineffective for reducing **1b**. To enhance the photocatalyst's redox power, we replaced the benzyl fragment on the hydroxycoumarin framework in **C1** with a thioaryl group (catalysts **C2**–**C5**). This modification was designed to leverage the sulfur lone pair to enhance electronic conjugation within the catalyst,[48] thus improving electron delocalization and stabilizing a charge-transfer (CT) state for more efficient redox activity.[49] The resulting 3-thiophenyl-4-hydroxycoumarin catalyst **C2** exhibited remarkable SET activity, affording the desired product **2a** in 98% yield from 4-chloroanisole **1a** and 50% yield from the fluoro substrate **1b**, successfully activating both C(sp^2)-Cl and C(sp^2)-F bonds.

Table 3.1 Reaction optimization of chloroanisole **1a** or fluoroanisole **2a**

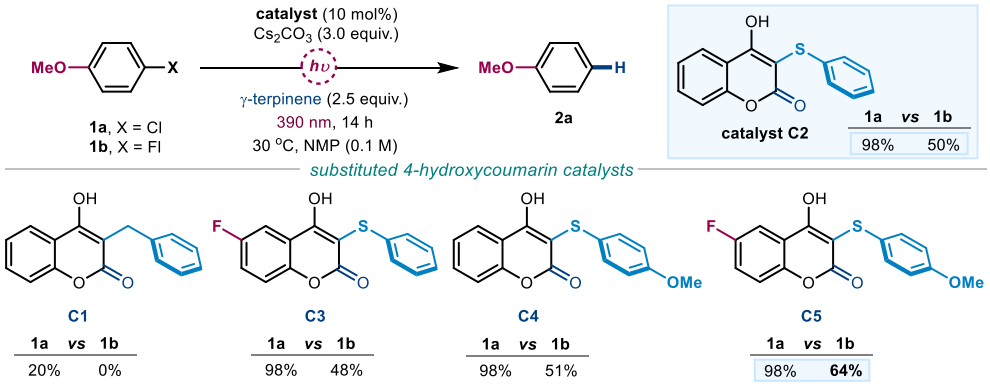

Control reactions using catalyst C2 (from **1a**)

entry	*deviation*	[%] yield **2a**	*entry*	*deviation*	[%] yield **2a**
1	none	**98**	7	Na_2CO_3 instead of Cs_2CO_3	82
2	no γ-terpinene	20	8	K_2CO_3 instead of Cs_2CO_3	93
3	*i*-Pr_2NEt or HCO_2Na instead of γ-terpinene	<35	9	TMG instead of Cs_2CO_3	28
4	no catalyst, no light or no base	0	10	DIPEA instead of Cs_2CO_3	trace
5	DMSO instead of NMP	0	11	Pyridine instead of Cs_2CO_3	trace
6	CH_3CN instead of NMP	16	12	Under air instead of N_2	0

Reactions performed on a 0.2 mmol scale. The yield of **2a** was determined by ^{1}H NMR analysis of the crude mixture using dimethylbromide as the internal standard.

[47] Mallik, S.; Sfreddo, E.; Wang, H.; Melchiorre, P. Radical Pathways for 2,4-Chromandione Synthesis via Photoexcitation of 4-Hydroxycoumarins. *Chem. Sci.* **2025**, *16*, 124–129.

[48] Wang, S.; Wang, H.; König, B. "Light-Induced Single-Electron Transfer Processes involving Sulfur Anions as Catalysts." *J. Am. Chem. Soc.* **2020**, *142*, 5165–5173.

[49] (a) Fukuzumi, S.; Kotani, H.; Ohkubo, K.; Ogo, S.; Tkachenko, N. V.; Lemmetyinen, H. "Electron-Transfer State of 9-Mesityl-10-methylacridinium Ion with a Much Longer Lifetime and Higher Energy Than That of the Natural Photosynthetic Reaction Center." *J. Am. Chem. Soc.* **2004**, *126*, 1600–1601; (b) McCarthy, B. G.; Pearson, R. M.; Lim, C.-H.; Sartor, S. M.; Damrauer, N. H.; Miyake, G. M. "Structure-Property Relationships for Tailoring Phenoxazines as Reducing Photoredox Catalysts." *J. Am. Chem. Soc.* **2018**, *140*, 5088–5101; (c) Bortolato, T.; Simionato, G.; Vayer, M.; Rosso, C.; Paoloni, L.; Benetti, E. M.; Sartorel, A.; Leboeuf, D.; Dell'Amico, L. "The Rational Design of Reducing Organophotoredox Catalysts Unlocks Proton-Coupled Electron-Transfer and Atom Transfer Radical Polymerization Mechanisms." *J. Am. Chem. Soc.* **2023**, *145*, 1835–1846.

Control experiments showed that the reaction performed worse in the absence of γ-terpinene (**Table 3.1**, entry 2), while alternative hydrogen donors, such as *i*-Pr_2NEt and sodium formate, led to moderate results (entry 3). Importantly, the absence of Cs_2CO_3 completely inhibited the reactivity (entry 4). Replacing NMP with other solvents, such as DMSO or CH_3CN, resulted in a significant decrease in yield (entries 5-6). Other carbonate bases, such as Na_2CO_3 and K_2CO_3, remained effective but gave slightly reduced yields (80% and 90%, respectively, entries 7-8), whereas organic bases (e.g., pyridine, *N*,*N*-diisopropylethylamine, and 1,1,3,3-tetramethylguanidine) failed to promote the reaction (entries 9-11). We also confirmed that the presence of the catalyst and light was essential for the reaction to occur (entry 4).

We then explored further catalyst modifications (catalysts **C3**–**C5**) to evaluate whether better results could be obtained in the reduction of fluorine substrate **1b**. Catalyst **C5**, featuring an electron-donating methoxy group on the thiophenyl scaffold and an electron-withdrawing fluorine atom on the coumarin core, exhibited enhanced efficiency in the photoreduction of **1b** compared to the simpler catalyst **C2** (**Table 3.1**). This observation suggests that a push-pull effect, by stabilizing charge-separated states, may enhance the redox activity of our photocatalysts.[50]

3.3.2 Mechanistic Insights Into SET Activity and Charge-Transfer State Formation

To understand the photocatalytic SET performance of our catalysts, we conducted both experimental and computational studies. Treatment of catalyst **C2** with Cs_2CO_3 (3 equiv.) in CD_3CN rapidly and quantitatively generated the electron-rich anion **C2**$^-$, as confirmed by ^1H NMR analysis (see **Section 3.5.19** in the Experimental Section for details). Absorption spectroscopic analysis (**Figure 3.16a**, see also **Section 3.5.17.1** in the Experimental Section) revealed that catalyst **C2** lacks significant absorption in the visible region. Deprotonation with Cs_2CO_3 to form **C2**$^-$ induced a minimal bathochromic shift, extending absorption to ~390 nm (the excitation wavelength used in this study) though the extinction coefficient remained low (ε_{390} = 81 M^{-1} cm^{-1} at 1 mM). Upon excitation at 354 nm of anion **C2**$^-$ in CH_3CN (*in situ*-generated by mixing **C2** with Cs_2CO_3), an emission maximum at 445 nm was detected, confirming that **C2**$^-$ could access an electronically excited state (**Figure 3.16b**). From the overlap of normalized UV-visible absorption and emission spectra, the 0−0 transition energy ($E_{0,0}$) was determined to be 3.35 eV at 370 nm. Next, electrochemical studies using cyclic voltammetry revealed that anion **C2**$^-$ exhibited an irreversible oxidation peak at +0.65 V vs

[50] Ahn, M.; Kim, M.-J.; Cho, D. W.; Wee, K. R. Electron Push-Pull Effects on Intramolecular Charge Transfer in Perylene-Based Donor-Acceptor Compounds. *J. Org. Chem.* **2021**, *86*, 403–413.

Ag/AgCl in CH_3CN (**Figure 3.16c**). Using the Rehm–Weller formalism,[51] the redox potential of the excited state of anion **C2**$^-$ (E(**I**/**C2**$^{-*}$)) was estimated to be −2.78 V vs SCE, confirming its strong reducing capability upon excitation. Further experimental evidence from Stern–Volmer quenching experiments (see **Section 3.5.17.6** and **Figure 3.47** for details) demonstrated that the fluorescence of excited **C2**$^-$ was quenched by 4-chloroanisole **1a** (K_{SV} = 1.5 × 10^{-3} M^{-1}; k_q = 5.0 x 10^5 M^{-1} s^{-1}), corroborating its potential for productive SET reactivity. Similar experiments were performed for photocatalysts **C3**–**C5**, and the results are reported in **Section 3.5.17** of the Experimental Section.

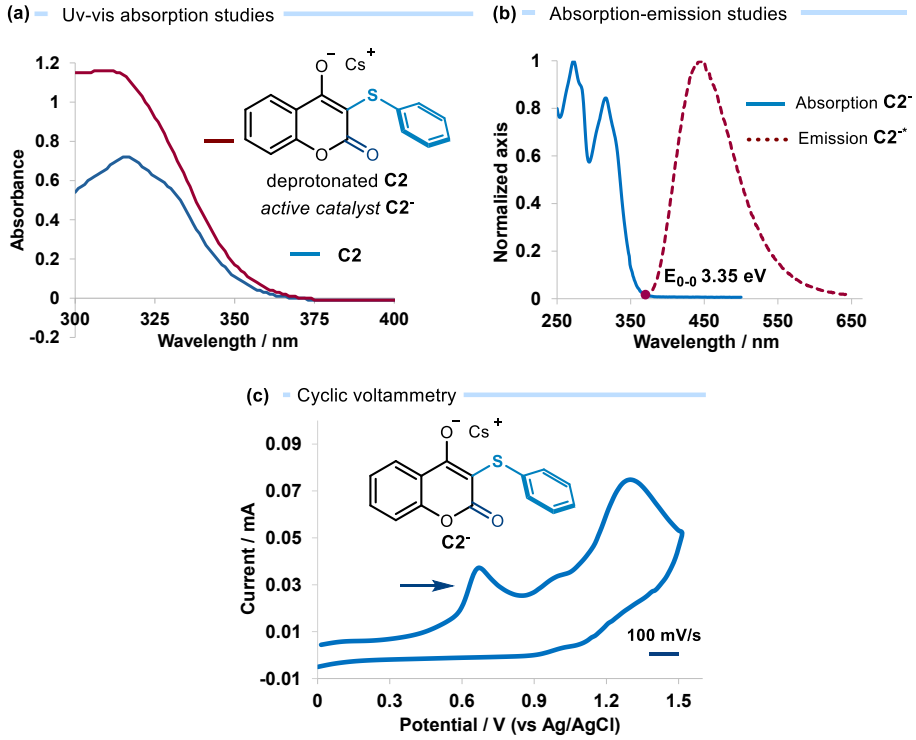

Figure 3.16. (**a**) UV–vis absorption spectra of catalyst **C2** and the corresponding anion **C2**$^-$ (formed in situ treating **C2** with 3 equiv. of Cs_2CO_3) in CH_3CN (10^{-4} M). (**b**) Emission of the excited anion **C2**$^{-*}$ in CH_3CN (formed in situ treating **C2** with Cs_2CO_3) upon irradiation at 354 nm and its intercept at 370 nm with the normalized absorption spectrum, with a 0–0 transition energy ($E_{0,0}$) of 3.35 eV. (**c**) Cyclic voltammetry measurements of the deprotonated catalyst anion **C2**$^-$ (oxidation onset) carried out in CH_3CN vs. Ag/AgCl at a scan rate of 100 mV s^{-1}. Estimated redox potential vs. SCE in CH_3CN.

Lastly, we determined the quantum yield (Φ) of the photochemical dechlorination using catalyst **C2**, γ-terpinene and Cs_2CO_3, which was measured to be as low as 0.13, suggesting

[51] Farid, S.; Dinnocenzo, J. P.; Merkel, P. B.; Young, R. H.; Shukla, D.; Guirado, G. "Reexamination of the Rehm–Weller Data Set Reveals Electron Transfer Quenching That Follows a Sandros–Boltzmann Dependence on Free Energy." *J. Am. Chem. Soc.* **2011**, *133*, 11580–11587.

that a radical chain mechanism is unlikely (see **Section 3.5.16** for details).

Based on the photophysical studies and control experiments described in **Figure 3.16** and **Table 3.1**, we propose the mechanism depicted in **Figure 3.17**, in which the electron-rich anion $\mathbf{C}^-$, formed *in situ* by deprotonation of catalyst **C**, would reach a highly reducing excited state ($\mathbf{C}^{-}$*****) under light irradiation. SET activation of a difficult-to-reduce electron-rich C(sp^2)–X substrate **1** would generate an aryl radical. γ-Terpinene, serving as a hydrogen atom donor, is expected to quench this aryl radical via hydrogen-atom transfer (HAT), yielding the reduced product **2**. The resulting cyclohexadienyl radical **II** would then undergo either SET or HAT[52] with the radical intermediate **I**, thereby regenerating the catalyst and completing the catalytic cycle.

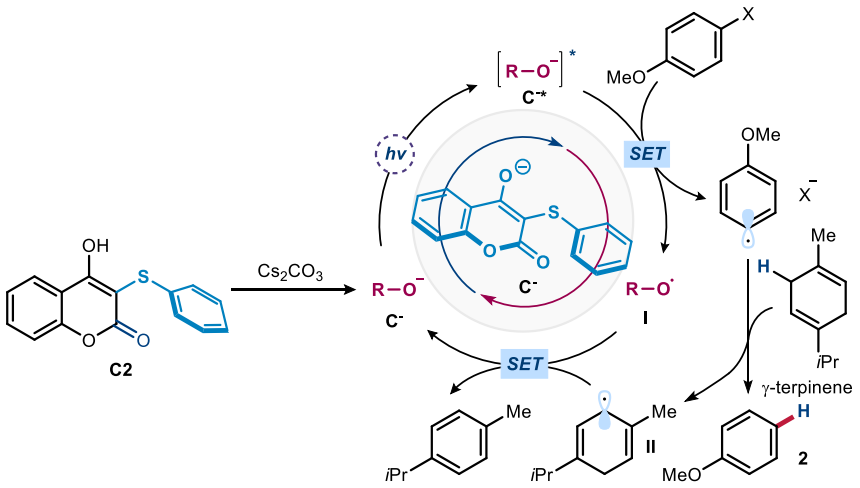

Figure 3.17. Proposed mechanism for the reduction of aryl halides **1**.

We then focused on the rationalization of the photoredox behavior of our catalysts **C**. Our experiments demonstrated that replacing the benzyl substituent in catalyst **C1** with the thiophenyl fragment in catalysts **C2** and **C5** significantly enhanced photoreductive performance. We therefore used a combination of photophysical data and computational investigations to rationalize the enhanced SET function of **C2** and **C5** (**Figure 3.18**). Photophysical characterization revealed that catalysts **C2** and **C5** exhibited similar singlet excited-state lifetimes (3.0 ns for deprotonated **C2** and 3.4 ns for deprotonated **C5**) as catalyst **C1** (5.1 ns). However, catalysts **C2** and **C5** displayed a more pronounced charge-transfer (CT) state,[50,53] as indicated by the increased Stokes shifts compared to **C1**. Given that the singlet

---

[52] A HAT path from the cyclohexadienyl radical **II** that reduces the hydroxycoumarin radical **I** to turnover catalyst **C** cannot be excluded, see: de Pedro Beato, E.; Mazzarella, D.; Balletti, M.; Melchiorre, P. "Photochemical Generation of Acyl and Carbamoyl Radicals Using a Nucleophilic Organic Catalyst: Applications and Mechanism Thereof." *Chem. Sci.* **2020**, *11*, 6312–6324.

[53] Chen, T.; Zheng, L.; Yuan, J.; An, Z.; Chen, R.; Tao, Y.; Li, H.; Xie, X.; Huang, W. Understanding the Control of Singlet-Triplet Splitting for Organic Exciton Manipulating: A Combined Theoretical and Experimental Approach. *Sci. Rep.* **2015**, *5*, 10923.

excited-state lifetimes and redox potentials of the excited states are comparable (**Figure 3.18a**, redox potential of the excited anion **C5**$^{-}$* estimated as −3.08 V vs. SCE), this suggests that the enhanced performance of **C2** and **C5** is not primarily due to thermodynamic differences but rather kinetic factors. The greater stabilization of the CT state in **C2** and **C5** may contribute to a more efficient SET process due to more stable excited-state dynamics and electron-transfer kinetics.[47-50]

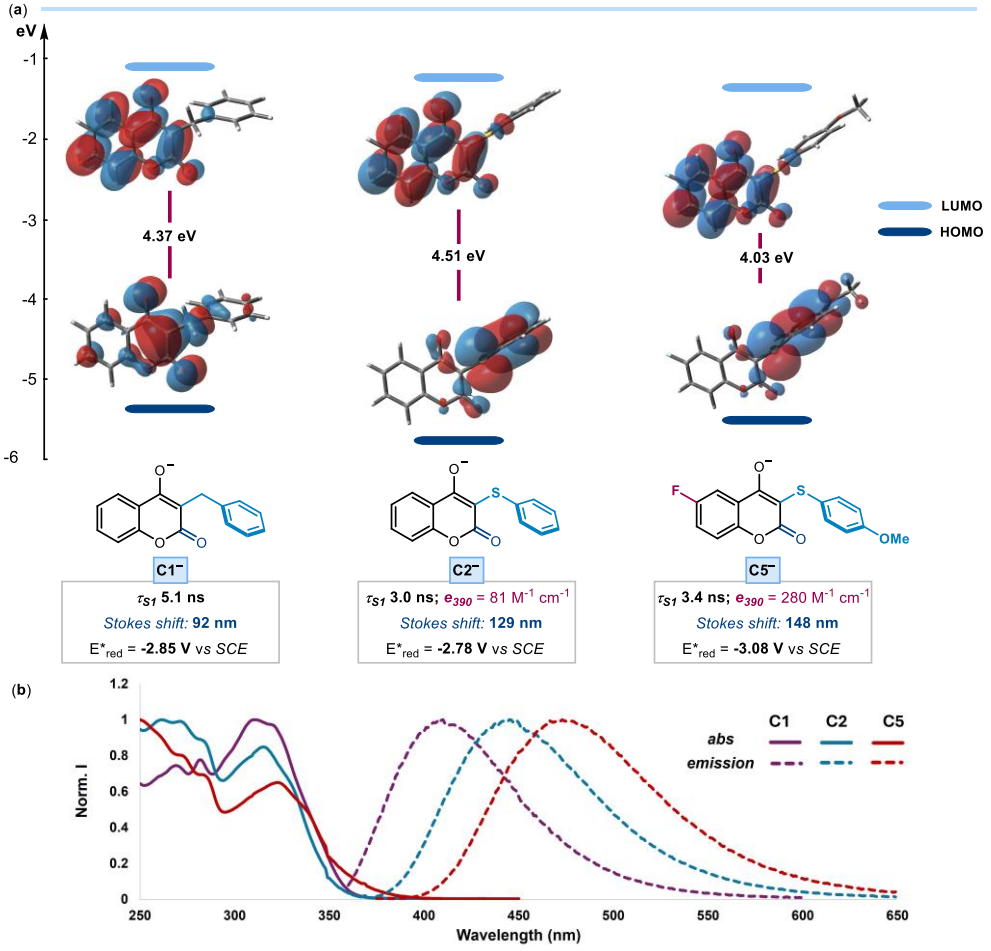

Figure 3.18. (a) DFT-calculated HOMO-LUMO orbitals for the deprotonated catalysts **C1**, **C2**, and **C5**, along with their experimentally measured photophysical properties; calculations were carried out at B3LYP/6-31+G** level of theory. τ_{S1} denotes the singlet excited-state lifetime, ε_{390} is the molar extinction coefficient at 390 nm (1 mM concentration), the Stokes shift refers to the difference in wavelength between the maxima of absorption and emission spectra of the deprotonated catalysts, and E^{*}_{red} indicates the excited-state reduction potentials. **(b)** Absorption and emission spectra of the deprotonated catalysts **C**$^{-}$ upon laser excitation at 354 nm (10^{-4} M solutions in CH_3CN obtained by mixing **C1**, **C2**, or **C5** in the presence of 3 equiv. of Cs_2CO_3).

To better understand the influence of the substituents on the photocatalyst scaffold, one of my colleagues (Dr. Bixiao Li) performed DFT calculations at the B3LYP/6-31+G** level of

theory, using the PCM solvent model to account for solvation effects. Time-dependent DFT (TDDFT) calculations revealed that the primary electronic transition ($S_0 \rightarrow S_1$) for all deprotonated catalysts **C1**–**C5** was governed by the HOMO-LUMO transition, with notable differences across the series (see **Figure 3.18a**, and **Section 3.5.20** in Experimental Section for details). Computational studies showed that in **C1**, the HOMO was predominantly localized on the carbonyl group of the hydroxycoumarin core, limiting electronic communication within the catalyst. In contrast, the incorporation of a thiophenyl substituent in **C2** shifted the HOMO to the thiophenyl ring, lowering its energy by 0.33 eV and enhancing electronic delocalization. This structural modification facilitated the formation of a more stabilized CT state, as corroborated by the observed Stokes shift differences of **C2** and **C5**. Further computational studies revealed that the introduction of additional substituents in **C5**, specifically a fluorine electron-withdrawing group on the hydroxycoumarin core and a methoxy electron-donating group on the thiophenyl fragment, lowered the HOMO-LUMO gap by 0.48 eV and further increased the Stokes shift. Overall, these studies, combined with the experimental data, support the conclusion that the enhanced CT state stabilization in **C2** and **C5** is key to their superior SET properties and improved catalytic performance.

To further validate our design strategy, we also computationally screened all possible permutations of MeO and F substituents across the X and Y positions, which confirmed that the substitution pattern in **C5** provides the most favorable redshift and push–pull characteristics (see **Section 3.5.20** in Experimental Section for details).

3.3.3 Further Synthetic Applications via SET Activation

To fully explore the applicability of our organophotocatalytic system, we focused on the SET activation of aryl halides characterized by highly negative reduction potentials ($E_{red} < -3.0$ V vs. SCE) and high bond dissociation energies (~125 ± 2 kcal/mol). To enable the SET reducing power of our system, we used catalyst **C2** in the presence of Cs_2CO_3 (3 equiv.). **C2** was chosen due to its low cost and easy accessibility; however, when its performance was insufficient, we evaluated catalyst **C5** as an alternative. We first examined a series of fluoroanisole derivatives, which underwent efficient reductive dehalogenation to afford the corresponding anisoles **2a-c** in good yields (**Figure 3.19**). To further assess the catalytic efficiency of **C2**, we extended the study to both electron-rich and electron-deficient chlorides. These substrates, known for their resistance to SET reduction,[54] were successfully converted into the desired hydrochlorination products **2a, 2d-h**, achieving high yields. In cases where lower yields were observed, a simple switch to catalyst **C5** led to significantly improved outcomes (e.g., **2c** and **2h**). Importantly, the high yield of products **2g** and **2h** demonstrates the compatibility of our

[54] Wu, S.; Schiel, F.; Melchiorre, P. A "General Light-Driven Organocatalytic Platform for the Activation of Inert Substrates." *Angew. Chem. Int. Ed.* **2023**, *62*, e202306364.

catalyst with heteroaromatic chlorides. The versatility of our catalytic system was further demonstrated by the successful reductive detosylation of *N*,*N*-diphenyl-*p*-toluenesulfonamide and *N*-(4-methoxy-phenyl)-4-methyl-benzenesulfonamide, affording products **2i** and **2j** in high yield (**Figure 3.19**).[55] On the other hand, substrates containing readily reducible functional groups, such as vinyl, formyl, polyfluoro, and carbonyl or pyridine substituents, were not reactive.

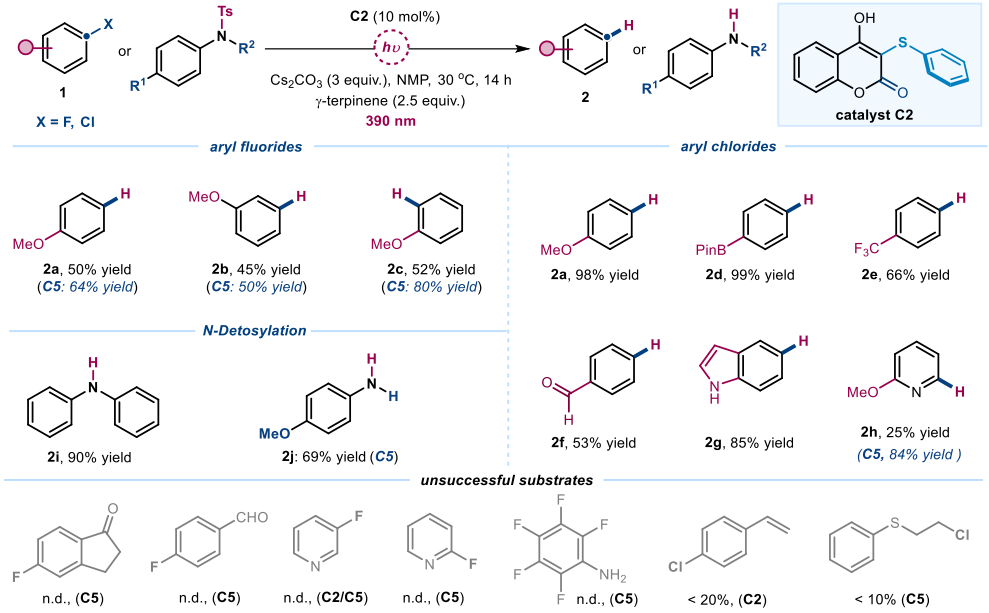

Figure 3.19. Synthetic applications via SET activation: reductive dehalogenation of aryl fluorides and chlorides and *N*-detosylation of selected amine substrates. Experiments performed on a 0.2 mmol scale. Yields of products **2** were determined by ^{1}H NMR analysis using dimethylbromide as an internal standard, except for **2g**, **2i**, and **2j**, which represent the yields of the isolated, purified product.

The synthetic utility of our platform was further demonstrated by intercepting the aryl radicals generated upon catalyst-mediated reductive cleavage of aryl chlorides (**Figure 3.20**).

[55] MacKenzie, I. A.; Wang, L.; Onuska, N. P. R.; Williams, O. F.; Begam, K.; Moran, A. M.; Dunietz, B. M.; Nicewicz, D. A. "Discovery and characterization of an acridine radical photoreductant." *Nature* **2020**, *580*, 76–80.

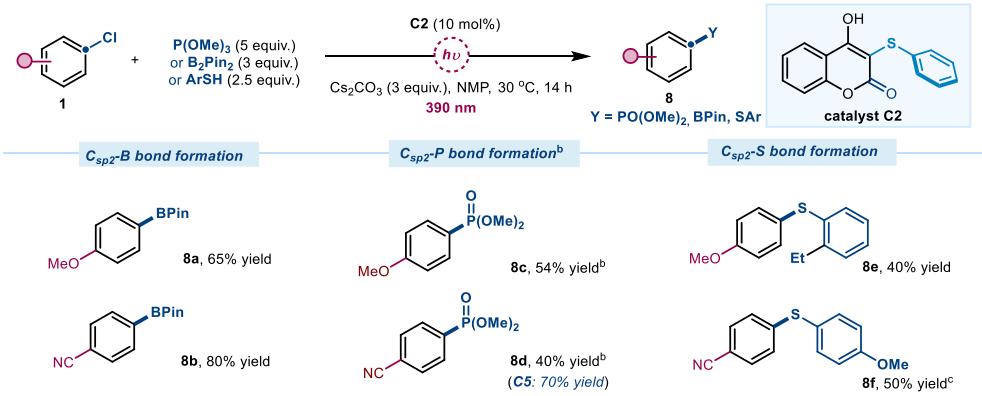

Figure 3.20. Photocatalytic borylation, phosphorylation, and thiolation of aryl chlorides performed on a 0.2 mmol scale. (**a**) The yields refer to isolated product **8**. (**b**) Performed using HCO_2Na (1 equiv.) instead of γ-terpinene. (c) tBuONa used instead of C_2CO_3.

Specifically, the use of bis(pinacolato)diboron (B_2pin_2) and trimethyl phosphite ($P(OMe)_3$) enabled efficient formation of C(sp^2)–B and C(sp^2)–P bonds within products **8a-b**[56] and **8c-d**,[57] respectively. C(sp^2)–S bond formation was also achieved by reacting aryl chlorides and aryl thiols, which afforded the target products **8e–f**. The experiments in **Figure 3.20** were performed using electron-rich (*para*-MeO) and electron-poor (*para*-CN) aryl chlorides, chosen as model substrates to demonstrate the feasibility of the process regardless of the electronic nature of the radical precursors.

In another application, catalyst **C2** was effective in the selective mono-defluorination of trifluorotoluene, achieved via SET reduction (**Figure 3.21**).[58] The resulting aryl-CF_2· radical was efficiently trapped with thiophenol, providing a streamlined approach to CF_2–S bond formation (product **8g**). Our catalyst's ability to efficiently reduce $PhCF_3$ (E_{red} = –3.04 V vs. SCE) was also applied in radical-mediated C–C bond formation via addition to unactivated olefins (**Figure 3.21**). In contrast to previous methods that required elevated temperatures,[59] our system operates smoothly at room temperature, delivering product **8h**. Also 1,3-bis(trifluoromethyl)benzene (E_{red} = –2.07 V vs. SCE) could be readily activated via SET to yield product **8i**.

---

[56] Zhang, L.; Jiao, L. Visible-Light-Induced Organocatalytic Borylation of Aryl Chlorides. *J. Am. Chem. Soc.* **2019**, *141*, 9124–9128.

[57] Xu, J.; Cao, J.; Wu, X.; Wang, H.; Yang, X.; Tang, X.; Toh, R. W.; Zhou, R.; Yeow, E. K. L.; Wu, J. Unveiling Extreme Photoreduction Potentials of Donor-Acceptor Cyanoarenes to Access Aryl Radicals from Aryl Chlorides. *J. Am. Chem. Soc.* **2021**, *143*, 13266–13273.

[58] Xu, J.; Liu, J.-W.; Wang, R.; Yang, J.; Zhao, K.-K.; Xu, H.-J. Construction of C–X (X = S, O, Se) Bonds via Lewis Acid-Promoted Functionalization of Trifluoromethylarenes. *ACS Catal.* **2023**, *13*, 7339–7346.

[59] Vogt, D. B.; Seath, C. P.; Wang, H.; Jui, N. T. Selective C-F Functionalization of Unactivated Trifluoromethylarenes. *J. Am. Chem. Soc.* **2019**, *141*, 13203–13211.

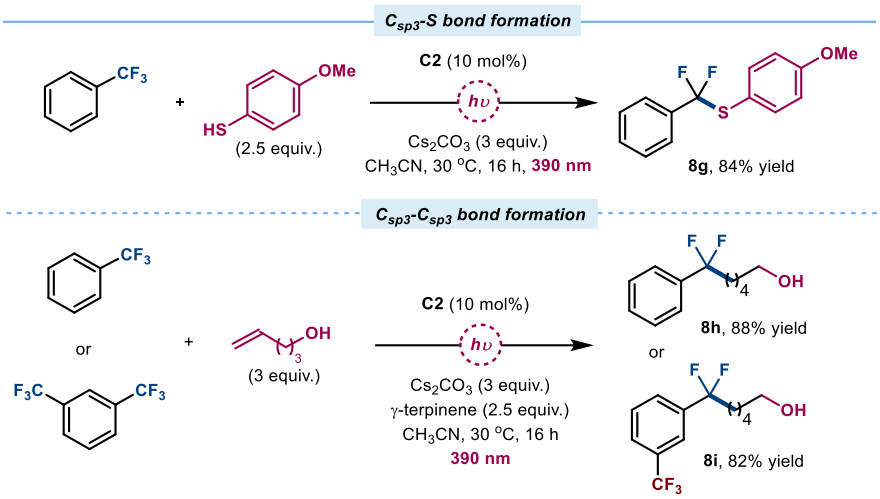

Figure 3.21. Selective mono-defluorination of trifluorotoluene followed by thiophenol trapping, yielding CF_2–S bond formation. The reaction performed on a 0.2 mmol scale with yields refer to isolated product **8**.

We also evaluated the capability of catalyst **C2** to drive light-induced Birch reductions of unactivated arenes (**Figure 3.22a**).[54,60] This transformation is particularly difficult due to the absence of leaving groups, which often leads to unproductive back-electron transfer. Our organic catalyst enabled the activation of naphthalene, affording the corresponding dihydro product in good yield (**9a**). In the case of anthracene-9-carbonitrile, the reaction proceeded via decyanation followed by Birch reduction (**9b**). As for more challenging substrates, such as *N*-methyl indole and benzofurane, the use of catalyst **C5** proved effective to achieve appreciable yields (adducts **9c-d**). We then showcased the versatility of our catalyst in driving radical cyclizations (**Figure 3.22b**). The chloro-substrate **10a** was successfully activated to afford 2,3-dehydrogenated benzofuran **11a**,[61] while the reductive imino cyclization from **10b** smoothly led to product **11b**. Finally, we used catalyst **C2** to promote a three-component difunctionalization of *para*-methoxy styrene with 4-cyano-chlorobenzene and 2,2,6,6-tetramethylpiperidin-1-ol (TEMPO-H), delivering product **12** (**Figure 3.22c**).[62] Overall, these results highlight the potential of our catalytic system for promoting diverse and complex SET-mediated radical transformations.

---

[60] Chatterjee, A.; König, B. Birch-Type Photoreduction of Arenes and Heteroarenes by Sensitized Electron Transfer. *Angew. Chem. Int. Ed.* **2019**, *58*, 14289–14294.

[61] Chmiel, A. F.; Williams, O. P.; Chernowsky, C. P.; Yeung, C. S.; Wickens, Z. K. "Non-innocent Radical Ion Intermediates in Photoredox Catalysis: Parallel Reduction Modes Enable Coupling of Diverse Aryl Chlorides." *J. Am. Chem. Soc.* **2021**, *143*, 10882–10889.

[62] Liang, K.; Liu, Q.; Shen, L.; Li, X.; Wei, D.; Zheng, L.; Xia, C. "Intermolecular oxyarylation of olefins with aryl halides and TEMPOH catalyzed by the phenolate anion under visible light." *Chem. Sci.* **2020**, *11*, 6996–7002.

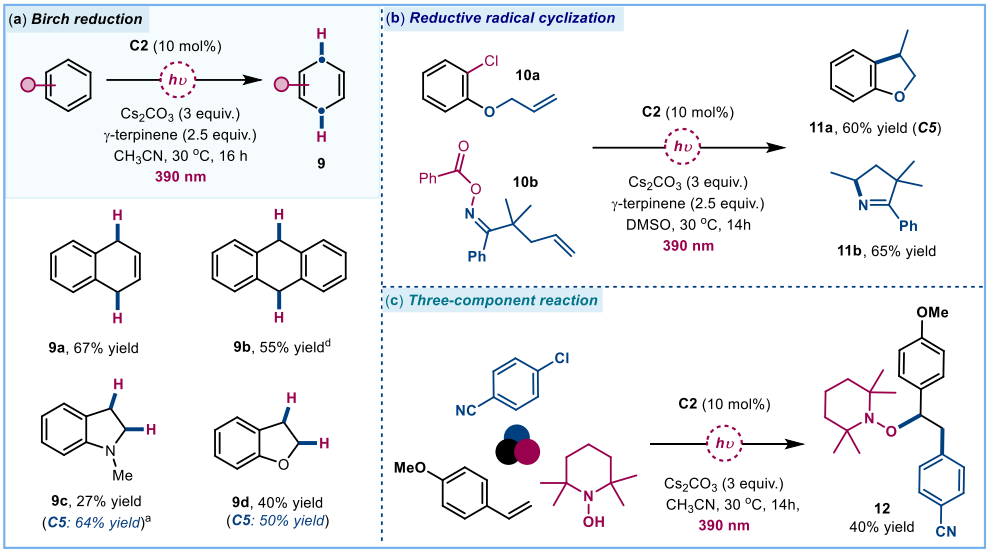

Figure 3.22. (**a**) Light-induced Birch reductions of unactivated arenes. (**b**) Radical cyclizations. (**c**) Three-component radical difunctionalization. Reactions performed on a 0.2 mmol scale using photocatalyst **C2** or **C5** (10 mol%) in a PhotoRedOx Box TCTM reactor under illumination by a Kessil lamp (max 52 W, λmax = 390 nm). Yields of products **9** were determined by ^{1}H NMR analysis using dimethylbromide as an internal standard, unless otherwise noted. Yields of products **9c**, **11**, and **12** refer to isolated materials after purification.

3.3.4 Developing Efficient Energy Transfer Catalysts

To evaluate the potential of our newly developed 3-thiophenyl-4-hydroxycoumarin-based compounds **C2**–**C5** to also serve as effective energy transfer catalysts, we first examined their ability to promote the *E*–*Z* photoisomerization[63] of methyl fumarate *E*-**3a** (E_T = 66.2 kcal/mol) to methyl maleate *Z*-**3a** (E_T = 71.0 kcal/mol, **Table 3.2**). The high triplet energy of methyl fumarate *E*-**3a** was selected to challenge our catalysts, pushing them to operate under conditions where a high triplet energy and long-lived excited states are crucial for driving the transformation. The reactions were performed in CH_3CN using 10 mol% of the EnT catalyst **C** and under 370 nm light irradiation. Conducting the reaction in the presence of 3 equiv. of Cs_2CO_3, previously used for SET activation, did not provide any *E*/*Z* isomerization (entry 1). In contrast, performing the reaction without any base afforded high selectivity for the desired product *Z*-**3a**, yielding an *E*:*Z* ratio of 8:92 (entry 2). Given this observation, the neutral forms of other catalysts were tested; however, catalysts **C3**–**C5** proved much less effective (entries 3-5). Finally, control experiments, conducted in the absence of either catalyst or light (entry 6), confirmed the necessity of both. In general, the neutral EnT catalysts performed worse under 390 nm irradiation—used to trigger SET processes— likely due to the poorer absorption

[63] Neveselý, T.; Wienhold, M.; Molloy, J. J.; Gilmour, R. Advances in the E → Z Isomerization of Alkenes Using Small Molecule Photocatalysts. *Chem. Rev.* **2022**, *122*, 2650–2694.

at this wavelength (see **Figure 3.29** in the **Experimental Section** for details).

Table 3.2 Reaction optimization for photoisomerization of *E*-methyl fumarate (**3a**)

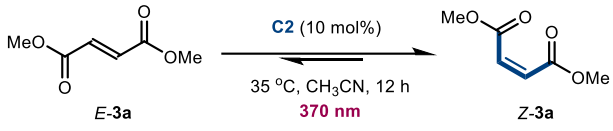

entry	deviation	*E*:*Z*
1	Cs_2CO_3 (3 equiv.)	99:1
2	none	**8:92**
3	**C3** instead of **C2**	36:64
4	**C4** instead of **C2**	79:21
5	**C5** instead of **C2**	32:68
6	no catalyst or no light	> 91:9

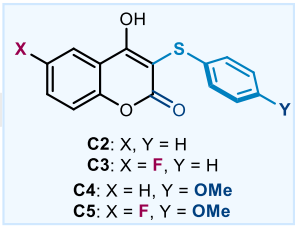

The *E*/*Z* ratio of **3a** was determined by ^{1}H NMR analysis of the crude mixture.

To rationalize these observations, we investigated the photophysical properties of catalysts **C2**–**C5** in their neutral forms, conducting studies in the absence of any base (**Figure 3.23a**). The triplet-state lifetimes and triplet energies were determined from emission studies in a 77 K frozen matrix (**Figure 3.23b** shows data for catalyst **C2**; see **Figure 3.46** in the Experimental Section for other studies). Catalyst **C2** exhibited a triplet energy E_T of 67.0 kcal/mol and a triplet-state lifetime of 9 μs.

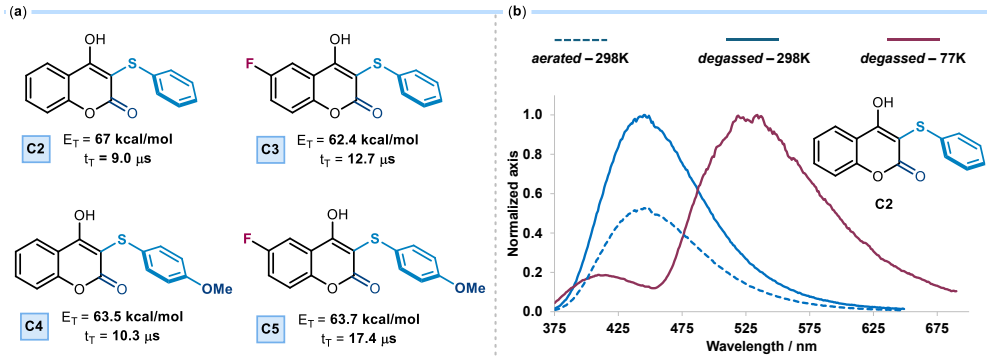

Figure 3.23. (**a**) Relevant photophysical properties of neutral catalysts **C2**–**C5**. (**b**) Normalized emission spectra of catalyst **C2** (10^{-4} M solution in CH_3CN): blue line represents the spectrum in degassed, deaerated CH_3CN at room temperature; dashed blue line represents the spectrum in aerated CH_3CN at room temperature; red line represents the spectrum in a 77 K solid matrix of degassed CH_3CN.

The presence of a triplet excited state was further confirmed by comparing the emission spectra of **C2** under degassed and aerated conditions at room temperature (**Figure 3.23b**, blue vs. dashed blue line), where oxygen quenching indicated the involvement of a long-lived triplet excited state. As for catalysts **C3**–**C5**, which were not effective in promoting *E*/*Z* isomerization, this was likely due to their lower triplet energies (E_T ranging from 62.4 to 63.7

kcal/mol), which may be insufficient to effectively activate *E*-**3a** via EnT sensitization.

To rationalize the difference in EnT activity between the neutral and deprotonated forms of catalyst **C2** in the photoisomerization of dimethyl fumarate *E*-**3a** (entries 1 & 2 in **Table 3.2**), we performed Stern–Volmer fluorescence quenching studies using *E*-**3a** as the quencher (**Figure 3.24a**, also see **section 3.5.17.6** for details). The deprotonated catalyst **C2**$^{-}$ displayed linear quenching behavior (K_{SV} = 5.3 × 10^{-2} M^{-1}), while GC-MS analysis confirmed the formation of dimethyl succinate, the reduced product derived from **3a** (see **Figure 3.50** in the Experimental Section for details), suggesting that a photoinduced SET mechanism is operative in the presence of a base. This is in line with the reduction potential of *E*-**3a** (E_{red} = –1.55 V vs Ag/AgCl),[64] which renders SET thermodynamically feasible for **C2**$^{-}$. In contrast, the neutral catalyst **C2** exhibited a non-linear, upward-curved and complex quenching profile (**Figure 3.24b**), which can be attributed to triplet–triplet EnT processes.[65] These studies therefore suggest that a mechanistic shift from EnT to SET takes place upon deprotonation of the catalyst.

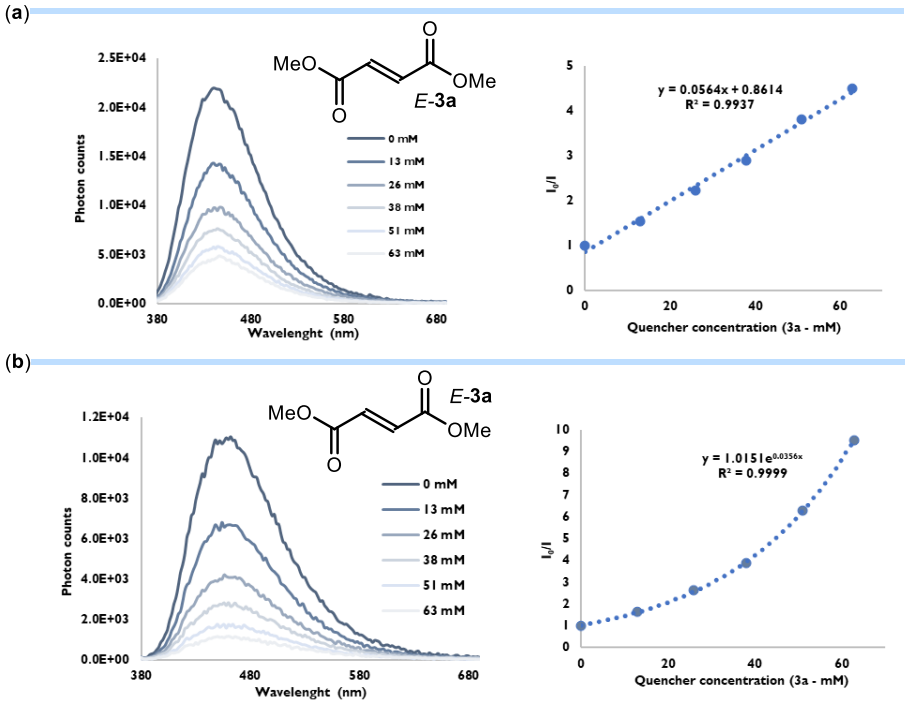

Figure 3.24. (**a**) Stern-Volmer fluorescence quenching studies of deprotonated **C2**$^{-}$ with **3a.** (**b**) Stern-Volmer fluorescence quenching studies of **C2** with **3a.**

[64] Doherty, A. P.; Scott, K. The Electrochemical Reduction of Dimethyl Maleate and Dimethyl Fumarate. *J. Electroanal. Chem.* **1998**, *442*, 35–40.

[65] Gehlen, M. H. The Centenary of the Stern-Volmer Equation of Fluorescence Quenching: From the Single Line Plot to the SV Quenching Map. *J. Photochem. Photobiol. C* **2020**, *42*, 100338.

Next, we explored the reactivity of various *E*-olefins **3** in the *E*/*Z* photoisomerization using the neutral catalyst **C2** (**Figure 3.25**). An unsymmetrical trisubstituted *E*-keto ester was isomerized to the corresponding *Z*-**3b** in good yield with high selectivity (97:3 *Z*/*E* ratio). The low 53:47 *Z*/*E* ratio observed for fumaronitrile **3c** is consistent with previous literature reports.[66] This result can be explained by the fact that both *E* and *Z* isomers of **3c** have a similar triplet energy of ≈ 60 kcal/mol, thus resulting in an approximately equilibrated ratio of isomers at the photostationary state.[66]

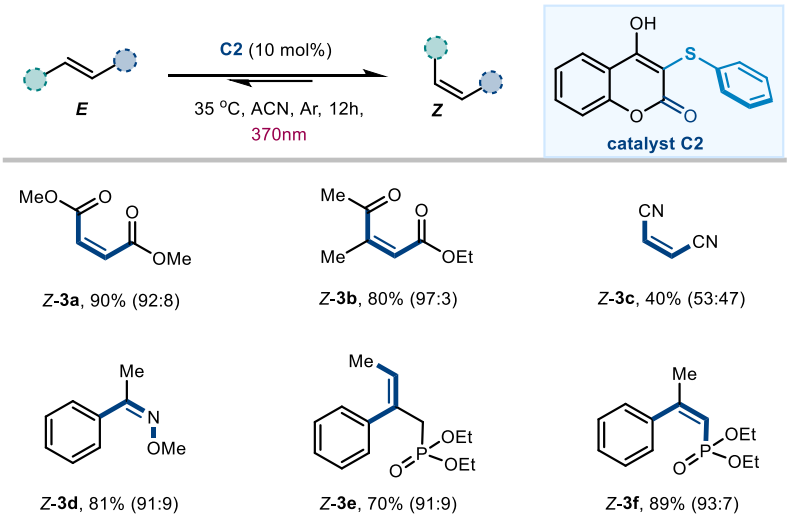

Figure 3.25. Exploring the substrate scope of the energy transfer-mediated E/Z photoisomerization; reactions performed on a 0.2 mmol scale with 10 mol % of catalyst **C2** in dry, degassed CH_3CN (1 mL). Yields refer to the isolated Z isomers of products **3**, with the Z/E ratio indicated in parentheses.

We then evaluated the EnT-based isomerization of the oxime derivative **3d**.[67] The recovered high selectivity (91:9 *Z*/*E* ratio) is congruent with the large triplet energy difference between the *E*-**3d** (59 kcal/mol) and *Z*-**3d** (72 kcal/mol)[68] isomers, which aligns well with the catalyst's triplet energies, enabling selective isomerization. To further extend the scope of photoisomerization, we investigated styrene derivatives. While *trans*-β-methylstyrene did not undergo efficient *E*/*Z* isomerization (see **Figure 3.27** in Experimental Section for a full list of unreactive or moderately reactive substrates), the introduction of a phosphonate group at the β-position (substrate **3e**) resulted in a *Z*/*E* ratio of 91:9 for *Z*-**3e**. This outcome is consistent with the reported strategy of leveraging destabilizing $A_{1,3}$-strain to deconjugate the *Z*-alkene

[66] Neveselý, T.; Molloy, C. McLaughlin, L. Brüss, C. G. Daniliuc, R. Gilmour, R. "Leveraging the n→π* Interaction in Alkene Isomerization by Selective Energy Transfer Catalysis." *Angew. Chem. Int. Ed.* **2022**, *61*, e202113600

[67] Zhang, X.; Rovis, T. "Photocatalyzed Triplet Sensitization of Oximes Using Visible Light Provides a Route to Nonclassical Beckmann Rearrangement Products." *J. Am. Chem. Soc.* **2021**, *143*, 21211–21217.

[68] Strieth-Kalthoff, F.; James, M. J.; Teders, M.; Pitzer, L.; Glorius, F. "Energy Transfer Catalysis Mediated by Visible Light: Principles, Applications, Directions." *Chem. Soc. Rev.* **2018**, *47*, 7190–7202.

chromophore, thereby increasing its triplet energy.[63,69] Also diethyl (*E*)-(2-phenylprop-1-en-1-yl)phosphonate was efficiently isomerized to *Z*-**3f** in a 93:7 *Z*/*E* ratio.[70]

Beyond *E*→*Z* isomerization, our new organic photocatalysts were suitable for mediating another hallmark transformation of energy transfer catalysis: [2+2] photocycloadditions.[71] Specifically, we focused on reactions previously reported in the literature and known to proceed via triplet-sensitization. In the absence of base, catalyst **C2** efficiently catalyzed the EnT-mediated *intermolecular* [2+2] cycloaddition of coumarin (E_T = 63.2 kcal/mol) and cyclohexene, yielding cyclobutene product **4** (**Figure 3.26**, upper panel).[72]

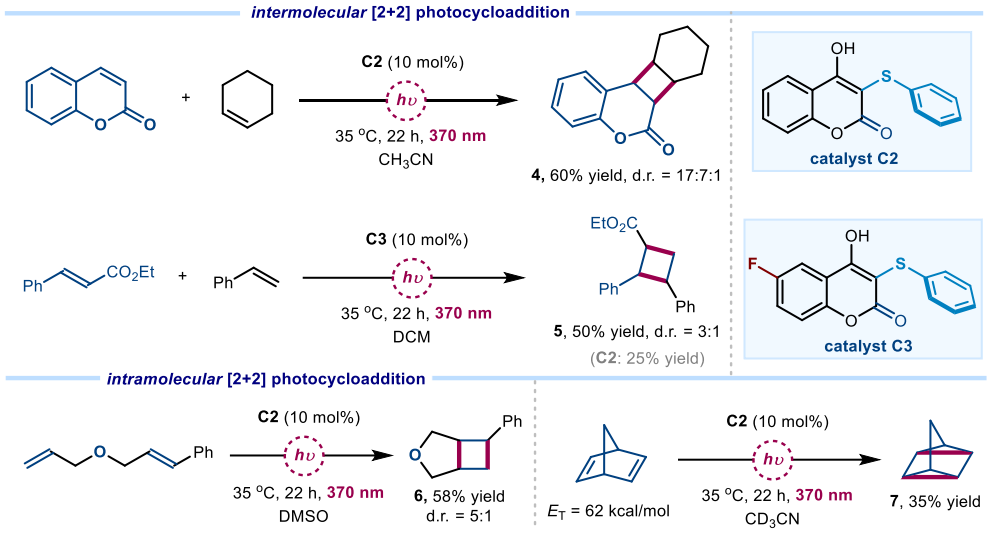

Figure 3.26. Intermolecular and intramolecular EnT-mediated [2 + 2] photocycloadditions; reactions performed on a 0.2 mmol scale with 10 mol % of catalyst **C2** or **C3** in dry, degassed solvent (1 mL); yields refer to the isolated products **4**–**6**, while the yield of **7** was measured by ^{1}H NMR analysis using dibromomethane as the internal standard.

In this reaction, we also detected a minor amount (~15%) of coumarin homodimerization, which was the only case where such byproducts were observed in our study. Interestingly, as depicted in **Figure 3.26**, catalyst **C3** outperformed **C2** in the EnT-driven [2+2] reaction

---

[69] (a) Dugave, C.; Demange, L. "Cis−Trans Isomerization of Organic Molecules and Biomolecules: Implications and Applications." *Chem. Rev.* **2003**, *103*, 2475–2532. (b) Pearson, C. M.; Snaddon, T. N. "Alkene Photo-Isomerization Inspired by Vision." *ACS Cent. Sci.* **2017**, *3*, 922–924. (c) Molloy, J. J.; Morack, T.; Gilmour, R. "Positional and Geometrical Isomerisation of Alkenes: The Pinnacle of Atom Economy." *Angew. Chem. Int. Ed.* **2019**, *58*, 13654–13664. (d) Metternich, J. B.; Gilmour, R. "A Bio-Inspired, Catalytic E → Z Isomerization of Activated Olefins." *J. Am. Chem. Soc.* **2015**, *137*, 11254–11257. (e) Metternich, J. B.; Gilmour, R. "One Photocatalyst, n Activation Modes Strategy for Cascade Catalysis: Emulating Coumarin Biosynthesis with (−)-Riboflavin." *J. Am. Chem. Soc.* **2016**, *138*, 1040–1045.

[70] Onneken, C.; Bussmann, K.; Gilmour, R. "Inverting External Asymmetric Induction via Selective Energy Transfer Catalysis: A Strategy to β-Chiral Phosphonate Antipodes." *Angew. Chem. Int. Ed.* **2020**, *59*, 330–334.

[71] Strieth-Kalthoff, F.; Glorius, F. "Triplet Energy Transfer Photocatalysis: Unlocking the Next Level." *Chem* **2020**, *6*, 1888–1903.

[72] Voloshkin, V. A.; Villa, M.; Martynova, E. A.; Beliš, M.; Van Hecke, K.; Ceroni, P.; Nolan, S. P. "Synthesis of cyclobutane-fused chromanones via gold-mediated photocatalysis." *Chem. Sci.* **2024**, *15*, 4571–4580.

between styrene and ethyl cinnamate ($E_T \approx 49$ kcal/mol for methyl cinnamate),[73] delivering product **5** in 50% yield (**C2** offered 25% yield). The results observed using different catalysts to promote the process in **Figure 3.26**, top panel, is consistent with the following scenario: when using catalyst **C2**, the triplet energy of the photocatalyst ($E_T = 67$ kcal/mol) surpasses that of styrene ($E_T = 61.7$ kcal/mol), enabling competitive quenching of the photocatalyst and leading to a loss in overall efficiency. In contrast, **C3**, with a triplet energy of 62.7 kcal/mol, is more selective for sensitizing ethyl cinnamate, resulting in a more efficient process for the target product **5**. These results demonstrate how structurally related catalyst variants can offer a versatile platform to fine-tune reactivity across different substrates and reaction types. Additionally, **C2** smoothly promoted the *intramolecular* [2+2] photocycloaddition of a styrene derivative (**Figure 3.26**, bottom panel),[74] delivering product **6** in 58% yield. **C2** proved also effective in the *intramolecular* [2+2] cycloaddition of norbornadiene ($E_T = 62.3$ kcal/mol)[29] to quadricyclane **7**, affording the product in moderate yield (**Figure 3.26**, bottom panel). Overall, these results highlight that our catalyst platform is useful for promoting diverse classical triplet-sensitized photochemical transformations.

3.4 Conclusion

In summary, we have introduced 3-thioaryl-4-hydroxycoumarins as a new class of inexpensive, organic bifunctional photocatalysts capable of mediating both SET and EnT processes. These metal-free catalysts combine strong reducing power—enabling the activation of redox-inert substrates—with high triplet energies, allowing for efficient energy transfer catalysis. Their ability to promote a wide array of C–C, C–S, C–P, and C–B bond-forming reactions, as well as photochemical isomerizations and cycloadditions, highlights their synthetic utility. Comprehensive mechanistic investigations, supported by photophysical and theoretical analyses, shed light on the basis of this dual activity, which is uncommon among small organic scaffolds. These mechanistic insights may provide a foundation for expanding the scope of organic photocatalysis as a sustainable alternative to transition-metal-based systems, while the concept of engineering charge-transfer excited states to unify SET and EnT pathways may prove useful in guiding future advances in photocatalyst design.

---

[73] Daub, M. E.; Jung, H.; Lee, B. J.; Won, J.; Baik, M. H.; Yoon, T. P. "Enantioselective [2+2] Cycloadditions of Cinnamate Esters: Generalizing Lewis Acid Catalysis of Triplet Energy Transfer." *J. Am. Chem. Soc.* **2019**, *141*, 9543–9547.

[74] Lu, Z.; Yoon, T. P. "Visible Light Photocatalysis of [2+2] Styrene Cycloadditions by Energy Transfer." *Angew. Chem. Int. Ed.* **2012**, *51*, 10329–10332.

3.5 Experimental Section

3.5.1 General Information

The ^{1}H NMR, $^{19}F\{^{1}H\}$ NMR, $^{13}C\{^{1}H\}$ NMR spectra are available in the literature[1] and are not reported in the present dissertation.

The NMR spectra were recorded at 400 MHz and 600 MHz for ^{1}H, 101 or 150 MHz for ^{13}C and 376 MHz for $^{19}F\{^{1}H\}$. The chemical shift (δ) for ^{1}H and ^{13}C are given in ppm relative to residual signals of the solvents (CHCl3 @ 7.26 ppm ^{1}H NMR and 77.16 ppm ^{13}C NMR). Coupling constants are given in Hertz. The following abbreviations are used to indicate the multiplicity: s, singlet; d, doublet; q, quartet; m, multiplet; br, broad signal.

High-resolution mass spectra (HRMS) were obtained from the Mass Facility unit on a Waters Xevo Q Tof spectrometer with electrospray ionization (ESI). UV-vis measurements were carried out on a Cary 3500 Multicell UV-vis spectrophotometer. Cyclic voltammetry studies were carried out on a PGSTAT204 potentiostat, offering compliance voltage up to ± 20 V (available at the counter electrode), ± 10 V scan range, and ±0.4 A current range. Fluorescence measurements were carried out on an Edinburgh FLSP920 spectrometer equipped with a 450 W xenon arc lamp, double excitation and single emission monochromators, and a Peltier-cooled Hamamatsu R928P photomultiplier tube (185−850 nm).

Yields refer to isolated materials of >95% purity as determined by ^{1}H NMR analysis. When specified, yields were determined by ^{1}H NMR analysis of the crude mixture using an internal standard, typically in cases where the product was too volatile for isolation or difficult to separate from the substrate.

General Procedures. All reactions were set up under an argon atmosphere in oven-dried glassware. Synthesis grade and anhydrous solvents were used as purchased from commercial sources. Chromatographic purification of products was accomplished using forced-flow chromatography (FC) on silica gel (230-400 mesh). For thin layer chromatography (TLC) analysis throughout this work, Merck pre-coated TLC plates (silica gel 60 GF254, 0.25 mm) were employed, using UV light as the visualizing agent and an acidic mixture of vanillin or basic aqueous potassium permanganate (KMnO4) stain solutions, and heat as developing agents. Organic solutions were concentrated under reduced pressure on a Büchi rotatory evaporator.

Materials. Commercial-grade reagents and solvents were purchased at the highest quality from commercial suppliers and used as received, unless otherwise stated.

3.5.2 Unreactive and Poorly Reactive Substrates

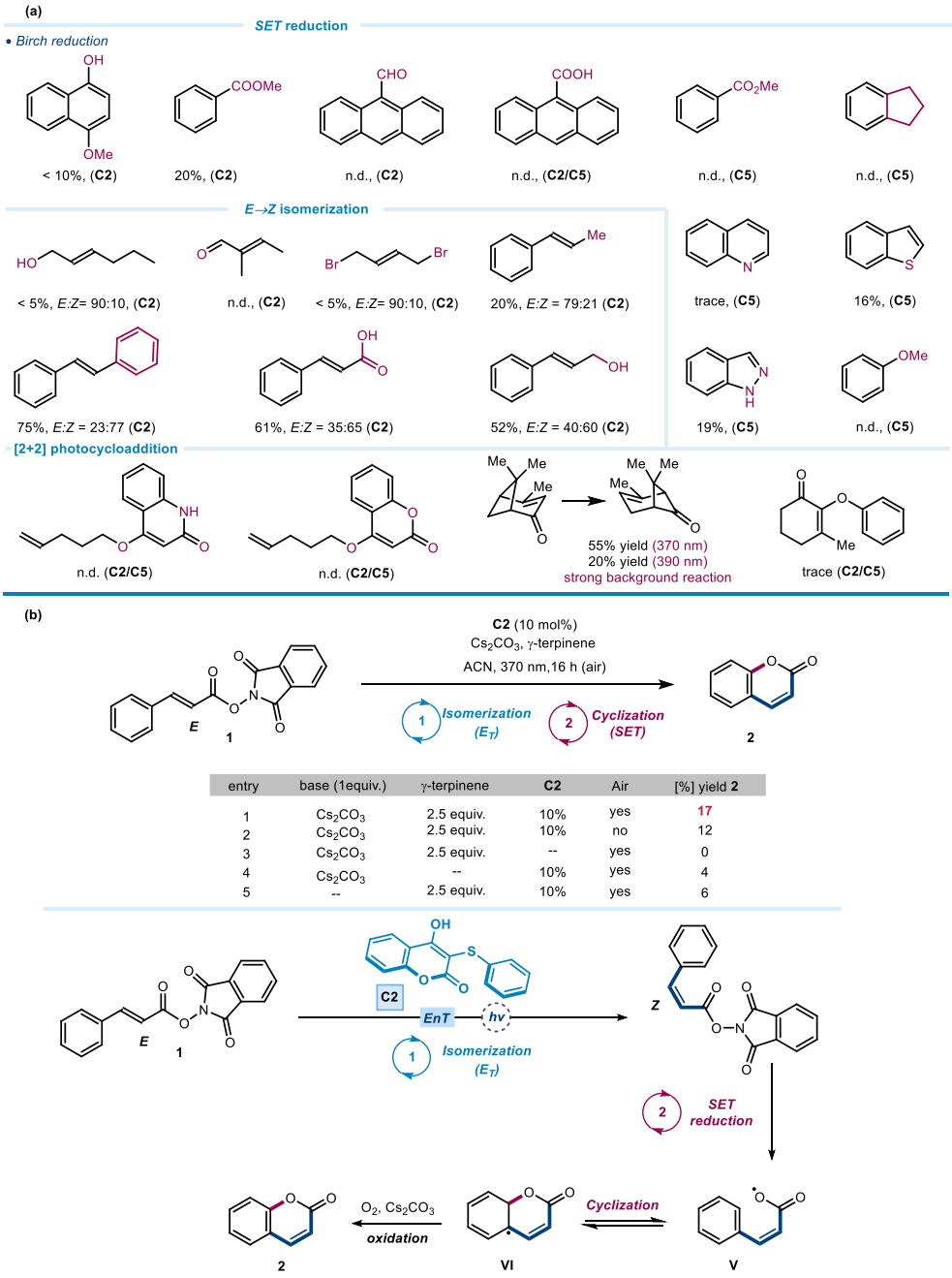

Figure 3.27. (a) Unsuccessful and moderately reactive substrates. Both SET reductions and *E*/*Z* photoisomerization reactions were carried out on a 0.2 mmol scale under the optimized conditions reported in **Section 3.4**, using either catalyst **C2** or **C5** as specified. Results are shown below each entry. *n.d. = product not detected.* **(b) Attempted tandem reaction** combining EnT-mediated *E*/*Z* isomerization and SET-driven radical cyclization along with some optimization results.

3.5.3 Synthesis of Substrates and Catalysts

Substrate Synthesis

The following substrates (**Figure 3.28**) were synthesized according to reported procedures.[75]

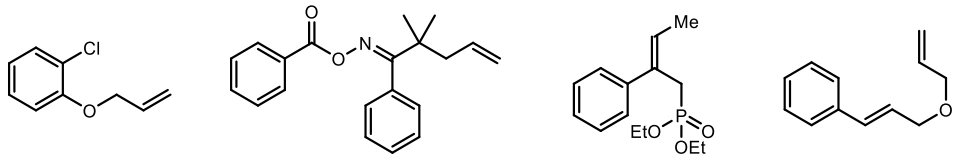

Figure 3.28. Starting materials synthesized according to known procedures.

General Procedure for the Synthesis of *N*-Ts Amine Derivatives

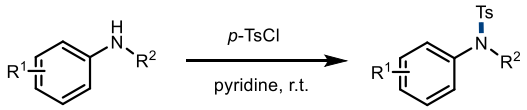

To a solution of the appropriate aniline (5 mmol, 1 equiv.) in pyridine (10 mL, 0.5 M) was added *p*-toluenesulfonyl chloride (5.5 mmol, 1.1 equiv.) at 0 °C. After the solution was stirred at ambient temperature for 2-3 hours, pyridine was removed by rotary evaporator, and the reaction mixture was poured into water. The product was extracted with CH_2Cl_2 (three times), the organic layers dried over Na_2SO_4 and concentrated in vacuo. The residue was purified by column chromatography on silica gel to give the corresponding product.

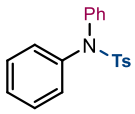

1i

***N,N*-diphenyl-p-toluenesulfonamide (1i):** Synthesized according to the General Procedure using diphenylamine (0.846g, 5 mmol, 1.0 equiv.). The crude mixture was purified by flash column chromatography on silica gel (20% ethyl acetate in hexanes as eluent) to afford **1i** (1.18g, 73% yield) as a white solid. **^{1}H NMR (400 MHz, $CDCl_3$)** δ 7.58 (d, *J* = 8.4 Hz, 2H), 7.33 – 7.25 (m, 12H), 2.43 (s, 3H). Matching reported literature data.[55]

---

[75] (a) Folgueiras-Amador, A. A.; Teuten, A. E.; Salam-Perez, M.; Pearce, J. E.; Denuault, G.; Pletcher, D.; Parsons, P. J.; Harrowven, D. C.; Brown, R. C. D."Cathodic Radical Cyclisation of Aryl Halides Using a Strongly-Reducing Catalytic Mediator in Flow." *Angew. Chem., Int. Ed.* **2022**, *61*, e202203694. (b) Su, H.; Li, F.; Xuan, Z.; Yu, W. "Copper-Catalyzed Cyclization and Azidation of γ,δ-Unsaturated Ketone O-Benzoyl Oximes." *Adv. Synth. Catal.* **2015**, *357*, 64–70. (c) Okamoto, R.; Tanaka, K. "Rhodium-Catalyzed Olefin Isomerization/Allyl Claisen Rearrangement/Intramolecular Hydroacylation Cascade." *Org. Lett.* **2013**, *15,* 2112−2115. (d) Duan, Z.; Hu, X.; Zhang, C.; Wang, D.; Yu, S.; Zheng, Z. "Highly Enantioselective Rh-Catalyzed Hydrogenation of β,γ-Unsaturated Phosphonates with Chiral Ferrocene-Based Monophosphoramidite Ligands." *J. Org. Chem.* **2009**, *74*, 9191–9194.

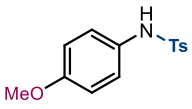

1j

***N*-Ts-4-Methoxyaniline (1j):** Synthesized according to the General Procedure using 4-methoxy-aniline (0.615g, 5 mmol, 1.0 equiv.). The crude mixture was purified by flash column chromatography on silica gel (10% ethyl acetate in hexanes as eluent) to afford **1j** (0.91g, 65% yield) as a white solid. **^{1}H NMR (400 MHz, $CDCl_3$)** δ 7.57 (d, *J* = 8.4 Hz, 2H), 7.21 (d, *J* = 8.6 Hz, 2H), 6.96 (d, *J* = 9.0 Hz, 2H), 6.76 (d, *J* = 9.1 Hz, 2H), 3.76 (s, 3H), 2.38 (s, 3H). Matching reported literature data.[55]

Synthesis of Ethyl (*E*)-3-methyl-4-oxohex-2-enoate (*E*-3b):

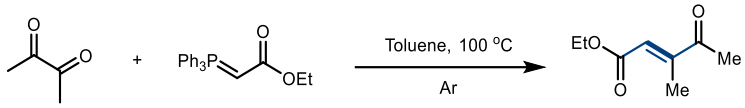

E-3b

To an oven-dried Schlenk tube, (carbethoxymethylene)triphenylphosphorane (1.75 g, 5 mmol, 1 equiv.) and dry toluene (5 mL) were added under an argon atmosphere. To the formed suspension, butane-2,3-dione (0.43g, 5 mmol, 1 equiv.) was added in one portion. The reaction mixture was stirred for 3 hours at 100 °C. Afterward, the mixture was allowed to cool to ambient temperature and was diluted with Et_2O (20 mL), which caused triphenylphosphine oxide to precipitate out. The precipitate was filtered off, the solid further washed with Et_2O and the collected organic layer was concentrated with the use of a rotary evaporator. The crude material was purified by flash column chromatography on silica gel (10% Et_2O in hexanes as eluent) to afford substrate *E*-**3b** (0.32 g, 41% yield) as a clear oil. **^{1}H NMR (400 MHz, $CDCl_3$)** δ 6.57 (q, *J* = 1.5 Hz, 1H), 4.24 (q, *J* = 7.1 Hz, 2H), 2.38 (s, 3H), 2.20 (d, *J* = 1.5 Hz, 3H), 1.32 (t, *J* = 7.1 Hz, 3H). Matching reported literature data.[66]

Synthesis of (*E*)-acetophenone *O*-methyloxime (*E*-3d)

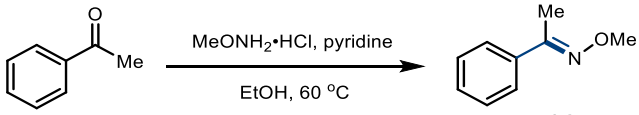

E-3d

To a solution of acetophenone (2.64 g, 22.0 mmol) and pyridine (5.0 mL, 61.8 mmol) in EtOH (10 mL) was added $MeONH_2$•HCl (2.80 g, 33.0 mmol) in one portion, and the reaction mixture was stirred at 60 °C for 2 h. The reaction was quenched by adding water and extracted twice with ethyl acetate. The combined organic layers were washed with 1N aqueous HCl and brine, dried over $MgSO_4$, and the solvent was removed in a rotary evaporator. The crude material was purified by flash column chromatography on silica gel (10% ethyl acetate in hexanes as eluent) to afford *E*-**3d** (2.90 g, 88% yield) as a clear oil. **^{1}H NMR (400 MHz,**

$CDCl_3$) δ 7.72 – 7.60 (m, 2H), 7.37 (dd, J = 5.3, 2.1 Hz, 3H), 4.02 (s, 3H), 2.24 (s, 3H). Matching reported literature data.[76]

Synthesis of diethyl (*E*)-(2-phenylprop-1-en-1-yl)phosphonate (*E*-3e)

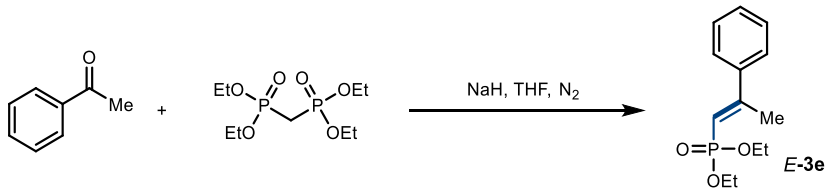

In an oven-dried Schlenk tube under argon atmosphere, sodium hydride (60% in mineral oil, 0.50g) was dissolved in dry tetrahydrofuran (10 mL) at 0 °C. Tetraethyl methylenediphosphonate (2.70 mL, 10.9 mmol, 1.27 equiv.) was added dropwise and the solution was stirred under an argon atmosphere at 0 °C for 1 hour. Acetophenone (1 mL, 8.57 mmol, 1.00 equiv.) was added via syringe and the solution was heated at 65 °C and stirred for three days. After the mixture was cooled to room temperature, water (30 mL) and ethyl acetate (40 mL) were added. The layers were separated and the aqueous layer was extracted with ethyl acetate (3 x 20 mL). The combined organic layers were dried over Na_2SO_4 and the solvent was removed in vacuo. The crude material was purified by flash column chromatography on silica gel (40% ethyl acetate in hexanes as eluent) to afford *E*-**3e** (0.81g, 37% yield) as a yellow oil. **^{1}H NMR (400 MHz, $CDCl_3$)** δ 7.46 (dt, *J* = 7.2, 1.8 Hz, 2H), 7.39 – 7.32 (m, 3H), 5.90 (dt, *J* = 16.6, 1.2 Hz, 1H), 4.16 – 4.09 (m, 4H), 2.50 (dd, *J* = 3.2, 1.5 Hz, 3H), 1.35 (td, *J* = 7.1, 1.5 Hz, 6H). Matching reported literature data.[70]

Catalyst Synthesis

Catalyst **C1** was synthesized following a previously reported procedure.[45]

Catalyst **C2** and the analogous 3-thiophenyl 4-hydroxycoumarin catalysts (**C3**-**C5**) were synthesized according to previously reported procedures,[77] with slight modifications as outlined below.

---

[76] Too, P. C.; Wang, Y. F.; Chiba, S. Rhodium (III)-catalyzed synthesis of isoquinolines from aryl ketone O-acyloxime derivatives and internal alkynes. *Org. Lett.* **2010**, *12*, 5688−5691.

[77] Parumalaa, S. K. R.; Peddinti, R. K. Iodine catalyzed cross-dehydrogenative C–S coupling by C(sp2)–H bond activation: direct access to aryl sulfides from aryl thiols. *Green Chem.* **2015**, *17*, 4068−4072.

General Procedure A

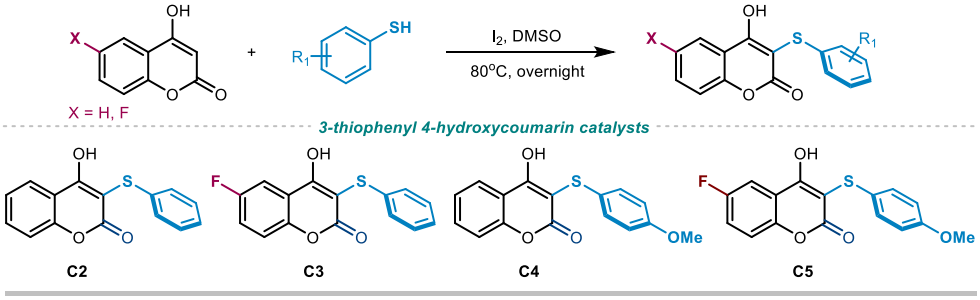

Figure 3.28. Synthesis of catalysts **C2-C5** according to procedure **A**.

An oven-dried Schlenk flask was charged with 4-hydroxycoumarin (1.0 equiv.), aryl thiol (1.0 equiv.), and iodine (10 mol%), which were dissolved in 0.2 M dimethyl sulfoxide. The reaction mixture was heated in a pre-heated oil bath at 80 °C overnight. The reaction was monitored by TLC analysis, then the reaction was diluted with ethyl acetate and quenched with a saturated aqueous solution of sodium thiosulfate.

*For the isolation of **C2**:* A crystalline solid precipitated in the ethyl acetate layer and was collected by filtration through a Büchner funnel. The solid was washed three times with water and ethyl acetate to afford the pure compound.

*For the isolation of **C3–C5:*** After quenching the reaction with a saturated aqueous solution of sodium thiosulfate, the organic layer was extracted with ethyl acetate, washed twice with brine, and dried over anhydrous Na_2SO_4. After filtration and concentration to dryness, the crude residue was washed with hexane, affording the corresponding pure products.

Characterization of Catalysts C

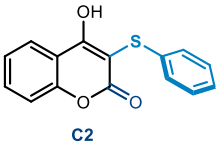

4-Hydroxy-3-(phenylthio)-2*H*-chromen-2-one (C2): Synthesized according to the general procedure **A** using 4-hydroxycoumarin (1.62 g, 10.00 mmol, 1.0 equiv.), thiophenol (1.10 g, 10.00 mmol, 1.0 equiv.) and iodine (0.126 g, 1.00 mmol, 10 mol%.) in DMSO. The crystalline compound was isolated by vacuum filtration to afford **C2** (2.75 g, 98% yield) as a white solid.

^{1}H NMR (600 MHz, DMSO) δ 7.95 (dd, *J* = 7.9, 1.5 Hz, 1H), 7.71 (ddd, *J* = 8.6, 7.3, 1.6 Hz, 1H), 7.43 – 7.38 (m, 2H), 7.30 (d, J = 8.6 Hz, 2H), 7.12 (d, J = 8.6 Hz, 2H), 1.23 (s, 9H).

^{13}C NMR (151 MHz, DMSO) δ 168.7, 161.4, 153.4, 148.7, 134.0, 133.0, 126.8, 126.4, 124.8, 124.7, 117.0, 116.3, 95.1, 34.6, 31.5.

HRMS: calculated for $C_{15}H_{10}O_3S$ ($M+Na^+$): 293.0243, found 293.0244.

Matching reported literature data.[77]

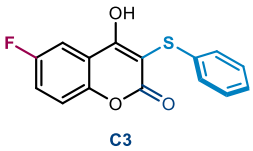

C3

6-Fluoro-4-hydroxy-3-(phenylthio)-2*H*-chromen-2-one (C3): Synthesized according to the general procedure **A** using 6-fluoro-4-hydroxycoumarin (0.214 g, 1.19 mmol, 1.0 equiv.), thiophenol (0.196 g, 1.78 mmol, 1.5 equiv.) and iodine (30.2 mg, 0.119 mmol, 10 mol%.) in DMSO. The crystalline compound was isolated by vacuum filtration to afford **C3** (0.298 g, 87% yield) as a yellow solid.

^{1}H NMR (600 MHz, DMSO) δ 7.67 (d, *J* = 8.7 Hz, 1H), 7.57 (t, *J* = 8.6 Hz, 1H), 7.47 (dd, *J* = 8.9, 4.3 Hz, 1H), 7.26 (t, *J* = 7.7 Hz, 2H), 7.15 (dd, *J* = 14.3, 7.8 Hz, 3H).

^{13}C NMR (151 MHz, DMSO) δ 167.7 (d, *J* = 22.9 Hz), 160.7 (d, *J* = 12.6 Hz), 158.0 (d, *J* = 241.2 Hz), 149.4 (d, *J* = 4.0 Hz), 135.8 (d, *J* = 17.1 Hz), 129.1, 126.3 (d, *J* = 9.9 Hz), 125.6 (d, *J* = 7.7 Hz), 120.9 (d, *J* = 24.6 Hz), 118.7 (d, *J* = 8.6 Hz), 118.2 – 116.6 (m), 109.8 (dd, *J* = 25.2, 3.8 Hz), 95.1 (d, *J* = 42.9 Hz).

^{19}F NMR (376 MHz, DMSO) δ -117.6.

HRMS: calculated for $C_{15}H_9FO_3S$ ($M+H^+$): 289.0329, found 289.0335.

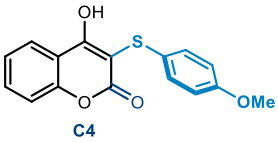

C4

4-Hydroxy-3-((4-methoxyphenyl)thio)-2*H*-chromen-2-one (C4): Synthesized according to the general procedure **A** using 4-hydroxycoumarin (1.00 g, 6.17 mmol, 1.0 equiv.), 4-methoxythiophenol (1.30 g, 9.25 mmol, 1.5 equiv.) and iodine (0.157 g, 0.617 mmol, 10 mol%.) in DMSO. The crystalline compound was isolated by vacuum filtration to afford **C4** (1.66 g, 90% yield) as a white solid.

^{1}H NMR (600 MHz, DMSO) δ 7.94 (dd, *J* = 7.9, 1.4 Hz, 1H), 7.67 (ddd, *J* = 8.4, 7.3, 1.6 Hz, 1H), 7.40 – 7.34 (m, 2H), 7.27 (d, *J* = 8.9 Hz, 2H), 6.88 (d, *J* = 8.9 Hz, 2H), 3.70 (s, 3H).

^{13}C NMR (151 MHz, DMSO) δ167.6, 161.2, 158.5, 153.1, 133.8, 130.3, 126.1, 124.6, 124.5, 116.7, 115.9, 115.1, 97.0, 55.5.

HRMS: calculated for $C_{16}H_{12}O_4S$ ($M+Na^+$): 323.0349, found 323.0352.

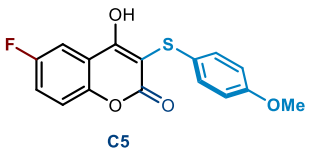

C5

6-Fluoro-4-hydroxy-3-((4-methoxyphenyl)thio)-2H-chromen-2-one (C5): Synthesized according to the general procedure **A** using 6-fluoro-4-hydroxycoumarin (0.22 g, 1.22 mmol, 1.0 equiv.), 4-methoxy thiophenol (0.171 g, 10.00 mmol, 1.0 equiv.) and iodine (31.0 mg, 0.122 mmol, 10 mol%.) in DMSO. The crystalline compound was isolated by vacuum filtration to afford **C5** (0.292 g, 75% yield) as a white solid.

^{1}H NMR (600 MHz, DMSO) δ 7.66 (dd, *J* = 8.7, 3.1 Hz, 1H), 7.55 (td, *J* = 8.4, 3.1 Hz, 1H), 7.45 (dd, *J* = 9.1, 4.4 Hz, 1H), 7.24 (d, *J* = 8.9 Hz, 2H), 6.87 (d, *J* = 8.9 Hz, 2H), 3.71 (s, 3H).

^{13}C NMR (151 MHz, DMSO) δ 166.7 (d, *J* = 18.7 Hz), 160.7 (d, *J* = 9.2 Hz), 158.3 (d, *J* = 5.5 Hz), 158.0 (d, *J* = 241.0 Hz), 149.3, 130.1 (d, *J* = 11.0 Hz), 125.7 (d, *J* = 17.3 Hz), 120.8 (dd, *J* = 24.5, 3.2 Hz), 118.6 (d, *J* = 8.5 Hz), 116.99 (m), 114.79 (s), 109.7 (d, *J* = 25.4 Hz), 97.4 (d, *J* = 34.0 Hz), 55.22 (s).

^{19}F NMR (376 MHz, DMSO) δ -117.9.

HRMS: calculated for $C_{16}H_{11}FO_4S$ ($M+Na^+$): 341.0254, found 341.0262.

3.5.4 Optimization Studies

Table 3.3. Optimization of the SET-based model reaction[a]

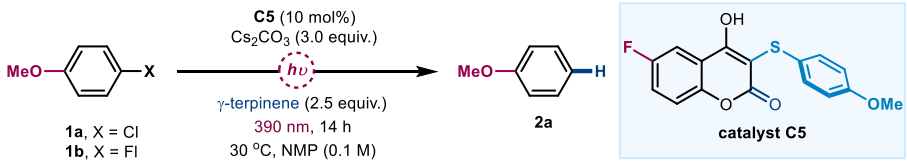

Entry	Substrate	Deviation	Yield % **2a**
1	**1a**	Irradiation @ 427 nm, using **C5**	70
2	**1b**	Irradiation @ 427 nm, using **C5**	19
3	**1a**	6 h instead of 14 h, using **C5**	60
4	**1b**	6 h instead of 14 h, using **C5**	49

[a] Reactions performed over 14 hours in 0.4 mL of NMP using 0.2 mmol of **1a**, 0.5 mmol of γ-terpinene, and base (3 equiv.) under irradiation by a Kessil lamp (λ_{max} = 390 nm, irradiance = 100 mW/cm^2). Yield of **2a** determined by ^{1}H NMR analysis of the crude mixture using dibromomethane as the internal standard.

General comment: Catalyst **C5**, which exhibits better absorption in the visible region compared to **C2**, was found to effectively promote the dechlorination of **1a** under 427 nm irradiation. However, when applied to the fluoro derivative **1b**, **C5** demonstrated poor reactivity at the same wavelength. To ensure consistent results, we opted to perform all subsequent SET-based reactions at 390 nm, even when using **C5**, as this wavelength provided more reliable and reproducible outcomes. Note that for *EnT*-based processes, irradiation at 370 nm was used instead, as it offered improved performance (see **Figure 3.29** in the following page).

Table 3.4. Optimization of the EnT-based [2+2] photocycloaddition[a]

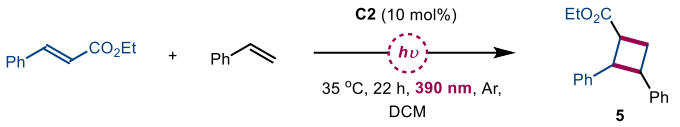

substituted 4-hydroxycoumarin catalysts

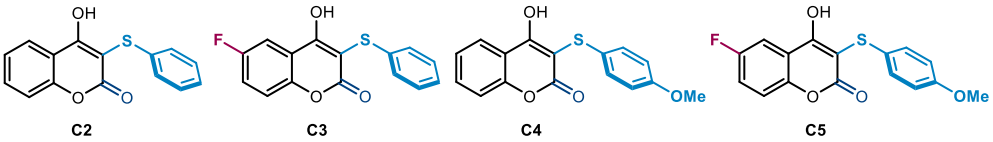

Entry	Deviation	Yield
1	none	20%
2	no catalyst or no light	0
3	CH_3CN instead of DCM	20%
4	370 nm instead of 390 nm	25%
5	**C3** instead of **C2** (370 nm)	50%
6	**C4** instead of **C2** (370 nm)	28%
7	**C5** instead of **C2** (370 nm)	30%

[a] Reactions performed over 22 hours in 1 mL of DCM using 0.2 mmol of ethyl cinnamate and styrene (1 mmol) under irradiation by a Kessil lamp (λ_{max} = 390 nm or 370 nm, irradiance = 100 mW/cm^2). Reaction yield determined by ^{1}H NMR analysis of the crude mixture using dibromomethane as the internal standard.

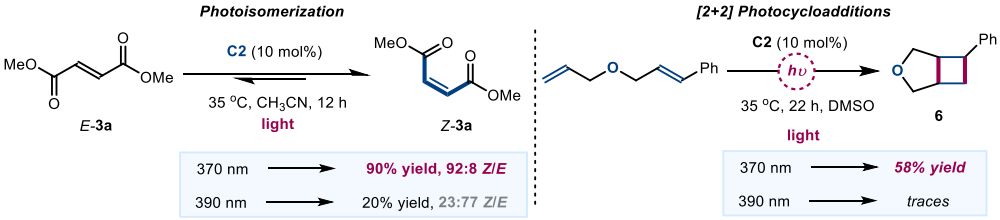

Figure 3.29. Effect of light irradiation (370 nm vs 390 nm) on the [2+2] photocycloaddition reaction.

3.5.5 Experimental Procedures

Experimental Setup

- ***Photochemical Set-up 1*** *390 nm Kessil lamp* with **PhotoRedOx Box TC™** (**Figure 3.30**)

The reactions were performed using a PhotoRedOx Box TC™ reactor under the illumination of a *Kessil* lamp (max 52 W, λ_{max} = 390 nm, positioned 2-3 cm away from the vial), with a fan to control the temperature. Under these conditions, the reaction temperature inside the vessel was measured using a thermometer and found to range between 30-32 ºC.

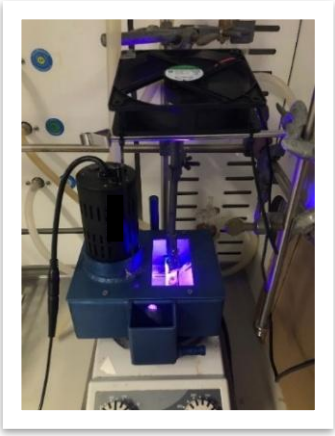

Figure 3.30. Reaction setup using PhotoRedOx Box TC™ reactor with 390 nm *Kessil lamp*.

- ***Photochemical Set-up 2*** *390 nm Kessil lamp* with **3D-printed photoreactor** (**Figure 3.31**)

The Birch reduction reactions were performed using a 3D-printed photoreactor reported in the literature[78] under the illumination of a Kessil lamp (max 52 W, λ_{max} = 390 nm, positioned 2-3 cm away from the vial). Under these conditions, the reaction temperature in the reactor was maintained at 30 °C using a circulating water cooling system.

[78] Schiel, F.; Peinsipp, C.; Kornigg, S.; Böse, D. "A 3D-Printed Open Access Photoreactor Designed for Versatile Applications in Photoredox- and Photoelectrochemical Synthesis." *ChemPhotoChem*. **2021**, *5*, 431–437.

Figure 3.31. Reaction setup using 3D-printed photoreactor[81] with 390 nm *Kessil lamp*.

- ***Photochemical Set-up 3*** *370 nm Kessil lamp* with a Fan (**Figure 3.32**)

The EnT reactions were performed under the illumination of a Kessil lamp (max 52 W, λ_{max} = 370 nm, positioned 3-5 cm away from the Schlenk tube), with a fan to control the temperature. Under these conditions, the reaction temperature inside the vessel was measured using a thermometer and found to range between 34-36 ºC.

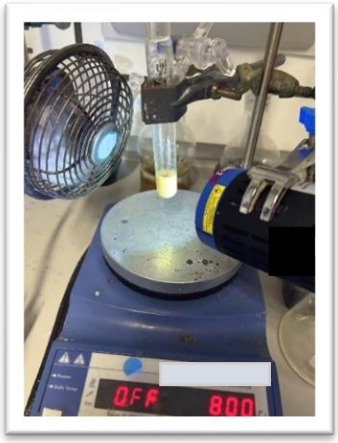

Figure 3.32. Reaction setup using a Fan with 370 nm or 390nm *Kessil lamp*.

3.5.6 General Procedure for the Reductive Dehalogenation of Aryl Fluorides and Chlorides

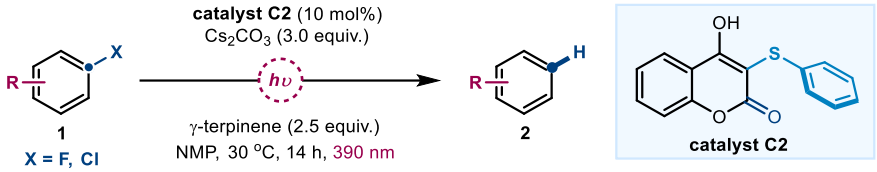

To a 4 mL glass vial, catalyst **C2** (5.4 mg, 0.02 mmol, 0.1 equiv.) or **C5** (6.4 mg, 0,02 mmol, 0.1 equiv. where specified), Cs_2CO_3 (0.6 mmol, 3 equiv.), and aryl halide **1** (*if solid*, 0.2 mmol, 1 equiv.) were sequentially added. The vial was sealed with a screw-top cap with a septum, evacuated, and backfilled with nitrogen three times. Then, aryl halide **1** (*if liquid*, 0.2 mmol, 1 equiv.), γ-terpinene (80 µL, 0.5 mmol, 2.5 equiv.), and argon-sparged NMP (0.5 M, 0.4 mL) were added via syringe. The vial was sealed with Parafilm and stirred under 390 nm Kessil lamp irradiation in a PhotoRedOx Box TC™ reactor for 14 hours using ***Set-up 1*** detailed in **Figure 3.30**.

NMR analyses (products **2a-2f**, **2h**): After irradiation at 390 nm for 14 hours, dibromomethane (34.8 mg, 0.2 mmol, 1 equiv.) was added to the crude reaction mixture as an internal standard, followed by 2 mL of H_2O and 1 mL of brine. The mixture was then extracted with 0.7 mL of $CDCl_3$, and the organic layer was analyzed by ^1H NMR spectroscopy.

Isolation of products **2g**: After completion of the reaction, the mixture was transferred to a separatory funnel, and 10 mL of H_2O and 2 mL of brine were added. The organic layer was extracted with EtOAc, washed twice with brine, and then dried over anhydrous Na_2SO_4. After filtration and concentration to dryness, the crude residue was purified by column chromatography, affording the corresponding products with the reported yields (>95% purity according to ^1H NMR analysis).

Characterization of Products

The ^1H NMR traces of products **2a-2f, 2h**, which are reported in the NMR Section I of the Supporting Information, matched the reported literature data.[54,55,79,80]

---

[79] Kuhlmann, J. H.; Dickoff, J. H.; Mancheño, O. G. Visible Light Thiyl Radical-Mediated Desilylation of Arylsilanes. *Chem. Eur. J.* **2023**, *29*, e202203347.

[80] Yamada, Y. M. A.; Watanabe, T.; Ohno, A.; Uozumi, Y. Development of Polymeric Palladium-Nanoparticle Membrane-Installed Microflow Devices and their Application in Hydrodehalogenation. *ChemSusChem*. **2012**, *5*, 293-299.

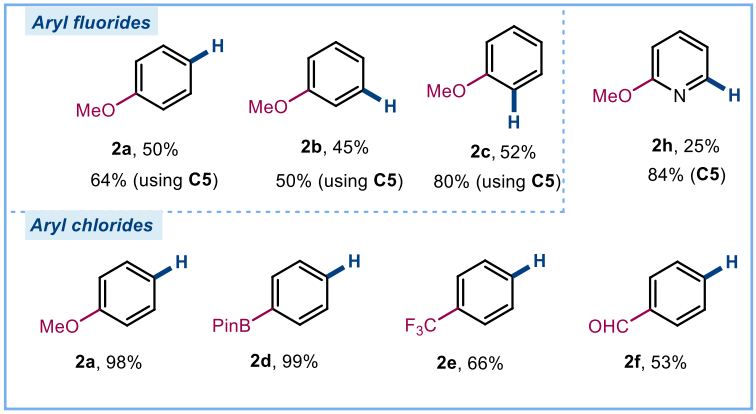

Figure 3.33. Compounds for which yields have been determined by ^{1}H NMR analysis using an internal standard.

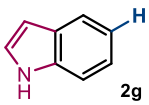

2g

1*H*-indole (2g): Synthesized according to the General Procedure using 5-chloro-1*H*-indole (30.2 mg, 0.2 mmol, 1.0 equiv.) and catalyst **C2**. The crude mixture was purified by flash column chromatography on silica gel (10% ethyl acetate in hexanes as eluent) to afford **2g** (19.8 mg, 85% yield) as a white solid.

^{1}H NMR (600 MHz, $CDCl_3$) δ 8.11 (s, 1H), 7.67 (d, J = 7.5 Hz, 1H), 7.41 (dq, J = 8.2, 0.9 Hz, 1H), 7.24 – 7.20 (m, 2H), 7.16 – 7.13 (m, 1H), 6.58 (ddd, J = 3.1, 2.0, 1.0 Hz, 1H).

^{13}C NMR (151 MHz, $CDCl_3$) δ 135.7, 127.8, 124.1, 121.9, 120.7, 119.8, 111.0, 102.6.

Matching reported literature data.[81]

3.5.7. General Procedure for *N*-Desotylation

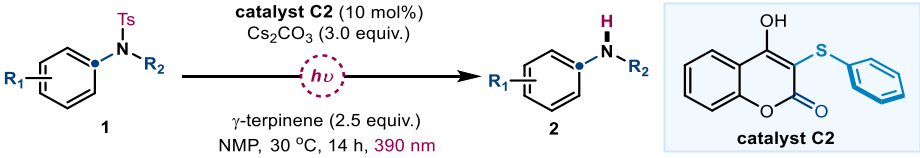

To a 4 mL glass vial, catalyst **C2** (5.4 mg, 0.02 mmol, 0.1 equiv.) or **C5** (6.4 mg, 0,02 mmol, 0.1 equiv. where specified), and Cs_2CO_3 (0.6 mmol, 3 equiv.) were sequentially added. The vial was sealed with a screw-top cap with a septum, evacuated, and backfilled with nitrogen three times. Then, *N*-Ts-amine **1** (0.2 mmol, 1 equiv.), γ-terpinene (80 µL, 0.5 mmol, 2.5 equiv.), and argon-sparged NMP (0.5 M, 0.4 mL) were added via syringe. The vial was sealed with Parafilm and stirred under 390 nm Kessil lamp irradiation in a PhotoRedOx Box TC™ reactor for 14 hours using ***Set-up 1*** detailed in **Figure 3.30**.

---

[81] Kanchupalli, V.; Joseph, D.; Katukojvala, S. "Pyridazine *N*-Oxides as Precursors of Metallocarbenes: Rhodium-Catalyzed Transannulation with Pyrroles." *Org. Lett.* **2015**, *17*, 5878–5881.

After irradiation at 390 nm for 14 hours, the reaction mixture was transferred to an extraction funnel. Then, 10 mL of water and 2 mL of brine were added, and the organic layer was extracted with ethyl acetate (EtOAc x 3). The organic layer was washed twice with brine. The combined organic layers were dried over anhydrous Na_2SO_4, filtered, and concentrated to dryness. The crude residue was purified by column chromatography to afford the corresponding product **2**.

Characterization of Products

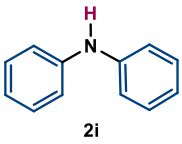

2i

Diphenylamine (2i): Synthesized according to the General Procedure using catalyst **C2** and *N,N*-diphenyl-p-toluenesulfonamide (64.7 mg, 0.2 mmol, 1.0 equiv.). The crude mixture was purified by flash column chromatography on silica gel (20% ethyl acetate in hexanes as eluent) to afford **2j** (30.5 mg, 90% yield) as a white solid.

^{1}H NMR (600 MHz, $CDCl_3$) δ 7.34 (q, *J* = 6.4 Hz, 4H), 7.15 (d, *J* = 5.1 Hz, 4H), 7.02 (t, *J* = 7.4 Hz, 2H), 5.73 (s, 1H). **^{13}C NMR (151 MHz, $CDCl_3$)** δ 143.2, 129.4, 121.1, 117.9.

Matching reported literature data.[54]

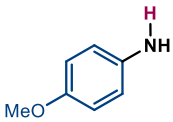

2j

4-Methoxy-aniline (2j): Synthesized according to the General Procedure using catalyst **C5** and *N*-(4-Methoxy-phenyl)-4-methyl-benzenesulfonamide (55.5 mg, 0.2 mmol, 1.0 equiv.). The crude mixture was purified by flash column chromatography on silica gel (5% ethyl acetate in hexanes as eluent) to afford **2k** (17.0 mg, 69% yield) as a brown solid.

^{1}H NMR (600 MHz, $CDCl_3$) δ 6.76 (d, *J* = 9.6 Hz, 2H), 6.65 (d, *J* = 7.5 Hz, 2H), 3.75 (s, 3H), 3.43 (s, 2H). **^{13}C NMR (151 MHz, $CDCl_3$)** δ 152.8, 140.1, 116.5, 114.9, 55.8.

Matching reported literature data.[82]

3.5.8. Borylation of Aryl Chlorides

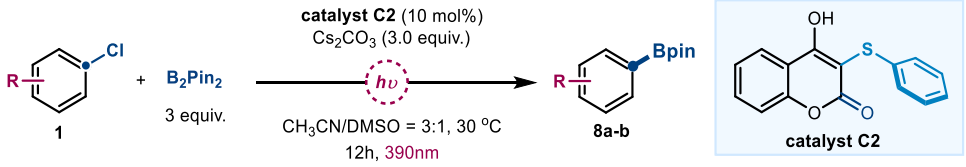

To a 4 mL glass vial, catalyst **C2** (5.4 mg, 0.02 mmol, 0.1 equiv.), cesium carbonate (195 mg,

[82] Garcia, N.; Garcia-Garcia, P.; Fernandez-Rodriguez, M.A.; Rubio, R.; Pedrosa, M. R.; Arnaiz, F. J.; Sanz, R. "Pinacol as a New Green Reducing Agent: Molybdenum-Catalyzed Chemoselective Reduction of Sulfoxides and Nitroaromatics." *Adv. Synth. Catal.* **2012**, *354*, 321–327.

0.6 mmol, 3 equiv.), B_2Pin_2 (152 mg, 0.6 mmol, 3 equiv.) and aryl chlorides **1** (*if solid*, 0.2 mmol, 1 equiv.) were added as solids. The vial was then evacuated and backfilled with argon three times. Next, aryl chlorides **1** (*if liquid*, 0.2 mmol, 1 equiv.) were added, followed by argon-sparged solvent (CH_3CN:DMSO = 3:1, 0.2 M) via syringe. The vial was sealed with Parafilm and stirred under irradiation from a 390 nm Kessil lamp using the PhotoRedOx Box TC™ reactor for 12 hours (***Set-up 1***, detailed in **Figure 3.30**).

After irradiation at 390 nm for 12 hours, the reaction mixture was transferred to an extraction funnel. Then, 10 mL of water and 2 mL of brine were added, and the organic layer was extracted with ethyl acetate (EtOAc). The organic layer was washed twice with brine. The combined organic layers were dried over anhydrous Na_2SO_4, filtered, and concentrated to dryness. The crude residue was purified by column chromatography to afford the corresponding product **8**.

Characterization of Products

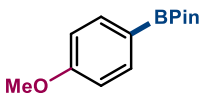

8a

2-(4-methoxyphenyl)-4,4,5,5-tetramethyl-1,3,2-dioxaborolane (**8a**): Synthesized according to the General Procedure using 1-chloro-4 methoxybenzene (28.5 mg, 0.2 mmol, 1.0 equiv.) and 4,4,4',4',5,5,5',5' octamethyl-2,2'-bi(1,3,2-dioxaborolane) (152.4 mg, 0.6 mmol, 3.0 equiv.). The crude mixture was purified by flash column chromatography on silica gel (3% ethyl acetate in hexanes as eluent) to afford **8a** (30.4 mg, 65% yield) as a white solid.

^{1}H NMR (600 MHz, $CDCl_3$) δ 7.75 (d, *J* = 8.7 Hz, 2H), 6.89 (d, *J* = 10.1 Hz, 2H), 3.83 (s, 3H), 1.33 (s, 12H). **^{13}C NMR** (151 MHz, $CDCl_3$) δ 162.1, 136.4, 113.2, 83.4, 55.0, 24.8.

Matching reported literature data.[83]

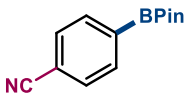

8b

2-(4-cyanophenyl)-4,4,5,5-tetramethyl-1,3,2-dioxaborolane (**8b**): Synthesized according to the General Procedure using 1-chloro-4-cyanobenzene (27.5 mg, 0.2 mmol, 1.0 equiv.) and 4,4,4',4',5,5,5',5' octamethyl-2,2'-bi(1,3,2-dioxaborolane) (152.4 mg, 0.6 mmol, 3.0 equiv.). The crude mixture was purified by flash column chromatography on silica gel (5% ethyl acetate in hexanes as eluent) to afford **8b** (36.6 mg, 80% yield) as a white solid.

^{1}H NMR (600 MHz, $CDCl_3$) δ 7.86 (d, *J* = 9.4 Hz, 2H), 7.62 (d, *J* = 8.4 Hz, 2H), 1.33 (s, 12H). **^{13}C NMR (151 MHz, $CDCl_3$)** δ 135.2, 131.2, 118.9, 114.6, 84.6, 24.9.

Matching reported literature data.[84]

---

[83] Zhao, J.-H.; Zhou, Z.-Z.; Zhang, Y.; Su, X.; Chen, X.-M.; Liang, Y.-M. "Visible-light-mediated borylation of aryl and alkyl halides with a palladium complex." *Org. Biomol. Chem.* **2020**, *18*, 4390–4394.

[84] Fan, Y.; Kang, D. W.; Labalme, S.; Li, J.; Lin, W. "Enhanced Energy Transfer in A π-Conjugated Covalent Organic Framework Facilitates Excited-State Nickel Catalysis." *Angew. Chem., Int. Ed.* **2023**, *62*, e202218908.

3.5.9 General Procedure for the Phosphorylation of Aryl Chlorides

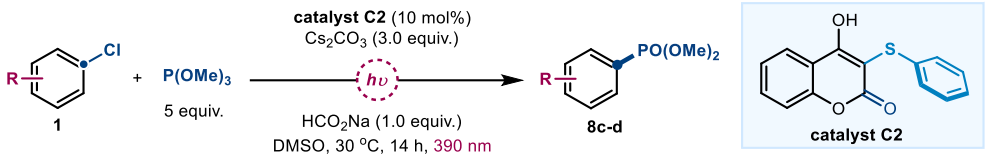

To a 4 mL glass vial, catalyst **C2** (5.4 mg, 0.02 mmol, 0.1 equiv.), cesium carbonate (163 mg, 0.4 mmol, 2 equiv.), sodium formate (13.6 mg, 0.2 mmol, 1 equiv.), and aryl chlorides **1** (*if solid*, 0.2 mmol, 1 equiv.) were added as solids. The vial was then evacuated and backfilled with argon three times. Next, aryl chlorides **1** (*if liquid*, 0.2 mmol, 1 equiv.) and trimethyl phosphite (118 µL, 1.0 mmol, 5.0 equiv.) were added, followed by argon-sparged DMSO (0.5 M, 0.4 mL) via syringe. The vial was sealed with Parafilm and stirred under irradiation from a 390 nm Kessil lamp using the PhotoRedOx Box TC™ reactor for 14 hours (***Set-up 1***, detailed in **Figure 3.30**).

After irradiation under 390 nm for 14 hours, the reaction mixture was transferred to an extraction funnel. Then, 10 mL of water and 2 mL of brine were added, and the organic layer was extracted with ethyl acetate (EtOAc). The organic layer was washed twice with brine. The combined organic layers were dried over anhydrous Na_2SO_4, filtered, and concentrated to dryness. The crude residue was purified by column chromatography to afford the corresponding product **8**.

Characterization of Products

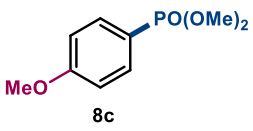

Dimethyl (4-methoxyphenyl)phosphonate (8c): Synthesized according to the General Procedure using 1-chloro-4-methoxybenzene (28.5 mg, 0.2 mmol, 1.0 equiv.) and trimethyl phosphite (124.0 mg, 1.0 mmol, 5.0 equiv.). The crude mixture was purified by flash column chromatography on silica gel (40% acetone in hexanes as eluent) to afford **8c** (23.3 mg, 54% yield) as a yellow liquid.

^{1}H NMR (400 MHz, $CDCl_3$) δ 7.73 (dd, J = 12.7, 8.9 Hz, 2H), 6.97 (dd, J = 8.9, 3.4 Hz, 2H), 3.85 (s, 3H), 3.74 (s, 3H), 3.72 (s, 3H).

^{13}C NMR (151 MHz, $CDCl_3$) δ 163.1, 134.0, 133.9, 118.6, 117.3, 114.2, 114.1, 55.4, 52.6.

^{31}P NMR (243 MHz, $CDCl_3$) δ = 22.77

Matching reported literature data.[54]

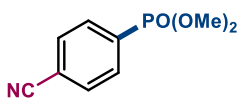

8d

Dimethyl (4-cyanophenyl)phosphonate (8d): Synthesized according to the General Procedure using 1-chloro-4-cyanobenzene (27.5 mg, 0.2 mmol, 1.0 equiv.) and trimethyl phosphite (124.0 mg, 1.0 mmol, 5.0 equiv.). The crude mixture was purified by flash column chromatography on silica gel (40% acetone in hexanes as eluent) to afford **8d** (16.9 mg, 40% yield) as a colorless oil.

^{1}H NMR (400 MHz, $CDCl_3$) δ 7.96 – 7.85 (m, 2H), 7.81 – 7.71 (m, 2H), 3.79 (s, 3H), 3.78 (s, 3H).

^{13}C NMR (151 MHz, $CDCl_3$) δ 133.4, 132.8, 132.7, 132.5, 132.4, 132.2, 118.1, 116.6, 116.6, 53.4, 53.4.

^{31}P NMR (243 MHz, $CDCl_3$) δ = 15.98

Matching reported literature data.[85]

3.5.10. Radical Trapping by Thiophenols

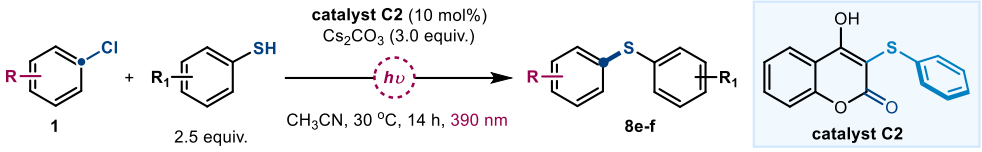

To a 4 mL glass vial, catalyst **C2** (5.4 mg, 0.02 mmol, 0.1 equiv.), cesium carbonate or sodium tert-butoxide (0.6 mmol, 3 equiv.) and aryl chlorides **1** (*if solid*, 0.2 mmol, 1 equiv.) were added as solids. The vial was then evacuated and backfilled with argon three times. Next, aryl chlorides **1** (*if liquid*, 0.2 mmol, 1 equiv.) and thiophenols (0.5 mmol, 2.5 equiv.) were added, followed by argon-sparged solvent (CH_3CN, 0.2 M) via syringe. The vial was sealed with Parafilm and stirred under irradiation from a 390 nm Kessil lamp using the PhotoRedOx Box TC™ reactor (***Set-up 1***, detailed in **Figure 3.30**).

After irradiation under 390 nm for 14 hours, the reaction mixture was transferred to an extraction funnel. Then, 10 mL of water and 2 mL of brine were added, and the organic layer was extracted with ethyl acetate (EtOAc). The organic layer was washed twice with brine. The combined organic layers were dried over anhydrous Na_2SO_4, filtered, and concentrated to dryness. The crude residue was purified by column chromatography to afford the corresponding product.

---

[85] Zhao, Y. L.; Wu, G. J.; Li, Y.; Gao, X. L.; Han, F. S. "[$NiCl_2$(dppp)]-Catalyzed Cross-Coupling of Aryl Halides with Dialkyl Phosphite, Diphenylphosphine Oxide, and Diphenylphosphine." *Chem. Eur. J.*, **2012**, *18*, 9622– 9627.

Characterization of Products

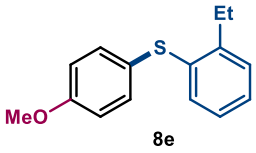

8e

(2-Ethylphenyl)(4-methoxyphenyl)sulfane (8e): Synthesized according to the General Procedure using 1-chloro-4-methoxybenzene (28.5 mg, 0.2 mmol, 1.0 equiv.) and 2-ethylbenzenethiol (54 uL, 0.4 mmol, 2.0 equiv.). The crude mixture was purified by flash column chromatography on silica gel (1% ethyl acetate in hexanes as eluent) to afford **8e** (19.5 mg, 40% yield) as a colorless oil.

^{1}H NMR (600 MHz, $CDCl_3$) δ 7.33 (d, *J* = 8.8 Hz, 2H), 7.21 (dd, *J* = 7.6, 1.5 Hz, 1H), 7.14 (td, *J* = 7.4, 1.4 Hz, 1H), 7.06 (td, *J* = 7.5, 1.6 Hz, 1H), 7.00 (dd, *J* = 7.8, 1.4 Hz, 1H), 6.88 (d, *J* = 8.8 Hz, 2H), 3.82 (s, 3H), 2.80 (q, *J* = 7.5 Hz, 2H), 1.25 (t, *J* = 7.5 Hz, 3H).

^{13}C NMR (151 MHz, $CDCl_3$) δ 159.6, 143.2, 136.6, 134.6, 129.8, 128.6, 126.6, 126.5, 125.2, 115.1, 55.5, 27.0, 14.6. Matching reported literature data.[86]

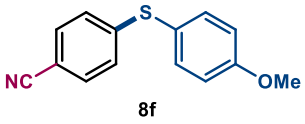

8f

4-((4-methoxyphenyl)thio)benzonitrile (8f): Synthesized according to the General Procedure using 1-chloro-4-cyanobenzene (27.5 mg, 0.2 mmol, 1.0 equiv.) and 4-methoxybenzenethiol (62 uL, 0.5 mmol, 2.5 equiv.). The crude mixture was purified by flash column chromatography on silica gel (1% ethyl acetate in hexanes as eluent) to afford **8f** (24.0 mg, 50% yield) as a colorless oil.

^{1}H NMR (600 MHz, $CDCl_3$) δ 7.45 (dd, *J* = 15.4, 8.8 Hz, 4H), 7.09 – 7.04 (m, 2H), 6.97 (d, *J* = 8.8 Hz, 2H), 3.86 (s, 3H).

^{13}C NMR (151 MHz, $CDCl_3$) δ 161.1, 147.5, 137.2, 132.4, 126.2, 120.5, 119.1, 115.7, 108.2, 55.6. Matching reported literature data.[87]

3.5.11. Mono-Defluorinative Radical Addition of Trifluorotoluenes to Olefins

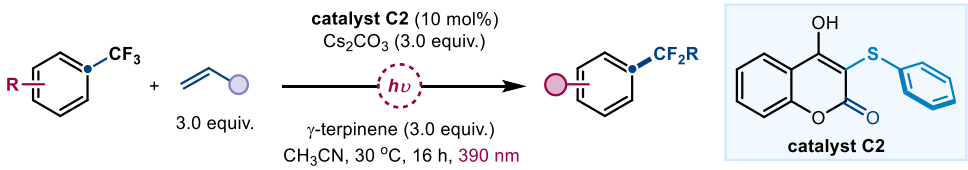

To a 4 mL glass vial, catalyst **C2** (5.4 mg, 0.02 mmol, 0.1 equiv.) and cesium carbonate (163

---

[86] Liang, G.; Wang, J-H.; Lei, T.; Cheng, Y-Y.; Zhou, C.; Chen, Y-J.; Ye, C.; Chen, B.; Tung, C-H.; Wu, L-Z. "Direct C–H Thiolation for Selective Cross-Coupling of Arenes with Thiophenols via Aerobic Visible-Light Catalysis." *Org. Lett.* **2021**, *23*, 8082−8087.

[87] Nikitin, M.; Babawale, F.; Tastekin, S.; Antonietti, M.; Ghosh, I.; König, B. "C(sp^2)–S cross-coupling reactions with nickel, visible light, and mesoporous graphitic carbon nitride." *Green Chem.* **2024**, *26*, 5845−5851.

mg, 0.4 mmol, 2 equiv.) were added as solids. The vial was then evacuated and backfilled with argon three times. Next, 1,3-bis(trifluoromethyl)benzene or *α,α,α*-trifluorotoluene (0.2 mmol, 1 equiv.), *γ*-terpinene (80 µL, 0.5 mmol, 2.5 equiv.) and unactivated alkenes (0.6 mmol, 3 equiv.) were added, followed by argon-sparged CH_3CN (0.1 M) via syringe. The vial was sealed with Parafilm and stirred under irradiation from a 390 nm Kessil lamp using the PhotoRedOx Box TC™ reactor for 16 hours (***Set-up 1***, detailed in **Figure 3.30**).

After irradiation under 390 nm for 16 hours, the reaction mixture was transferred to an extraction funnel. Then, 10 mL of water and 2 mL of brine were added, and the organic layer was extracted with ethyl acetate (EtOAc). The organic layer was washed twice with brine. The combined organic layers were dried over anhydrous Na_2SO_4, filtered, and concentrated to dryness. The crude residue was purified by column chromatography to afford the corresponding product.

Characterization of Products

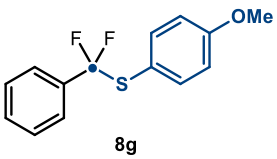

8g

(Difluoro(phenyl)methyl)(4-methoxyphenyl)sulfane (8g): Synthesized according to the General Procedure using α,α,α-trifluorotoluene (29.2 mg, 0.2 mmol, 1.0 equiv.) and 4-methoxybenzenethiol (62 uL, 0.5 mmol, 2.5 equiv.). The crude mixture was purified by flash column chromatography on silica gel (2% ethyl acetate in hexanes as eluent) to afford **8g** (44.7 mg, 84% yield) as a white solid.

^{1}H NMR (600 MHz, $CDCl_3$) δ 7.58 – 7.50 (m, 4H), 7.47 – 7.36 (m, 3H), 6.92 – 6.87 (m, 2H), 3.83 (s, 3H). **^{19}F NMR (376 MHz, $CDCl_3$)** δ -72.8.

Matching reported literature data.[88]

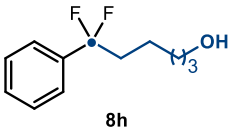

8h

6,6-difluoro-6-phenylhexan-1-ol (8h): Synthesized according to the General Procedure using α,α,α-trifluorotoluene (29.2 mg, 0.2 mmol, 1.0 equiv.) and 4-Penten-1-ol (51.7 mg, 0.6 mmol, 2.0 equiv.). The crude mixture was purified by flash column chromatography on silica gel (20% ethyl acetate in hexanes as eluent) to afford **8h** (37.7 mg, 88% yield) as a colorless oil.

^{1}H NMR (400 MHz, $CDCl_3$) δ 7.51 – 7.36 (m, 5H), 3.61 (t, J = 6.5 Hz, 2H), 2.21 – 2.05 (m, 2H), 1.60 – 1.51 (m, 2H), 1.47 – 1.38 (m, 4H). **^{19}F NMR (376 MHz, $CDCl_3$)** δ -95.5 (t, J = 16.3 Hz). Matching reported literature data.[89]

---

[88] Brigham, C. E.; Malapit, C. A.; Lalloo, N.; Sanford, M. S. "Nickel-Catalyzed Decarbonylative Synthesis of FluoroalkylThioethers." *ACS Catal.* **2020**, *10*, 8315−8320.

[89] Li, S-Y.; Yang, X-Y.; Shen, P-H.; Xu, L.; Xu, J.; Zhang, Q.; Xu, H-J. "Selective Defluoroalkylation and Hydrodefluorination of Trifluoromethyl Groups Photocatalyzed by Dihydroacridine Derivatives." *J. Org. Chem.* **2023**, *88*, 17284−17296.

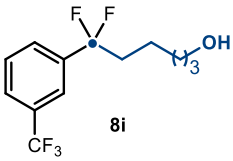

8i

6,6-difluoro-6-phenylhexan-1-ol (8i): Synthesized according to the General Procedure using 1,3-bis(trifluoromethyl)benzene (42.8 mg, 0.2 mmol, 1.0 equiv.) and 4-Penten-1-ol (51.7 mg, 0.6 mmol, 2.0 equiv.). The crude mixture was purified by flash column chromatography on silica gel (20% ethyl acetate in hexanes as eluent) to afford **8i** (46.2 mg, 82% yield) as a colorless oil.

^{1}H NMR (400 MHz, $CDCl_3$) δ 7.80 – 7.71 (m, 1H), 7.71 – 7.62 (m, 2H), 7.56 (t, *J* = 7.8 Hz, 1H), 3.62 (t, *J* = 6.5 Hz, 2H), 2.22 – 2.06 (m, 2H), 1.66 – 1.52 (m, 2H), 1.49 – 1.33 (m, 4H). **^{19}F NMR (376 MHz, $CDCl_3$)** δ -62.8, -96.1 (t, *J* = 16.5 Hz). Matching reported literature data.[90]

3.5.12. Birch Reduction

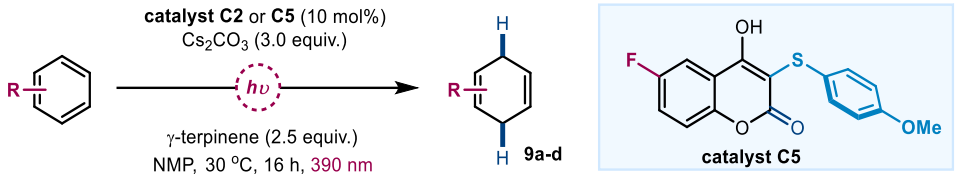

To a 4 mL glass vial, catalyst **C2** (5.4 mg, 0.02 mmol, 0.1 equiv.) or **C5** (6.4 mg, 0,02 mmol, 0.1 equiv. where specified), Cs_2CO_3 (0.4 mmol, 2 equiv.) and arenes (*if solid*, 0.2 mmol, 1 equiv.) were sequentially added. The vial was sealed with a screw-top cap with the septum and then evacuated and backfilled with argon three times. Next, arenes **4** (*if liquid*, 0.2 mmol, 1 equiv.) and γ-terpinene (80 µL, 0.5 mmol, 2.5 equiv.) were added, followed by argon-sparged NMP (0.5 M, 0.4 mL) via syringe. The vial was sealed with Parafilm and stirred under the irradiation of a 390 nm Kessil lamp in the PhotoRedOx Box TC™ reactor for 16 hours using ***Set-up 2***, as detailed in **Figure 3.31**.

NMR analyses (products **9a, 9b, 9d**): dibromomethane was added as the internal standard (34.8 mg, 0.2 mmol, 1 equiv.) to the crude reaction mixture, followed by 2 mL H_2O and 1 mL of brine. Then, the solution was extracted with 0.7 mL of $CDCl_3$ and the reactions were analyzed via ^{1}H NMR spectroscopy of the $CDCl_3$ layer.

For the isolation of product **9c**: After irradiation under 390 nm for 16 hours, the reaction mixture was transferred to an extraction funnel, 10 mL of H_2O and 2 mL of brine were added and the organic layer was extracted with EtOAc. The organic layer was washed twice with brine, the combined organic layers were dried over anhydrous Na_2SO_4, filtered, and concentrated to dryness. The crude residue was purified by column chromatography to afford

[90] Wang, H.; Jui, N. T. "Catalytic Defluoroalkylation of Trifluoromethylaromatics with Unactivated Alkenes." *J. Am. Chem. Soc.* **2018**, *140*, 163−166.

the corresponding products with the reported yields (>95% purity according to ^{1}H NMR analysis).

The crude ^{1}H NMR of products **9a, 9b,** and **9d**, which are reported in the NMR Section I of the Supporting Information, matched the reported literature data.[54, 60, 91]

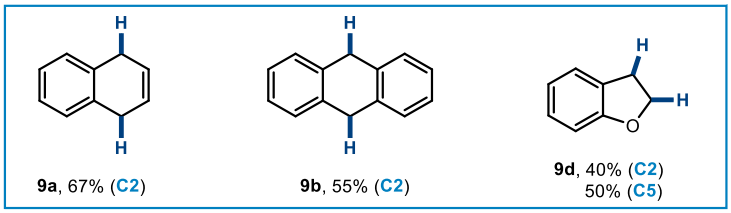

Figure 3.34. Compounds for which yields have been determined by ^{1}H NMR analysis using an internal standard.

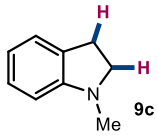

1-Methylindoline (9c): Synthesized according to the General Procedure using 1-methyl-1H-indole (26.2 mg, 0.2 mmol, 1.0 equiv.) and **C5** (6.4 mg, 0.02 mmol, 10 mol%). The crude mixture was purified by flash column chromatography on silica gel (4% ethyl acetate in hexanes as eluent) to afford **9c** (17.0 mg, 64% yield) as an orange oil. **^{1}H NMR (400 MHz, $CDCl_3$)** δ 7.16 – 7.00 (m, 2H), 6.75 – 6.61 (m, 1H), 6.49 (d, J = 7.0 Hz, 1H), 3.29 (d, J = 15.9 Hz, 2H), 2.95 (t, J = 8.5 Hz, 2H), 2.76 (s, 3H). **^{13}C NMR (151 MHz, $CDCl_3$)** δ 153.7, 130.7, 127.7, 124.6, 118.1, 107.6, 56.5, 36.6, 29.1. Matching reported literature data.[92]

3.5.13. Reductive Radical Cyclization

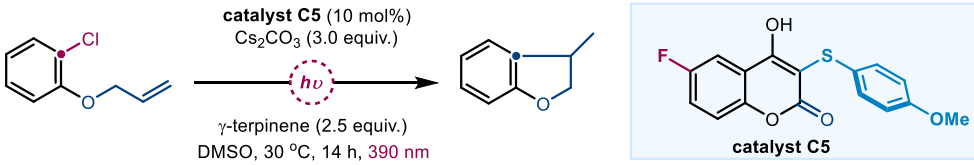

To a 4 mL glass vial, catalyst **C5** (6.4 mg, 0.02 mmol, 0.1 equiv.) and caesium carbonate (130.4 mg, 0.4 mmol, 2 equiv.) were added as solids. The vial was then evacuated and backfilled with argon three times. Next, allyl 2-chlorophenyl ether (33.8 mg, 0.2 mmol, 1 equiv.) and γ-terpinene (64.2 µL, 0.4 mmol, 2.0 equiv.) were added, followed by argon-sparged DMSO (1 mL) via syringe. The vial was sealed with Parafilm and then stirred under

[91] Szostak, M.; Spain, M.; Procter, D. J. "Determination of the Effective Redox Potentials of SmI_2, $SmBr_2$, $SmCl_2$, and their Complexes with Water by Reduction of Aromatic Hydrocarbons. Reduction of Anthracene and Stilbene by samarium (II) Iodide–Water Complex." *J. Org. Chem.* **2014**, *79*, 2522–2537.

[92] Peng, Y.; Wang, G.; Klare, H. F. T. Oestreich, M. "Ring Contraction of Saturated Cyclic Amines and Rearrangement of Acyclic Amines Through Their Corresponding Hydroxylamines." *Angew. Chem. Int. Ed.* **2024**, *63*, e202410483.

the irradiation of 390 nm *Kessil* lamp with PhotoRedOx Box TC™ reactor for 14 hours using ***Set-up 1*** detailed in **Figure 3.30**.

After irradiation under 390 nm for 14 hours, the reaction mixture was transferred to an extraction funnel. Then, 10 mL of water and 2 mL of brine were added, and the organic layer was extracted with ethyl acetate (EtOAc). The organic layer was washed twice with brine. The combined organic layers were dried over anhydrous Na_2SO_4, filtered, and concentrated to dryness). The crude mixture was purified by flash column chromatography on silica gel (1% ethyl acetate in hexanes as eluent) to afford **11a** (16.1 mg, 60% yield) as a colorless oil.

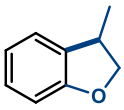

11a

3-methyl-2,3-dihydrobenzofuran (11a)

^{1}H NMR (600 MHz, $CDCl_3$) δ 7.16 (d, *J* = 8.7 Hz, 1H), 7.12 (t, *J* = 7.3 Hz, 1H), 6.87 (t, *J* = 7.3 Hz, 1H), 6.79 (d, *J* = 8.1 Hz, 1H), 4.68 (t, *J* = 8.7 Hz, 1H), 4.12 – 4.01 (m, 1H), 3.55 (h, *J* = 6.8 Hz, 1H), 1.33 (d, *J* = 6.9 Hz, 3H).

Matching reported literature data.[93]

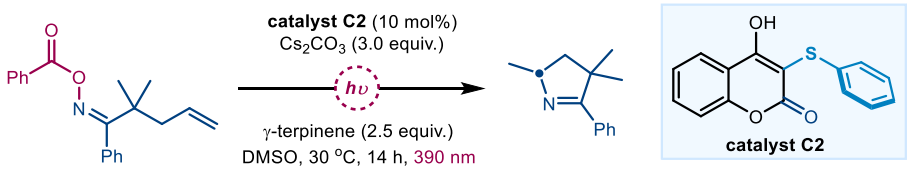

To a 4 mL glass vial, catalyst **C2** (2.7 mg, 0.01 mmol, 0.1 equiv.), γ,δ-unsaturated *O*-benzoyl ketoxime (30.7 mg, 0.1 mmol, 1.0 equiv.), and cesium carbonate (32.6 mg, 0.1 mmol, 1.0 equiv.) were added as solids. The vial was then evacuated and backfilled with argon three times. Next, γ-terpinene (32.1 µL, 0.2 mmol, 2.0 equiv.) was added, followed by argon-sparged DMSO (0.1 M, 0.4 mL) via syringe. The vial was sealed with Parafilm and stirred under the irradiation of a 390 nm Kessil lamp in the PhotoRedOx Box TC™ reactor for 14 hours using ***Set-up 1***, as detailed in **Figure 3.30**.

After irradiation under 390 nm for 14 hours, the reaction mixture was transferred to an extraction funnel. Then, 10 mL of water and 2 mL of brine were added, and the organic layer was extracted with ethyl acetate (EtOAc). The organic layer was washed twice with brine. The combined organic layers were dried over anhydrous Na_2SO_4, filtered, and concentrated to dryness. The crude mixture was purified by flash column chromatography on silica gel (20% ethyl acetate in hexanes as eluent) to afford **11b** (12.2 mg, 65% yield) as a yellow oil.

---

[93] Cowper, N. G. W.; Chernowsky, C. P.; Williams, O. P.; Wickens, Z. K. "Potent Reductants via Electron-Primed Photoredox Catalysis: Unlocking Aryl Chlorides for Radical Coupling." *J.Am. Chem. Soc.* **2020**, *142*, 2093−2099.

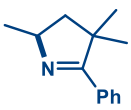

11b

2,4,4-trimethyl-5-phenyl-3,4-dihydro-2H-pyrrole (11b)

^{1}H NMR (600 MHz, $CDCl_3$) δ 7.73 – 7.63 (m, 2H), 7.37 (dd, J = 5.2, 2.0 Hz, 3H), 4.17 – 4.01 (m, 1H), 2.11 (dd, J = 12.4, 6.7 Hz, 1H), 1.50 (dd, J = 12.4, 8.6 Hz, 1H), 1.38 (d, J = 6.8 Hz, 3H), 1.35 (s, 3H), 1.33 (s, 3H).

Matching reported literature data.[94]

3.5.14. Difunctionalization of Alkenes

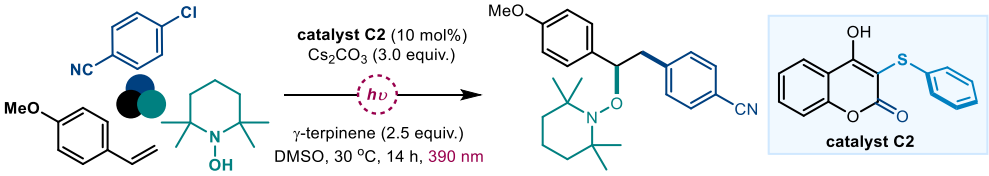

To a 4 mL glass vial, catalyst **C2** (5.5 mg, 0.02 mmol, 0.1 equiv.), TEMPO-H (38 mg, 0.24 mmol, 1.2 equiv.) and caesium carbonate (163 mg, 0.6 mmol, 3 equiv.) were added as solids. The vial was then evacuated and backfilled with argon three times. Next, 4-chlorobenzonitrile (27.5 mg, 0.2 mmol, 1 equiv.) and 4-methoxystyrene (40 µL, 0.3 mmol, 1.5 equiv.) were added, followed by argon-sparged DMSO (1 mL) via syringe. The vial was sealed with Parafilm and stirred under the irradiation of a 390 nm Kessil lamp in the PhotoRedOx Box TC™ reactor for 14 hours using ***Set-up 1***, as detailed in **Figure 3.34**.

After irradiation under 390 nm for 14 hours, the reaction mixture was transferred to an extraction funnel. Then, 10 mL of water and 2 mL of brine were added, and the organic layer was extracted with ethyl acetate (EtOAc). The organic layer was washed twice with brine. The combined organic layers were dried over anhydrous Na_2SO_4, filtered, and concentrated to dryness. The crude residue was purified by column chromatography to afford the corresponding product **12** (31 mg, 40% yield) as a white solid.

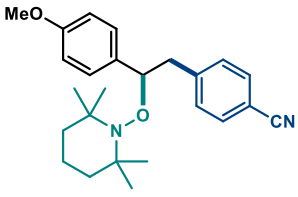

12

4-(2-(4-Methoxyphenyl)-2-((2,2,6,6-tetramethylpiperidin-1-yl)oxy)ethyl)benzonitrile (12)

^{1}H NMR (600 MHz, $CDCl_3$) δ 7.41 (d, *J* = 8.3 Hz, 2H), 6.98 (dd, *J* = 8.4, 3.7 Hz, 4H), 6.74 (d, *J* = 8.6 Hz, 2H), 4.74 (dd, *J* = 9.8, 4.7 Hz, 1H), 3.77 (s, 3H), 3.63 (dd, *J* = 12.7, 4.7 Hz, 1H), 2.95 (dd, *J* = 12.7, 9.8 Hz, 1H), 1.54 – 1.25 (m, 12H), 1.19 – 1.00 (m, 6H). **^{13}C NMR (151 MHz, $CDCl_3$)** δ 159.0, 144.7, 134.1, 131.8, 130.6, 129.1, 119.3, 113.2, 109.8, 87.4, 60.2, 59.9, 55.2, 43.2, 40.5, 29.8, 20.5, 17.3.

Matching reported literature data.[62]

---

[94] Usami, K.; Yamaguchi, E.; Tada, N.; Itoh, A. "Visible-Light-Mediated Iminyl Radical Generation from BenzylOxime Ether: Synthesis of Pyrroline via Hydroimination Cyclization." *Org. Lett.* **2018**, *20*, 5714−5717.

3.5.15 Energy Transfer Catalysis

General Procedure for the *E*/*Z* Photoisomerization

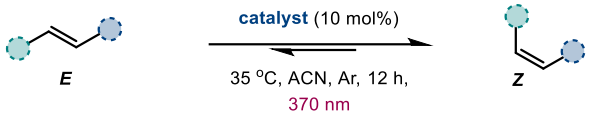

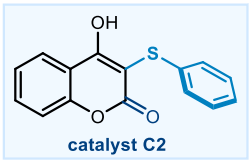

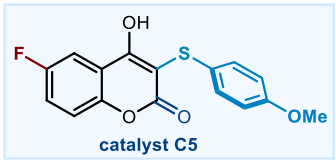

To a 10 mL Schlenk tube, catalyst (0.02 mmol, 0.1 equiv.) and *E* alkenes (0.2 mmol, 1 equiv.) were sequentially added, followed by argon-sparged CH_3CN (0.2 M, 1 mL) via syringe. The Schlenk tube was sealed, frozen in liquid nitrogen, and evacuated. This process was repeated three times, followed by three cycles of freezing, evacuating, and backfilling with argon. The reaction mixture was then stirred under 370 nm Kessil lamp irradiation for 12 hours, using ***Set-up 3***, as detailed in **Figure 3.32**.

After irradiation under 370 nm for 12 hours, the reaction mixture was concentrated to dryness. The crude residue was purified by column chromatography to afford the corresponding product *Z*-**3**.

Characterization of Products

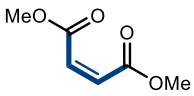

Z-3a

Dimethyl maleate (*Z*-3a): Synthesized according to the General Procedure C using dimethyl fumarate (28.8 mg, 0.2 mmol, 1.0 equiv.) and **C2** (5.4 mg, 0.02 mmol, 10 mol%.). The crude mixture was purified by flash column chromatography on silica gel (20% diethyl ether in hexanes as eluent, $\mathbf{R_f}$ = 0.4) to afford *Z*-**3a** (26.0 mg, 90% yield) as a colorless oil. The ratio of isomers in the crude mixture was determined via ^{1}H NMR analysis - *Z*:*E* = 92:8.

^{1}H NMR (600 MHz, $CDCl_3$) δ 6.29 – 6.20 (m, 2H), 3.84 – 3.70 (m, 6H).

^{13}C NMR (151 MHz, $CDCl_3$) δ 166.0, 130.1, 52.5. Matching reported literature data.[69]

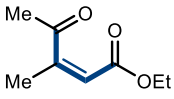

Z-**3b**

Ethyl (*Z*)-3-methyl-4-oxopent-2-enoate (*Z*-3b): Synthesized according to the General Procedure C using Ethyl (*E*)-3-methyl-4-oxohex-2-enoate (31.2 mg, 0.2 mmol, 1.0 equiv.), **C2** (5.4 mg, 0.02 mmol, 10 mol%.). The crude mixture was purified by flash column chromatography on silica gel (10% diethyl ether in hexanes as eluent, $\mathbf{R_f}$ = 0.24) to afford *Z*-**3b** (25.0 mg, 80% yield)

as a colorless oil. The ratio of isomers in the crude mixture was determined via ^{1}H NMR - *Z:E* = 97:3.

^{1}H NMR (600 MHz, $CDCl_3$) δ 5.68 (q, *J* = 1.6 Hz, 1H), 4.16 (q, *J* = 7.1 Hz, 2H), 2.36 (s, 3H), 1.99 (d, *J* = 1.6 Hz, 3H), 1.26 (t, *J* = 7.2 Hz, 4H).

^{13}C NMR (151 MHz, $CDCl_3$) δ 206.6, 165.5, 157.5, 117.4, 61.1, 29.0, 20.6, 14.4.

Matching reported literature data.[66]

Z-**3c**

Maleonitrile (*Z*-3c): Synthesized according to the General Procedure C using 1,2-Dicyanoethylene (15.6 mg, 0.2 mmol, 1.0 equiv.), **C2** (5.4 mg, 0.02 mmol, 10 mol%). After completion of the reaction, dibromomethane was added as the internal standard (34.8 mg, 0.2 mmol, 1 equiv.) to the crude reaction mixture, the ratio of isomers in the crude mixture was determined via ^{1}H NMR - *Z:E* = 53:47 with a 40% yield. Matching reported literature data.[95]

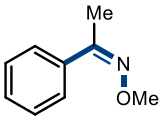

Z-**3d**

(*Z*)-1-phenylethan-1-one *O*-methyl oxime (*Z*-3d): Synthesized according to the General Procedure C using (*E*)-1-phenylethan-1-one O-methyl oxime (30.0 mg, 0.2 mmol, 1.0 equiv.), **C2** (5.4 mg, 0.02 mmol, 10 mol%.), which were stirred under the irradiation of a 390 nm Kessil lamp in the PhotoRedOx Box TC™ reactor for 24 hours using *Set-up 3*, as detailed in Figure S6. After completion, the crude mixture was purified by flash column chromatography on silica gel (10% diethyl ether in hexanes as eluent, $\mathbf{R_f}$ = 0.6) to afford *Z*-**3d** (24.3 mg, 81% yield) as a colorless oil. The ratio of isomers in the crude mixture was determined via ^{1}H NMR - *Z:E* = 91:9.

^{1}H NMR (600 MHz, $CDCl_3$) δ 7.52 – 7.44 (m, 2H), 7.44 – 7.31 (m, 3H), 3.85 (s, 3H), 2.21 (s, 3H). **^{13}C NMR (151 MHz, $CDCl_3$)** δ 154.2, 134.8, 129.3, 128.5, 128.2, 62.1, 22.0.

Matching reported literature data.[96]

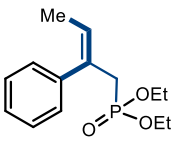

Z-**3e**

Diethyl (*Z*)-(2-phenylbut-1-en-1-yl)phosphonate (*Z*-3e): Synthesized according to the General Procedure C using Diethyl (*E*)-(2-phenylbut-1-en-1-yl)phosphonate (26.8 mg, 0.1 mmol, 1.0 equiv.), **C5** (3.2 mg, 0.01 mmol, 10 mol%.) and Cs_2CO_3 (5.0 mg, 0.015 mmol, 15 mol%.), which were stirred under the irradiation of a 390 nm Kessil lamp in the PhotoRedOx Box TC™ reactor for 24 hours using *Set-up 3*, as detailed in Figure S6. After completion, the crude mixture was purified by flash column chromatography on silica gel

---

[95] Kaplaneris, N.; Bisticha, A.; Papadopoulos, G. N.; Limnios, D.; Kokotos, C. G. "Photoorganocatalytic synthesis of lactones via a selective C–H activation–alkylation of alcohols." *Green Chem.* **2017**, *19*, 4451–4456.

[96] Noverges, B.; Mollar, C.; Medio-Simon, M.; Asensio, G. "Palladium-Catalyzed Suzuki–Miyaura Cross-Coupling of α-Halomethyl Oxime Ethers and Site-Selective Cross-Coupling of Dihalo Derivatives." *Adv. Synth. Catal.* **2013**, *355*, 2327–2342.

(ethyl acetate as eluent, $\mathbf{R_f}$ = 0.26) to afford *Z*-**3e** (18.9 mg, 70% yield) as a colorless oil. The ratio of isomers in the crude mixture was determined via ^{1}H NMR - *Z:E* = 91:9.

^{1}H NMR (600 MHz, $CDCl_3$) δ 7.37 – 7.29 (m, 2H), 7.26 – 7.21 (m, 3H), 5.81 (s, 1H), 4.02 – 3.83 (m, 4H), 2.91 (d, J = 21.4 Hz, 2H), 1.64 (t, J = 6.5 Hz, 3H), 1.17 (t, J = 7.1 Hz, 6H).

^{13}C NMR (151 MHz, $CDCl_3$) δ 140.4 (d, *J* = 3.8 Hz), 131.5 (d, *J* = 10.6 Hz), 129.1, 128.4, 127.3 (d, *J* = 12.0 Hz), 127.2, 62.0 (d, *J* = 6.8 Hz), 36.3 (d, *J* = 138.3 Hz), 16.6 (d, *J* = 6.2 Hz), 15.5 (d, *J* = 3.0 Hz).

^{31}P NMR (243 MHz, $CDCl_3$) δ 27.33 (ddp, *J* = 21.4, 14.6, 6.9 Hz).

HRMS: calculated for $C_{14}H_{22}O_3P$ ($M+H^+$): 269.1301, found 269.1308.

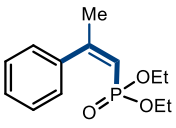

Z-**3f**

Diethyl (*Z*)-(2-phenylprop-1-en-1-yl)phosphonate (*Z*-3f): Synthesized according to the General Procedure C using diethyl (*E*)-(2-phenylprop-1-en-1-yl)phosphonate (50.9 mg, 0.2 mmol, 1.0 equiv.), **C5** (6.4 mg, 0.02 mmol, 10 mol%), which were stirred under the irradiation of a 370 nm Kessil lamp with a fan for 22 hours using *Set-up 3*, as detailed in Figure S6. After completion, the crude mixture was purified by flash column chromatography on silica gel (30% ethyl acetate in hexanes as eluent, $\mathbf{R_f}$ = 0.3) to afford *Z*-**3f** (45.3 mg, 89% yield) as a colorless oil. The ratio of isomers in the crude mixture was determined via ^{1}H NMR - *Z:E* = 93:7.

^{1}H NMR (600 MHz, $CDCl_3$) δ 7.41 – 7.37 (m, 2H), 7.37 – 7.29 (m, 3H), 5.73 (dd, *J* = 17.3, 1.5 Hz, 1H), 3.94 – 3.66 (m, 4H), 2.23 (s, 3H), 1.07 (t, *J* = 7.0 Hz, 6H).

^{13}C NMR (151 MHz, $CDCl_3$) δ 159.3, 159.3, 140.9, 140.8, 128.6, 128.3, 127.7, 127.6, 115.8, 114.5, 61.7, 61.6, 28.8, 28.7, 16.4.

^{31}P NMR (243 MHz, $CDCl_3$) δ = 16.20 (dp, *J* = 15.8, 7.7 Hz).

HRMS: calculated for $C_{13}H_{19}NaO_3P$ ($M+Na^+$): 277.0964, found 277.0966.

Matching reported literature data.[76]

General Procedure D for the Intermolecular [2+2] Photocycloadditions

To a 10 mL Schlenk tube, catalyst **C** (0.02 mmol, 0.1 equiv.), the EnT-responsive substrate (0.2 mmol, 1 equiv.), and an alkene were sequentially added, followed by argon-sparged solvent (0.2 M, 1 mL) via syringe. The Schlenk tube was sealed, frozen in liquid nitrogen, and evacuated. This process was repeated three times, followed by three cycles of freezing, evacuating, and backfilling with argon. The reaction mixture was then stirred under irradiation of 370 nm *Kessil* lamp with a fan for 22 hours using ***Set-up 3*** detailed in **Figure 3.32**.

After the reaction was completed, the reaction mixture was transferred to an extraction funnel, 10 mL of H_2O and 2 mL of brine were added and the organic layer was extracted with EtOAc. The organic layer was washed twice with brine, the combined organic layers were dried over

anhydrous Na_2SO_4, filtered, and concentrated to dryness. The crude residue was purified by column chromatography to afford the corresponding products with the reported yields.

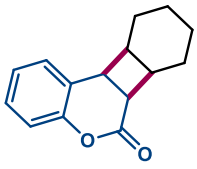

4

6a,6b,7,8,9,10,10a,10b-Octahydro-benzo(3,4)cyclobuta[1,2-c]chromen-6-on (4): Synthesized according to the General Procedure D using coumarin (30.0 mg, 0.2 mmol, 1.0 equiv.), cyclohexene (49.3 mg, 0.6 mmol, 3 equiv.), and catalyst **C2** (5.4 mg, 0.02 mmol, 10 mol%.), dry CH_3CN (1 mL). The crude mixture was purified by flash column chromatography on silica gel (10% diethyl ether in hexanes as eluent) to afford **4** (27.5 mg, 60% yield) as a colorless oil. The ratio of isomers in the crude mixture was determined via ^{1}H NMR analysis to be d.r. = 17:7:1 (see section I for details).

^{1}H NMR (600 MHz, $CDCl_3$) δ 7.18 – 7.14 (m, 1H), 7.03 – 6.99 (m, 2H), 6.97 – 6.94 (m, 1H), 3.77 (t, *J* = 8.9 Hz, 1H), 3.51 – 3.43 (m, 1H), 3.04 – 2.92 (m, 1H), 2.80 – 2.73 (m, 1H), 1.67 – 1.54 (m, 2H), 1.38 – 0.98 (m, 6H).

^{13}C NMR (151 MHz, $CDCl_3$) δ 168.4, 152.4, 128.9, 128.5, 124.7, 121.4, 117.5, 38.1, 38.0, 36.8, 36.6, 24.0, 23.9, 22.2, 21.9.

Matching reported literature data.[72]

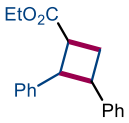

5

Ethyl 2,3-diphenylcyclobutane-1-carboxylate (5): Synthesized according to the General Procedure D using ethyl cinnamate (32.4 mg, 0.2 mmol, 1.0 equiv.), styrene (104.1mg, 1 mmol, 5 equiv.) and catalyst **C3** (5.8 mg, 0.02 mmol, 10 mol%.), dry DCM (1 mL). The crude mixture was purified by flash column chromatography on silica gel (4% ethyl acetate in hexanes as eluent) to afford **5** (27.8 mg, 50% yield) as a colorless oil. The ratio of isomers in the crude mixture was determined via ^{1}H NMR analysis to be d.r. = 3:1.

^{1}H NMR (600 MHz, $CDCl_3$) δ 7.26 – 7.19 (m, 8H), 7.15 (t, *J* = 7.1 Hz, 2H), 4.15 – 4.07 (m, 2H), 3.78 (t, *J* = 9.8 Hz, 1H), 3.51 – 3.41 (m, 1H), 3.15 – 3.04 (m, 1H), 2.60 – 2.48 (m, 1H), 2.33 (q, *J* = 10.4 Hz, 1H), 1.21 (t, *J* = 7.1 Hz, 4H).

^{13}C NMR (151 MHz, $CDCl_3$) δ 174.5, 143.6, 142.6, 128.8, 127.2, 127.0, 127.0, 126.9, 60.9, 51.0, 43.6, 42.1, 30.1, 29.9, 14.6. Matching reported literature data.[73]

General Procedure E for the Intramolecular [2+2] Photocycloadditions

To a 10 mL Schlenk tube, catalyst **C2** (5.4 mg, 0.02 mmol, 10 mol%.) and the substrate (0.2 mmol, 1 equiv.) were sequentially added, followed by argon-sparged solvent (0.2 M, 1 mL) via syringe. The Schlenk tube was sealed, frozen in liquid nitrogen, and evacuated. This process was repeated three times, followed by three cycles of freezing, evacuating, and backfilling with argon. The reaction mixture was then stirred under irradiation of 370 nm *Kessil* lamp with a fan for 22 hours using ***Set-up 3*** detailed in **Figure 3.32**.

After the reaction was completed, the reaction mixture was transferred to an extraction funnel, 10 mL of H_2O and 2 mL of brine were added, and the organic layer was extracted with EtOAc. The organic layer was washed twice with brine, the combined organic layers were dried over anhydrous Na_2SO_4, filtered, and concentrated to dryness. The crude residue was purified by column chromatography to afford the corresponding products with the reported yields.

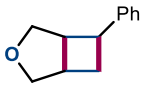

6

6-Phenyl-3-oxa-bicyclo[3.2.0]heptane (6): Synthesized according to the General Procedure E using (*E*)-(3-(allyloxy)prop-1-en-1-yl)benzene (34.8 mg, 0.2 mmol, 1.0 equiv.) and catalyst **C2** (5.4 mg, 0.02 mmol, 10 mol%.), dry DMSO (1mL). The mixture was purified by flash column chromatography on silica gel (10% diethyl ether in hexanes as eluent) to afford **6** (20.2 mg, 58% yield) as a colorless oil. The ratio of isomers in the crude mixture was determined via ^{1}H NMR analysis to be d.r. = 5:1.

^{1}H NMR (600 MHz, $CDCl_3$) δ 7.35 – 7.28 (m, 2H), 7.25 (d, *J* = 6.0 Hz, 2H), 7.22 – 7.16 (m, 1H), 4.03 – 3.94 (m, 2H), 3.61 (dd, *J* = 8.9, 6.0 Hz, 1H), 3.51 (dd, *J* = 9.3, 4.1 Hz, 1H), 3.23 (dd, *J* = 12.4, 9.6 Hz, 1H), 3.05 – 2.90 (m, 2H), 2.35 – 2.24 (m, 1H), 2.21 – 2.12 (m, 1H).

^{13}C NMR (151 MHz, $CDCl_3$) δ 146.2, 128.6, 126.5, 126.1, 74.6, 74.1, 47.3, 42.1, 35.4, 31.9. Matching reported literature data.[74]

7

Quadricyclo[2.2.1.0.0]heptane (7): Synthesized according to the General Procedure E using bicyclo[2.2.1]hepta-2,5-diene (18.4 mg, 0.2 mmol, 1.0 equiv.) and catalyst **C2** (5.4 mg, 0.02 mmol, 10 mol%.) using CD_3CN as solvent. After completion of the reaction, dibromomethane was added as the internal standard (34.8 mg, 0.2 mmol, 1 equiv.) to the crude reaction mixture. The yield of **7** (35% yield) was determined via ^{1}H NMR analysis of the crude mixture. Characterization data matching reported literature data.[75]

3.5.16. Quantum Yield Determination

-Experimental Setup

The experiments for the quantum yield determination were conducted under illumination by a 390 Kessil lamp (setup depicted in **Figure 3.35**), using a 3D printed photoreactor. The intensity was fixed to the maximum value.

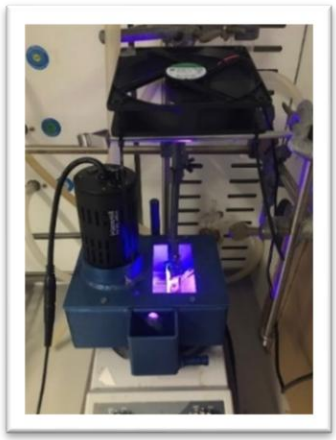

Figure 3.35. Kessil lamp set-up for the quantum yield determination

General Procedure for photon Flux (F) determination:[97]

$$\Phi = M / (F \cdot t \cdot f) \quad (1)$$

$$f = 1\text{-}10^{-A} \quad (2)$$

M is the moles of product formed (mol), **F** is the number of photons emitted per second (einstein s−1), **t** is the time (s) and **f** is fraction of light absorbed which can be calculated using eq. 2, Rwhere **A** is the measured absorbance at 390 nm.

The number of photons emitted per second was determined using azobenzene as actinometer.[98,99] Using the reaction setup depicted in **Figure 3.35**, a glass vial was filled with a solution of *Z*-azobenzene (0.1 mmol) in CD_3OD (0.1M) and irradiated at 390 nm. The *trans-cis* isomerization was monitored by ^1H NMR analysis using dibromomethane as an internal standard (**Figure 3.36**).

---

[97] Cismesia, M. A.; Yoon, T. P. "Characterizing chain processes in visible light photoredox catalysis." *Chem. Sci.*, **2015**, *6*, 5426−5434.

[98] Leeuwen, T. V.; Buzzetti, L.; Perego, L. A.; Melchiorre, P. "A Redox-Active Nickel Complex that Acts as an Electron Mediator in Photochemical Giese Reactions." *Angew. Chem., Int. Ed.* **2019**, *58*, 4953−4957.

[99] Ladányi, V.; Dvořák, P.; Anshori, J. A.; Vetráková, L.; Wirz, J.; Heger, D. "Azobenzene photoisomerization quantum yields in methanol redetermined." *Photochem. Photobiol. Sci.*, **2017**, *16*, 1757−1761.

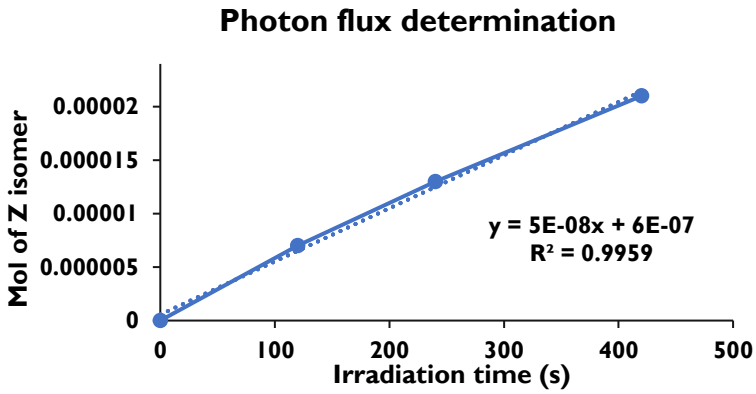

Figure 3.36. Plot of moles of *cis*-azobenzene formed vs irradiation time (s)

The actinometer solution was irradiated for 0 min, 2 min, 4 min, and 7 min. According to the equations (**1**) and (**2**), and an estimated quantum yield of *trans-cis* isomerization process at 390 nm ($\Phi = 0.262$), the number of photons emitted per time unit (**F**) was determined (2.08×10^{-8} mol s^{-1}).

Quantum Yield Determination:

Following the general procedure, five model dechlorination reactions using 4-chlorophenylboronic acid pinacol ester **1d**, catalyst **C2**, γ-terpinene and Cs_2CO_3, leading to product **2d**, were performed separately. Each reaction mixture was irradiated for 0 h, 2 h, 4 h, 6 h, and 8 h. After irradiation, the reactions were worked up and the amount of product **2d** formed was determined by ^{1}H NMR analysis of the crude using mesitylene as the internal standard. Fraction of light absorbed *f* was recognized as 1. The moles of the formed product **2d** are plotted against the number of incident photons (**Figure 3.37**). The quantum yield was calculated to be $\Phi = 0.13$ based on the slope and eq. (**1**), (**2**).

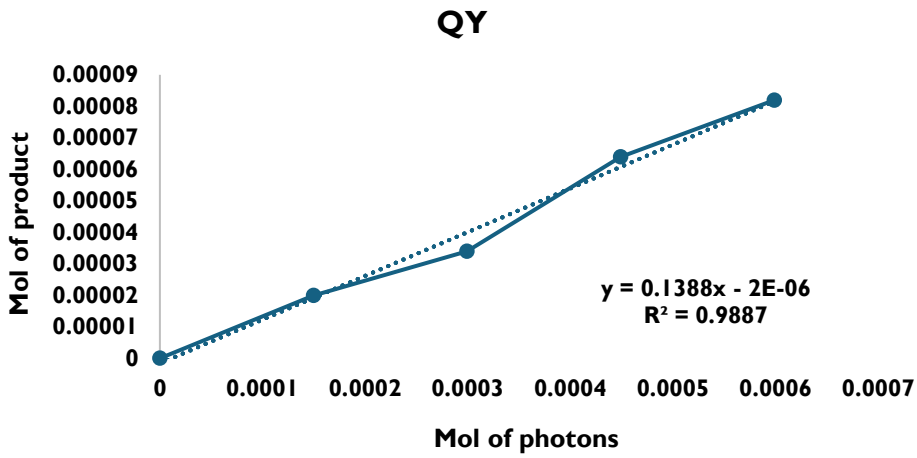

Figure 3.37. Plot of moles of incident photons vs moles of product **2d** formed.

3.5.17. Photophysical Characterization of the Photocatalysts C

Sample Preparation: Eight 25 mL glass vials, each containing either catalyst **C2**, **C3**, **C4**, or **C5**, or their mixture with Cs_2CO_3 (3 equiv.) as the base, were sealed with septa and degassed. Then, dry, degassed CH_3CN (20 mL) was added to each vial to prepare 0.1 M solutions of the catalysts. From these stock solutions, **C2** to **C5** were prepared at concentrations of 10^{-3} M and 10^{-4} M, and similarly, **C2** to **C5** with Cs_2CO_3 (3 equivalents) were prepared at the same concentrations. Then, 2.5 mL of each solution was transferred into an argon-filled quartz cuvette (10 x 10 mm light path) equipped with a septum.

3.5.17.1. UV-Vis Absorption Studies

UV-Vis measurements were carried out on a Cary 3500 Multicell UV-Vis spectrophotometer equipped with two silicon diode detectors, double beam optics and Xenon pulse light (**Figure 3.38-3.40**).

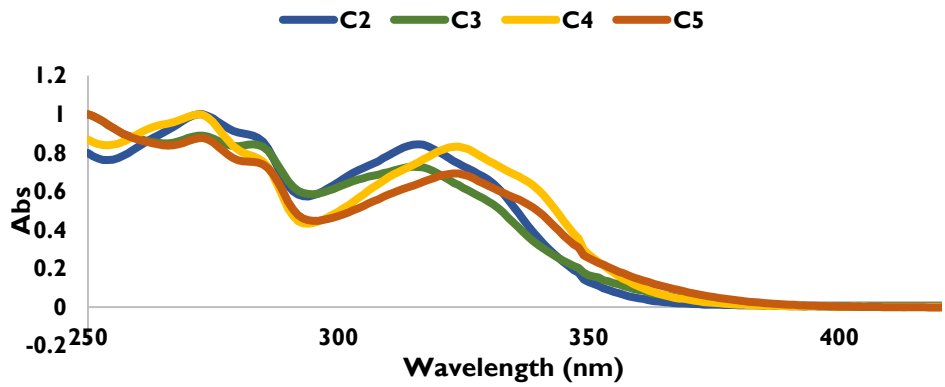

Figure 3.38 – Absorption profiles of 10^{-4} M solutions of catalysts **C2-C5** in dry, degassed acetonitrile at 298K.

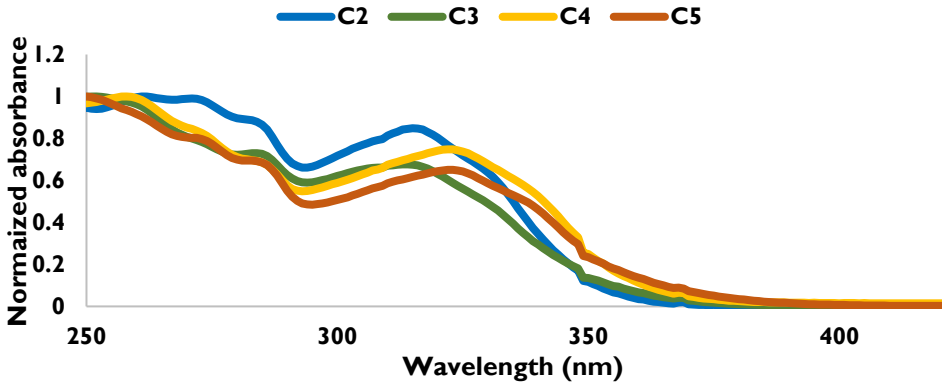

Figure 3.39 – Absorption profiles of 10^{-4}M solutions of catalysts **C2-C5** in dry, degassed, acetonitrile after the *addition of 3 equiv. of Cs_2CO_3* at 298K.

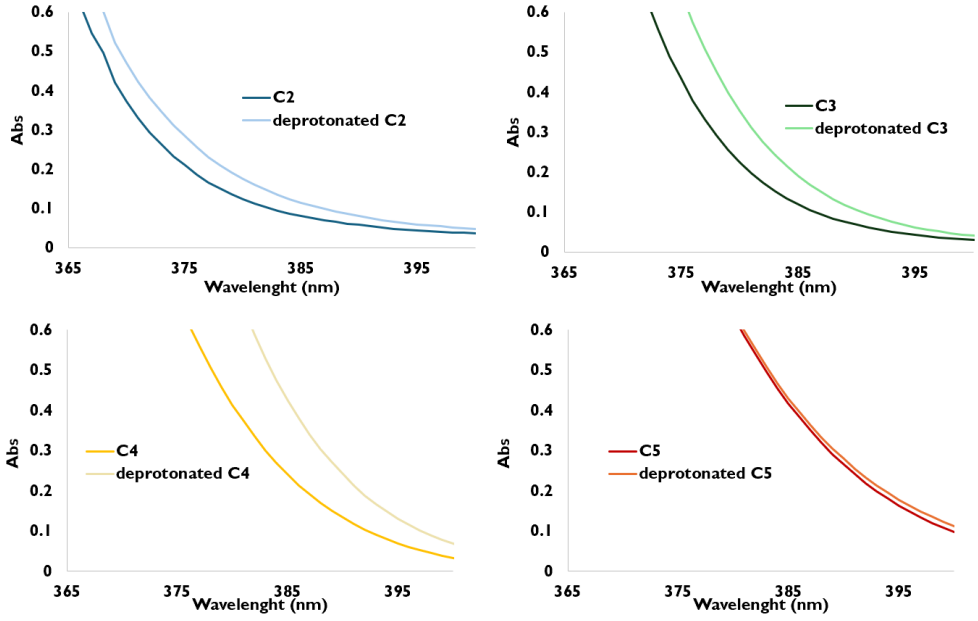

Figure 3.40 – Absorption profiles of 10^{-3}M solutions of catalysts **C2-C5** in dry, degassed, acetonitrile before and after the addition of 3 equiv. of Cs_2CO_3 at 298 K (only tails of absorption are shown for simplicity).

3.5.17.2 Photophysical Characterization of Catalysts C2-C5: Summary of Relevant Data

Table 3.5. Representative parameters for catalysts **C2-C5** ***at 298K*** 10^{-4}M CH_3CN solutions

Catalyst	Excitation 298 K[a]		Emission 298 K[a]		Δ exc-em
	λ_{exc}(nm)	λ_{em}(nm)	τ (ns) S^1	τ (μs) T^1	Δ(nm)
C2	357	445	2.8	9	88
C3	352	449	2.9	12.7	97
C4	363	459	4.6	10.3	96
C5	374	472	3	17.4	98

[a] Degassed samples

Table 3.6. Representative parameters for catalysts **C2-C5** ***at 77K*** of 10^{-4}M CH_3CN solutions

Catalyst	Excitation 77 K[a]	Emission 77 K[a]			Δ exc-em	Triplet energy
	λ_{exc}(nm)	λ_{em}(nm)	τ_{ox} (ns) S^1	τ_{ox} (μs) T^1	Δ(nm)	Kcal/mol
C2	347	513	1.2	0.9 (53%), 7.3 (47%)	166	67.0
C3	366	540	1.2	1.1 (62%), 8.8 (38%)	174	62.4
C4	354	540	1.2 (20%) 10.3 (80%)	0.6 (18%), 5.0 (82%)	186	63.5
C5	356	547	1.2	0.7 (20%), 6.0 (79%)	191	63.7

[a] In a glassy matrix of CH_3CN

Table 3.7. Representative parameters for the ***deprotonated*** catalysts **C2-C5** at 298K of 10^{-4}M CH_3CN solutions;

Catalyst	Excitation 298 K[a,b]	Emission 298 K[a,b]			Δ exc-em
	λ(nm)	λ_{em}(nm)	τ (ns) S[1]	τ (μs) T[1]	Δ(nm)
C2	354	445	3.0	13.4	91
C3	360	449	3.1	18.0	89
C4	359	466	5.0	21.1	107
C5	367	473	3.4	15.2	106

[a] After stirring with 3 equiv. of Cs_2CO_3 and filtrating the excess of base. [b] Degassed samples.

3.5.17.3 Photophysical Characterization of Catalysts C2-C5

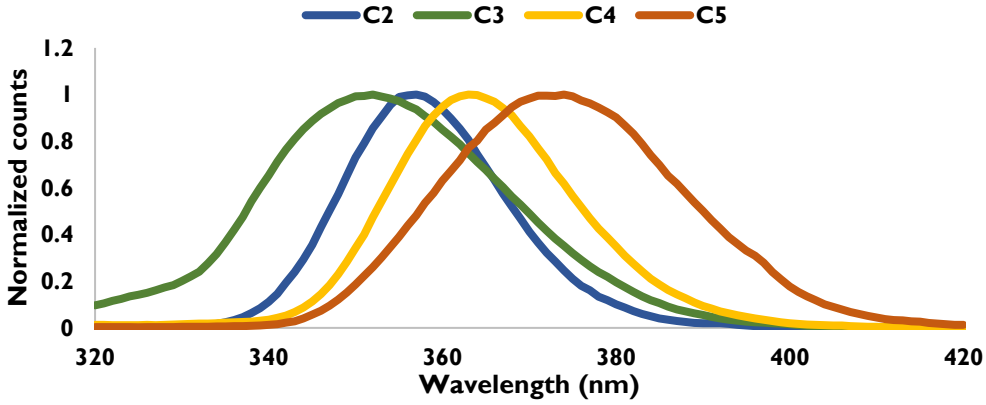

Figure 3.41. Excitation profiles of 10^{-4}M CH_3CN solutions of catalysts **C2-C5** *at 298K*

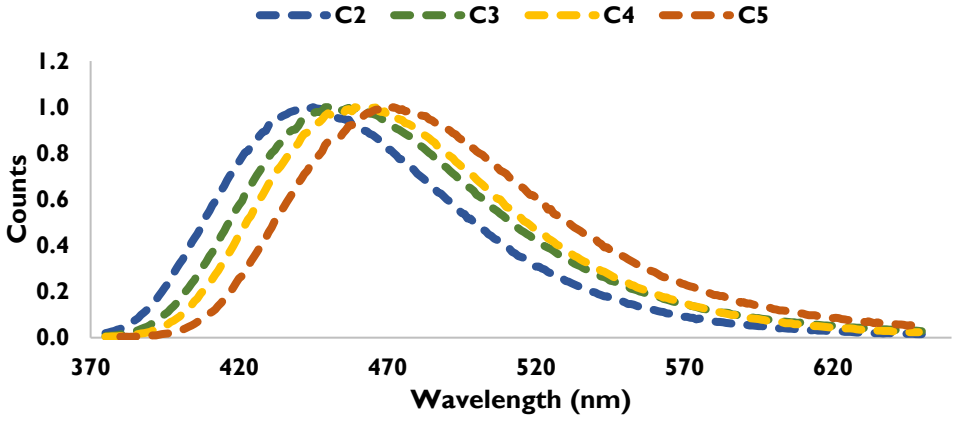

Figure 3.42. Emission profiles of 10^{-4}M CH_3CN solutions of catalysts **C2-C5** *at 298K*

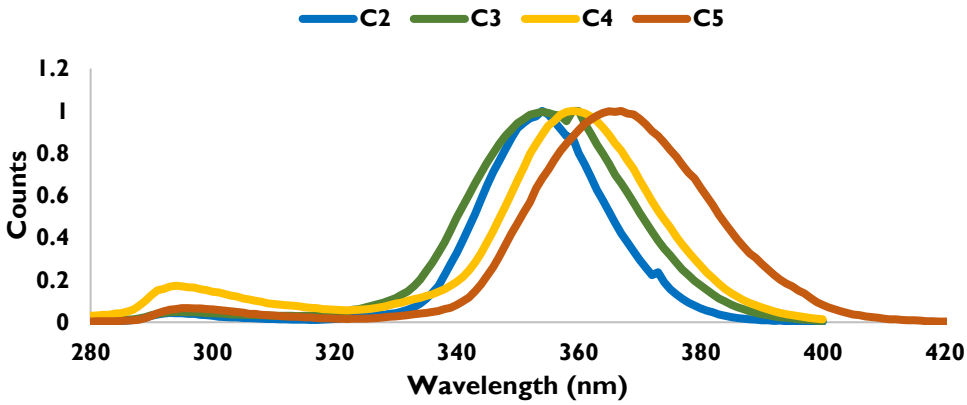

Figure 3.43. Excitation profiles of 10^{-4}M CH_3CN solutions of *deprotonated* catalysts **C2-C5** in the presence of 3 equiv. of Cs_2CO_3 at 298K.

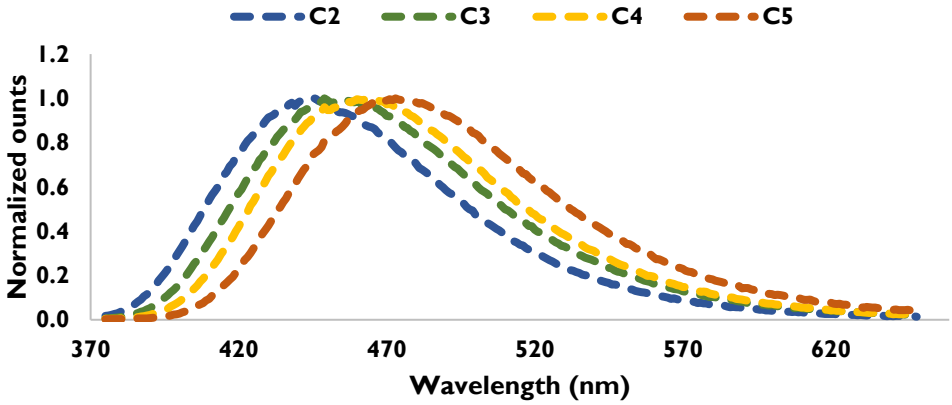

Figure 3.44. Emission profiles of 10^{-4}M CH_3CN solutions of *deprotonated* **C2-C5** in the presence of 3 equivalents of Cs_2CO_3

3.5.17.4 E(0,0) Determination of the Deprotonated Catalysts C2-C5

Fluorescence measurements were carried out on an Edinburgh FLSP920 spectrometer equipped with a 450 W xenon arc lamp, double excitation and single emission monochromators, and a Peltier-cooled Hamamatsu R928P photomultiplier tube (185−850 nm).

The emission spectrum of the deprotonated catalysts **C2-C5** (formed *in situ* from **C2-C5** upon addition of 3 equivalents of Cs_2CO_3 in dry, degassed CH_3CN) was superimposed with the absorption spectra (**Figure 3.45**).

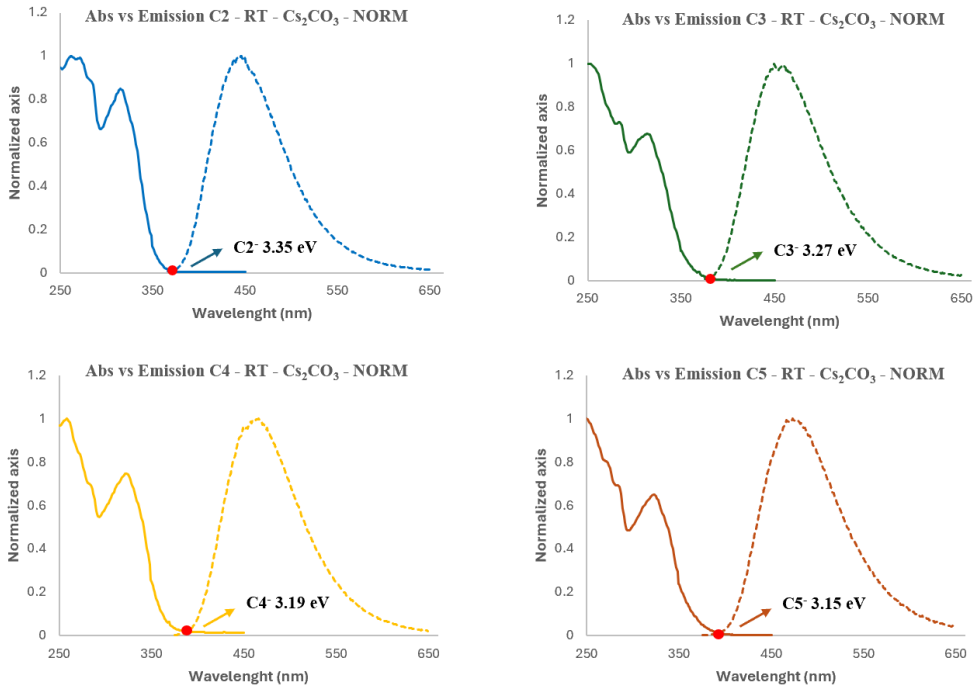

Figure 3.45. Absorption-emission overlap of 10^{-4}M solutions of catalysts **C2-C5** in dry, degassed, acetonitrile after the addition of 3 equiv. of Cs_2CO_3 at 298K.

3.5.17.5 Triplet Energy Measurement of the Neutral Catalysts C2-C5

Triplet measurements of neutral catalysts **C2-C5** were obtained from low temperature (77 K) emission measurement. The low temperature emission spectrum was measured in FLS900 Fluorescence spectrometer (*Edinburgh Instrument*).

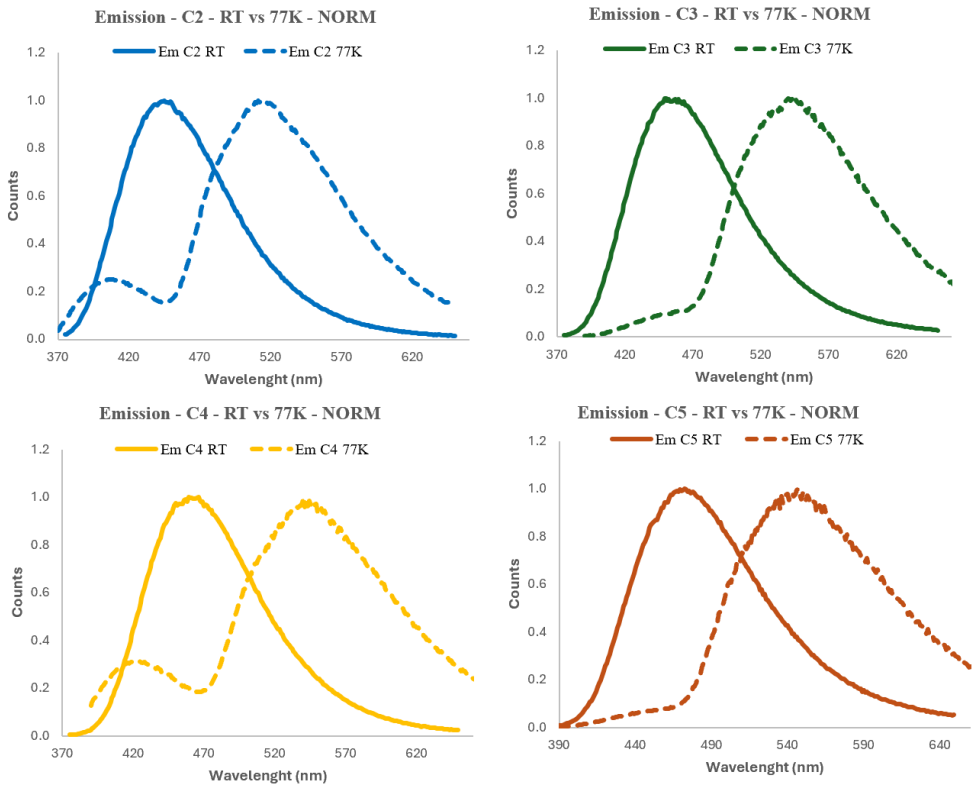

Figure 3.46. Comparison between emission of **C2-C5** solutions 10^{-4}M in CH_3CN to emission profile of glassy matrix at 77K

In **Figure 3.46**, the room temperature emission and glass temperature emission spectra are presented for catalysts **C2-C5**. The red-shifted emission observed at glass temperature is safely assigned to the emission from the triplet state. Since assignment of vibronic peaks was not possible, the crossing point of the tangent for the onset of emission was used for its determination.

3.5.17.6. Stern-Volmer Quenching Studies

Fluorescence measurements were carried out on an Edinburgh FLSP920 spectrometer equipped with a 450 W xenon arc lamp, double excitation and single emission monochromators. The excitation wavelength was fixed at 350 nm for all the experiments.

Stern-Volmer Quenching Studies with 4-Chloroanisole 1a

A 1.0 M solution of the quencher substrate (4-chloroanisole **1a**) in dry, degassed, CH_3CN (HPLC grade) was prepared and 40 µL of this stock solution were added to the solution (10^{-4}M HPLC grade CH_3CN) of the *deprotonated* catalyst **C2**$^-$, prepared according to the procedure detailed at the beginning of **section 3.5.17**. The addition of the substrate solution **1a** was repeated four times. After each addition, the solution was mixed, and the emission spectra of the excited catalyst was acquired from 320 nm to 600 nm (the excitation wavelength was fixed at 350 nm). A solvent blank was subtracted from all the measurements.

The results shown in **Figure 3.47** indicate that substrate **1a** quenched the excited-state emission of the deprotonated **C2**. The Stern-Volmer plot shows a linear correlation between the amounts of substrates and the ratio I_0/I, following the relationship: $\mathbf{I_0/I = 1 + K_{SV}[Q]}$ **(Q = Quencher)** (**Figure 3.47**).

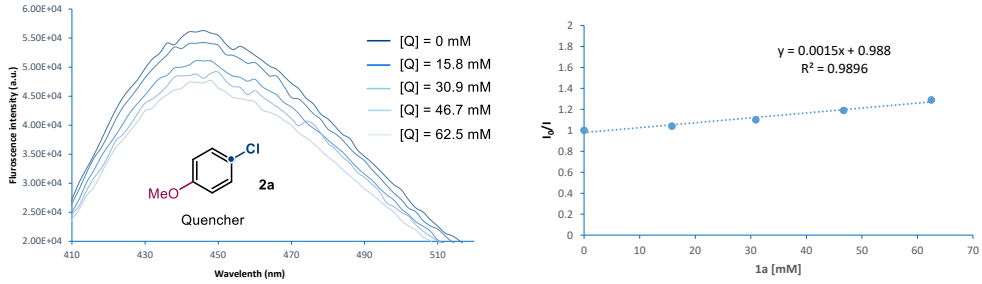

Figure 3.47. Stern-Volmer quenching studies of the excited deprotonated catalyst **C2**$^-$ with substrate **1a**

Stern-Volmer Quenching Studies with Methyl Fumarate *E*-3a

A 1.0 M solution of the quencher substrate (methyl fumarate *E*-**3a**) in dry, degassed, CH_3CN (HPLC grade) was prepared, and 40 µL of this stock solution were added to a 10^{-4} M solution (HPLC grade CH_3CN) of either the deprotonated catalyst **C2**$^-$ or the neutral catalyst **C2**. The solutions of the catalyst were prepared according to the procedure detailed at the beginning of **section 3.5.17**. The addition of the substrate solution **3a** was repeated five times. After each addition, the solution was mixed, and the emission spectra of the excited catalyst was acquired from 380 nm to 690 nm (the excitation wavelength was fixed at 350 nm). A solvent blank was subtracted from all the measurements.

The results shown in **Figures 3.48** (quenching studies on *deprotonated* catalyst **C2**$^-$) and **3.53** (quenching studies on *neutral* catalyst **C2**) indicate that substrate **3a** quenched the excited-state emission of both the deprotonated **C2**$^-$ or neutral **C2** with a different behavior.

Stern Volmer quenching studies with 3a and deprotonated C2$^-$

The Stern-Volmer plot for the quenching studies performed on *deprotonated* **C2**$^-$ (**Figure 3.48** – right) with **3a** (dimethyl fumarate) shows a linear correlation between the amounts of

substrates and the ratio $\mathbf{I_0/I}$, following the relationship: $\mathbf{I_0/I = 1 + K_{SV}[Q]}$ **(Q = Quencher)**.

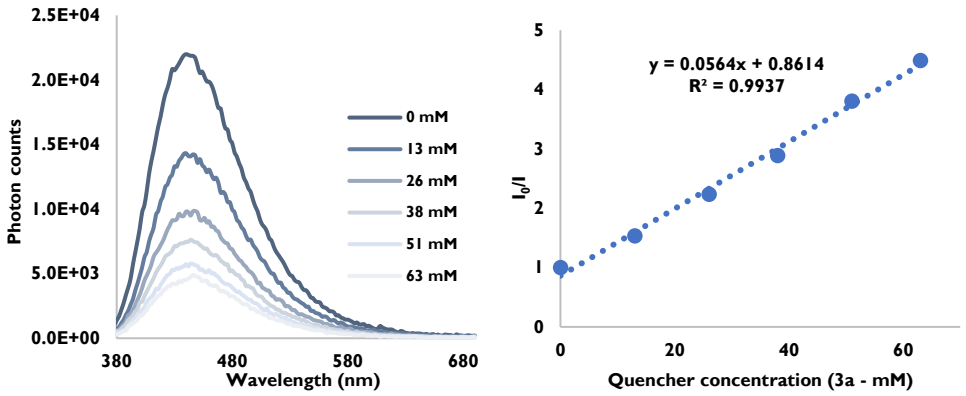

Figure 3.48 – Stern-Volmer fluorescence quenching studies of deprotonated **C2⁻** with **3a.**

Stern Volmer quenching studies with 3a and neutral C2

The Stern-Volmer plot for quenching studies of *neutral* **C2** (**Figure 3.49** – right) with **3a** (dimethyl fumarate) reveals a departure from the expected linear relationship between substrate concentration and the fluorescence intensity ratio I_0/I. Instead, the data fits an exponential curve with an upward deviation from linearity. This behavior could stem from several factors, such as the simultaneous presence of dynamic and static quenching or the influence of more intricate quenching mechanisms like Förster resonance energy transfer (FRET) or Dexter energy transfer.[100] As a result, a Stern-Volmer quenching constant was not determined for this system.

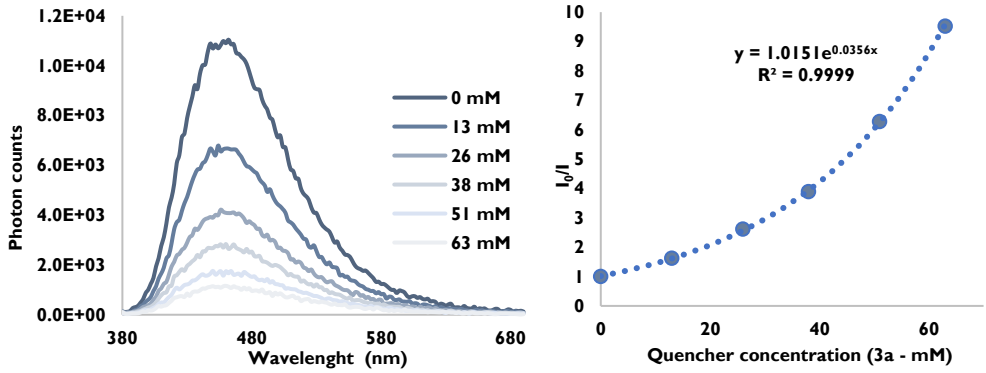

Figure 3.49 – Stern-Volmer fluorescence quenching studies of **C2** with **3a.**

[100] Gehlen, M. H. "The centenary of the Stern–Volmer equation of fluorescence quenching: From the single line plot to the SV quenching map." *J. Photochem. Photobiol.*, C **2020**, *42*, 100338.

Based on the experimental results discussed in the **section 3.4** (e.g., the inability of the deprotonated catalyst to drive the *E/Z* photoisomerization of **3a**, **Table 3.2**), the different behaviors observed for deprotonated **C2**$^{-}$ and neutral **C2** catalysts during the quenching studies can be explained by distinct quenching mechanisms. *When the catalyst is deprotonated, single-electron reduction is likely at play, whereas energy transfer is the dominant process when the catalyst is in its neutral form*. This mechanistic distinction accounts for the differences in the Stern-Volmer plots and the observed deviation from linearity in the case of the triplet energy transfer with catalyst **C2**.

Further Studies on the Behavior of Deprotonated Catalyst C2^{-} in the Activation of Fumarate 3a

When the *E/Z* photoisomerization of dimethyl fumarate (*E*-**3a**) was carried out using catalyst **C2** in the presence of Cs_2CO_3, no isomerization was observed (see **Table 3.2**, entry 1 in the **section 3.4**). This suggests that the deprotonated form of catalyst **C2**$^{-}$ is inactive in this transformation, likely due to its incompatibility with an EnT mechanism. In contrast, the neutral catalyst **C2** efficiently promoted the isomerization, confirming its effectiveness as an EnT photocatalyst (**Table 3.2**, entry 2 in the **section 3.4**).

To further investigate the reactivity of the deprotonated species, the same model reaction was performed in the presence of γ-terpinene as a hydrogen donor (see below).

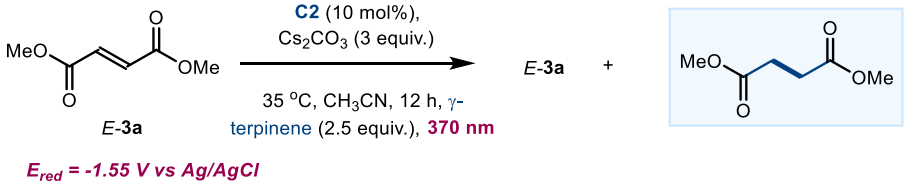

E_{red} = -1.55 V vs Ag/AgCl

Under these conditions, and using the deprotonated catalyst **C2**$^{-}$, GC-MS analysis after 12 hours revealed the formation of dimethyl succinate, the reduced product from **3a** (see **Figure 3.50**). This observation provides evidence that **C2**$^{-}$ engages in SET with *E*-**3a** (E_{red} = -1.55V vs Ag/AgCl),[64] consistent with a mechanistic shift from EnT to SET upon deprotonation of the catalyst.

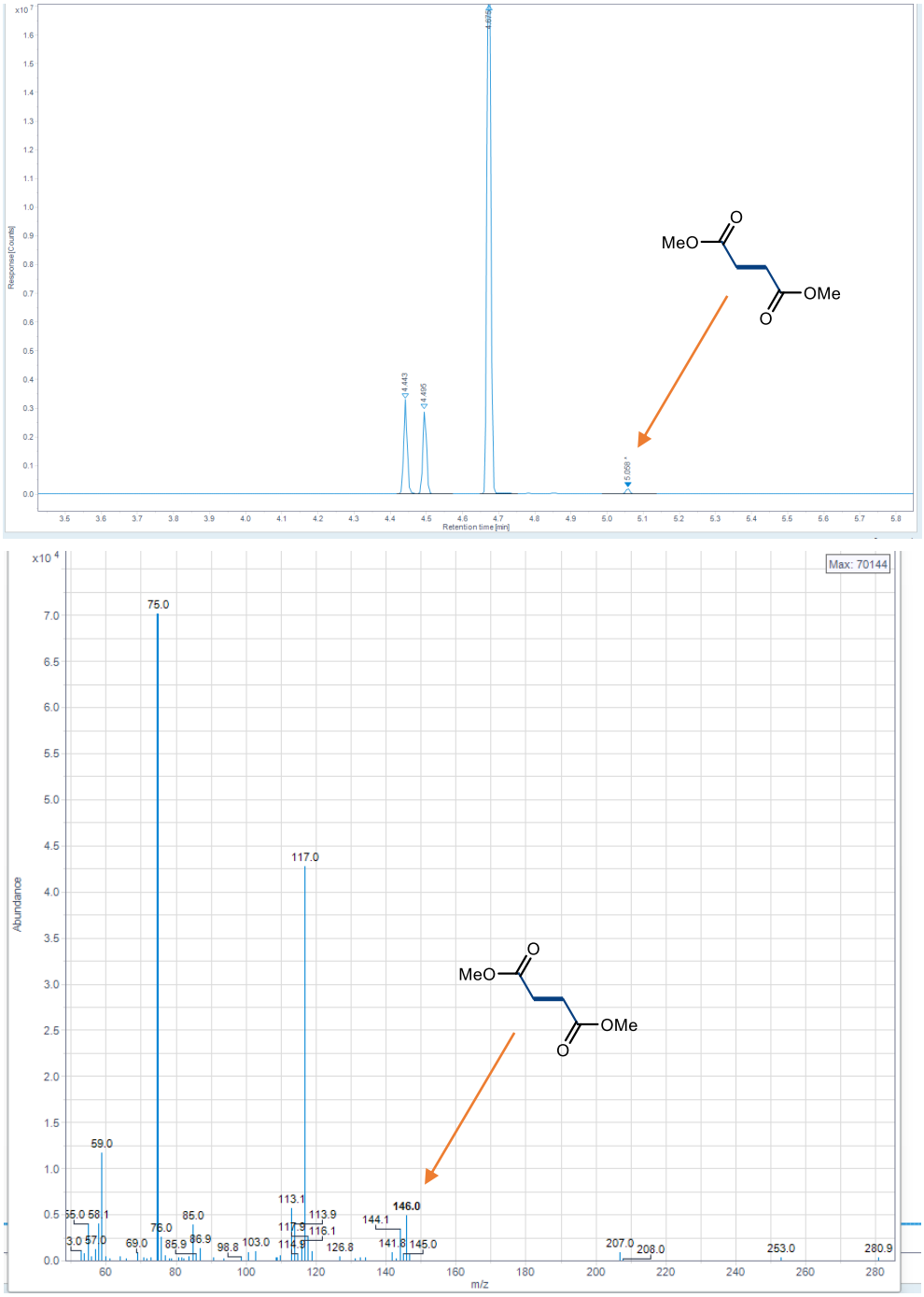

Figure 3.50. GC-MS analysis of the reaction between *E*-**3a** catalyzed by the deprotonated **C2** in the presence of γ-terpinene.

3.5.18. Electrochemical Studies

Cyclic voltammetry studies were carried out on a PGSTAT204 potentiostat, offering compliance voltage up to ± 20 V (available at the counter electrode), ± 10 V scan range and ±0.4 A current range with a glassy carbon disk electrode (diameter: 3 mm) as working electrode. A silver wire coated with AgCl immersed in a 3.0 M aqueous solution of KCl and separated from the analyte by a fritted glass disk was employed as the reference electrode and a Pt wire counter-electrode completed the electrochemical setup. The scan rate was 100 mV/s unless otherwise stated. The substrates were measured at concentration of 2 mM in CH_3CN after the addition and filtration of 3 equivalents of Cs_2CO_3, with $TBAPF_6$ (0.1 M) as electrolyte.

Oxidation Peaks for the Deprotonated Catalysts C2-C5

Potentials are quoted with the following notation: E_p^A (E_{Ox}) refers to the anodic peak potential while E_p^C (E_{Red}) refers to the cathodic peak potential (**Figure 3.51** to **3.54**).

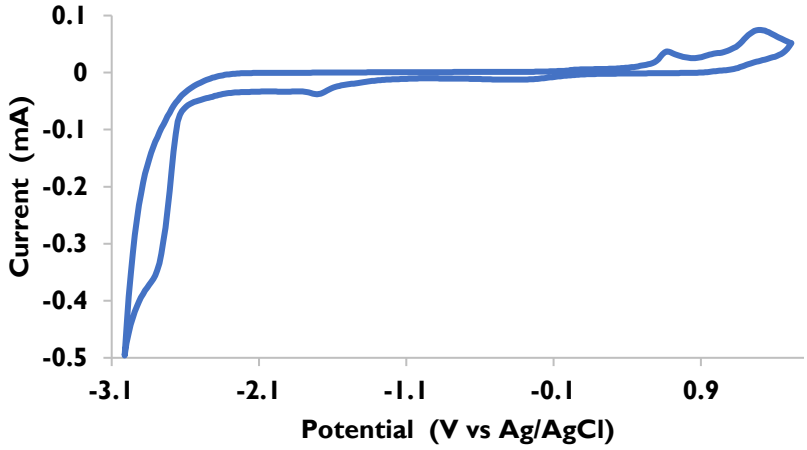

Figure 3.51. CV of the deprotonated catalyst **C2**$^{2-}$ in CH_3CN starting with the oxidation, irreversible oxidation and reduction, Ep^A = 0.65 V with a sweep rate of 100 mV/s.

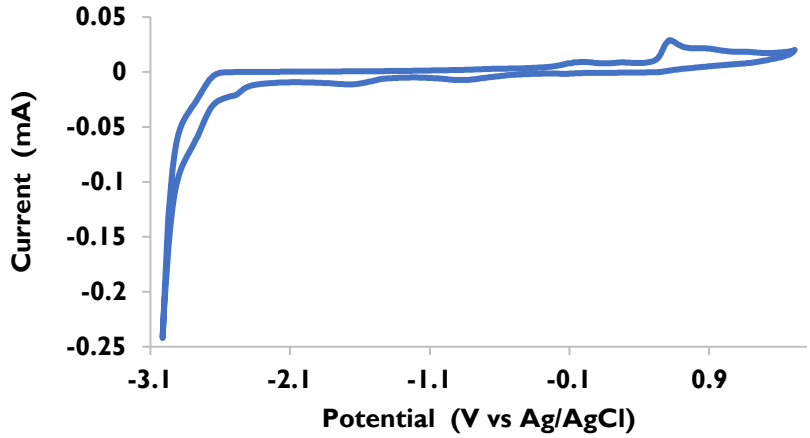

Figure 3.52. CV of **C3**$^{-}$ in CH_3CN starting with the oxidation, irreversible oxidation and reduction, Ep^A = 0.63 V with a sweep rate of 100 mV/s.

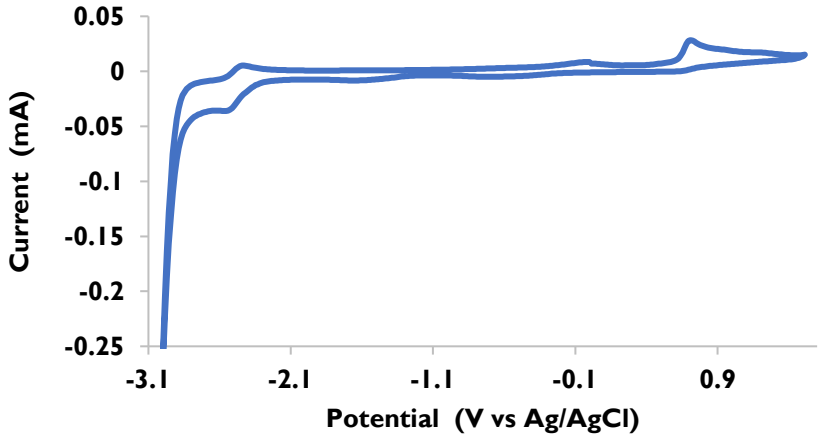

Figure 3.53. CV of **C4**$^{-}$ in CH_3CN starting with the oxidation, irreversible oxidation and reduction, Ep^A = 0.71 V with a sweep rate of 100 mV/s.

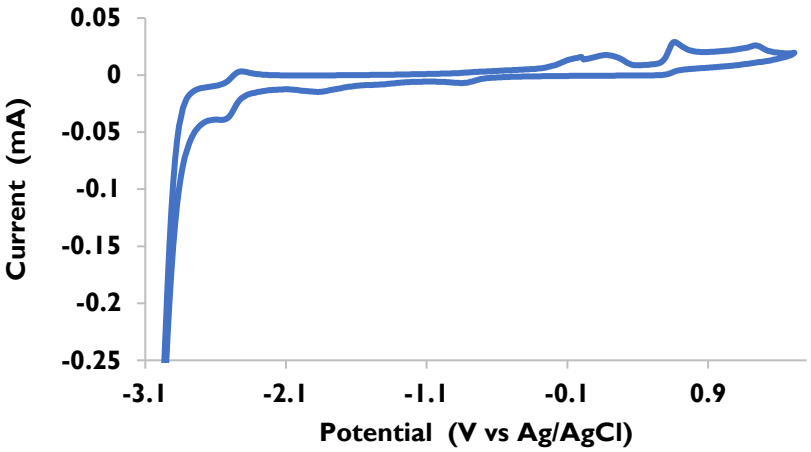

Figure 3.54. CV of **C5**$^{-}$ in CH_3CN starting with the oxidation, irreversible oxidation and reduction, Ep^A = 0.15 V with a sweep rate of 100 mV/s.

Conversion of the Potential from Ag/AgCl to SCE for Catalysts C2-C5

The conversion of the redox potential from Ag/AgCl to SCE was done according to the literature by measuring the redox potential of ferrocene as reference in CH_3CN (**Figure 3.55**).[101]

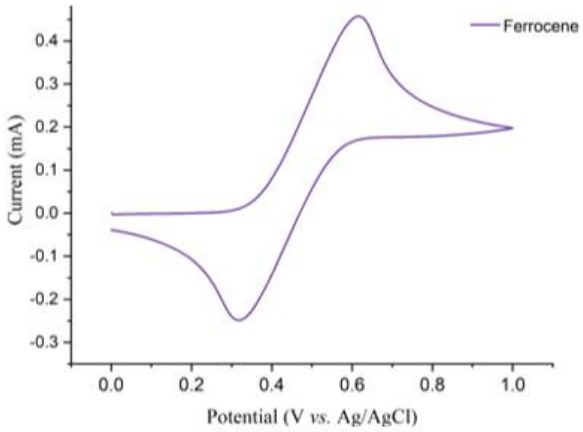

Figure 3.55. CV of ferrocene in CH_3CN, reversible reduction and oxidation $E_{1/2}$ = 0.46 V.

With the reference CV, the redox potential vs. SCE for the deprotonated catalyst **C2-C5** in CH_3CN was calculated using the following equations:

---

[101] V.V. Pavlishchuk, A.W. Addison. "Conversion constants for redox potentials measured versus different reference electrodes in acetonitrile solutions at 25°C." *Inorganica Chim. Acta.* **2000**, *298*, 97–102.

C2^{-} E_p^A (E_{Ox}) (**Ag/AgCl to Fc/Fc**$^{+}$) = 0.65 - 0.46 = 0.19 V vs. Fc/Fc^{+}

C2^{-} E_p^A (E_{Ox}) **Fc**$^{+}$ **to SCE**) = 0.19 + 0.38= 0.57 V vs. SCE

C3^{-} E_p^A (E_{Ox}) (**Ag/AgCl to Fc/Fc**$^{+}$) = 0.63 - 0.46 = 0.17 V vs. Fc/Fc^{+}

C3^{-} E_p^A (E_{Ox}) **Fc**$^{+}$ **to SCE**) = 0.17 + 0.38= 0.55 V vs. SCE

C4^{-} E_p^A (E_{Ox}) (**Ag/AgCl to Fc/Fc**$^{+}$) = 0.71 - 0.46 = 0.25 V vs. Fc/Fc^{+}

C4^{-} E_p^A (E_{Ox}) **Fc**$^{+}$ **to SCE**) = 0.25 + 0.38= 0.63 V vs. SCE

C5^{-} E_p^A (E_{Ox}) (**Ag/AgCl to Fc/Fc**$^{+}$) = 0.15 - 0.46 = -0.31 V vs. Fc/Fc^{+}

C5^{-} E_p^A (E_{Ox}) **Fc**$^{+}$ **to SCE**) = -0.31 + 0.38= 0.07 V vs. SCE

Evaluation of the Excited-state Potential of the Deprotonated Catalysts C2-C5

Using the data collected from the CV studies (**Figure 3.51-3.54**) and from the absorption and emission spectra overlap (**Figure 3.46**) of deprotonated catalysts **C2-C5**, we could estimate the redox potential of the excited state with the following equation:

$$E(\mathbf{C}^{\bullet+}/\mathbf{C}^{*}) = E(\mathbf{C}^{\bullet+}/\mathbf{C}) - E_{0\text{-}0}(\mathbf{C}^{*})/(\mathbf{C})$$

Since the electrochemical oxidation of deprotonated catalysts **C2-C5** is irreversible (**Figure 3.46-3.49**), the irreversible oxidation peak potential anode $\mathbf{Ep^A}$ was used for E(**Pc**$^{\bullet+}$**/Pc**).

$E_{0\text{-}0}$(**C***)/(**C**) was approximately determined spectroscopically from the overlap of the tail of absorption spectrum with the emission spectrum for every catalyst (**Figure 3.46**).

The redox potential of the excited **C2**$^{-}$***:**

$$E(\mathbf{C}^{\bullet+}/\mathbf{C}^{*}) = 0.65 - 3.35 = \mathbf{-2.7\ V} \text{ vs. Ag/AgCl}$$

$$E(\mathbf{C}^{\bullet+}/\mathbf{C}^{*}) = 0.57 - 3.35 = \mathbf{-2.78\ V} \text{ vs. SCE}$$

The redox potential of the excited **C3**$^{-}$***:**

$$E(\mathbf{C}^{\bullet+}/\mathbf{C}^{*}) = 0.63 - 3.27 = \mathbf{-2.64\ V} \text{ vs. Ag/AgCl}$$

$$E(\mathbf{C}^{\bullet+}/\mathbf{C}^{*}) = 0.55 - 3.27 = \mathbf{-2.72\ V} \text{ vs. SCE}$$

The redox potential of the excited **C4**$^{-}$***:**

$$E(\mathbf{C}^{\bullet+}/\mathbf{C}^{*}) = 0.71 - 3.19 = \mathbf{-2.48\ V} \text{ vs. Ag/AgCl}$$

$$E(\mathbf{C}^{\bullet+}/\mathbf{C}^{*}) = 0.63 - 3.19 = \mathbf{-2.56\ V} \text{ vs. SCE}$$

The redox potential of the excited **C5**$^{-}$***:**

$$E(\mathbf{C}^{\bullet+}/\mathbf{C}^{*}) = 0.15 - 3.15 = \mathbf{-3.00\ V} \text{ vs. Ag/AgCl}$$

$$E(\mathbf{C}^{\bullet+}/\mathbf{C}^{*}) = 0.07 - 3.15 = \mathbf{-3.08\ V} \text{ vs. SCE}$$

3.5.19. NMR Studies of the Deprotonated Catalysts

To assess the extent of catalyst deprotonation under the reaction conditions, NMR studies were conducted in CD_3CN. ^1H NMR spectra were recorded for 100 mM solutions of catalysts **C2**–**C5** in deuterated acetonitrile, both before and after the addition of 3 equivalents of Cs_2CO_3 (**Figure 3.56–3.59**). A significant shift was observed for all aromatic signals, indicating the formation of an electron-rich phenate ion, which enhances shielding across the conjugated system.

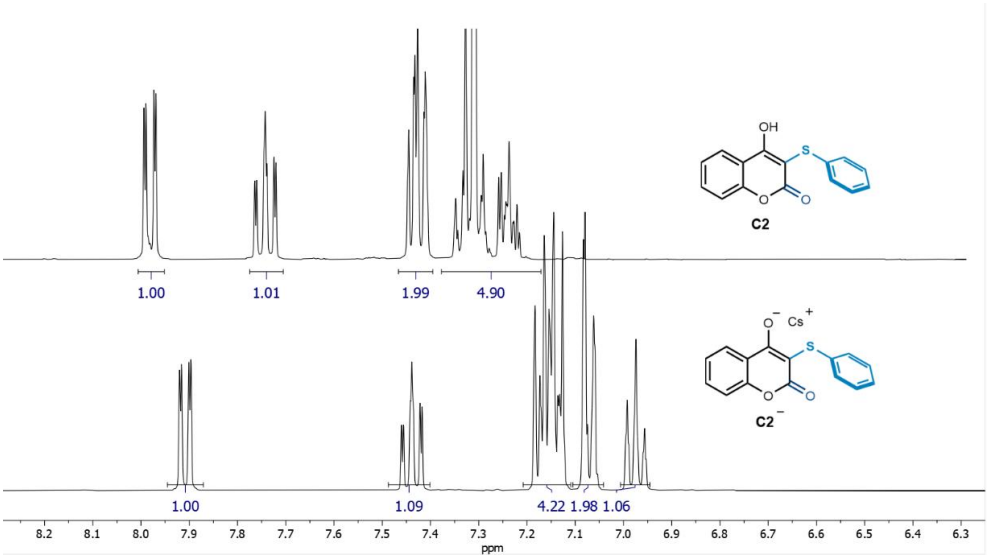

Figure 3.56. NMR studies of catalyst **C2** (up) and deprotonated **C2** (down) in CD_3CN (100 mM); zoom on the aromatic signals.

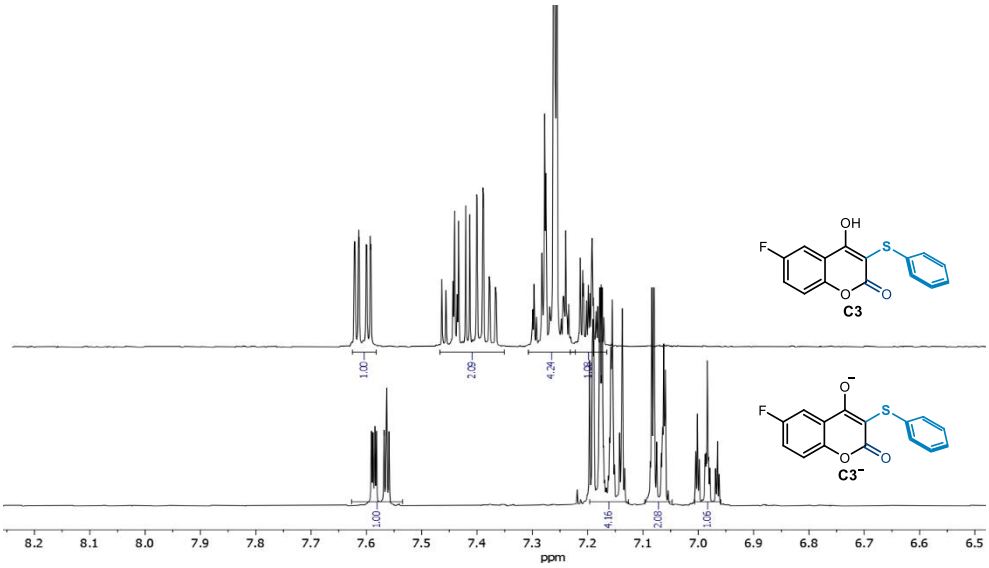

Figure 3.57 – NMR studies of **C3** (up) and deprotonated **C3** (down) in CD_3CN (100 mM); zoom on the aromatic signals.

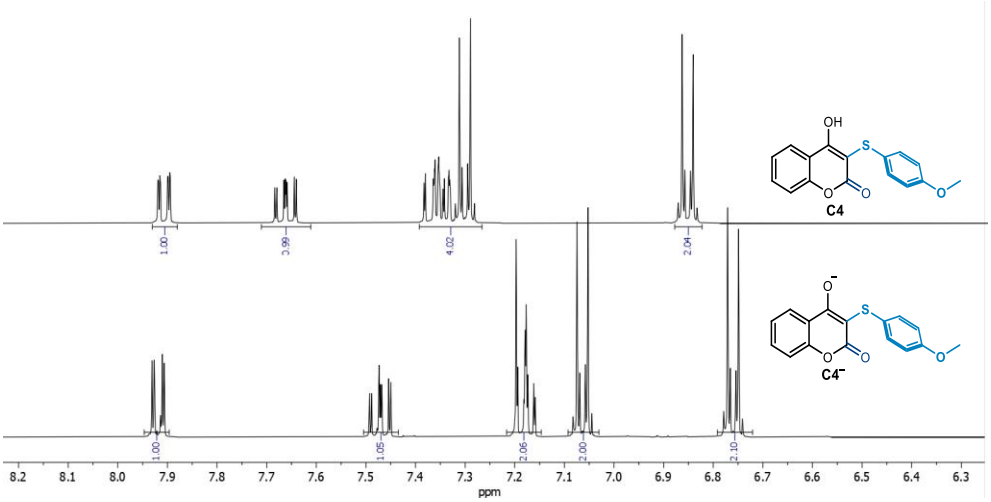

Figure 3.58 – NMR studies of **C4** (up) and deprotonated **C4** (down) in CD_3CN (100 mM); zoom on the aromatic signals.

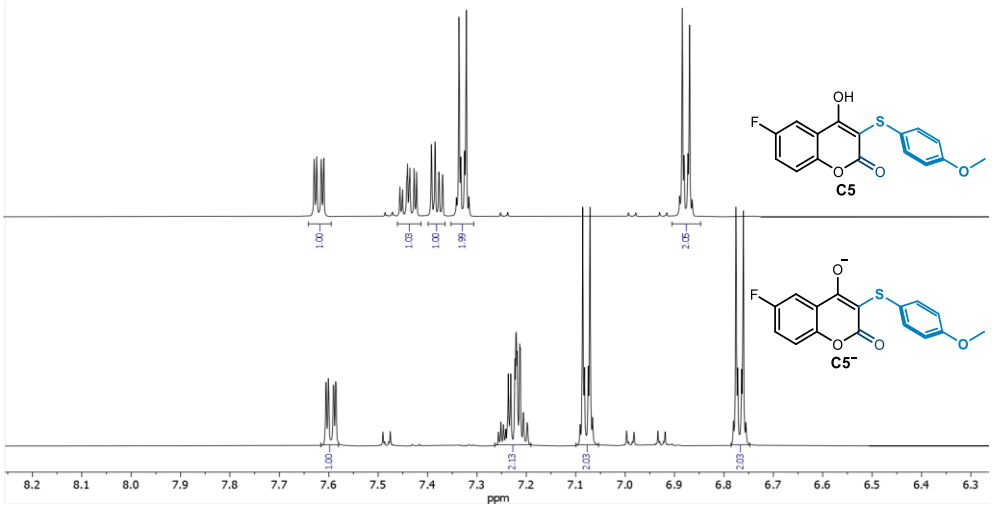

Figure 3.59 – NMR studies of **C5** (up) and deprotonated **C5** (down) in CD_3CN (100 mM); zoom on the aromatic signals.

3.5.20. Computational Studies

All the calculations were performed with the GAUSSIAN16, Revision A.03 program package.[102] Structure optimizations were carried out at B3LYP/6-31+G** level of theory[103] with the polarizable continuum model (PCM)[104] for the solvation effects of DMSO or ACN. The vibrational frequencies were computed at the same level to confirm each optimized structure as stationary points. NBO analysis was performed after full geometry and energy optimization for MO visualization (for **C1-C5** structures). TD-DFT calculations were conducted with the optimized geometries at the same level of theory with n states =10.

---

[102] Frisch, M. J.; Trucks, G. W.; Schlegel, H. B.; Scuseria, G. E.; Robb, M. A.; Cheeseman, J. R.; Scalmani, G.; Barone, V.; Petersson, G.A.; Nakatsuji, H.; Li, X.; Caricato, M.; Marenich, A.V.; Bloino, J.; Janesko, B. G.; Gomperts, R.; Mennucci, B.; Hratchian, H. P.; Ortiz, J.V.; Izmaylov, A. F.; Sonnenberg, J. L.; Williams-Young, D.; Ding, F.; Lipparini, F.; Egidi, F.; Goings, J.; Peng, B.; Petrone, A.; Henderson, T.; Ranasinghe, D.; Zakrzewski, V. G.; Gao, J.; Rega, N.; Zheng, G.; Liang, W.; Hada, M.; Ehara, M.; Toyota, K.; Fukuda, R.; Hasegawa, J.; Ishida, M.; Nakajima, T.; Honda, Y.; Kitao, O.; Nakai, H.; Vreven, T.; Throssell, K.; Montgomery, J. A., Jr.; Peralta, J. E.; Ogliaro, F.; Bearpark, M. J.; Heyd, J. J.; Brothers, E. N.; Kudin, K. N.; Staroverov, V. N.; Keith, T. A.; Kobayashi, R.; Normand, J.; Raghavachari, K.; Rendell, A. P.; Burant, J. C.; Iyengar, S. S.; Tomasi, J.; Cossi, M.; Millam, J. M.; Klene, M.; Adamo, C.; Cammi, R.; Ochterski, J. W.; Martin, R. L.; Morokuma, K.; Farkas, O.; Foresman, J. B.; Fox, D. J. *Gaussian 16*, Revision C.01; *Gaussian, Inc., Wallingford CT*, **2016**

[103] (a) Becke, A. D. "A new mixing of Hartree–Fock and local density-functional theories." *J. Chem. Phys.* **1993**, *98*, 1372–1377; (b) Lee, C.; Yang, W.; Parr., R. G. "Development of the Colle-Salvetti correlation-energy formula into a functional of the electron density." *Phys. Rev. B.* **1988**, *37*, 785-789; (c) Hariharan, P. C.; Pople, J. A. "Theor The influence of polarization functions on molecular orbital hydrogenation energies." *Chim. Acta.* **1973**, *28*, 213-222; (d) Francl, M. M.; Petro, W. J.; Hehre, W. J.; Binkley, J. S.; Gordon, M. S.; DeFrees, D. J.; Pople, J. A. "Self-consistent molecular orbital methods. XXIII. A polarization-type basis set for second-row elements." *J. Chem. Phys.* **1982**, *77*, 3654-3665.

[104] (a) Miertuš, S.; Scrocco, E.; Tomasi, J. "Electrostatic Interaction of a Solute with a Continuum. A Direct Utilization of ab Initio Molecular Potentials for the Prediction of Solvent Effects." *Chem. Phys.* **1981**, *55*, 117–129. (b) Miertuš, S.; Tomasi, J. "Approximate Evaluations of the Electrostatic Free Energy and Internal Energy Changes in Solution Processes." *Chem. Phys.* **1982**, *65*, 239–245. (c) Pascual-Ahuir, J. L.; Silla, E.; Tuñón, I. "GEPOL: An Improved Description of Molecular Surfaces. III. A New Algorithm for the Computation of a Solvent-Excluding Surface." *J. Comput. Chem.* **1994**, *15*, 1127–1138.

Rational Photocatalyst Design via Computed UV-Vis Spectra

To explore the influence of substituents on the photophysical properties of thiophenyl-coumarin catalysts, we screened a selection of compounds having fluorine (-F) or methoxy (-OMe) substituents at X and Y positions of the catalysts scaffold. We analyzed both the catalysts already synthesized and tested (**C2**–**C5**), as well as all remaining permutations involving fluorine (-F) and methoxy (-OMe) groups at the X and Y positions (**C6**–**C10**). In total, nine structures (**C2**–**C10**) were examined, whose phenate anion geometries were first optimized and then UV-Vis spectra were obtained through TD-DFT (B3LYP/6-31+G**; SMD=acetonitrile; NStates=10).

The obtained UV-Vis spectra and candidate's structures are shown below (**Figure 3.60**):

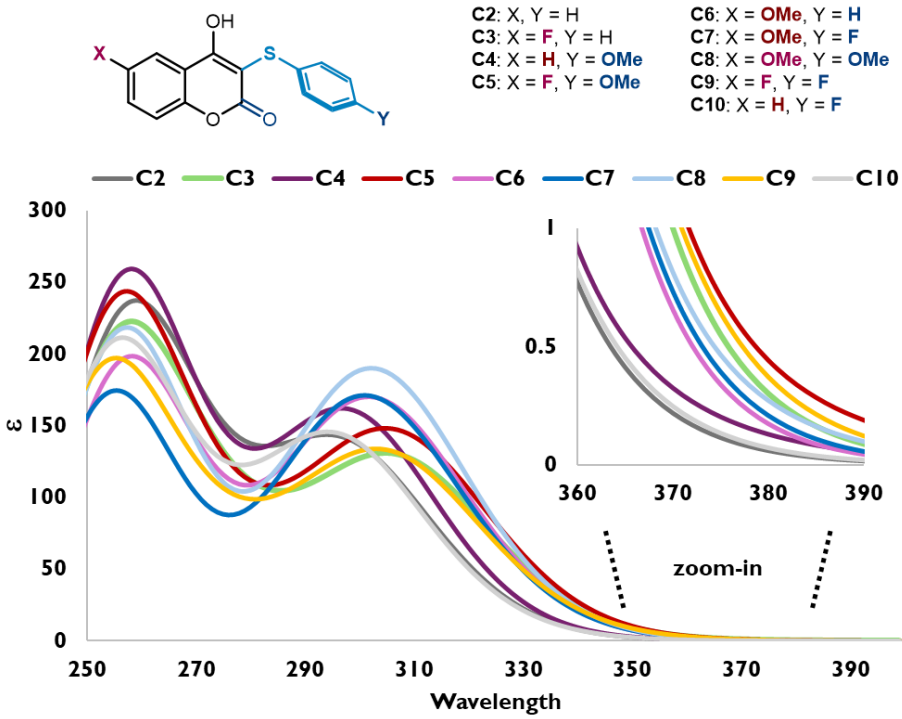

Figure 3.60. Calculated UV-Vis absorption profiles of family **C2-C10** with TD-DFT (B3LYP/6-31+G**; SMD=acetonitrile; NStates=10).

As shown in **Figure 3.60** (top right corner), fluorine substitution at the X position has the most significant effect in red-shifting the absorption spectrum (notably in **C5**, **C9**, and **C3**). Additionally, catalyst **C5**, featuring a *para*-methoxy group at position Y and a fluorine atom at position X on the hydroxycoumarin core, exemplifies our push-pull design strategy, as supported by the results presented in the **section 3.4**.

Based on these findings and the practical availability of starting materials, we selected the subfamily **C2**–**C5** for further investigation of photoreduction and energy transfer processes.

Computational study of excited states for C1-C5

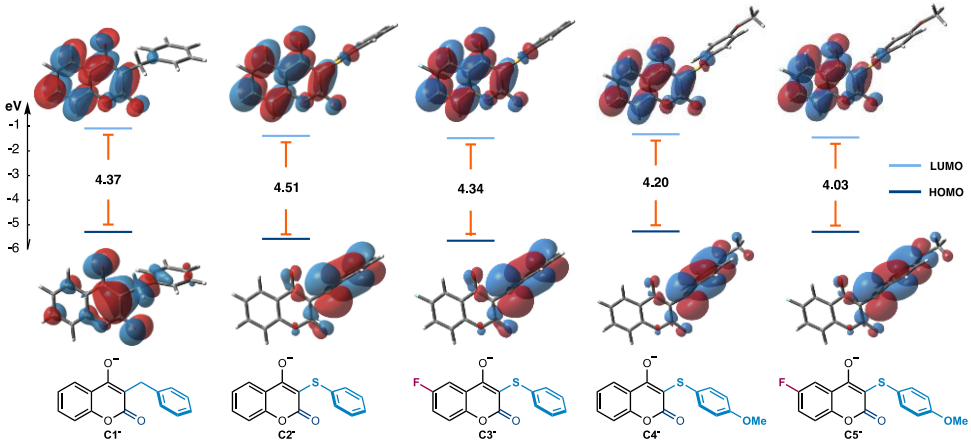

Figure 3.61. Calculated HOMO-LUMO graph and energy gaps of deprotonated **C1**-**C5**.

Table 3.8. HOMO and LUMO energies of all the catalysts[a] Deprotonated. [b] Energies are given in eV.

PC[a]	E_{HOMO}[b]	E_{LUMO}[b]
C1⁻	-5.42	-1.05
C2⁻	-5.75	-1.24
C3⁻	-5.77	-1.43
C4⁻	-5.43	-1.23
C5⁻	-5.45	-1.42

Table 3.9. Computational spectral data and most relevant transition involved in the formation of the lowest excited state

PC[a]	Transition	ΔE(eV)/ λ(nm) (experimental)[b]	Transition Character
C1⁻	$S_0 \rightarrow S_1$	3.90/317 (314)	Orbital 66 (HOMO) → Orbital 67 (LUMO) 97%
C2⁻	$S_0 \rightarrow S_1$	3.85/322 (315)	Orbital 70 (HOMO) → Orbital 71 (LUMO) 97%
C3⁻	$S_0 \rightarrow S_1$	3.69/336 (314)	Orbital 74 (HOMO)→Orbital 75 (LUMO) 98%
C4⁻	$S_0 \rightarrow S_1$	3.59/345 (323)	Orbital 78 (HOMO)→Orbital 79 (LUMO) 98%
C5⁻	$S_0 \rightarrow S_1$	3.43/361 (322)	Orbital 82 (HOMO)→Orbital 83 (LUMO) 98%

[a] Deprotonated. [b] Experimental absorption peaks are marked in parentheses.

Optimized geometries and Enthalpy and Gibbs free energies (in Hartree):

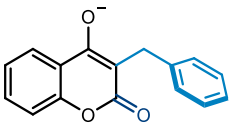

C1

C1$^-$

E = -841.983299

G = -842.042480

-1 1

C	-4.71312000	0.02997500	0.91179300
C	-3.73216000	1.01813400	0.88456600
C	-2.48802400	0.73202500	0.30784500
C	-2.20799700	-0.52695400	-0.24166000
C	-3.21434100	-1.50800800	-0.20117800
C	-4.45612200	-1.23950200	0.36736200
H	-5.67951000	0.24711400	1.35744200
H	-3.91027900	2.00518700	1.29971000
C	-0.87280200	-0.78768600	-0.84105400
H	-2.99147100	-2.48106200	-0.62671100
H	-5.22376000	-2.00713700	0.39106500
C	0.04798400	0.29399900	-0.81221900
C	-0.27949800	1.55229800	-0.25026000
C	1.42113400	0.13613700	-1.42424600
H	1.37104000	-0.71743100	-2.11134900
H	1.66655300	1.01987200	-2.02386100
C	2.56623400	-0.10747000	-0.44802800
C	2.42570000	-0.98596300	0.63877100
C	3.81013700	0.51376500	-0.63748200
C	3.49413000	-1.23883700	1.50422600
H	1.46887900	-1.47208500	0.80730200
C	4.88303300	0.26683400	0.22656000
H	3.93932700	1.20338800	-1.46873600
C	4.72986900	-0.61322100	1.30219300

H	3.36161300	-1.92405800	2.33748000
H	5.83460200	0.76511100	0.06091100
H	5.55969900	-0.80661200	1.97613600
O	-0.61890300	-1.92556100	-1.33709600
O	0.44467800	2.55840900	-0.18342100
O	-1.56097900	1.73647100	0.30520100

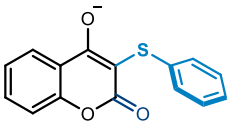

C2

C2$^-$

E = -1200.882044

G = -1200.943005

-1 1

C	-4.82166900	-0.45040200	0.85494000
C	-3.95203200	0.62751800	0.99922100
C	-2.67991500	0.56026100	0.41794700
C	-2.26494200	-0.56516200	-0.30389400
C	-3.15937900	-1.64151800	-0.43532700
C	-4.42708000	-1.59101100	0.13590600
H	-5.80955000	-0.40396900	1.30360800
H	-4.23758200	1.51707800	1.55145000
C	-0.90515000	-0.59937000	-0.90789600
H	-2.82974900	-2.51068500	-0.99498200
H	-5.10901300	-2.42873300	0.02734200
C	-0.10996300	0.57371600	-0.69385900
C	-0.56452600	1.69757600	0.06106400
C	2.65023100	0.01872800	-0.28156500
C	2.28300700	-0.47253200	0.97833900
C	4.00335300	-0.00834300	-0.66231200
C	3.25694000	-0.98195800	1.84358000
H	1.24048200	-0.45652500	1.27970400
C	4.96944000	-0.51844900	0.20721600
H	4.30073700	0.36936100	-1.63744600

C	4.60305000	-1.00852600	1.46650500
H	2.95673000	-1.35903700	2.81758400
H	6.01102700	-0.53205600	-0.10190400
H	5.35543800	-1.40452300	2.14189300
O	-0.53445700	-1.61413900	-1.54742600
O	0.04066400	2.74020000	0.32348700
O	-1.86405200	1.64540100	0.59248000
S	1.48100300	0.69963900	-1.46342300

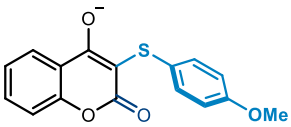

C3

C3$^-$

E = -1300.129384

G = -1300.192386

-1 1

C	-4.55365700	0.09853000	0.85167700
C	-3.58931700	1.09335700	0.98619100
C	-2.32513000	0.91150700	0.41159300
C	-2.00722700	-0.25230700	-0.29756600
C	-2.98338000	-1.25410600	-0.43045800
C	-4.22403100	-1.05663600	0.14266700
H	-5.54148900	0.20991400	1.28518100
H	-3.80315100	2.00727800	1.52990600
C	-0.65304900	-0.41365200	-0.89646300
H	-2.74925400	-2.16033000	-0.97720400
C	0.23684200	0.68962200	-0.69544800
C	-0.11910000	1.85620800	0.04971500
C	2.94077100	-0.09315300	-0.28171000
C	2.53814700	-0.53301400	0.98614700
C	4.28402500	-0.24438000	-0.66797200
C	3.46800600	-1.11522900	1.85400500
H	1.50284100	-0.42143000	1.29198900

C	5.20589400	-0.82663500	0.20419300
H	4.60815400	0.09238800	-1.64953900
C	4.80429300	-1.26597500	1.47140400
H	3.14097900	-1.45155800	2.83425300
H	6.24041800	-0.93674100	-0.10924700
H	5.52225900	-1.71855100	2.14869000
O	-0.37441700	-1.46666400	-1.51901300
O	0.57437700	2.84309900	0.30451900
O	-1.41870400	1.92230900	0.57955900
S	1.83005100	0.66969700	-1.47047100
F	-5.17668300	-2.03232200	0.01390500

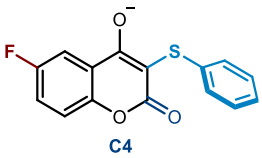

C4

C4$^-$

E = -1315.376300

G = -1315.442738

-1 1

C	5.30866300	-1.31332700	-0.73184700
C	4.52593700	-0.33825700	-1.34470900
C	3.33348300	0.06460700	-0.73096100
C	2.91242600	-0.49119900	0.48298300
C	3.71805100	-1.47501500	1.08211300
C	4.90622600	-1.88614000	0.48617600
H	6.23458200	-1.62963800	-1.20301800
H	4.81881900	0.11557500	-2.28603300
C	1.63909700	-0.03601100	1.10459500
H	3.38435100	-1.90244400	2.02190900
C	0.93357600	0.98232700	0.38425000
C	1.38728900	1.51158700	-0.86220000
C	-1.89370700	0.68665900	0.47703900
C	-1.72930200	-0.41651300	-0.37343800
C	-3.18914800	1.03601800	0.87821300

C	-2.83316100	-1.14640200	-0.80987800
H	-0.73440200	-0.70625300	-0.69611000
C	-4.30356900	0.30807000	0.44534800
H	-3.34469000	1.88656600	1.53720300
C	-4.12811200	-0.79115800	-0.40527700
H	-2.70268400	-1.99983100	-1.46871200
H	-5.28938900	0.61053200	0.77794200
O	1.25785100	-0.54682400	2.18625900
O	0.84900900	2.36109400	-1.57708400
O	2.60081000	1.02346300	-1.37657900
S	-0.52959300	1.68918100	1.09053500
O	-5.14746000	-1.57152800	-0.88973900
C	-6.48624000	-1.25022300	-0.50929300
H	-7.12061100	-1.98728400	-1.00211000
H	-6.61877100	-1.32243100	0.57639700
H	-6.76462800	-0.24514300	-0.84683100
H	5.52017900	-2.64632100	0.95927000

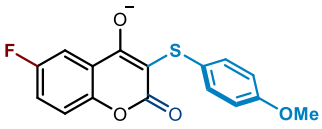

C5

C5^{-}

E = -1414.623656

G = -1414.692540

-1 1

C	5.08811700	-0.64922800	-1.05581700
C	4.20459400	0.33420900	-1.49189800
C	3.00566400	0.54185000	-0.79834800
C	2.67309800	-0.22080400	0.32678700
C	3.56729200	-1.21286900	0.76299100
C	4.74498500	-1.40183400	0.06736800
H	6.02426400	-0.83355600	-1.57139800
H	4.43194000	0.94187600	-2.36118800

C	1.38899700	0.02412700	1.04079800
H	3.32040300	-1.81025900	1.63313700
C	0.58428500	1.07887300	0.50312900
C	0.95086400	1.82594800	-0.65912200
C	-2.21374600	0.57815700	0.59174700
C	-1.99094200	-0.41245900	-0.37585900
C	-3.52720700	0.82170000	1.01174000
C	-3.05617700	-1.13567400	-0.90846900
H	-0.98119800	-0.61842000	-0.71618500
C	-4.60288300	0.09771400	0.48445800
H	-3.72756800	1.58554800	1.75886900
C	-4.36943000	-0.88827600	-0.48296500
H	-2.88088400	-1.90117700	-1.65856000
H	-5.60470300	0.31638800	0.83441500
O	1.09342500	-0.68079300	2.03586400
O	0.32249900	2.72652000	-1.21957100
O	2.17716000	1.52080100	-1.27418100
S	-0.90131200	1.55447800	1.34436700
F	5.61830500	-2.36782900	0.49224100
O	-5.34723800	-1.65346300	-1.06656100
C	-6.70254600	-1.43914200	-0.66946400
H	-7.29779600	-2.14368800	-1.25068000
H	-6.83970500	-1.64017000	0.39933300
H	-7.02506100	-0.41599300	-0.89465100

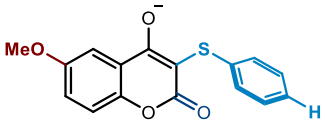

C6

C6^{-}

E = -1315.541079

G = -1315.357709

-1 1

C	-4.20791200	0.43099300	0.75755000

C	-3.18615200	1.36076300	0.97083100
C	-1.91798100	1.15056100	0.42412800
C	-1.65972100	0.00448000	-0.34194300
C	-2.68490300	-0.92227900	-0.55029000
C	-3.95328200	-0.71707100	-0.00839000
H	-3.36268600	2.25478100	1.56096000
C	-0.29764000	-0.21795900	-0.92521400
H	-2.46720700	-1.80424100	-1.14368400
C	0.65262900	0.81787400	-0.63690300
C	0.36120700	1.97650300	0.15815500
C	3.27866100	-0.18980300	-0.26954700
C	2.81966700	-0.74429900	0.93465600
C	4.62747300	-0.37686600	-0.62654400
C	3.68848900	-1.46329600	1.75766100
H	1.78057600	-0.60805700	1.21555800
C	5.49009200	-1.09701000	0.19967300
H	4.99745700	0.04757000	-1.55702700
C	5.02862900	-1.64734300	1.40131500
H	3.31072200	-1.88502000	2.68649400
H	6.52867900	-1.22773500	-0.09684700
O	-0.08022100	-1.24836300	-1.59271200
O	1.09588900	2.90076500	0.47314800
O	-0.96490100	2.09212100	0.66903900
S	2.25248900	0.74225000	-1.39168000
H	5.70020200	-2.20845100	2.04585900
H	-5.18432400	0.61527600	1.19132900
O	-4.89722900	-1.69428000	-0.27501900
C	-6.19540200	-1.52570200	0.25595600
H	-6.77115400	-2.39522800	-0.06932200
H	-6.18642100	-1.49118500	1.35505500
H	-6.67711100	-0.61293200	-0.12370600

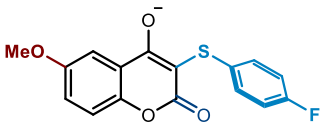

C7

C7$^-$

E = -1414.784038

G = -1414.610408

-1 1

C	4.47771800	0.07679500	-0.91309900
C	3.51091700	1.01746500	-1.27935200
C	2.25985900	1.01873800	-0.65816800
C	1.96376600	0.07556000	0.33667900
C	2.93387600	-0.86365500	0.69726000
C	4.18523400	-0.86879300	0.08192500
H	3.71748400	1.75640100	-2.04740500
C	0.62015100	0.08004500	0.99896200
H	2.68751100	-1.58757000	1.46706200
C	-0.27077200	1.10591600	0.53690900
C	0.05681500	2.05072700	-0.49307600
C	-2.96304700	0.22353300	0.49648300
C	-2.59046800	-0.62206900	-0.55885200
C	-4.30439500	0.21765000	0.92079700
C	-3.52933100	-1.45071000	-1.17897000
H	-1.55792600	-0.62849200	-0.89108700
C	-5.25144300	-0.60698900	0.31038700
H	-4.61141800	0.86693700	1.73679000
C	-4.84292700	-1.42802400	-0.73258500
H	-3.24565400	-2.10749600	-1.99543600
H	-6.28779900	-0.61390300	0.63350600
O	0.36414600	-0.77538200	1.86906800
O	-0.63097500	2.94169500	-0.96869000
O	1.36015900	1.95919600	-1.06091400
S	-1.83055100	1.31021200	1.34774300
F	-5.77037200	-2.24254100	-1.33973100

H	5.44189200	0.09496500	-1.40851500
O	5.07369100	-1.83891100	0.51253600
C	6.35286300	-1.88082600	-0.08580300
H	6.88411600	-2.70667500	0.39270900
H	6.29243600	-2.07075400	-1.16718800
H	6.91246100	-0.94889700	0.08027800

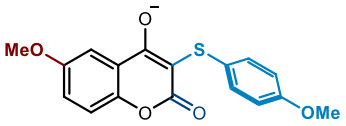

C8

C8$^-$

E = -1430.067087

G = -1429.855423

-1 1

C	4.79891100	-0.19578300	-0.98657500
C	3.87872700	0.76735200	-1.41039700
C	2.65013600	0.90164400	-0.75923400
C	2.33002000	0.07049100	0.32417800
C	3.25343800	-0.89177800	0.74214500
C	4.48202700	-1.02938700	0.09703700
H	4.10442800	1.42122600	-2.24719100
C	1.01030600	0.21639300	1.01858800
H	2.98846900	-1.52778700	1.58037700
C	0.16600400	1.24910000	0.48926700
C	0.51765400	2.07852300	-0.62816600
C	-2.58100100	0.54727400	0.57555000
C	-2.29467400	-0.41069600	-0.41074100
C	-3.90729600	0.66661900	1.01107400
C	-3.30037800	-1.21398100	-0.94048100
H	-1.27302400	-0.52136600	-0.75867700
C	-4.92573000	-0.13833800	0.48609100
H	-4.15798400	1.40115400	1.77279100
C	-4.62199500	-1.08514500	-0.49708700

H	-3.07429900	-1.95405000	-1.70277800
H	-5.93842800	-0.00997900	0.85260700
O	0.73507400	-0.54099200	1.97020900
O	-0.12809000	2.96678400	-1.16401000
O	1.79620800	1.85687400	-1.22037700
S	-1.35524200	1.61718100	1.31712300
O	-5.54735200	-1.93051300	-1.08569300
C	-6.89212200	-1.83294800	-0.66249300
H	-7.44725800	-2.57565000	-1.24021900
H	-6.99914500	-2.05567000	0.40884300
H	-7.31029700	-0.83563600	-0.86082100
H	5.74623600	-0.28165600	-1.50691200
O	5.32467400	-2.01131500	0.59001000
C	6.57864900	-2.18577200	-0.03664500
H	7.07510600	-2.99782200	0.49957300
H	6.47158900	-2.46612000	-1.09460800
H	7.19829900	-1.27964800	0.02925300

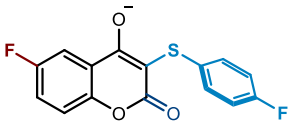

C9

C9^{-}

E = -1399.501656

G = -1399.366201

-1 1

C	4.80147500	-0.37102800	-0.94948900
C	3.91128900	0.64364900	-1.29568800
C	2.66215600	0.72258800	-0.66192600
C	2.29587400	-0.20998100	0.31724600
C	3.19422400	-1.23129000	0.66205600
C	4.41966000	-1.28973900	0.02719100
H	4.16465800	1.38084300	-2.05075900
C	0.96038100	-0.11621300	0.98678500

H	2.89898900	-1.94864000	1.42036000
C	0.14794100	0.98215500	0.54898600
C	0.54182000	1.91640300	-0.46602100
C	-2.60445400	0.31177700	0.50707000
C	-2.30464400	-0.53523100	-0.56978400
C	-3.93909400	0.39901800	0.94291900
C	-3.30842900	-1.27557100	-1.19994700
H	-1.27823600	-0.61326100	-0.91165900
C	-4.95051900	-0.33686300	0.32262200
H	-4.18991100	1.05092100	1.77580600
C	-4.61324700	-1.16276200	-0.74180800
H	-3.08157000	-1.93322400	-2.03324200
H	-5.98203100	-0.27212100	0.65452700
O	0.64800500	-0.96673400	1.84296000
O	-0.07325200	2.86498200	-0.92574100
O	1.83737700	1.73283900	-1.04344500
S	-1.38748600	1.29064200	1.37340300
F	-5.60400400	-1.88978100	-1.35849900
H	5.77431800	-0.45610200	-1.42267200
F	5.30510500	-2.28675900	0.36091400

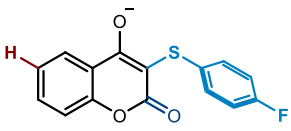

C10

C10^{-}

E = -1300.259242

G = -1300.114032

-1 1

C	5.03610800	-1.01032500	-0.75932700
C	4.24565600	0.03426300	-1.23191300
C	2.99923700	0.28263100	-0.63616400
C	2.54117300	-0.50783600	0.42604900

C	3.35222600	-1.55575400	0.88555700
C	4.59180000	-1.81207700	0.30460200
H	4.56695200	0.66726500	-2.05343100
C	1.21036700	-0.23048100	1.05049500
H	2.96850000	-2.15094500	1.70878500
H	5.21128000	-2.62679000	0.67043400
C	0.49926500	0.87995900	0.48189000
C	0.98623500	1.66452900	-0.61473200
C	-2.29861400	0.43262100	0.45362500
C	-2.05507400	-0.55162100	-0.51563200
C	-3.62760000	0.67460400	0.84662900
C	-3.10762400	-1.27550100	-1.08208400
H	-1.03373900	-0.74901600	-0.82299700
C	-4.68764900	-0.04314800	0.28928000
H	-3.83524100	1.43420200	1.59600200
C	-4.40489700	-1.00795400	-0.66882600
H	-2.92421700	-2.03882600	-1.83185000
H	-5.71481400	0.14100200	0.58843400
O	0.80908500	-0.95356000	1.98413000
O	0.46252500	2.60817400	-1.18616000
O	2.26985600	1.31247100	-1.13859500
S	-1.01627600	1.40080200	1.23266200
F	-5.44395400	-1.71864400	-1.22318400
H	6.00191400	-1.20206200	-1.22101700

Chapter IV

General Conclusions

The work presented in this doctoral thesis has established new photochemical strategies based on the intrinsic excited-state reactivity of 4-hydroxycoumarins. By exploiting their capacity to undergo photoexcitation, this research redefined their role from ground-state nucleophiles to versatile light-responsive scaffolds capable of mediating both electron-transfer and energy-transfer transformations.

In Chapter II, a previously unrecognized radical mechanism was uncovered for the synthesis of 3,3-disubstituted 2,4-chromandiones through the direct photoexcitation of 4-hydroxycoumarins. Upon deprotonation and irradiation with near-UV light, 4-hydroxycoumarin anions act as strong single-electron transfer (SET) donors, activating alkyl and perfluoroalkyl halides to form carbon-centered radicals that couple regioselectively at the C3 position. This strategy resolved the longstanding chemoselectivity problem between *O*- and *C*-alkylation, providing a mild, catalyst-free route to valuable chromandione scaffolds containing a quaternary stereocenter.

Building upon this mechanistic foundation, Chapter III introduced a new class of bifunctional organic photocatalysts derived from 4-hydroxycoumarins. Rational molecular design led to 3-thioaryl-4-hydroxycoumarins, capable of merging strong photoreductive power ($E^*_{red} \approx -3.0$ V vs SCE) with high triplet energy ($E_T \approx 67$ kcal·mol^{-1}). These catalysts operate through dual photochemical manifolds, promoting both SET-driven radical reactions—such as the reduction of inert aryl halides—and energy-transfer processes, including *E/Z* isomerization and [2+2] photocycloadditions. The bifunctional behavior originates from charge-transfer excited states that balance strong reducing power with effective triplet sensitization in a single organic scaffold.

Overall, this thesis demonstrates that 4-hydroxycoumarins represent a unified platform for accessing distinct excited states with programmable reactivity. By rationally modulating their structure and electronic environment, it is possible to design sustainable, metal-free photocatalysts that control chemical reactivity through light. These findings expand the chemical reactivity of 4-hydroxycoumarins beyond traditional polar chemistry, establishing them as practical tools for visible-light-driven synthesis and the foundation for future developments in excited-state catalysis